antioxidants

Special Issue Reprint

Antioxidant Compounds and Health Benefits of Citrus Fruits

Edited by
Sergio Marques Borghi and Wander Rogério Pavanelli

mdpi.com/journal/antioxidants

MDPI

Antioxidant Compounds and Health Benefits of Citrus Fruits

Antioxidant Compounds and Health Benefits of Citrus Fruits

Guest Editors

Sergio Marques Borghi
Wander Rogério Pavanelli

MDPI

Basel • Beijing • Wuhan • Barcelona • Belgrade • Novi Sad • Cluj • Manchester

Guest Editors

Sergio Marques Borghi
Departament of Pathology
Londrina State University
Londrina
Brazil

Wander Rogério Pavanelli
Biosciences and Biotechnology
Postgraduate Program
Carlos Chagas Institute
(ICC/Fiocruz/PR)
Curitiba
Brazil

Editorial Office
MDPI AG
Grosspeteranlage 5
4052 Basel, Switzerland

This is a reprint of the Special Issue, published open access by the journal *Antioxidants* (ISSN 2076-3921), freely accessible at: https://www.mdpi.com/journal/antioxidants/special_issues/antioxidant_citrus_fruits.

For citation purposes, cite each article independently as indicated on the article page online and as indicated below:

Lastname, A.A.; Lastname, B.B. Article Title. *Journal Name* **Year**, *Volume Number*, Page Range.

ISBN 978-3-7258-4399-2 (Hbk)
ISBN 978-3-7258-4400-5 (PDF)
https://doi.org/10.3390/books978-3-7258-4400-5

Contents

antioxidants

MDPI

Editorial

Antioxidant Compounds and Health Benefits of Citrus Fruits

Sergio Marques Borghi [1,2,*] and Wander Rogério Pavanelli [3,*]

[1] Laboratory of Pain, Inflammation, Department of Pathology, Neuropathy and Cancer, Londrina State University, Londrina 86057-970, Brazil
[2] Center for Research in Health Sciences, University of Northern Paraná, Londrina 86041-140, Brazil
[3] Laboratory of Immunoparasitology of Neglected Diseases and Cancer, State University of Londrina, Londrina 86057-970, Brazil
* Correspondence: sergio.borghi@cogna.com.br (S.M.B.); wanderpavanelli@uel.br (W.R.P.)

Recent evidence emanating from epidemiological prospective studies shows that increased intakes of antioxidant-rich fruits, vegetables, and legumes are associated with a lower risk of developing chronic oxidative stress-related diseases like cardiovascular diseases and cancer, as well as with a lower risk of cardiovascular, cancer, and all-cause mortality rates [1–3]. Functional food ingredients (also referred to as nutraceuticals) are highly nutritious food-derived products that naturally offer or are modified aiming to promote powerful additional health benefits that go beyond basic nutrition factors. The bioactive compounds present in these dietary items have been extensively studied in recent decades as potential molecules capable of interfering with the pathophysiological mechanisms associate with several diseases. The general benefits provided by the regular consumption of fruits and vegetables are proposed to be conferred by their nutritional compounds, including vitamins, and non-flavonoid and flavonoid polyphenols [4]. Important components of functional foods include citrus fruits produced by the flowering plants from the genus *Citrus* L. (Rutaceae family) [5,6]. Fruits in this group include oranges, mandarin, tangerine, clementine, grapefruit, pomelo, lemons, and lime. Citrus fruits are rich in sugars, vitamins, organic acids (such as hydroxycinnamic, hydroxybenzoic, citric, and succinic acids), coumarins, terpenoids, and flavonoids (including flavanones, flavones, flavonols, and anthocyanins). The biological properties of citrus fruit phytochemicals range from antioxidant and anti-inflammatory to antimutagenic and anticarcinogenic effects, among others [6–8].

Oxidative stress denotes a condition provoked by endogenous or exogenous processes in which an imbalance between the generation of free radicals and the cellular ability to neutralize them occurs, thus favoring the overproduction of reactive species. This phenomenon represents a harmful event for cells and tissues, in which the cell membrane, mitochondria and nucleus are highly vulnerable, consequently contributing to the pathogenesis and progression of several diseases [9]. Therefore, targeting oxidative stress in disease has been proposed as a potential approach for diseases prevention and therapy [10]. In this sense, a better comprehension of the mechanisms by which different antioxidants (both natural or synthetic) acts may provide helpful insights and a rationale for successful pharmacological approaches. Antioxidant mechanisms related to citrus fruits compounds are diversified. The inhibition of pro-oxidant enzymes (e.g., xanthine oxidase) and induction of antioxidant enzymes (e.g., catalase, superoxide dismutase, and glutathione peroxidase) [11–13], the modulation of redox-sensitive pathways such as nuclear factor κB (NFκB) and nuclear factor E2-related protein 2 (Nrf2) [14–18], reactive oxygen/nitrogen species (ROS/RNS) scavenging [19,20], and the chelation with transition metals [20,21] are some of the effects or actions described for the antioxidant compounds of citrus fruits to combat oxidative stress [6]. Despite these advances, unravelling new potential mechanisms by which citrus fruit-derived compounds may modulate pathological conditions will contribute to bringing new knowledge on their properties and therapeutic applicability. This Special Issue on the

"Antioxidant compounds and health benefits of citrus fruits" contains nine contributions, comprising six research articles and three reviews.

In the first original article, Bussmann et al. [17] demonstrated the mechanism by which the synthetic flavonoid hesperidin methyl chalcone (HMC; $C_{29}H_{36}O_{15}$) protects the kidneys from damage caused by the non-steroidal anti-inflammatory drug (NSAID) diclofenac. HMC is generated via methylation of the flavanone hesperidin (hesperidin-7-rhamnoglucoside) [22]. The data showed that HMC acts by boosting antioxidant parameters and by reducing oxidative damage and pro-inflammatory cytokines both systemically and in renal tissue. In the kidneys, HMC additionally led to an increased production of anti-inflammatory cytokine IL-10 and a reduction in histopathological damage, edema, and the levels of active tubular pathology marker neutrophil gelatinase-associated lipocalin (NGAL), with these effects being attributed to the activation of the Nrf2/antioxidant responsive elements (ARE) pathway [17]. Lai et al. [23] evaluated the effects of five different drying methods (freeze drying, shade drying, hot-air oven drying at 50 °C, hot-air oven drying at 70 °C, and microwave drying) on the bioactive phytochemicals and antioxidant capacity of navel orange peel. Through HPLC analysis, they identified thirteen flavonoids (three flavanone glycosides and ten polymethoxyflavones) in navel orange peel. The authors found that the use of hot-air oven drying at 50 °C or 70 °C for the drying of orange peel delivered the best results, contributing to the maintenance of bioactive compounds in the peel as well as the improvement of its antioxidant capacity, thus advancing the understanding of the useful methods for the viability and antioxidant potential of navel orange peel compounds [23]. Cioni and colleagues [24] conducted comparative chemical analyses among peel and pulp essential oils and methanolic extracts of different *Citrus australasica* varieties (Red, Collette, Pink Ice, and Yellow Sunshine), as well as analyses of the hybrid faustrime (caviar lime). Additionally, the antioxidant activity of peel and pulp extracts using an A31 mouse embryo fibroblast cell line was also investigated. The peels' essential oils exhibited higher total phenolic contents with greater antioxidant activity. Collette peels showed the highest concentration of flavonoids, including luteolin, isosakuranetin, and poncirin derivatives, and delphinidin and petunidin glycosides. Pink Ice pulps were also shown to be an additional source of flavonoids, and Collette and Red peels presented the highest in vitro antioxidant activity, which was attributed to the presence of anthocyanins, thus identifying finger lime fruits as good sources of phytocompounds within the context of promoting healthy benefits [24]. In another interesting original research article, Ju et al. [25] investigated the antioxidant effects of *Citrus junos* peel fractions (ethanol acetate, hexane, and butanol) using human primary dermal fibroblast and immortalized keratinocyte, and murine melanoma cell lineages. They showed that Yuja peel fractions possessed anti-wrinkle effects by inhibiting metalloproteinases 1, 9, and 13 at mRNA and protein levels, as well as by inducing type I pro-collagen and hyaluronic acid in evaluated UVB-irradiated cells. Moreover, the Yuja peel fractions induced the production of proteins relating to skin hydration, and they decreased melanin content, thus promoting advances in the understanding of the skin benefits provided by Yuja peel fractions, which may contribute to the development of novel pharmaceuticals and cosmetics [25]. In the in vitro study of Nakashima et al. [26], new pharmacological insights into the ways in which high doses of flavonoids quercetin ($C_{15}H_{10}O_7$) and hesperidin ($C_{28}H_{34}O_{15}$) differentially modulate cell viability, tight junction integrity, and cell shape are provided. Considering that the barrier function of tight junctions may block the absorption of some molecules, the identification of reversible modifiers of its integrity are desirable as drug absorption enhancers [27]. They conclude by suggesting both quercetin and hesperidin are promising compounds for developing a naturally occurring drug absorption enhancer for the paracellular route, with hesperidin being the most attractive for such a technology [26]. Finally, García-Nicolás et al. [28] conducted a spatial metabolomic analysis for the characterization of phenolic compounds in juices and fruit tissue extracts of lemons, limes, and mandarins. Flavonoids were mainly found in the citrus peel (flavedo and albedo) and carboxylic acids in segments,

facilitating the extraction of the latter in juices. Limonoids were also distributed in the albedo and segments. The radical scavenging activity was attributed to the flavonoids, and the antioxidant effects were attributed to the combined action of flavonoids and limonoids. These data regarding the fractionation of the extracts advance the comprehension of the antioxidant effects of the family compounds identified [28].

In the first review article, Saini et al. [29] highlighted in their compilation of data the composition and associated health benefits of some components of citrus fruits, notably, carotenoids, flavonoids, limonoids, and terpenes. In their conclusions, the authors propose that bioactive flavonoids of citrus fruits may represent important molecules with antioxidant ant inflammatory properties capable of minimizing the risk of many non-communicable chronic diseases, as well as suggesting that those essential oils rich in limonoids and terpenes possess potential antioxidant and antimicrobial effects. Additionally, the authors pointed to interesting potential future investigations in this field aiming to elucidate some gaps that still exist regarding the composition, content, and health effects of citrus fruit bioactives [29]. In the second review article, Fideles et al. discuss the neuroprotective effects of the flavonol quercetin on nervous system regeneration and functional recovery [30]. Quercetin, one of the most studied and abundant flavonoids in edible vegetables, fruits, and wines, is a pentahydroxyflavone that has hydroxy groups placed at the 3-, 3′-, 4′-, 5-, and 7-positions [31]. The result reported by the authors provided evidence for beneficial effects in preclinical spinal cord injury and peripheral nerve injury models, demonstrating that quercetin can induce effective recovery of neurological functions, contributing to the regeneration of both central and peripheral nervous tissues [30]. Finally, Madureira et al. [32] conducted a comprehensive review regarding the evidence of two antioxidant flavanones, naringenin ($C_{15}H_{12}O_5$) and hesperidin, on the prevention and therapy of breast cancer. Through DNA damage, oxidative stress may trigger genetic alterations that predispose tumorigenicity and tumor progression [33]. The main mechanisms of these flavonoids to counteract breast cancer are properly addressed in the article and are especially associated with anti-proliferative, anti-tumorigenic, and anti-metastatic actions, as well as with the epigenetic modulatory effects upon estrogen receptors [32]. Thus, within effective and safe concentrations, citrus fruits components may represent promising nutraceuticals as anti-cancer substances for breast cancers treatment.

In conclusion, the original research and review articles address several interesting experimental conditions aiming to explore the antioxidant potential of citrus fruit compounds in the context of health benefits. The progress regarding the best methods for its utilization, the elucidation of the mechanistic actions of each bioactive, and the identification of the most effective doses, with guaranteed safety of each antioxidant compound of citrus fruits, will help to develop a rationale to obtain advanced technology which will be useful to optimize its beneficial effects.

Author Contributions: Conceptualization, data curation, writing—original draft preparation, writing—review and editing, visualization, supervision, and project administration, S.M.B. and W.R.P. All authors have read and agreed to the published version of the manuscript.

Funding: This research received no external funding.

Conflicts of Interest: The authors declare no conflict of interest.

References

1. Wang, X.; Ouyang, Y.; Liu, J.; Zhu, M.; Zhao, G.; Bao, W.; Hu, F.B. Fruit and vegetable consumption and mortality from all causes, cardiovascular disease, and cancer: Systematic review and dose-response meta-analysis of prospective cohort studies. *BMJ* **2014**, *349*, g4490. [CrossRef] [PubMed]
2. Aune, D. Plant Foods, Antioxidant Biomarkers, and the Risk of Cardiovascular Disease, Cancer, and Mortality: A Review of the Evidence. *Adv. Nutr.* **2019**, *10*, S404–S421. [CrossRef] [PubMed]
3. Aune, D.; Keum, N.; Giovannucci, E.; Fadnes, L.T.; Boffetta, P.; Greenwood, D.C.; Tonstad, S.; Vatten, L.J.; Riboli, E.; Norat, T. Dietary intake and blood concentrations of antioxidants and the risk of cardiovascular disease, total cancer, and all-cause mortality: A systematic review and dose-response meta-analysis of prospective studies. *Am. J. Clin. Nutr.* **2018**, *108*, 1069–1091. [CrossRef] [PubMed]

4. Kaparapu, J.; Pragada, P.M.; Geddada, M.N.R. Fruits and Vegetables and its Nutritional Benefits. In *Functional Foods and Nutraceuticals Bioactive Components, Formulations and Innovations*, 1st ed.; Egbuna, C., Tupas, G.D., Eds.; Springer: Cham, Switzerland, 2020.
5. Wu, G.A.; Terol, J.; Ibanez, V.; Lopez-Garcia, A.; Perez-Roman, E.; Borreda, C.; Domingo, C.; Tadeo, F.R.; Carbonell-Caballero, J.; Alonso, R.; et al. Genomics of the origin and evolution of Citrus. *Nature* **2018**, *554*, 311–316. [CrossRef] [PubMed]
6. Zou, Z.; Xi, W.; Hu, Y.; Nie, C.; Zhou, Z. Antioxidant activity of Citrus fruits. *Food Chem.* **2016**, *196*, 885–896. [CrossRef]
7. Ballistreri, G.; Fabroni, S.; Romeo, F.V.; Timpanaro, N.; Amenta, M.; Rapisarda, P. Anthocyanins and Other Polyphenols in Citrus Genus: Biosynthesis, Chemical Profile, and Biological Activity. In *Polyphenols in Plants Isolation, Purification and Extract Preparation*, 2nd ed.; Watson, R.R., Ed.; Academic Press: Cambridge, MA, USA, 2019.
8. Ladaniya, M.S. Nutritive and medicinal value of citrus fruits. In *Citrus Fruit Biology, Technology and Evaluation*; Ladaniya, M.S., Ed.; Academic Press: Cambridge, MA, USA, 2008.
9. Hajam, Y.A.; Rani, R.; Ganie, S.Y.; Sheikh, T.A.; Javaid, D.; Qadri, S.S.; Pramodh, S.; Alsulimani, A.; Alkhanani, M.F.; Harakeh, S.; et al. Oxidative Stress in Human Pathology and Aging: Molecular Mechanisms and Perspectives. *Cells* **2022**, *11*, 552. [CrossRef]
10. Forman, H.J.; Zhang, H. Author Correction: Targeting oxidative stress in disease: Promise and limitations of antioxidant therapy. *Nat. Rev. Drug Discov.* **2021**, *20*, 652. [CrossRef]
11. Sun, Y.; Liu, M.; Tao, W.; Ye, X.; Sun, P. Effects of edible whole citrus fruits on endogenous antioxidant enzymes of HepG2 cells. *Food Qual. Saf.* **2022**, *6*, fyac029. [CrossRef]
12. Nakao, K.; Murata, K.; Itoh, K.; Hanamoto, Y.; Masuda, M.; Moriyama, K.; Shintani, T.; Matsuda, H. Anti-hyperuricemia effects of extracts of immature Citrus unshiu fruit. *J. Tradit. Med.* **2011**, *28*, 10–15. [CrossRef]
13. Ali, M.M.; El Kader, M.A. The influence of naringin on the oxidative state of rats with streptozotocin-induced acute hyperglycaemia. *Z. Naturforsch C J. Biosci.* **2004**, *59*, 726–733. [CrossRef]
14. Liu, X.; Wang, N.; Fan, S.; Zheng, X.; Yang, Y.; Zhu, Y.; Lu, Y.; Chen, Q.; Zhou, H.; Zheng, J. The citrus flavonoid naringenin confers protection in a murine endotoxaemia model through AMPK-ATF3-dependent negative regulation of the TLR4 signalling pathway. *Sci. Rep.* **2016**, *6*, 39735. [CrossRef] [PubMed]
15. Yang, G.; Li, S.; Yuan, L.; Yang, Y.; Pan, M.H. Effect of nobiletin on the MAPK/NF-kappaB signaling pathway in the synovial membrane of rats with arthritis induced by collagen. *Food Funct.* **2017**, *8*, 4668–4674. [CrossRef] [PubMed]
16. Arredondo, F.; Echeverry, C.; Abin-Carriquiry, J.A.; Blasina, F.; Antunez, K.; Jones, D.P.; Go, Y.M.; Liang, Y.L.; Dajas, F. After cellular internalization, quercetin causes Nrf2 nuclear translocation, increases glutathione levels, and prevents neuronal death against an oxidative insult. *Free Radic. Biol. Med.* **2010**, *49*, 738–747. [CrossRef]
17. Bussmann, A.J.C.; Zaninelli, T.H.; Saraiva-Santos, T.; Fattori, V.; Guazelli, C.F.S.; Bertozzi, M.M.; Andrade, K.C.; Ferraz, C.R.; Camilios-Neto, D.; Casella, A.M.B.; et al. The Flavonoid Hesperidin Methyl Chalcone Targets Cytokines and Oxidative Stress to Reduce Diclofenac-Induced Acute Renal Injury: Contribution of the Nrf2 Redox-Sensitive Pathway. *Antioxidants* **2022**, *11*, 1261. [CrossRef] [PubMed]
18. Bussmann, A.J.C.; Borghi, S.M.; Zaninelli, T.H.; Dos Santos, T.S.; Guazelli, C.F.S.; Fattori, V.; Domiciano, T.P.; Pinho-Ribeiro, F.A.; Ruiz-Miyazawa, K.W.; Casella, A.M.B.; et al. The citrus flavanone naringenin attenuates zymosan-induced mouse joint inflammation: Induction of Nrf2 expression in recruited CD45(+) hematopoietic cells. *Inflammopharmacology* **2019**, *27*, 1229–1242. [CrossRef]
19. Saleem, M.; Durani, A.I.; Asari, A.; Ahmed, M.; Ahmad, M.; Yousaf, N.; Muddassar, M. Investigation of antioxidant and antibacterial effects of citrus fruits peels extracts using different extracting agents: Phytochemical analysis with in silico studies. *Heliyon* **2023**, *9*, e15433. [CrossRef]
20. Amitava, D.; Kimberly, K. Antioxidant Vitamins and Minerals. In *Antioxidants in Food, Vitamins and Supplement Prevention and Treatment of Disease*, 1st ed.; Elsevier: Amsterdam, The Netherlands, 2014; pp. 227–294.
21. Kim, M.Y. Free radical scavenging and ferrous ion chelating activities of citrus fruits derived from induced mutations with gamma irradiation. *Life Sci. J.* **2022**, *19*, 53–56. [CrossRef]
22. Pinho-Ribeiro, F.A.; Zarpelon, A.C.; Mizokami, S.S.; Borghi, S.M.; Bordignon, J.; Silva, R.L.; Cunha, T.M.; Alves-Filho, J.C.; Cunha, F.Q.; Casagrande, R.; et al. The citrus flavonone naringenin reduces lipopolysaccharide-induced inflammatory pain and leukocyte recruitment by inhibiting NF-kappaB activation. *J. Nutr. Biochem.* **2016**, *33*, 8–14. [CrossRef]
23. Lai, C.; Liang, Y.; Zhang, L.; Huang, J.; Kaliaperumal, K.; Jiang, Y.; Zhang, J. Variations of Bioactive Phytochemicals and Antioxidant Capacity of Navel Orange Peel in Response to Different Drying Methods. *Antioxidants* **2022**, *11*, 1543. [CrossRef]
24. Cioni, E.; Migone, C.; Ascrizzi, R.; Muscatello, B.; De Leo, M.; Piras, A.M.; Zambito, Y.; Flamini, G.; Pistelli, L. Comparing Metabolomic and Essential Oil Fingerprints of Citrus australasica F. Muell (Finger Lime) Varieties and Their In Vitro Antioxidant Activity. *Antioxidants* **2022**, *11*, 2047. [CrossRef]
25. Jung, Y.Y.; Ha, I.J.; Lee, M.; Ahn, K.S. Skin Improvement with Antioxidant Effect of Yuja (Citrus junos) Peel Fractions: Wrinkles, Moisturizing, and Whitening. *Antioxidants* **2022**, *12*, 51. [CrossRef] [PubMed]
26. Nakashima, M.; Goda, N.; Tenno, T.; Kotake, A.; Inotsume, Y.; Amaya, M.; Hiroaki, H. Pharmacologic Comparison of High-Dose Hesperetin and Quercetin on MDCK II Cell Viability, Tight Junction Integrity, and Cell Shape. *Antioxidants* **2023**, *12*, 952. [CrossRef] [PubMed]
27. Deli, M.A. Potential use of tight junction modulators to reversibly open membranous barriers and improve drug delivery. *Biochim. Biophys. Acta* **2009**, *1788*, 892–910. [CrossRef] [PubMed]

28. Garcia-Nicolas, M.; Ledesma-Escobar, C.A.; Priego-Capote, F. Spatial Distribution and Antioxidant Activity of Extracts from Citrus Fruits. *Antioxidants* **2023**, *12*, 781. [CrossRef]
29. Saini, R.K.; Ranjit, A.; Sharma, K.; Prasad, P.; Shang, X.; Gowda, K.G.M.; Keum, Y.S. Bioactive Compounds of Citrus Fruits: A Review of Composition and Health Benefits of Carotenoids, Flavonoids, Limonoids, and Terpenes. *Antioxidants* **2022**, *11*, 239. [CrossRef]
30. Fideles, S.O.M.; de Cassia Ortiz, A.; Buchaim, D.V.; de Souza Bastos Mazuqueli Pereira, E.; Parreira, M.; de Oliveira Rossi, J.; da Cunha, M.R.; de Souza, A.T.; Soares, W.C.; Buchaim, R.L. Influence of the Neuroprotective Properties of Quercetin on Regeneration and Functional Recovery of the Nervous System. *Antioxidants* **2023**, *12*, 149. [CrossRef]
31. Borghi, S.M.; Pinho-Ribeiro, F.A.; Fattori, V.; Bussmann, A.J.; Vignoli, J.A.; Camilios-Neto, D.; Casagrande, R.; Verri, W.A., Jr. Quercetin Inhibits Peripheral and Spinal Cord Nociceptive Mechanisms to Reduce Intense Acute Swimming-Induced Muscle Pain in Mice. *PLoS ONE* **2016**, *11*, e0162267. [CrossRef]
32. Madureira, M.B.; Concato, V.M.; Cruz, E.M.S.; Bitencourt de Morais, J.M.; Inoue, F.S.R.; Concimo Santos, N.; Goncalves, M.D.; Cremer de Souza, M.; Basso Scandolara, T.; Fontana Mezoni, M.; et al. Naringenin and Hesperidin as Promising Alternatives for Prevention and Co-Adjuvant Therapy for Breast Cancer. *Antioxidants* **2023**, *12*, 586. [CrossRef]
33. Reuter, S.; Gupta, S.C.; Chaturvedi, M.M.; Aggarwal, B.B. Oxidative stress, inflammation, and cancer: How are they linked? *Free Radic. Biol. Med.* **2010**, *49*, 1603–1616. [CrossRef]

antioxidants

MDPI

Article

Pharmacologic Comparison of High-Dose Hesperetin and Quercetin on MDCK II Cell Viability, Tight Junction Integrity, and Cell Shape

Mio Nakashima [1], Natsuko Goda [1], Takeshi Tenno [1,2], Ayaka Kotake [3], Yuko Inotsume [3], Minako Amaya [3] and Hidekazu Hiroaki [1,2,4,*]

[1] Laboratory of Structural Molecular Pharmacology, Graduate School of Pharmaceutical Sciences, Nagoya University, Furocho, Chikusa-ku, Nagoya 464-8601, Aichi, Japan
[2] BeCerllBar, LLC, Business Incubation Building, Nagoya University, Furocho, Chikusa ku, Nagoya 464-8601, Aichi, Japan
[3] Cosmetics Research Department, Nicca Chemical Co., Ltd., Fukui 910-8670, Fukui, Japan
[4] Center for One Medicine Innovative Translational Research, Gifu University Institute for Advanced Study, Yanagito, Gifu 501-1112, Gifu, Japan
* Correspondence: hiroaki.hidekazu.j7@f.mail.nagoya-u.ac.jp; Tel.: +81-52-789-4535

Abstract: The modulation of tight junction (TJ) integrity with small molecules is important for drug delivery. High-dose baicalin (BLI), baicalein (BLE), quercetin (QUE), and hesperetin (HST) have been shown to open TJs in Madin-Darby canine kidney (MDCK) II cells, but the mechanisms for HST and QUE remain unclear. In this study, we compared the effects of HST and QUE on cell proliferation, morphological changes, and TJ integrity. HST and QUE were found to have opposing effects on the MDCK II cell viability, promotion, and suppression, respectively. Only QUE, but not HST, induced a morphological change in MDCK II into a slenderer cell shape. Both HST and QUE downregulated the subcellular localization of claudin (CLD)-2. However, only QUE, but not HST, downregulated CLD-2 expression. Conversely, only HST was shown to directly bind to the first PDZ domain of ZO-1, a key molecule to promote TJ biogenesis. The TGFβ pathway partially contributed to the HST-induced cell proliferation, since SB431541 ameliorated the effect. In contrast, the MEK pathway was not involved by both the flavonoids, since U0126 did not revert their TJ-opening effect. The results offer insight for using HST or QUE as naturally occurring absorption enhancers through the paracellular route.

Keywords: tight junction integrity; absorption enhancer; dynamic equilibrium of tight junction; claudin-ZO-1 interaction; TGFβ pathway; MEK pathway

1. Introduction

The tight junction (TJ) is the apical-most intercellular adhesion complex found in epithelial and endothelial cells [1–3]. TJs are a proteinous complexes, containing integral membrane proteins, such as occludin (OCLN) and claudins (CLDs), as well as cytosolic scaffold proteins, such as zonula occludens (ZO)-1 (and its close paralog ZO-2), which connect these membranous components to the actin cytoskeleton [4–7]. As the key physicochemical function of TJ is to limit the free translocation of solvents, solutes, and cells through the paracellular pathway, TJs play a pivotal role in the barrier function of the paracellular transport pathway. TJs have a barrier function in the paracellular pathway, since they restrict the free translocation of solvents, solutes, and cells across the epithelial cell layers. Hence, TJs are particularly important for the digestive organs, respiratory tract, skin, and blood vessels. In a pharmacological context, the barrier function of TJs sometimes hampers the absorption of medium-sized drugs, including peptides and oligonucleotides, across paracellular pathways. Accordingly, the reversible modifiers of TJ integrity are expected to act as drug absorption enhancers.

ZO-1 and ZO-2 are essential components that promote TJ biogenesis and maintain TJ integrity [7,8]. These scaffold proteins harbor N-terminal three copies of the postsynaptic density 95 (PSD-95)/discs large/ZO-1 (PDZ) domains, followed by the Src-homology 3 domain and a guanylate kinase domain [4,9,10]. Among these three PDZ domains of ZO-1/2, the first PDZ domain of ZO-1 (ZO-1 (PDZ1)) acts as the molecular interface to bind the C-terminal PDZ-binding motifs (PBMs) of CLDs [11]. This specific interaction has been shown to be indispensable for TJ formation and maintenance [7]. For example, the cells of ZO-1 and ZO-2 double knockdown decreased some (but not all) CLD localizations in the TJ area, with an abnormal accumulation of apical actin [12]. Similarly, ZO-1 knockout/ZO-2 knockdown resulted in abnormal and immature organization of CLDs in the TJ compartment [13]. The fact that the point mutations in the PBMs of CLDs exhibited TJ-defective phenotypes partly supports the relevance of the ZO-1(PDZ1)–CLD interaction [14]. The number of examples of molecules that directly bind to ZO-1(PDZ1)) with TJ-opening activities is also increasing [15–19].

To discover milder and safer TJ modifiers, we focused on TJ-modulating flavonoids. Flavonoids are generally believed to be beneficial with regards to consumption from foods, medical herbs, and traditional medicines, and this is the result of their antioxidant and anti-inflammatory properties [20]. In this study, we focused on the other pharmacological activity of flavonoids, rather than their antioxidative activity. In our previous studies, baicalin (BLI) and baicalein (BLE) showed specific binding to ZO-1(PDZ1) using nuclear magnetic resonance (NMR) methods, with mild TJ-opening activity in two epithelial cells: Madin–Darby canine kidney (MDCK) II cell and Caco-2 cell [18]. We also reported that a high-dose administration of hesperetin (HST) and quercetin (QUE) against MDCK II cells resulted in reduced subcellular localization of CLD-2 to the TJ compartment and decreased TJ integrity [21]. Note that there are no previous investigations into the TJ-opening activity of HST. In contrast, the reported TJ opening of QUE seems controversial, since many other groups have reported barrier-enhancing and/or barrier-protecting activity of QUE for epithelial cells [22]. Nevertheless, nephrotoxicity was also reported by an overdose administration of QUE [23]. Thus, elucidation of the pharmacological mechanism of the TJ opening of HST and QUE may facilitate the development of a safer TJ-opening modulator from natural sources, especially from citrus fruits.

In this study, we compared the effects of flavonoids on cell viability, cell shape morphology, TJ modulating activity, and mechanisms of TJ opening with regards to the effects of flavonoids on MDCK II cells. We also assessed the direct interaction of ZO-1(PDZ1) with either HST or QUE through NMR titration experiments using ^{15}N-labelled ZO-1(PDZ1). Finally, we discussed the application potential of HST and QUE as 'safer' drug absorption enhancers.

2. Materials and Methods

2.1. Materials

HST (>96% pure), QUE (practical grade), SB431542, and U0126 were purchased from FUJIFILM Wako Pure Chemical Corporation (Osaka, Japan). All compounds used for NMR and cell experiments were dissolved into d_6-dimethylsulfoxide (DMSO) as a 100 mM solution and stored at -20 °C until needed.

The rabbit anti-CLD-2 antibody and anti-OCLN antibody were obtained from Sigma-Aldrich (St. Louis, MO, USA). The rabbit anti-ZO-1 antibody was obtained from Invitrogen (Carlsbad, CA, USA). Mouse anti-β-actin antibody was purchased from Wako. Rhodamine–phalloidin was purchased from Cytoskeleton, Inc. (Denver, CO, USA). For immunofluorescence microscopy, the anti-rabbit immunoglobulin G (IgG) and the F(ab')2 fragment-Cy3 antibody were obtained from Sigma-Aldrich. For Western blotting analysis, anti-rabbit and mouse IgG horseradish peroxidase (HRP) conjugates were acquired from Promega (Madison, WI, USA).

2.2. Cell Culture and Morphology Analysis

The culture of MDCK II cells, a kind gift from Mikio Furuse (National Institute for Physiological Sciences, Okazaki, Aichi, Japan), and their morphology analysis was performed according to our previous reports [18,21]. For this process, Dulbecco's modified Eagle's medium (DMEM) supplemented with 10% fetal bovine serum (FBS; Biosera, Ringmer, UK), 1% penicillin/streptomycin (Gibco, NY, USA, or Wako Pure Chemical Co.), and six-well, 35-mm plate (AGC Techno Glass Co., Shizuoka, Japan) were used, and 30×10^4 cells per well were plated. To observe the flavonoids' and the inhibitors' effect, the culture medium was changed to a medium containing 100 μM of HST and QUE, or 5, 10, and 20 μM of SB431542 and U0126, supplemented with a final concentration of 0.1% of d_6-DMSO, after twenty-four hours after plating. Cells treated by 0.1% d_6-DMSO were used as controls. The cells were analyzed using immunofluorescent microscopy, Western blotting, real-time polymerase chain reaction (PCR), a WST-8 assay, and cell morphology analysis (differential interference contrast (DIC) images) after 48 h of exposure to the compounds.

The cell viability after compound exposure was monitored by WST-8 assay. 1.5×10^4 cells per well were plated on a 96-well, 7-mm plate (AGC Techno Glass Co.). The culture medium was changed to a medium containing 100 μM of HST and QUE, or 5, 10, and 20 μM of SB431542 and U0126, with a final concentration of 0.1% of d_6-DMSO added after one day after plating. After two days of treatment with the compounds, cell viability was measured using a Cell Counting Kit-8 (DOJINDO, Kumamoto, Japan). An EnSpire plate reader (Perkin-Elmer Japan, Kanagawa, Japan), excited at 450 nm, was used.

To obtain the morphological parameters of the cell shape, DIC-images were digitalized and subjected to ImageJ software (National Institute of Health, Rockville Pike, Bethesda, MD, USA). All parameters were normalized against their corresponding values from the control cells.

2.3. Immunofluorescence Microscopy

After fixation of the cells with cold 1 × phosphate-buffered saline, containing 4% paraformaldehyde, the cells were incubated with primary antibodies (anti-CLD-2, OCLN, ZO-1, and actin) for 24 h at 4 °C. The cells were then incubated with secondary antibodies for 1 h. The fluorescence images were obtained using fluorescence microscopy (IX-71, Olympus, Tokyo, Japan; scale bar: 20 μm) equipped with a color charge-coupled device camera DP-70 (Olympus, Shinjuku, Tokyo, Japan). For CLD-2 and actin immunostaining, brightness (+85%) and contrast (+10%) in Figures 2, 3, and 6 were modified for clarity. The original figures are found in the Supplementary Figures.

2.4. Western Blotting

Western blot analysis was performed according to our previous reports [18,21]. The cells were rinsed, and crude proteins were extracted with 100 μL of the buffer, containing sodium dodecyl sulfate (SDS). Mild sonication, using a Bioruptor (BM Equipment Co., Tokyo, Japan), for 5 min (duty cycle 50%), was used for this process. Each crude protein sample was analyzed by SDS–polyacrylamide gel electrophoresis. The samples were then electroblotted to the poly(vinylidene fluoride) (PVDF) membrane (ATTO, Tokyo, Japan) and blocked with 3% skim milk for overnight with the primary antibodies. The membrane was washed four times and treated with corresponding secondary antibodies. Detection of the corresponding proteins was achieved using a Chemi-Lumi One Super solution (Nacalai Tesque, Kyoto, Japan) and the LAS-3000 analyzer (Fuji Film, Tokyo, Japan). For quantification of the results from the Western blotting, the experiments were repeated at least three times. The number of the repeats was indicated in the figure legends.

2.5. Real-Time PCR

The RNA was purified using the RNeasy Plus Mini Kit (QIAGEN, Tokyo, Japan), based on the manufacturer's instructions. Then, cDNA was prepared using the ReverTra® Ace qPCR RT Master Mix (Toyobo Co., Osaka, Japan), based on the manufacturer's in-

structions. Quantitative real-time PCR was performed using the LightCycler® System (Roche Diagnostics, Tokyo, Japan). The primer sequences are as follows: *GAPDH* (GenBank accession number: NM_001003142) (Fw 5′-CAACTCC-CTCAAGATTGTCAGCAA-3′ and Rev 5′-CATGGATGACTTTGGCTAGAG-GA-3′), *CLD-2* (GenBank accession number: NM_001003089) (Fw 5′-CGCTCCGACTACTATGACTCCT-3′ and Rev 5′-GGCCTTGGAG-AGCCTCTAGT-3′), *OCLN* (GenBank accession number: NM_001003195) (Fw 5′-CTGGAG-CAGGACCACTATGAGA -3′ and Rev 5′-CTCCTCCAGCTCGTCACAC-3′), and *TJP1* (GenBank accession number: NM_001003140) (Fw 5′-GGAG-ATTCCGGGGT-CTTCG-3′ and Rev 5′-CTGGCTGAGCTGACAAATCCTC-3′). An aliquot of 1 μL of template cDNA with 0.6 μL of forward and reverse primers was mixed with 10 μL of THUNDERBIRD® SYBR® qPCR Mix (TOYOBO, Osaka, Japan) and adjusted to a total solution volume to 20 μL.

2.6. Protein Expression and Purification

The expression and purification of the mouse ZO-1(PDZ1) (residues 18–110) has been previously described with a slight modification [24]. In brief, ZO-1(PDZ1) was expressed as the glutathione-S-transferase (GST)-tagged form by Escherichia coli BL21 (*DE3*). For the NMR sample, 1 L M9 minimal media with ^{15}N-ammonium chloride as the sole nitrogen source was used [24]. The fusion protein was captured using GST-accept (Nacalai Tesque). To obtain ^{15}N-labeled ZO-1(PDZ1), the fusion protein was digested "on-column" using PreScission™ Protease. Finally, the sample was further purified by size-exclusion chromatography using a Superdex 75 column (Cytiva, Tokyo, Japan).

2.7. NMR Titration Experiments

To assess the direct interaction between ZO-1(PDZ1) and the flavonoids, NMR titration experiments were employed, in which a series of 2D ^{1}H-^{15}N heteronuclear single quantum coherence (HSQC) spectra at 25 °C were analyzed. The sample was dissolved in 5% D_2O–95% H_2O containing 20 mM of MES buffer (pH 5.9). In the titration, up to two molar equivalences of HST and QUE were added to 0.1 mM ^{15}N-ZO-1(PDZ1), and the normalized chemical shift changes $\Delta\delta_{normalized}$ in the 1H-^{15}N HSQC spectra upon ligand titration were analyzed as follows (Equation (1)),

$$\Delta\delta_{normalized} = \{\Delta\delta(^{1}H)^2 + [\Delta\delta(^{15}N)/5]^2\}^{1/2} \quad (1)$$

where $\Delta\delta(^{1}H)$ and $\Delta\delta(^{15}N)$ are the chemical shift changes in the amide proton and amide nitrogen, respectively [25]. The results were visualized using the molecular graphics tool PyMOL program (The PyMOL Molecular Graphics System, Version 2.0, Schrödinger, LLC., Broadway, New York, USA) onto the ribbon representation of the ZO-1(PDZ1) structure (the Protein Data Bank (PDB) ID = 2H3M). Each threshold value was calculated using the method developed by Schumann et al. [26].

2.8. Molecular Docking Based on NMR Chemical Shift Perturbations

Structural models of the ZO1-HST and ZO1-QUE complexes were calculated with the NMR structure of ZO-1(PDZ1) (PDB ID of 2RRM) [16] using HADDOCK software (HADDOCK2.4, Utrecht University, Heidelberglaan, Utrecht, The Netherlands), which derives the docking model, fulfilling the chemical shift perturbations (CSPs) [27,28]. We used the first model registered in 2RRM for the docking experiment. The data of CSPs were used as the restraints to generate the NMR-based docking model, according to the user manual. Thus, the residues of ZO-1(PDZ1) that showed marked CSPs were defined as the binding sites of ZO-1(PDZ1). The ZO1-HST structure with the lowest Z score was selected and displayed using PyMOL. The coordinates of the flavonoids were obtained from the webserver (https://molview.org (accessed on 1 December 2021)) and converted into pdb format. The other details are described in Supplementary Information.

2.9. Statistical Analysis

Statistical analyses were performed by one-way ANOVA followed by a Tukey–Kramer test. A difference of $p < 0.05$ was considered significant. All values are expressed as means with their standard errors of mean.

3. Results

3.1. Cell Viability of HST or QUE

We assessed the conditions (concentrations and time points) of the HST and QUE treatments that did not damage the MDCK II cells severely. The MDCK II cells began to form TJs approximately 24 h after seeding. We chose this time point for treatment with flavonoids and examined the effects on the proliferation of MDCK II cells. As shown in Figure 1D, the cells treated with HST showed an increased viability of up to 130%, whereas those treated with QUE showed a decreased viability of 60% compared to the control. This drop in cell viability after exposure to 100 μM if QUE raises the concern of toxicity of a high-dose QUE treatment, although QUE is considered a beneficial flavonoid.

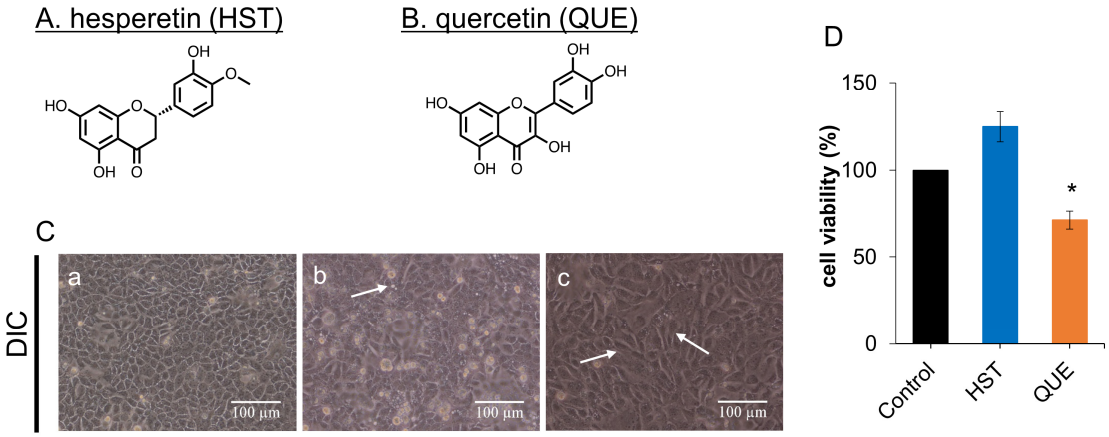

Figure 1. Chemical structures of (**A**) hesperetin (HST) and (**B**) quercetin (QUE). (**C**) Morphological change in Madin-Darby canine kidney (MDCK) II cells induced by flavonoids. Bright-field differential interference contrasts (DIC) images with corresponding flavonoids that are arrayed. Cells were exposed to flavonoids at a concentration of 100 μM for 48 h. Arrows show the changes. (**a**) Control (DMSO), (**b**) HST, and (**c**) QUE. Scale bar = 100 μm. (**D**) Effects of flavonoids on cell viability in MDCK II cells. Cells were treated with flavonoids at a concentration of 100 μM for 48 h. Error bars indicate standard deviations. Turkey-Kramer multiple comparison tests were applied as statistical analyses. Difference from the value of the control cells, * $p < 0.05$. HST, QUE: $n = 4$.

3.2. Changes in Cell Morphology Induced by QUE

We then assessed the morphological changes in the MDCK II cells exposed to 100 μM of HST and QUE under a bright-field phase contrast microscope. In our previous studies, we reported pharmacological effect of several flavonoids against MDCK II cells at the concentration between 50 and 100 μM, and moderate effect were observed after 48 to 96 h of exposure [18,21]. Thus, in this study, we also chose 100 μM and 48 h as the fixed experimental conditions. It is worth noting that the concentration is below the 50% cytotoxicity concentration of QUE (2500 μM) and HST (2900 μM) against MDCK cells [29]. When the cells were exposed to HST, the cell monolayer seemed normal and healthy in terms of shape and size. However, we found many white granular spots (white spots) (Figure 1C panel b, arrow, Supplementary Figure S2). Similar white spots, such as oil droplets, were repeatedly observed in our previous study [21]. Moreover, when the cells were exposed to high concentrations (200 μM) of HST, several holes in the cell monolayer formed due to unknown cellular stress of HST.

By contrast, the cells treated with QUE showed significant morphological changes compared to the typical cobblestone-like morphology of untreated MDCK II cells, which

exhibited an elongated and slenderized cell shape similar to a fibroblast-like appearance (Figure 1C panel c, arrows). It should be noted that we also reported similar morphological changes and a fibroblast-like phenotype of MDCK II cells when the cells were exposed to a high dose of BLE [18].

We quantitatively analyzed these morphological changes using QUE by estimating the length of the transverse and longitudinal axes of the cells using the cell areas from microscopic images. We found that the cells elongated by 180% in the long-axis direction. When the cells were treated with QUE for 96 h, the elongation reached 220%, with 130% elongation of the short axis. As a result, the relative cell area became more than 300% (Supplementary Figure S1). Surprisingly, these morphological changes were irreversible. The cells did not recover and were re-transformed into a native shape even after 48 h of the removal of QUE (Supplementary Figure S1). These changes seemed specific to QUE and were not observed in the cells exposed to rutin, a 3-rutinoside of QUE [21].

We hypothesized that the QUE-induced morphological changes could be one of the important steps of the "partial" epithelial–mesenchymal transition (EMT), which we previously observed in BLE treatment [18]. If so, then this observation is somewhat controversial in the many reported QUE activities, as QUE can prevent EMT in many cancer cells [30,31]. Thus, we assessed whether the observed morphological changes were signs of partial EMT. For this purpose, we assessed the subcellular distributions of CLD-2, OCLN, ZO-1, and actin cytoskeleton, as the disintegration of the intercellular cell–cell junctions is one of the critical checkpoints of EMT. The localization of TJ-related proteins (CLD-2, ZO-1, and OCLN) was observed using immunofluorescence microscopy. As shown in Figure 2, the significant morphological changes in the MDCK II cells exposed to QUE were readily more visible using fluorescent immunological microscopy with paraformaldehyde fixed cells than using bright-field microscopy (Figure 2F,I). In addition, the amount of CLD-2, which was localized at the cell–cell interaction membrane compartment, decreased (to be discussed later). However, the localization of ZO-1 and OCLN was not affected by QUE treatment, suggesting that EMT did not occur (Figure 2F,I). We also assessed the amount and direction of cortical actin bundles. We could not find any significant changes in actin compared to the control (Figure 2L), suggesting that the regulatory pathway of the actin cytoskeleton might not be a direct target of QUE.

The same experiment was performed for HST, and similar to QUE, the membrane localization of OCLN, ZO-1, and actin fibers was not affected. Therefore, although we observed cell slenderizing induced by QUE, neither QUE nor HST induced partial EMT and rearrangement of the actin cytoskeleton of MDCK II cells.

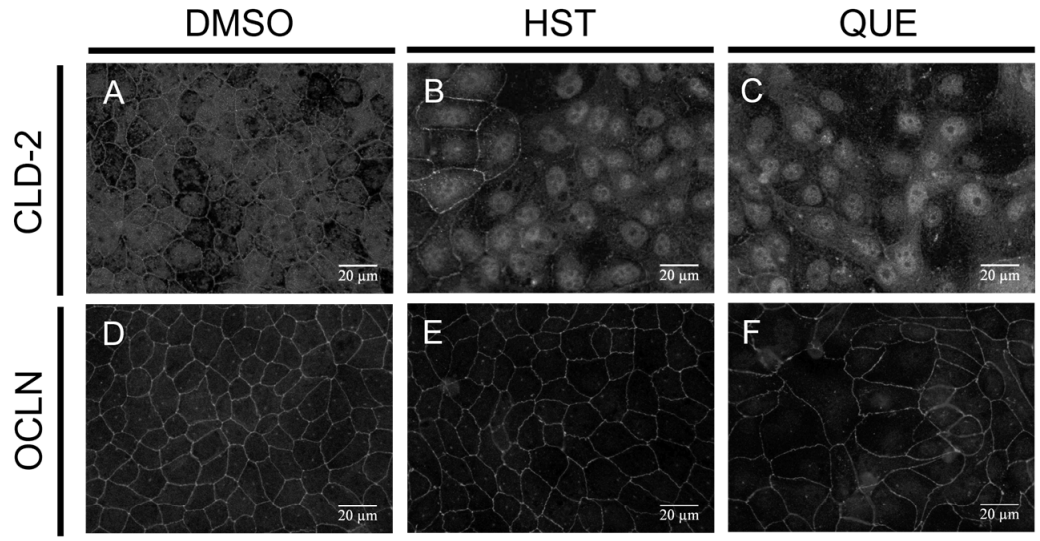

Figure 2. *Cont.*

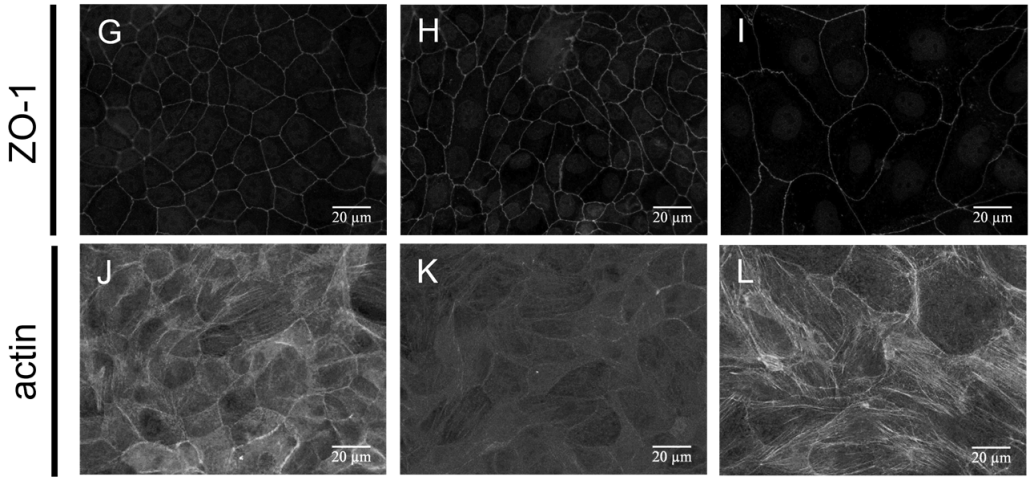

Figure 2. Changes on TJ integrity of MDCK II cells induced by flavonoids. Immuno-fluorescence staining of CLD-2, ZO-1, OCLN, and actin were applied to the MDCK II cells exposed to flavonoids at a concentration of 100 μM for 48 h. (**A**,**D**,**G**,**J**) control (DMSO); (**B**,**E**,**H**,**K**) HST; (**C**,**F**,**I**,**L**) QUE. Scale bar = 20 μM. Brightness of images was modified to 160%.

3.3. TJ Reduction Activity of HST or QUE

During the assessment of the possibility of partial EMT by QUE or HST through immunofluorescence microscopy, we succeeded in reproducing the TJ-opening activity of QUE and HST (Figure 2B,C), which we previously reported [21]. The amount of CLD-2 in the TJ compartment significantly decreased after 48 h of exposure to 100 μM QUE or HST. As CLD-2 is considered the most abundant CLD in MDCK II cells [32], we supposed that these changes were related to the decreased integrity of TJ. We then examined the reversibility of the flavonoid-induced TJ-opening of MDCK II cells and continued observing the recovery of TJ-accumulated CLD-2 48 h after QUE was washed out. The amount of TJ-accumulated CLD-2 was partially restored after 48 h in the medium without QUE after QUE treatment (Figure 3B, panel e). The same experiment was also performed for the HST. In the bright-field observation of living MDCK cells, the white spots on the cell monolayer surface induced by HST vanished due to HST removal. Accordingly, the TJ-accumulated CLD-2 was restored after a 48-h culture in the medium without HST after HST treatment (Figure 3A panel e). Therefore, the effects of QUE or HST on CLD-2 attenuation in the TJ compartment were partially reversible, whereas the effect of QUE on cell morphology seemed irreversible.

We then examined the protein expression level of CLD-2 in cells treated with QUE and HST using Western blotting. Figure 4A shows the results of the amount of CLD-2 extracted from cells treated with 100 μM HST or QUE after 48 h of exposure. Figure 4B is a bar graph of the protein level of CLD-2 treated with 100 μM HST or QUE normalized to the untreated cells. The CLD-2 protein level decreased to 65% and 35% compared to the controls with HST and QUE treatment, respectively. These changes were dose-dependent, and treatment with 10 μM of HST or QUE did not induce observable changes in the CLD-2 levels in our preliminary experiments. Accordingly, we examined the reversibility of CLD-2 reduction by analyzing the cells that were first exposed to either HST or QUE and then incubating with HST- or QUE-free medium for 48 h. Western blot analysis showed that the removal of HST or QUE from the medium could restore CLD-2 protein levels.

As shown previously, we also analyzed the effects of HST and QUE on the other TJ-related proteins, ZO-1 and OCLN. ZO-1 is a protein that serves as a scaffold during TJ formation, and its mislocalization from TJ decreases TJ integrity. After exposure to either HST or QUE, we observed the subcellular localization of ZO-1 in the MDCK II cells (Figure 2H,I). Similarly, the subcellular localization of OCLN was also monitored (Figure 2E,F). However, the amount of ZO-1 and OCLN localized in the lateral membrane of MDCK II cells was not affected, regardless of the decrease in CLD-2. This suggests that

the decrease in the subcellular localization of CLD-2 is independent from those of OCLN and ZO-1 upon HST or QUE treatment.

In addition, we examined the changes in CLD-2 mRNA levels upon HST and QUE treatment using quantitative PCR. The CLD-2 mRNA level was significantly decreased by HST or QUE (Figure 4C). QUE was more potent than HST in terms of CLD-2 transcription suppression. Surprisingly, although the protein levels of OCLN and ZO-1 were not drastically changed, their mRNA levels were suppressed by HST and QUE.

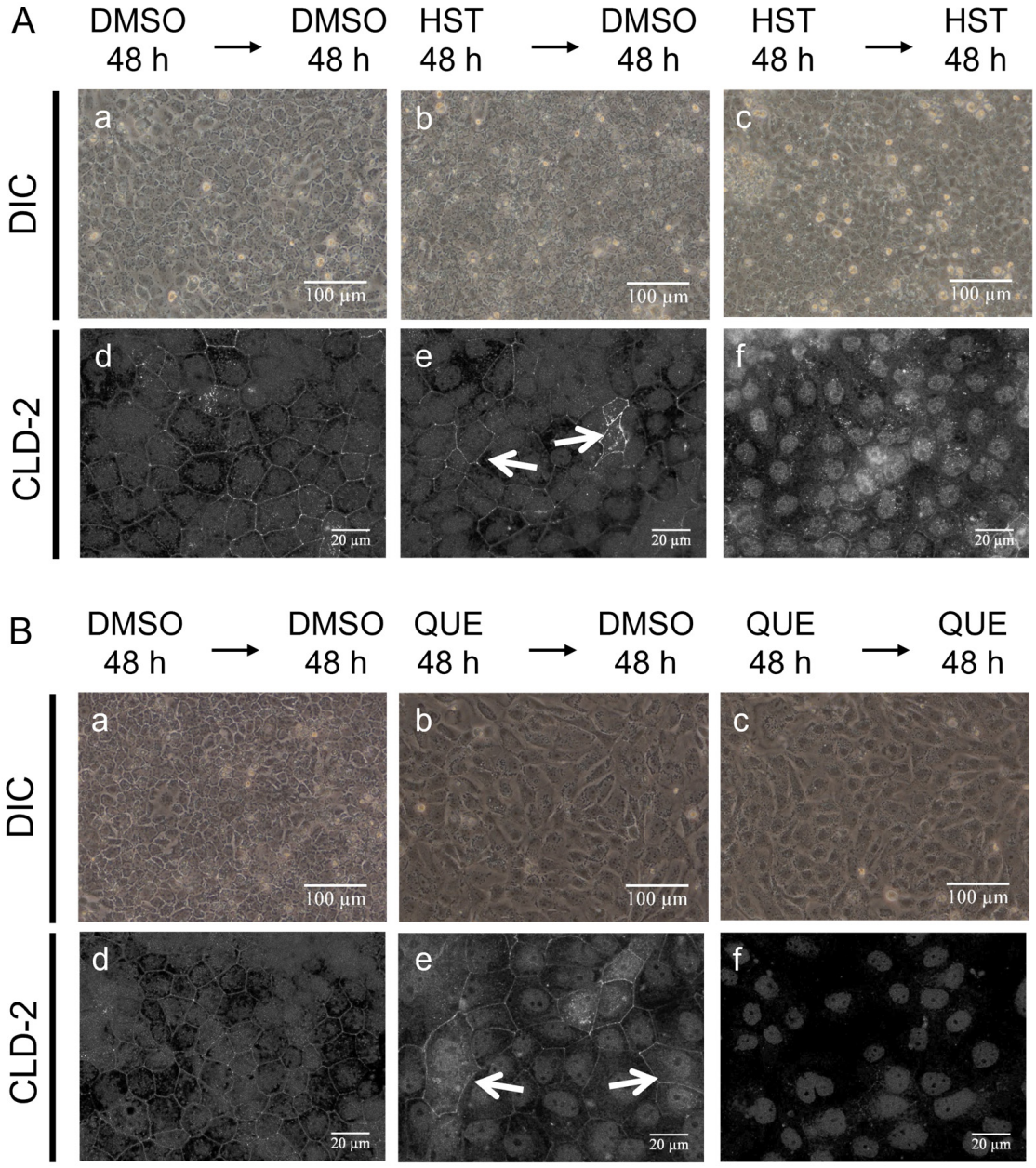

Figure 3. Partially irreversible changes of morphology and TJ integrity of MDCK II cells induced by (**A**) HST or (**B**) QUE. DIC images (**a**–**c**) and immunofluorescence-stained images of CLD-2 (**d**–**f**) of MDCK II cells are shown. The cells were exposed to HST or QUE at a concentration of 100 μM for 48 h and then treated with HST, QUE, or DMSO at a concentration of 100 μM for 48 h after washing with the medium. (**a**,**d**) Control (DMSO–DMSO), (**b**,**e**) flavonoid–DMSO, and (**c**,**f**) flavonoid–flavonoid. Scale bar = 100 μm (**a**–**c**), 20 μm (**d**–**f**). For immunofluorescence staining, brightness was modified to 160%. Arrows indicate CLD-2 localized at regenerated tight junctions.

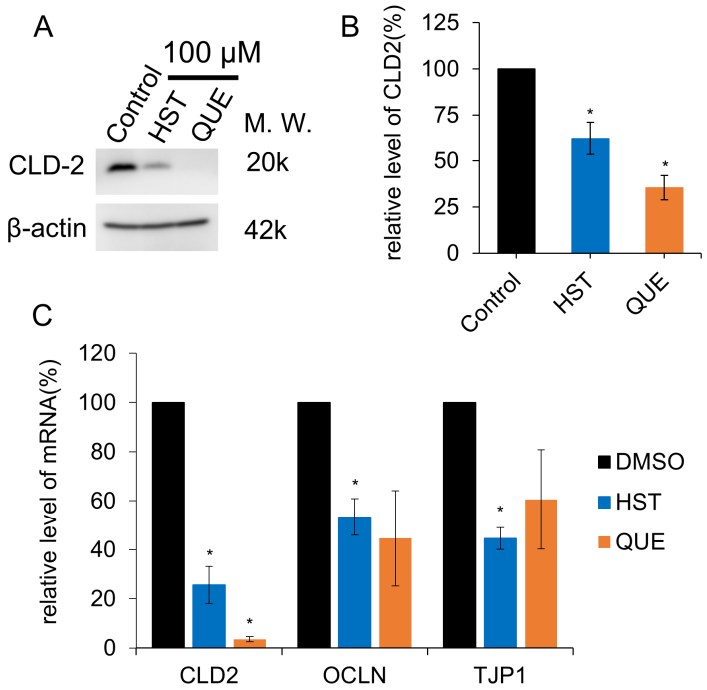

Figure 4. Semi-quantitative analyses of protein or mRNA levels of CLD-2, OCLN, and ZO-1 (TJP1) after 100 μM flavonoid exposure for 48 h in MDCK II cells. (**A**) Western blotting analysis of CLD-2 expression in cell lysates from the control (DMSO) and 100 μM flavonoid-treated MDCK II cells. (**B**) Quantitative analysis with densitometry of 100 μM flavonoid-treated MDCK II cells. HST, QUE: n = 8. (**C**) RT-qPCR analysis of CLD-2, OCLN, and TJP1 expressions in cell lysates from the control (DMSO) and 100 μM flavonoid-treated MDCK II cells. Error bars indicate standard deviations. Statistical analyses were performed using the Turkey–Kramer multiple comparison tests. Difference from the value of the control cells, * $p < 0.05$. HST, QUE: n = 3.

3.4. NMR Evidence of Direct Binding of HST but Not QUE to ZO-1(PDZ1)

We previously succeeded in determining the solution structure of mouse ZO-1(PDZ1) using solution NMR experiments found that the C-terminal peptide of CLD-3 and phosphatidylinositol phosphate competitively bound to the canonical peptide binding site of ZO-1(PDZ1) [16]. In a recent study, ZO-1(PDZ1) was directly inhibited by glycyrrhizin, which prolongs TJ-opening induced by deoxycholate in the Caco-2 cell monolayer [33]. These results suggest that the direct binding of a small molecule ligand to the CLD binding site of ZO-1(PDZ1) may inhibit the physiologically important interaction between ZO-1(PDZ1) and CLDs, which may result in the malformation of TJ or at least disturb TJ integrity in epithelial cells. According to this hypothesis, the flavonoids BLI and BLE directly bound to the CLD binding site of ZO-1(PDZ1) and reduced TJ integrity [18]. Thus, we again examined whether HST and QUE directly bound to ZO-1(PDZ1) using the solution NMR technique. In the HSQC spectra of ^{15}N-labeled ZO-1(PDZ1), small but certain chemical shift perturbations (CSP) were observed with the addition of two equivalents of HST (Supplementary Figure S5A). The major residues with a marked CSP of the amide signals were found to surround the canonical peptide-binding pocket of ZO-1(PDZ1) (Supplementary Figure S5A panels b,c). The binding mode of HST to ZO-1(PDZ1) was predicted by the NMR-based HADDOCK approach, and the putative complex structure seemed reasonable (Supplementary Figure S5A panel d,e). HADDOCK is one of the docking simulation software for both protein–protein and protein–small ligdocking, which is specialized to utilize the data from NMR titration experiments with the user-friendly interface [28]. As a result, HADDOCK succeeded in predicting the binding site of HST as same as the canonical CLD binding site on ZO-1(PDZ1) [16]. Thus, we hypothesized that the direct inhibition of HST to ZO-1(PDZ1) is one of the mechanisms that promotes TJ-opening.

By contrast, although the chemical structure of QUE is similar to HST, no remarkable CSP of ZO-1(PDZ1) upon QUE titration was observed (Supplementary Figure S5B panel b,c) in 2 molecular equivalents. Thus, we performed HADDOCK simulation without NMR-based restraints. As a result, the binding sites of QUE were not converged into the canonical ligand binding pocket (Supplementary Figure S5B panel d). Nevertheless, interestingly, one of the best five models fitted the equivalent binding site of HST (panel e). The difference between the two flavonoids is the relative orientation between A and B rings of flavanone (HST) and flavonol (QUE), respectively, may explain the difference of ZO-1 binding. In detail, the A and B rings of QUE are kept planar, whereas the A and B rings of HST are skewed (Supplementary Figure S5B panel f). In addition, it should be noted that QUE suppressed the expression of the CLD-2 gene (Figure 4C). It is likely that QUE loosened TJ integrity through a mechanism other than the direct inhibition of ZO-1.

3.5. Pharmacological Investigation of the Mechanism of TJ-Opening Using HST or QUE

As mentioned above, not only the direct inhibition of the ZO-1(PDZ1)–CLD interaction, but also the other signaling pathways, are considered TJ-opening mechanisms using HST and QUE. In this context, we previously demonstrated that both BLI and BLE contributed to TJ-opening, partly through the ALK5-dependent pathway [18]. In addition, the inhibition of the MEK pathway signal partially reverted BLE-induced cell morphological changes [18]. Based on these considerations, we employed SB431542 or U0126 as ALK5 and MEK inhibitors, respectively, to determine whether they could revert the TJ-opening and the slender cell shape induced by either HST or QUE.

We first measured the number of viable cells using the WST-8 assay. The viable cells were 130% after treatment with HST and 60% after treatment with QUE compared to the control (Figure 5). When SB431542 was co-administered with HST, the enhanced cell proliferation reverted to the normal level. Therefore, HST is seemingly potent for the proliferation enhancement of MDCK II cells through the activation of the TGFβ pathway. To the contrary, either SB431542 or U0126 failed to revert the weak cytotoxicity using QUE, suggesting that the TGFβ and MEK pathways were not involved in QUE toxicity.

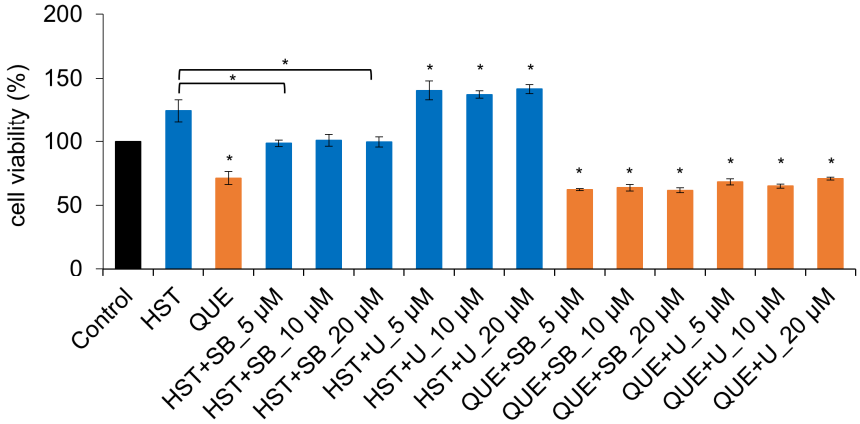

Figure 5. Comparison of cell viability in MDCK II cells exposed to flavonoids and inhibitors. Cells were treated with flavonoids at a concentration of 100 μM and/or SB431542 (labelled as SB)/U0126 5 (labelled as U), 10, and 20 μM for 48 h. Error bars indicate standard deviations. Statistical analyses were performed using Turkey-Kramer multiple comparison tests. These were different from the value of the control (DMSO) or HST-treated cells, * $p < 0.05$. HST, QUE: $n = 4$.

We also examined the effects of SB431542 and U0126 on morphological changes in MDCK II cells under bright-field microscopy. The bright-field observation of viable cells showed that the co-exposure of HST with SB431542 resulted in the disappearance of white spots (Figure 6A panel e). This suggests that TGFβ/ALK5 could be involved in the appearance of white spots induced by HST. For the cell shape changes induced by QUE,

either SB431542 or U0126 did not ameliorate the slenderized morphology of MDCK II cells (Figure 6A panel f,i). Thus, we ruled out that the QUE-induced slender cell shape was downstream of either the TGFβ or MEK pathway. Finally, we examined the recovery of the membrane localization and protein expression of CLD-2 using these inhibitors. SB431542 partially recovered the decreased localization of CLD-2 induced by HST (Figure 6B panel e). In addition, SB431542 could also weakly reverse the decreased CLD-2 by QUE at the TJ-area (Figure 6B panel f). However, in the Western blotting analysis, we did not observe a remarkable recovery of the CLD-2 amount through the co-administration of either SB431542 or U0126 (Figure 7A,B).

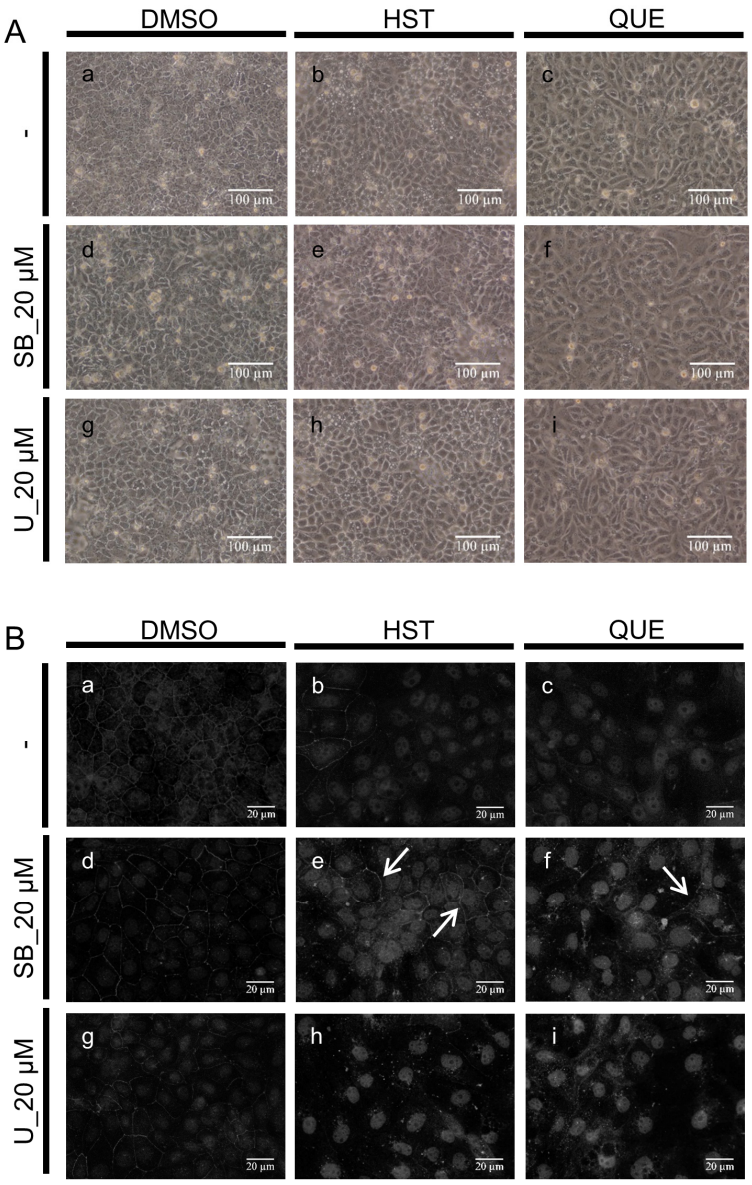

Figure 6. Effects of flavonoids on the morphology and TJ integrity of MDCK II cells. (**A**) DIC images with corresponding flavonoids are presented. Cells were exposed to flavonoids at a concentration of 100 μM and/or SB431542 or U0126 20 μM for 48 h. (**a**,**d**,**g**) control (DMSO); (**b**,**e**,**h**) HST; (**c**,**f**,**i**) QUE. Scale bar = 100 μM. (**B**) Immunofluorescence staining of CLD2 images are shown. Cells were treated with flavonoids at a concentration of 100 μM and/or SB431542/U0126 20 μM for 48 h. (**a**,**d**,**g**) control (DMSO); (**b**,**e**,**h**) HST; (**c**,**f**,**i**) QUE. Scale bar = 20 μM. Brightness is modified to 160%. Arrows indicate CLD-2 localized at partially restored tight junctions.

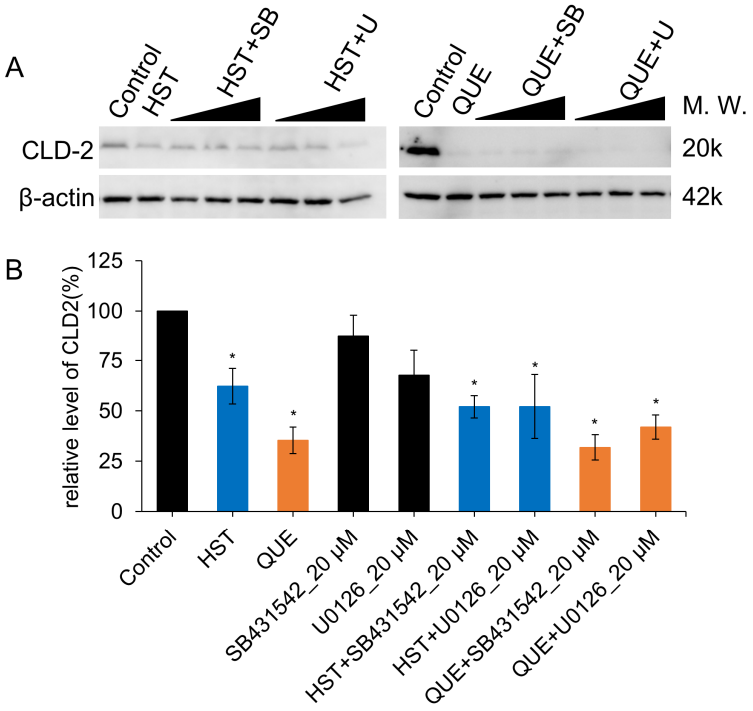

Figure 7. Changes in the relative amount of protein of CLD-2 after compounds treatment for 48 h in MDCK II cells. (**A**) Western blotting analysis of CLD-2 expressed in control (DMSO) and 100 μM flavonoid- and/or 5, 10, 20 μM SB431542/U0126 -treated MDCK II cells. (**B**) Quantitative analysis with densitometry of 100 μM flavonoid- and/or 5, 10, 20 μM SB431542/U0126- treated MDCK II cells. Turkey-Kramer multiple comparison tests were applied as statistical analyses. Error bars show standard deviations. Different from the value of the control cells, * $p < 0.05$. HST, QUE: $n = 8$.

4. Discussion

HST is one of the major components of citrus flavonoids. It is found in the peels, fruits, and albedos of many citrus species. For example, fruits or fruit peels of *Citrus aurantium* L. (Rutaceae) contain HST, hesperidin (HSD), narirutin (NRT), neohesperidin (NHD), and kaempferol [34]. Conversely, several citrus fruits contain naringin (NAR) and naringenin (NRG), rather than HST-related flavonoids. In this study, we demonstrated a weak, but certain, TJ-opening activity of HST against MDCK II cells. However, we previously showed that NAR and NRG, but not NRT, had remarkable TJ-enhancing activity on MDCK II cells [21]. In the case of the NAR-related flavonoids, namely, NAR, NRG, and NRT, we previously showed that aglycone (NAR) exhibited stronger pharmacological effects than its glycosides. NRG, the neohesperidoside of NAR, showed mild TJ-enhancing activity, whereas NRT, the rutinoside of NAR, had no effect on TJ biogenesis. However, in the case of the glycosides of HST, including NHD and HSD, the neohesperidoside and the rutinoside of HST, respectively, showed TJ-enhancing activity, which is the opposing pharmacological action of TJ-opening induced by their aglycone HST [21]. It should be noted that some extracts from citrus peels or albedos are used as skin-conditioning ingredients for many cosmetics. However, the active ingredients of these citrus extracts must contain both TJ-enhancing and TJ-opening flavonoids. Therefore, when using citrus extracts as an additive for cosmetics for skin protection purposes, the extraction method of citrus may become particularly important. In this context, further studies on the quantitative comparison of the pharmacological effects of the TJ-opening activity of HST in simultaneous administration of other TJ-enhancing flavonoids, such as NAR and NRG, are needed.

Accordingly, some studies have reported the pharmacological activities of HST independent to its antioxidant activity, such as hypolipidemic (cholesterol-lowering) activity, anti-cancer activity, anti-metastatic activity, and anti-aromatase activity [34–37]. According to this hypolipidemic activity, HST has been reported to increase the expression of

low-density lipid receptor gene probably via sterol regulatory element (SRE)-binding proteins [35]. HST has also been reported to reduce the expression of genes encoding acyl-coenzyme A: cholesterol acyltransferase (ACAT1 and ACAT2) toward lowering cholesterol levels [38]. Another beneficial effect of HST includes activation of Nrf2 signaling pathway in several cells [36–38]. HST may have antioxidant, anti-inflammatory, anti-allergic, and vaso-protective actions [20]. HST also inhibits snake venom protease [39], as well as some virus genome-derived proteases, including zika, chikungunya, and dengue viruses [40–42]. HSP was previously suggested as a template molecule to develop new anti-arrhythmic drugs, as it blocks slowly-inactivating currents carried by the type 3 long QT syndromes (LQT3)-associated voltage-gated Na^+ channel (hNaV1.5) channel mutant R1623Q, an arrhythmogenic gain-of-function mutant of hNaV1.5 [43]. Finally, HST is expected to become a potential neuroprotective prophylactic (reviewed in [44]). None of these pieces of pharmacological evidence foreshadowed HST's TJ-opening activity shown in this study.

Therefore, we systematically examined how a high-dose treatment of both HST and QUE against epithelial cells had a suppressive effect on the subcellular localization of CLD-2 in the TJ compartment of the lateral membrane. Note that the TJ-opening activity of flavonoids is thought to be independent from their antioxidative property. In general, oxidative stress has a detrimental effect against TJ-integrity [45,46]. Accordingly, close examination revealed that the pharmacological activity of HST to suppress the protein level of CLD-2 was weaker than that of QUE. Similarly, HST was milder than QUE in suppressing the mRNA levels of TJ-related genes, including *CLD-2*, *OCLN*, and *TJP1* (ZO-1). One of the differences in the biological mechanisms between HST and QUE is the presence or absence of a direct interaction between the flavonoids and ZO-1(PDZ1), which is the responsible interface of ZO-1 to the C-terminal PDZ-binding motifs of CLDs [7]. Although the physiologically relevant target of QUE in MDCK II cells is still unclear, we demonstrated that QUE revealed a strong suppression of the expression of the three TJ-related genes. We also showed that both HST and QUE partly activated the TGFβ signaling pathway in a different manner. We concluded that the pharmacological actions of HST and QUE in the proliferation and TJ opening of MDCK II cells were only partly dependent on the TGFβ/ALK5 pathway, regardless of whether the other unknown signaling pathway exists, especially for regulating the expression of TJ-related genes. Figure 8 summarizes the pathways affected by the HST and QUE examined in this study. Table 1 presents the pharmacological effects of the four flavonoids: HST, QUE, BLI, and BLE. As BLI and BLE are also known to have TJ-opening activities by stimulating the TGFβ pathway [18], the pharmacological action of HST resembles that of BLI, rather than QUE, because HST did not induce the morphological changes. However, according to the subcellular localization of TJ-components, HST and QUE are distinct from BLI and BLE because the former decreased OCLN and ZO-1 level. We further assessed these pharmacological activities against some antioxidant capacity parameters, such as Trolox equivalent antioxidant capacity (TEAC), ferric reducing antioxidant power (FRAP), 2,2-diphenyl-1-picrylhydrazyl (DPPH) assay, and Folin-Ciocalteu reducing capacity (FCR) from the literature (Table 1) [47,48]. All these parameters suggested that Que (and BLE) are stronger antioxidants than HST. Contrary to our expectations, we found a weak positive correlation between typical antioxidant capacities and TJ-opening activity. In general, oxidative stress is thought to be harmful against TJ integrity [49]. Finally, it should be noted that HST, BLI, and BLE showed weak, but certain, direct interaction to the canonical ligand binding pocket of ZO-1(PDZ1). Currently, however, critical functional groups of flavonoids for PDZ-binding remain unclear. Not only the number and the position of hydroxyl groups, but also the molecular shape, may be important for ZO-1(PDZ1) interaction, as suggested by our HADDOCK study (Supplementary Figure S5). Recently, BLI has been reported as an efficient absorption enhancer of oral administration of insulin to rats when combined with $AlCl_3$ nanoparticles [50]. Conversely, QUE and BLE exhibited the activity of morphological changes in the epithelial cell shapes, which become concerning in relation to the adverse effects of

these flavonoids. Therefore, HST is considered as another flavonoid candidate for naturally occurring epithelial drug absorption enhancers, such like BLI.

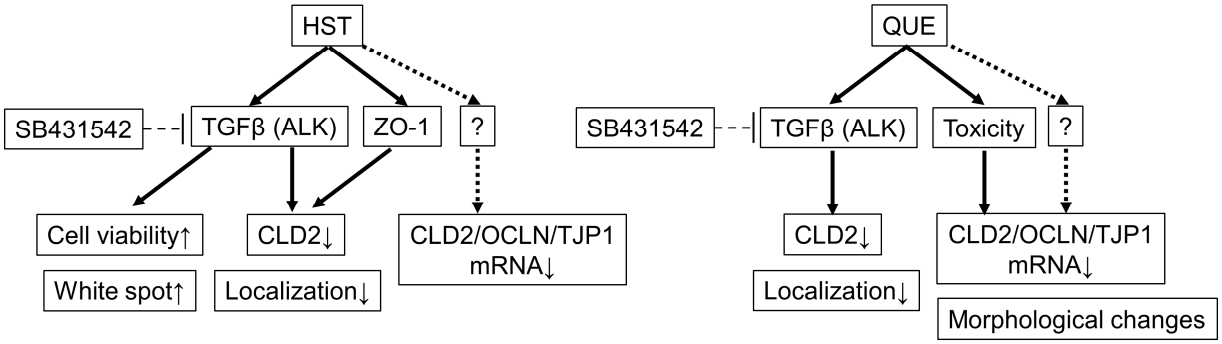

Figure 8. Putative molecular mechanisms underlying TJ modulation induced by HST (**left panel**) and QUE (**right panel**). Solid arrows indicate either stimulation or enhancement, dashed arrows indicate the possibility of stimulation, and dashed long left tacks indicate inhibition. "?" represents an unknown factor. ↑: increase; ↓: decrease.

Table 1. Comparison of pharmacological effects of flavonoids against TJ of MDCK II cells.

	HST	**QUE**	**BLI** [a]	**BLE** [a]
CLD-2				
TJ localization	− −	− − −	− − −	− − −
mRNA expression	−	− − −	−	−
OCLN				
TJ localization	−	−	+/−	+/−
mRNA expression	−	− − −	n.ex.	n.ex.
ZO-1 expression				
TJ localization	−	−	+/−	+/−
mRNA expression	−	− − −	n.ex.	n.ex.
MDCK II cell				
Proliferation	+ +	− −	+/−	−
Slenderer cell shape	no	yes	no	yes
Direct ZO1(PDZ1) interaction	yes	no	yes	yes
Other signaling pathways				
TGFβ	partially	partially	yes	yes
MEK/ERK	partially	no	partially	yes
Antioxidant capacity from literature				
TEAC (trolox equiv./mmol) [b]	2.01 ± 0.04	5.72 ± 0.16		
FCR (chlorogenic acid equiv./mmol [b]	0.53 ± 0.03	1.24 ± 0.09		
DPPH (trolox equiv./mmol) [b]	0.48 ± 0.04	2.25 ± 0.09		
FRAP (ferrous equiv./μmol) [c]	21.1 ± 0.4	95.9 ± 5.4		38.9 ± 2.5

[a] Hisada et al., 2020 [18]; [b] Zhang et al., 2011 [47]; [c] Firuzi et al., 2005 [48]; n.ex. Not examined. Symbols +, −, and +/− indicates increase, decrease, and un-changed, respectively. The number of the symbols reflects degree of change.

5. Conclusions

This study demonstrated that HST and QUE downregulated the subcellular localization of CLD-2 in the TJ compartment of the lateral membrane. HST promoted the proliferation of MDCK II cells, partly through the TGFβ pathway, whereas QUE suppressed the cells. QUE, but not HST, induced morphological changes in MDCK II into a slenderer cell shape. QUE, but not HST, attenuated the gene expression of TJ-related genes, including CLD-2, occludin, and ZO-1. Only HST, but not QUE, was directly bound to ZO-1(PDZ1), which was the responsible interface between ZO-1 and CLDs' C-terminal. These

results suggest that HST is an attractive candidate for developing a naturally occurring drug absorption enhancer for the paracellular route.

Supplementary Materials: The following supporting information can be downloaded at: https://www.mdpi.com/article/10.3390/antiox12040952/s1, Figure S1: Effects of quercetin (QUE) on cell morphology in MDCK II cells; Figure S2: Close-up view of HST-treated cells. Effects of HST on the morphology of MDCK II cells (enlarged one); Figure S3: Effects of flavonoids on TJ integrity of MDCK II cells (original figures); Figure S4: Effects of flavonoids on the shape and TJ integrity of MDCK II cells (original figures); Figure S5: Direct interaction between ZO-1(PDZ1) and the flavonoids; Figure S6: Effects of flavonoids on the morphology and TJ integrity of MDCK II cells (original figures); Figure S7: 600MHz ^{1}H NMR spectra of the commercially purchased reagents used in study.

Author Contributions: Conceptualization, Y.I., M.A. and H.H.; investigation, M.N., N.G., T.T. and A.K.; data curation, M.N., A.K., Y.I., T.T. and H.H.; resources, N.G., A.K. and T.T.; visualization, M.N. and N.G.; writing the original draft, H.H.; writing the review and editing, M.A. and H.H.; supervision, H.H.; project administration, M.A. and H.H.; funding acquisition, M.A. and H.H. All authors have read and agreed to the published version of the manuscript.

Funding: This research received no external funding.

Institutional Review Board Statement: Not applicable.

Informed Consent Statement: Not applicable.

Data Availability Statement: The data are contained within this article and Supplementary Materials.

Acknowledgments: The authors would like to thank Mikio Furuse for providing MDCK II cells.

Conflicts of Interest: Among the authors, T.T. and H.H. are the founders of a Nagoya University-based spinoff startup company, called BeCellBar. LLC. A.K., Y.I., and M.A. were employed by Nicca Chemical Co., Ltd. The remaining authors declare no conflicts of interest.

References

1. Förster, C. Tight Junctions and the Modulation of Barrier Function in Disease. *Histochem. Cell Biol.* **2008**, *130*, 55–70. [CrossRef] [PubMed]
2. Furuse, M.; Hata, M.; Furuse, K.; Yoshida, Y.; Haratake, A.; Sugitani, Y.; Noda, T.; Kubo, A.; Tsukita, S. Claudin-Based Tight Junctions Are Crucial for the Mammalian Epidermal Barrier. *J. Cell Biol.* **2002**, *156*, 1099–1111. [CrossRef] [PubMed]
3. Tsukita, S.; Furuse, M.; Itoh, M. Multifunctional Strands in Tight Junctions. *Nat. Rev. Mol. Cell Biol.* **2001**, *2*, 285–293. [CrossRef] [PubMed]
4. Fanning, A.S.; Mitic, L.L.; Anderson, J.M. Transmembrane Proteins in the Tight Junction Barrier. *J. Am. Soc. Nephrol.* **1999**, *10*, 1337–1345. [CrossRef]
5. Furuse, M.; Fujita, K.; Hiiragi, T.; Fujimoto, K.; Tsukita, S. Claudin-1 and -2: Novel Integral Membrane Proteins Localizing at Tight Junctions with No Sequence Similarity to Occludin. *J. Cell Biol.* **1998**, *141*, 1539–1550. [CrossRef]
6. Paris, L.; Tonutti, L.; Vannini, C.; Bazzoni, G. Structural Organization of the Tight Junctions. *Biochim. Biophys. Acta* **2008**, *1778*, 646–659. [CrossRef]
7. Itoh, M.; Furuse, M.; Morita, K.; Kubota, K.; Saitou, M.; Tsukita, S. Direct Binding of Three Tight Junction-Associated MAGUKs, ZO-1, ZO-2, and ZO-3, with the COOH Termini of Claudins. *J. Cell Biol.* **1999**, *147*, 1351–1363. [CrossRef]
8. Tokuda, S.; Higashi, T.; Furuse, M. ZO-1 Knockout by TALEN-Mediated Gene Targeting in MDCK Cells: Involvement of ZO-1 in the Regulation of Cytoskeleton and Cell Shape. *PLoS ONE* **2014**, *9*, e104994. [CrossRef]
9. González-Mariscal, L.; Betanzos, A.; Nava, P.; Jaramillo, B.E. Tight Junction Proteins. *Prog. Biophys. Mol. Biol.* **2003**, *81*, 1–44. [CrossRef]
10. González-Mariscal, L.; Betanzos, A.; Avila-Flores, A. MAGUK Proteins: Structure and Role in the Tight Junction. *Semin. Cell Dev. Biol.* **2000**, *11*, 315–324. [CrossRef]
11. Nomme, J.; Antanasijevic, A.; Caffrey, M.; van Itallie, C.M.; Anderson, J.M.; Fanning, A.S.; Lavie, A. Structural Basis of a Key Factor Regulating the Affinity between the Zonula Occludens First PDZ Domain and Claudins. *J. Biol. Chem.* **2015**, *290*, 16595–16606. [CrossRef] [PubMed]
12. Fanning, A.S.; van Itallie, C.M.; Anderson, J.M. Zonula Occludens-1 and -2 Regulate Apical Cell Structure and the Zonula Adherens Cytoskeleton in Polarized Epithelia. *Mol. Biol. Cell* **2012**, *23*, 577–590. [CrossRef] [PubMed]
13. Ikenouchi, J.; Umeda, K.; Tsukita, S.; Furuse, M.; Tsukita, S. Requirement of ZO-1 for the Formation of Belt-like Adherens Junctions during Epithelial Cell Polarization. *J. Cell Biol.* **2007**, *176*, 779–786. [CrossRef] [PubMed]

14. Furuse, M. Knockout Animals and Natural Mutations as Experimental and Diagnostic Tool for Studying Tight Junction Functions in Vivo. *Biochim. Biophys. Acta* **2009**, *1788*, 813–819. [CrossRef]
15. Fu, Q.; Wang, H.; Xia, M.; Deng, B.; Shen, H.; Ji, G.; Li, G.; Xie, Y. The Effect of Phytic Acid on Tight Junctions in the Human Intestinal Caco-2 Cell Line and Its Mechanism. *Eur. J. Pharm. Sci.* **2015**, *80*, 1–8. [CrossRef]
16. Hiroaki, H.; Satomura, K.; Goda, N.; Nakakura, Y.; Hiranuma, M.; Tenno, T.; Hamada, D.; Ikegami, T. Spatial Overlap of Claudin- and Phosphatidylinositol Phosphate-Binding Sites on the First PDZ Domain of Zonula Occludens 1 Studied by NMR. *Molecules* **2018**, *23*, 2465. [CrossRef]
17. Tenno, T.; Kataoka, K.; Goda, N.; Hiroaki, H. NMR-Guided Repositioning of Non-Steroidal Anti-Inflammatory Drugs into Tight Junction Modulators. *Int. J. Mol. Sci.* **2021**, *22*, 2583. [CrossRef]
18. Hisada, M.; Hiranuma, M.; Nakashima, M.; Goda, N.; Tenno, T.; Hiroaki, H. High Dose of Baicalin or Baicalein Can Reduce Tight Junction Integrity by Partly Targeting the First PDZ Domain of Zonula Occludens-1 (ZO-1). *Eur. J. Pharmacol.* **2020**, *887*, 173436. [CrossRef]
19. Tenno, T.; Goda, N.; Umetsu, Y.; Ota, M.; Kinoshita, K.; Hiroaki, H. Accidental Interaction between PDZ Domains and Diclofenac Revealed by NMR-Assisted Virtual Screening. *Molecules* **2013**, *18*, 9567–9581. [CrossRef]
20. Parhiz, H.; Roohbakhsh, A.; Soltani, F.; Rezaee, R.; Iranshahi, M. Antioxidant and Anti-Inflammatory Properties of the Citrus Flavonoids Hesperidin and Hesperetin: An Updated Review of Their Molecular Mechanisms and Experimental Models. *Phytother. Res.* **2015**, *29*, 323–331. [CrossRef]
21. Nakashima, M.; Hisada, M.; Goda, N.; Tenno, T.; Kotake, A.; Inotsume, Y.; Kameoka, I.; Hiroaki, H. Opposing Effect of Naringenin and Quercetin on the Junctional Compartment of MDCK II Cells to Modulate the Tight Junction. *Nutrients* **2020**, *12*, 3285. [CrossRef] [PubMed]
22. Gamero-Estevez, E.; Andonian, S.; Jean-Claude, B.; Gupta, I.; Ryan, A.K. Temporal Effects of Quercetin on Tight Junction Barrier Properties and Claudin Expression and Localization in MDCK II Cells. *Int. J. Mol. Sci.* **2019**, *20*, 4889. [CrossRef] [PubMed]
23. Ferry, D.R.; Smith, A.; Malkhandi, J.; Fyfe, D.W.; deTakats, P.G.; Anderson, D.; Baker, J.; Kerr, D.J. Phase I Clinical Trial of the Flavonoid Quercetin: Pharmacokinetics and Evidence for in Vivo Tyrosine Kinase Inhibition. *Clin. Cancer Res.* **1996**, *2*, 659–668. [PubMed]
24. Umetsu, Y.; Goda, N.; Taniguchi, R.; Satomura, K.; Ikegami, T.; Furuse, M.; Hiroaki, H. ^{1}H, ^{13}C, and ^{15}N Resonance Assignment of the First PDZ Domain of Mouse ZO-1. *Biomol. NMR Assign.* **2011**, *5*, 207–210. [CrossRef] [PubMed]
25. Grzesiek, S.; Bax, A.; Clore, G.M.; Gronenborn, A.M.; Hu, J.S.; Kaufman, J.; Palmer, I.; Stahl, S.J.; Wingfield, P.T. The Solution Structure of HIV-1 Nef Reveals an Unexpected Fold and Permits Delineation of the Binding Surface for the SH3 Domain of Hck Tyrosine Protein Kinase. *Nat. Struct. Biol.* **1996**, *3*, 340–345. [CrossRef]
26. Schumann, F.H.; Riepl, H.; Maurer, T.; Gronwald, W.; Neidig, K.-P.; Kalbitzer, H.R. Combined Chemical Shift Changes and Amino Acid Specific Chemical Shift Mapping of Protein-Protein Interactions. *J. Biomol. NMR* **2007**, *39*, 275–289. [CrossRef]
27. Dominguez, C.; Boelens, R.; Bonvin, A.M.J.J. HADDOCK: A Protein−Protein Docking Approach Based on Biochemical or Biophysical Information. *J. Am. Chem. Soc.* **2003**, *125*, 1731–1737. [CrossRef] [PubMed]
28. Van Zundert, G.C.P.; Rodrigues, J.P.G.L.M.; Trellet, M.; Schmitz, C.; Kastritis, P.L.; Karaca, E.; Melquiond, A.S.J.; Van Dijk, M.; De Vries, S.J.; Bonvin, A.M.J.J. The HADDOCK2.2 Web Server: User-Friendly Integrative Modeling of Biomolecular Complexes. *J. Mol. Biol.* **2016**, *428*, 720–725. [CrossRef]
29. Morimoto, R.; Hanada, A.; Matsubara, C.; Horio, Y.; Sumitani, H.; Ogata, T.; Isegawa, Y. Anti-Influenza A Virus Activity of Flavonoids in Vitro: A Structure–Activity Relationship. *J. Nat. Med.* **2023**, *77*, 219–227. [CrossRef]
30. Bhat, F.A.; Sharmila, G.; Balakrishnan, S.; Arunkumar, R.; Elumalai, P.; Suganya, S.; Raja Singh, P.; Srinivasan, N.; Arunakaran, J. Quercetin Reverses EGF-Induced Epithelial to Mesenchymal Transition and Invasiveness in Prostate Cancer (PC-3) Cell Line via EGFR/PI3K/Akt Pathway. *J. Nutr. Biochem.* **2014**, *25*, 1132–1139. [CrossRef]
31. Lin, Y.-S.; Tsai, P.-H.; Kandaswami, C.C.; Cheng, C.-H.; Ke, F.-C.; Lee, P.-P.; Hwang, J.-J.; Lee, M.-T. Effects of Dietary Flavonoids, Luteolin, and Quercetin on the Reversal of Epithelial-Mesenchymal Transition in A431 Epidermal Cancer Cells. *Cancer Sci.* **2011**, *102*, 1829–1839. [CrossRef]
32. Furuse, M.; Furuse, K.; Sasaki, H.; Tsukita, S. Conversion of Zonulae Occludentes from Tight to Leaky Strand Type by Introducing Claudin-2 into Madin-Darby Canine Kidney I Cells. *J. Cell Biol.* **2001**, *153*, 263–272. [CrossRef] [PubMed]
33. Hibino, E.; Goda, N.; Hisada, M.; Tenno, T.; Hiroaki, H. Direct Inhibition of the First PDZ Domain of ZO-1 by Glycyrrhizin Is a Possible Mechanism of Tight Junction Opening of Caco-2 Cells. *Food Funct.* **2022**, *13*, 1953–1964. [CrossRef] [PubMed]
34. Kawaii, S.; Tomono, Y.; Katase, E.; Ogawa, K.; Yano, M. Quantitation of Flavonoid Constituents in Citrus Fruits. *J. Agric. Food Chem.* **1999**, *47*, 3565–3571. [CrossRef] [PubMed]
35. Morin, B.; Nichols, L.A.; Zalasky, K.M.; Davis, J.W.; Manthey, J.A.; Holland, L.J. The Citrus Flavonoids Hesperetin and Nobiletin Differentially Regulate Low Density Lipoprotein Receptor Gene Transcription in HepG2 Liver Cells. *J. Nutr.* **2008**, *138*, 1274–1281. [CrossRef]
36. Zhu, C.; Dong, Y.; Liu, H.; Ren, H.; Cui, Z. Hesperetin Protects against H_2O_2-Triggered Oxidative Damage via Upregulation of the Keap1-Nrf2/HO-1 Signal Pathway in ARPE-19 Cells. *Biomed. Pharmacother.* **2017**, *88*, 124–133. [CrossRef]
37. Chen, Y.-J.; Kong, L.; Tang, Z.-Z.; Zhang, Y.-M.; Liu, Y.; Wang, T.-Y.; Liu, Y.-W. Hesperetin Ameliorates Diabetic Nephropathy in Rats by Activating Nrf2/ARE/Glyoxalase 1 Pathway. *Biomed. Pharmacother.* **2019**, *111*, 1166–1175. [CrossRef]

38. Li, J.; Wang, T.; Liu, P.; Yang, F.; Wang, X.; Zheng, W.; Sun, W. Hesperetin Ameliorates Hepatic Oxidative Stress and Inflammation via the PI3K/AKT-Nrf2-ARE Pathway in Oleic Acid-Induced HepG2 Cells and a Rat Model of High-Fat Diet-Induced NAFLD. *Food Funct.* **2021**, *12*, 3898–3918. [CrossRef]
39. Vander Dos Santos, R.; Villalta-Romero, F.; Stanisic, D.; Borro, L.; Neshich, G.; Tasic, L. Citrus Bioflavonoid, Hesperetin, as Inhibitor of Two Thrombin-like Snake Venom Serine Proteases Isolated from Crotalus Simus. *Toxicon* **2018**, *143*, 36–43. [CrossRef]
40. Eberle, R.J.; Olivier, D.S.; Amaral, M.S.; Willbold, D.; Arni, R.K.; Coronado, M.A. Promising Natural Compounds against Flavivirus Proteases: Citrus Flavonoids Hesperetin and Hesperidin. *Plants* **2021**, *10*, 2183. [CrossRef]
41. Lim, W.Z.; Cheng, P.G.; Abdulrahman, A.Y.; Teoh, T.C. The Identification of Active Compounds in Ganoderma Lucidum Var. Antler Extract Inhibiting Dengue Virus Serine Protease and Its Computational Studies. *J. Biomol. Struct. Dyn.* **2020**, *38*, 4273–4288. [CrossRef] [PubMed]
42. Eberle, R.J.; Olivier, D.S.; Pacca, C.C.; Avilla, C.M.S.; Nogueira, M.L.; Amaral, M.S.; Willbold, D.; Arni, R.K.; Coronado, M.A. In Vitro Study of Hesperetin and Hesperidin as Inhibitors of Zika and Chikungunya Virus Proteases. *PLoS ONE* **2021**, *16*, e0246319. [CrossRef]
43. Alvarez-Collazo, J.; López-Requena, A.; Galán, L.; Talavera, A.; Alvarez, J.L.; Talavera, K. The Citrus Flavanone Hesperetin Preferentially Inhibits Slow-Inactivating Currents of a Long QT Syndrome Type 3 Syndrome Na^+ Channel Mutation. *Br. J. Pharmacol.* **2019**, *176*, 1090–1105. [CrossRef] [PubMed]
44. Evans, J.A.; Mendonca, P.; Soliman, K.F.A. Neuroprotective Effects and Therapeutic Potential of the Citrus Flavonoid Hesperetin in Neurodegenerative Diseases. *Nutrients* **2022**, *14*, 2228. [CrossRef]
45. Nagira, M.; Tomita, M.; Mizuno, S.; Kumata, M.; Ayabe, T.; Hayashi, M. Ischemia/Reperfusion Injury in the Monolayers of Human Intestinal Epithelial Cell Line Caco-2 and Its Recovery by Antioxidants. *Drug Metab. Pharm.* **2006**, *21*, 230–237. [CrossRef] [PubMed]
46. Kim, H.J.; Lee, E.K.; Park, M.H.; Ha, Y.M.; Jung, K.J.; Kim, M.-S.; Kim, M.K.; Yu, B.P.; Chung, H.Y. Ferulate Protects the Epithelial Barrier by Maintaining Tight Junction Protein Expression and Preventing Apoptosis in Tert-Butyl Hydroperoxide-Induced Caco-2 Cells. *Phytother. Res.* **2013**, *27*, 362–367. [CrossRef] [PubMed]
47. Zhang, D.; Chu, L.; Liu, Y.; Wang, A.; Ji, B.; Wu, W.; Zhou, F.; Wei, Y.; Cheng, Q.; Cai, S.; et al. Analysis of the Antioxidant Capacities of Flavonoids under Different Spectrophotometric Assays Using Cyclic Voltammetry and Density Functional Theory. *J. Agric. Food Chem.* **2011**, *59*, 10277–10285. [CrossRef]
48. Firuzi, O.; Lacanna, A.; Petrucci, R.; Marrosu, G.; Saso, L. Evaluation of the Antioxidant Activity of Flavonoids by "Ferric Reducing Antioxidant Power" Assay and Cyclic Voltammetry. *Biochim. Biophys. Acta* **2005**, *1721*, 174–184. [CrossRef]
49. Rao, R. Oxidative Stress-Induced Disruption of Epithelial and Endothelial Tight Junctions. *Front. Biosci.* **2008**, *13*, 7210–7226. [CrossRef]
50. Jia, X.; Yuan, Z.; Yang, Y.; Huang, X.; Han, N.; Liu, X.; Lin, X.; Ma, T.; Xu, B.; Wang, P.; et al. Multi-Functional Self-Assembly Nanoparticles Originating from Small Molecule Natural Product for Oral Insulin Delivery through Modulating Tight Junctions. *J. Nanobiotechnol.* **2022**, *20*, 116. [CrossRef]

antioxidants

MDPI

Article

Spatial Distribution and Antioxidant Activity of Extracts from Citrus Fruits

María García-Nicolás [1], Carlos A. Ledesma-Escobar [2,3,4,5,*] and Feliciano Priego-Capote [2,3,4,5,*]

[1] Department of Analytical Chemistry, Faculty of Chemistry, Regional Campus of International Excellence "Campus Mare Nostrum", University of Murcia, E-30100 Murcia, Spain
[2] Department of Analytical Chemistry, Annex Marie Curie Building, Campus of Rabanales, University of Córdoba, E-14014 Córdoba, Spain
[3] Maimónides Institute of Biomedical Research (IMIBIC), Reina Sofía University Hospital, University of Córdoba, 14004 Córdoba, Spain
[4] Nanochemistry University Institute (IUNAN), Campus of Rabanales, University of Córdoba, E-14014 Córdoba, Spain
[5] CIBER Fragilidad y Envejecimiento Saludable (CIBERFES), Instituto de Salud Carlos III, 28029 Madrid, Spain
* Correspondence: z32leesc@uco.es (C.A.L.-E.); feliciano.priego@uco.es (F.P.-C.)

Abstract: Citrus fruits are recommended components of the human diet because of their enriched composition in bioactive compounds and health benefits. Among their notable components are phenols, with a special emphasis on flavonoids, limonoids, and carboxylic acids. In this research, we have carried out a spatial metabolomics analysis for the characterization of these bioactive families in three citrus fruits, namely, lemons, limes, and mandarins. Sampling was undertaken, for which the juices and three fruit tissues, namely, albedo, flavedo, and segments, were analyzed. This characterization allowed for the determination of 49 bioactive compounds in all the samples. The composition of the different extracts was correlated with the antioxidant capacity measured by the DPPH radical scavenging activity and β-carotene bleaching assays. Flavonoids, found in the albedo and flavedo at higher concentrations, were the main components responsible for DPPH radical scavenging activity. On the other hand, the combined action of flavonoids and limonoids contributed to explaining the antioxidant activity measured by the β-carotene bleaching assay. Generally, the antioxidant capacity of juices was lower than that estimated for extracts from citrus tissues.

Keywords: citrus fruits; metabolomics; spatial distribution; antioxidant activity; flavonoids; limonoids; carboxylic acids

1. Introduction

Citrus fruits constitute a characteristic element of the Mediterranean diet and are extensively researched due to their bioactive composition and health benefits. Among the most known citrus fruits, lemons (Citrus limon), mandarins (Citrus reticulata), and Persian limes (Citrus latifolia) have been demonstrated to be outstanding sources of bioactive compounds such as ascorbic acid, limonoids, and flavonoids [1].

Flavonoids are the most predominant phenolic compounds in citrus fruits and are the main sources of their flavor and coloration [2]. These phytochemicals have been described as beneficial to human health and are used to prevent some diseases [3] because of their anti-inflammatory, anti-cancer, or anti-obesity properties [4–7]. Citrus flavonoids' phenolic activities, such as their free radical scavenging activity, pro-oxidant metal ion chelation, and ability to act as enzyme cofactors, explain their beneficial properties.

Limonoids have also received great attention because of their anti-inflammatory, anti-aging, anti-tumor, immunomodulatory, and antioxidant activity [8]. Limonoids can be found as glucosides (water soluble) or aglycones (water insoluble), which contribute to the unflavored or bitter taste of citrus fruits. In a recent study, a total of 18 limonoid glucosides

and 55 limonoid aglycones were reported in citrus fruits [9]. The most representative limonoid glucoside is limonin-17-β-D-glucopyranoside, while the most abundant aglycones are limonin and nomilin [10,11]. The presence of limonoids has mainly been detected in essential oils obtained from citrus flavedo, and these oils have received special attention in previous years because of their high antimicrobial and preservative activity in various foods [12–14].

Limonoids and flavonoids have been determined by different techniques, with the most extensive being liquid chromatography coupled with diode array detection (LC–DAD) [15]; however, this technique requires the use of analytical standards for identification. For this reason, in the few last years, the use of liquid chromatography coupled with high-resolution tandem mass spectrometry (LC–MS/HRMS) has been increasing. Although this technique also requires standards for confirmation, it provides better identification capacity by comparing MS2 spectra with those included in databases. Most citrus fruits have been characterized by this technique, for example, limes, oranges, tangerines, lemons, grapefruit, etc. [16–22].

The antioxidant properties of citrus limonoids and flavonoids have been previously described using various techniques, including 2,2-diphenyl-1-picrylhydrazyl (DPPH) antioxidant capacity and β-carotene blenching assay studies. The DPPH method relies on the strength of a 30 min radical scavenging time, which allows DPPH to react efficiently, even with weak antioxidants providing high sensitivity, while β-carotene test allows both lipophilic and hydrophilic samples to be analyzed with high reproducibility [23]. The combination of these two assays has been used for the determination of the antioxidant activity of limonoid and flavonoid extracts from different tissues [17,24]. Specifically, grapefruit seeds [25], *Rutaceae* species peel [26], albedo and flavedo from *pompia* fruits [16], kinnow peel [27], and Spanish clementine fresh pulp [28] have been analyzed for the presence of these high valuable compounds using both antioxidant determination assays. Moreover, changes in the limonin and nomilin concentrations in different tissues from pummelo and mandarin varieties have been studied during fruit growth and maturation [29]. However, although citrus antioxidant activity has been widely studied, to the best of our knowledge, the spatial distribution of the antioxidant capacity in the different tissues (flavedo, albedo, pulp segments, and juice) of citrus fruits and the synergistic interaction between limonoids and flavonoids have not been studied in detail. For this reason, the aim of this research was to characterize the limonoid and flavonoid fractions of three Citrus fruits, namely, lemons, limes, and mandarins. For this purpose, three main tissues (albedo, flavedo, and pulp segment) and their respective juices were studied. A highly selective and sensitive LC–MS/HRMS approach was used for the characterization of these citrus tissues. In addition, their antioxidant activity was evaluated through the DPPH radical scavenging activity and β-carotene bleaching assays to ascertain the properties of limonoids and flavonoids and elucidate any synergistic interactions.

2. Materials and Methods

2.1. Samples

Limes, mandarins, and lemons were purchased in two local markets in Cordoba and Murcia (La Corredera and Veronicas local markets, Spain) in October 2022. Fruits were washed and processed to separate the albedo, flavedo, pulp segments, and juice. The solid samples were lyophilized and subsequently ground. The powder was stored in the dark at −20 °C.

2.2. Reagents

Ethanol (EtOH), methanol (MeOH), ethyl acetate (EA), acetone, chloroform, acetonitrile (ACN), and formic acid were purchased from Scharlab (Barcelona, Spain). n-Hexane was obtained from Sigma−Aldrich (St. Louis, MO, USA). All solvents were LC- or MS-grade. Simplicity® UV Millipore equipment (Burlington, MA, USA) was used to generate purified Milli-Q-water. Syringaldehyde (SA), used as external standard, was acquired from

Sigma−Aldrich. For antioxidant assays, we used 1,1-diphenyl-2-picrylhydrazyl (DPPH), linoleic acid, Tween-20, and β-carotene standards obtained from Sigma-Aldrich. Silica gel 60 (0.06–0.2 mm particle size) from Merck (Darmstadt, Germany) was used for the fractionation of extracts.

2.3. Instrumentation and Software

The analytical equipment consisted of a 1200 series LC system from Agilent Technologies (Palo Alto, CA, USA) coupled with a dual electrospray ionization source and a high-resolution Agilent 6540 quadrupole–time of flight detector QTOF (LC–MS/HRMS).

Agilent MassHunter Workstation (version B6.00 Profinder, Agilent Technologies, Santa Clara, CA, USA) was used for data acquisition. MassHunter Qualitative v7.0 software and MetaboAnalyst 5.0 (https://metaboanalyst.ca/, accessed on 9 January 2023) were used for targeted extraction of MS/MS information, metabolomics data analysis, and interpretation.

2.4. Metabolites Extraction

Albedo, flavedo, and pulp segments of mandarins, limes, and lemons were crushed and homogenized after lyophilization. A total of 1 g of each tissue was extracted in 10 mL of n-hexane while stirring at 1000 rpm for 30 min at 30 °C to remove the lipidic fraction. The n-hexane extract was discarded, and the solids were recovered and dried under gentle nitrogen flow prior to the triplicate extraction of bioactive compounds with 10 mL of (50:25:25 $v/v/v$) EA/acetone/EtOH for 30 min at 30 °C. The three fractions were mixed, evaporated under vacuum, and then reconstituted in 1 mL of MeOH containing SA at 1 μg/mL. Six extracts were obtained from each tissue (three extracts for triplicate analysis of the antioxidant activity and three extracts for fractionation).

Lyophilized juice samples of the three fruits were solubilized in water at 150 mg of total solids/mL. A total of 10 mL of reconstituted juice was extracted with 5 mL of EA for 10 min at 30 °C. The EA fraction was dried under vacuum and reconstituted in 1 mL of MeOH with SA at 1 μg/mL.

2.5. LC–MS/HRMS Analysis

Chromatographic separation of the extracts was performed by using a Zorbax Eclipse Plus C18 chromatographic column (1.8 μm particle size, 150 × 3.0 mm i.d., Agilent Technologies). The injection volume was 2 μL, and the mobile phases were composed of 0.1% of formic acid in both deionized water (phase A) and acetonitrile (phase B). Flow rate was constant at 0.25 mL/min. Chromatographic gradient was programmed as follows: 4% phase B was selected as initial composition; then, from min 0 to 1, mobile phase B was increased to 25%; from min 1 to 6, phase B was changed to 40%; from min 6 to 8, phase B was modified to 60%; and from min 8 to 10, mobile phase B was increased from 60 to 100%. The latter composition was maintained for 12 min to guarantee the elution of metabolites and the sterilization of the column. A post-time of 13 min was set to equilibrate the initial conditions for the next analysis.

The dual electrospray ionization source (ESI) was operated in both positive and negative ionization modes. ESI parameters were as follows: nebulizer gas at 50 psi and drying gas flow rate and temperature at 10 L/min and 325 °C, respectively. The capillary voltage was set at 3500 V, while the fragmentor, skimmer, and octapole voltages were 130, 65, and 750 V, respectively. Data were acquired in centroid mode in the extended dynamic range (2 GHz). Full scan was carried out at 6 spectra/s within the m/z range of 60–1200, with subsequent activation of the three most intense precursor ions (allowed charge: single or double) by MS/MS using a collision energy of 20 eV and 40 eV at 3 spectra/s within the m/z range of 30–1200. An active exclusion window was programmed for 0.75 min to avoid repetitive fragmentation of the most intense precursor ions, thus increasing the detection coverage. To assure the desired mass accuracy of recorded ions, continuous internal calibration was performed during analyses with the use of signals at m/z 121.0509 (protonated purine) and m/z 922.0098 (protonated hexakis (1H, 1H, 3H-tetrafluoropropoxy)

phosphazene or HP-921) in the positive ionization mode and m/z of 112.9856 (trifluoroacetic acid anion) and m/z 1033.9881 (HP-921) in the negative ionization mode. A quality control sample (QC) obtained by mixing aliquots of extracts was used to ensure the reproducibility and robustness of the methodology and chemometric results.

2.6. Data processing and Statistical Analysis

MassHunter Profinder (version B10.00; Agilent Technologies, Santa Clara, CA, USA) was used to process the data obtained by LC–MS/HRMS. Treatment of the raw data file started with the extraction of potential molecular features (MFs) by the applicable algorithm included in the software. The recursive extraction algorithm considered all ions exceeding 5000 counts as cut-off value. Additionally, the isotopic distribution used to determine whether a molecular feature is valid should be defined by two or more ions (with a peak spacing tolerance of m/z 0.0025 plus 10.0 ppm in mass accuracy). Apart from $[M + H]^+$ and $[M-H]^-$ ions, adduct formation in the positive (Na^+) and negative ionization ($HCOO^-$, Cl^-) modes and neutral loss by dehydration were included to identify features corresponding to the same potential metabolite. Thus, ions with identical elution profiles and related *m/z* values (representing different adducts or isotopes of the same compound) were extracted as entities characterized by their retention time (RT), the intensity at the apex chromatographic peak, and accurate mass. Then, a recursion step assured correct integration of the entities in all analyses.

Identification was achieved following the methodology previously described by Ledesma-Escobar et al. [17]. After extraction and alignment of all MFs, the software MassHunter Qualitative v.7.0 was used for targeted extraction of MS2 information associated with the monitored MFs in the whole dataset. This information was used for tentative identification of metabolites by searching the MoNA-MassBank of North America (https://mona.fiehnlab.ucdavis.edu/spectra/search, accessed on 13 December 2022) database and others developed by the research group. Additionally, some compounds were confirmed according to both their MS2 information and retention time by using commercially available standards. Finally, the compounds that were not found in the databases, or whose commercial standards were unavailable, were identified via an analysis of neutral mass losses combined with the characteristic fragmentation patterns of their derivatives confirmed by commercial standards.

Quantitative analysis was carried out in relative terms by preparing calibration models for limonin, nomilin, hesperidin, and quercetin as standard compounds (determination coefficients > 0.98; calibration range between 50 ng/mL and 20 μg/mL). Syringaldehyde (1 μg/mL) was used as external standard. Flavonoid glucosides and aglycones were quantitated with models prepared with hesperidin or quercetin, respectively, while limonoids were determined using their corresponding aglycone standards.

2.7. Silica Gel Column Fractionation of Crude Extracts

Crude extracts (1 mL) were fractioned by being passed through a normal-phase silica gel (5 g) column. The solid phase was conditioned with hexane and the metabolites were eluted with 2 mL of EA (fraction 1), 2 mL of 1:1 (v/v) EtOH/acetone (fraction 2), and 2 mL of 1:1 (v/v) EtOH/H_2O (fraction 3). Each fraction was evaporated under vacuum and dissolved with 1 mL of MeOH. The solutions were stored at −80 °C in darkness until use.

2.8. Antioxidant Assays

2.8.1. DPPH Radical Scavenging Activity

DPPH radical scavenging activity was evaluated by mixing 100 μL of sample (either crude extract or fraction) with 900 μL of 20 mg/L DPPH solution in MeOH. The mixture was stirred for 30 min at room temperature and the absorbance was measured at 517 nm. Reference solution was prepared following the same procedure but using MeOH

instead of sample. The antiradical scavenging potential was expressed as the percentage of decoloration of DPPH solution according to the following equation:

$$\%Radical\ scavenging = \left[1 - \frac{A_s}{A_R}\right] * 100 \quad (1)$$

where: *As*, absorbance of the sample; A_R, absorbance of the reference solution.

2.8.2. β-Carotene Bleaching Assay

A stock solution for this test was prepared as follows: 500 µL of Tween-20 was dissolved in 50 mL of water previously saturated with O_2 by air bubbling and mixed with 25 µL of linoleic acid and 500 µL of 1 mg/mL β-carotene solution in chloroform. The mixture was subjected to rotary evaporator under reduced pressure at 30 °C to remove chloroform. Then, the mixture was shaken vigorously until a crystalline emulsion was obtained (approximately 5 min) with the characteristic orange color of β-carotene. Stock solution was immediately used after preparation.

For the measurement of antioxidant activity, 100 µL of the crude extract or fraction was added to 900 µL of the β-carotene/linoleic acid stock solution and stirred for 2 h at 50 °C. The absorbance of the samples was measured at 470 nm immediately after preparation (time 0 min) and after 2 h (time 120 min). A control sample was prepared with MeOH instead of sample. The blank was composed of water, Tween-20, and linoleic acid at the same proportions as those used in the stock solution. The antioxidant activity was calculated as the ability to inhibit the discoloration of β-carotene using the following equation:

$$\%Antioxidant\ activity = \left[1 - \frac{\left(A_s^0 - A_s^{120}\right)}{\left(A_c^0 - A_c^{120}\right)}\right] * 100 \quad (2)$$

where: *As*, Absorbance of the sample; *Ac*, absorbance of control; 0 and 120 refer to time (min).

3. Results

3.1. Characterization of Bioactive Compounds in Citrus Fruits

The analysis of the sample citrus extracts led to the identification of 49 compounds distributed in 31 flavonoids, 9 limonoids, 6 simple phenols, and 3 carboxylic acids by following the methodology previously described by the authors [17]. Thirty-two metabolites were successfully identified as confirmed by the analytical standards. In addition, six isomers (MS2 spectrum correlation with that of the standard above 0.9) were detected at different retention times. The rest of the 11 metabolites were tentatively identified via the detection of neutral mass losses and fragmentation patterns. Thus, for the tentative identification of flavonoid derivatives, the MS2 spectrum should include the product ion of the aglycone as the dominating peak and the neutral loss of the distinctive glucoside. Concerning limonoids, their product ion at m/z 161.0595 in the positive ionization mode dominated the MS2 spectra together with the precursor ion. The identification parameters are summarized in Table S1.

3.2. Locations of the Bioactive Compounds in Citrus Fruits

Flavonoids were the most abundant phenolic compounds among the studied metabolites, followed by limonoids, simple phenols, and carboxylic acids. However, each metabolite class was distributed in a different proportion depending on the fruit. Figure 1 shows that flavonoids constituted the most abundant bioactive fraction in limes and mandarins, representing 64.4% and 73.1% of the total content of identified compounds, respectively. In addition, carboxylic acids were the second largest group in both fruits (36.7% in limes and 23.3% in mandarins). However, acids predominated in lemons, constituting 58.9% of the total quantified compounds, followed by flavonoids (34.2%), limonoids (5.6%), and simple phenols (1.3%).

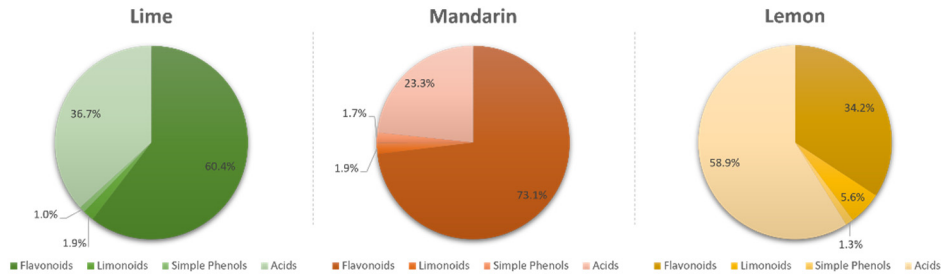

Figure 1. Proportion of flavonoids, limonoids, simple phenols, and carboxylic acids in limes, mandarins, and lemons.

A spatial analysis was carried out to determine the distribution of these metabolites in the analyzed fractions (flavedo, albedo, segments, and juice). Generally, we observed that flavonoids were mostly located in the flavedo and albedo, while carboxylic acids were abundant in the segments and juice. Regarding limonoids, they were mostly found in albedo and segments, while simple phenols were equally distributed in all parts. Despite the similar distribution of the monitored families in the analyzed samples, our results revealed that the fruit was also determinant (Figure 2).

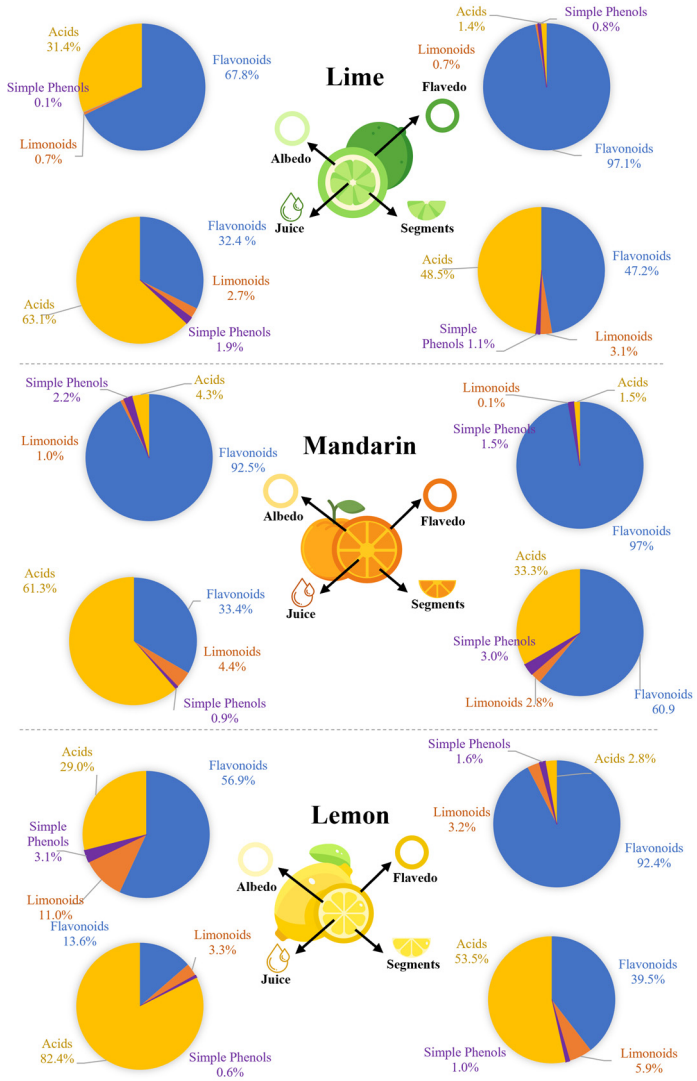

Figure 2. Spatial distribution of flavonoids, limonoids, simple phenols, and carboxylic acids in citrus fruits.

Finally, the concentration of simple phenols was mainly represented by pyrogallol among the three studied fruits. The concentrations of individual metabolites can be found in Table S2. Calibration curves were obtained for limonin, nomilin, hesperidin, and quercetin, which were used also to quantify the rest of the flavonoid glucosides, aglycones, and limonoids.

To confirm the observed differences among the fruits and samples, a non-supervised principal component analysis (PCA) was conducted by grouping the matrix by fruit or by sample, including the QCs (Supplementary Figure S1). This analysis revealed clear discrimination in the 3D scores plot for both grouping cases. Once clustering was confirmed, a multivariate analysis by partial least squares discriminant analysis (PLS-DA) was applied by (i) grouping the matrix by fruit (Figure 3A) and (ii) by sample (Figure 3B). The results of these two analyses revealed that the most important variables distinguishing the fruits were flavonoids and coumaric acid (especially naringenin derivatives, tangeritin, and luteolin, Figure 3C). On the other hand, discrimination by samples was mainly explained by limonoid and carboxylic acid concentrations (Figure 3D).

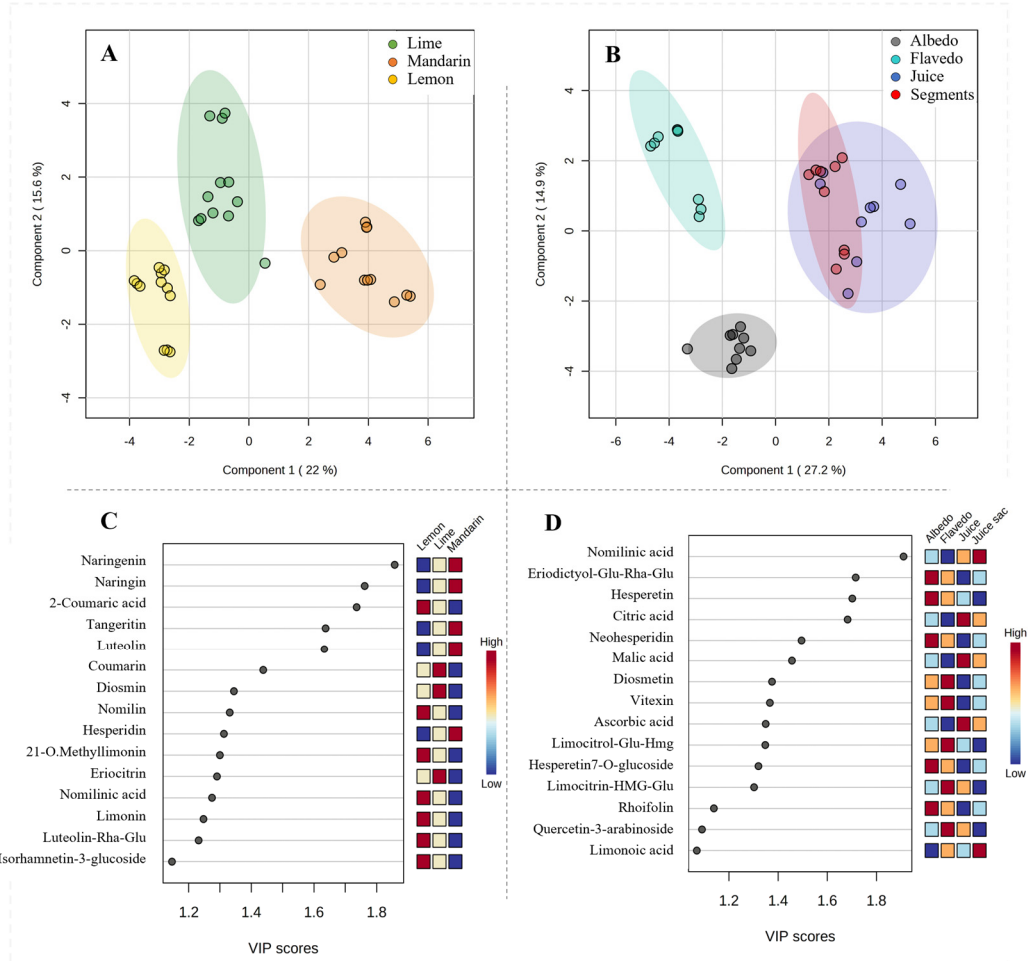

Figure 3. Multivariate PLS-DA for discrimination of citrus fruits (**A**) and samples (**B**) based on the composition of extracts. Variable importance projection (VIP) scores for identification of metabolites with the highest discrimination capability of citrus fruits (**C**) and samples (**D**).

3.3. Antioxidant Activity of Extracts from Different Citrus Fruit Tissues

Concerning the antioxidant activity measured by the β-carotene assay (Figure 4A), our results revealed that, generally, the lemon extracts from the flavedo, albedo, and segments possessed the highest antioxidant activity followed by those from limes and mandarins; however, it was observed that mandarin juice has superior activity compared to lemon

and lime juices. Considering the composition of the extracts, it is possible to assume that limonoids play a key role with respect to antioxidant capacity since this class of metabolites is particularly concentrated in the extracts from the flavedo, albedo, and segments of lemons as well as in mandarin juice. Moreover, a Spearman correlation supported this assumption for limonoids (Figure 4B). The mechanism of the β-carotene bleaching assay supports the ability of bioactive compounds to minimize the peroxidation of linoleic acid, given that hydroperoxides from linoleic acid can react with β-carotene. Therefore, greater activities determined by this assay indicate a higher capacity to prevent the oxidation of lipids.

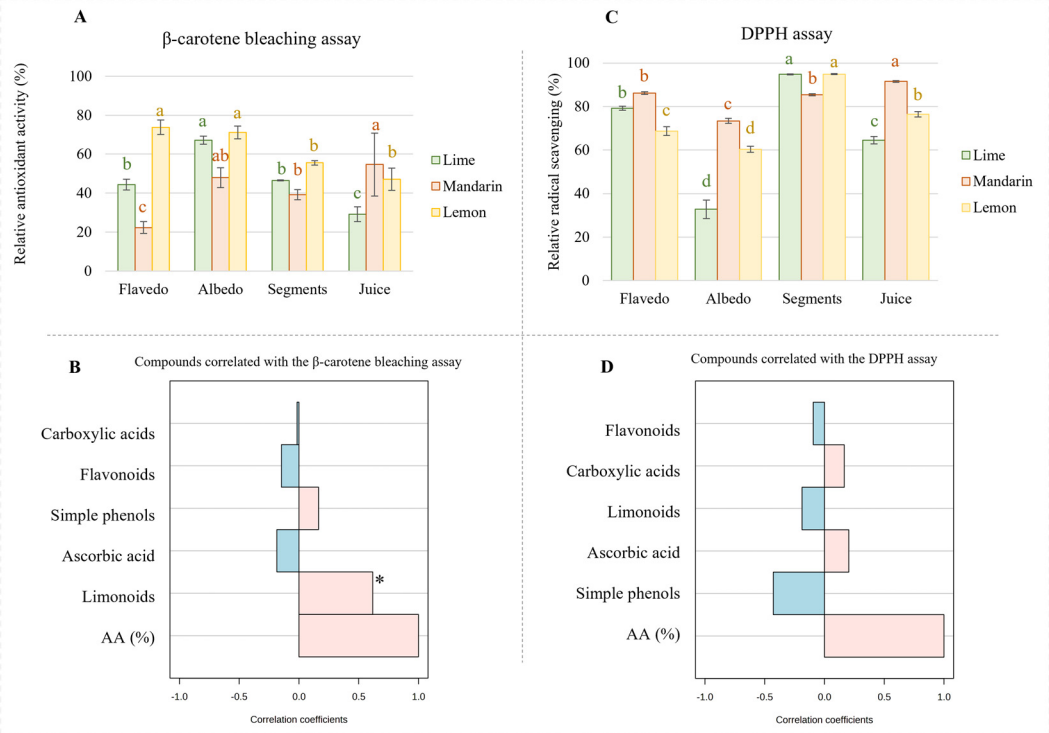

Figure 4. Antioxidant activity (**A**) and radical scavenging capacity (**B**) measured in extracts from citrus fruits. Spearman correlation between antioxidant assays and concentrations of families of metabolites (β-carotene test, (**C**); DPPH assay, (**D**)). Different letters for the same fruit indicate significant differences among tissues extracts in terms of antioxidant or radical scavenging activity. * p-value < 0.001.

On the other hand, the DPPH assay is based on the ability of bioactive compounds to stabilize free radicals by donating protons. In this sense, this study revealed that the mandarin extracts obtained from flavedo had higher radical scavenging potential than those from limes and lemons (Figure 4C), which could be attributed to a higher proportion of flavonoids (see Figure 2A–C). This assumption is not supported by the analysis of the radical scavenging activity in other samples. Thus, the mandarin extracts obtained from albedo, which were highly enriched in flavonoids, presented greater antioxidant activity than lemons, even when their content in flavonoids was very similar. On the other hand, the lime extracts exhibited almost half of the radical scavenging potential of lemons or mandarins, whose concentrations of flavonoids were only 20%, approximately. These discrepancies were also observed in the segment extracts that were expected to provide the highest radical scavenging activity due to their flavonoid content. Particularly, lemon and lime extracts, which proportionally had lower content in flavonoids than mandarins, provided greater scavenging potential. Finally, similar inconsistencies were observed regarding lemon juice, for which higher scavenging activity was reported compared to that of limes despite the reduced content of flavonoids in the former. According to the extracts'

compositions, it seems that the content of carboxylic acids should have affected antioxidant capacity. In fact, the Spearman correlation revealed that acids, especially ascorbic acid, greatly influence radical scavenging potential despite the content of flavonoids (Figure 4D).

3.4. Antioxidant Activity of Three Fractions of the Extracts from Different Citrus Fruits

To disclose the observed complexity of the studied fruits' antioxidant activity and radical scavenging potential, the extracts were partially purified by using a chromatographic column packed with silica. The purification of complex mixtures such as citrus extracts is not simple; however, three defined fractions were collected: (i) the less polar fraction (L) (with high content of limonin and nomilin), the major limonoids in the extracts, aglycone flavonoids, the minor flavonoids, and a low concentration of conjugated flavonoids; (ii) the mid-polar fraction (F), which is mainly composed of major flavonoids, simple phenols, and, to a lesser extent, conjugated limonoids (minor fraction); and, finally, (iii) the polar fraction, (A) containing mainly carboxylic acids and small amounts of flavonoids and simple phenols (Supplementary Figure S1). As expected, the activity of the three fractions was lower than that of the unfractionated extracts. Nevertheless, the obtained results suggest a synergic effect since the addition of the activities of the three fractions resulted in a higher value than those observed in the crude extracts (Figure 5).

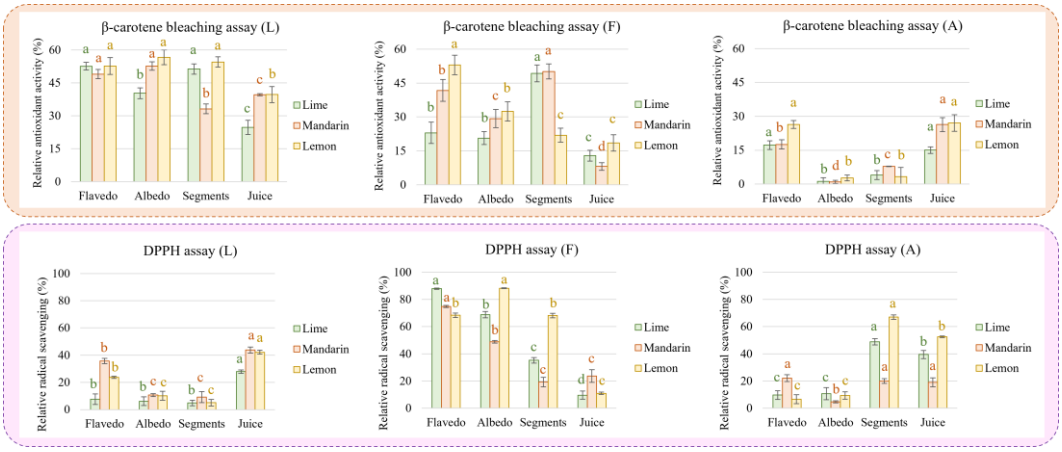

Figure 5. Antioxidant activity (β-carotene bleaching assay) and radical scavenging potential (DDPH assay) measured in fractions enriched in limonoids (L), flavonoids (F), and carboxylic acids (A) obtained by separation of extracts from citrus fruits. Different letters for the same fruit and fraction indicate significant differences in antioxidant or radical scavenging activity.

4. Discussion

In this report, the spatial distribution and antioxidant activity of bioactive compounds in limes, lemons, and mandarin tissues were studied. We observed that flavonoids were predominant in the flavedo and albedo of the three fruits (97.1% and 67.8%, respectively, in limes; 97.0% and 92.5% in mandarins; and 92.4% and 56.9% in lemons). However, hesperidin, diosmin, and eriocitrin were the most concentrated flavonoids in limes; hesperidin and naringin were predominant in mandarins; and apigenin and diosmetin derivatives and hesperidin were highly concentrated in lemons. The presence of these functional ingredients has been previously described in other citrus limon varieties but not distributed in the different tissues of the fruit [16]. Similarly, limonin derivatives were the most concentrated limonoids in limes and mandarins, while nomilin derivatives were the most abundant in lemons.

The highest proportion of carboxylic acids was found in lemons, followed by mandarins and limes, with citric acid being the most concentrated in all cases, followed by malic and ascorbic acids. However, it is worth noting that lemons were the richest fruit in terms of carboxylic acids (Figure 1), especially ascorbic acid, which was found at a twofold higher concentration in lemons than in limes and mandarins. The presence of the identified

carboxylic acids along with others was examined in lemons prior to this study and thus confirms this statement [17].

The antioxidant activity and radical scavenging capacity of citrus fruits have been widely discussed in the literature, but most studies have targeted two main sources: juice and industrial residue extracts [24]. Generally, citrus fruit's antioxidant activity is mainly attributed to ascorbic acid, phenols, and, to a lesser extent, other minor compounds such as limonoids [24]. Measuring the antioxidant activity of complex mixtures such as citrus juices or extracts is not an easy task since this act is affected by diverse aspects such as the structural [30], pH [31], or synergistic effects precipitated by different chemical families [32,33]. In this study, we evaluated the antioxidant activity in extracts from different citrus fruits to discern the contribution of the studied compounds to bioactivity. For this purpose, we used the β-carotene bleaching assay and the radical scavenging potential test (DPPH assay).

The β-carotene assay, which accounted for the composition of the extracts, showed that limonoids are crucial for antioxidant capacity given that this class of metabolites is particularly concentrated in mandarin juice and in the extracts from flavedo, albedo, and segments of lemons. Our DPPH assay revealed that despite their flavonoid content, carboxylic acids are believed to influence antioxidant capacity. Altunkaya et al. [31] demonstrated that the antioxidant activity of lettuce extracts also depended on the pH and level of synergism with added phenols. Hence, the content of carboxylic acids alters the total antioxidant activity of extracts.

Finally, the purification of the extracts was carried out using a column packed with silica defining three fractions (less, mid, and polar). Concerning the limonoid fraction (L), we observed that the antioxidant activity was like that of the extract, with only an approximate decrease of 20% for all samples. This result reinforces the hypothesis that limonoids play a key role in reducing the formation of hydroperoxides from linoleic acid and thus lipidic peroxidation. In addition, the antioxidant activity was generally lower in the juices compared to the extracts from fruit tissues. On the contrary, the radical scavenging activity in juice was reduced by more than 50% compared to the extract. In this case, juices demonstrated higher capacity than the extracts from fruit tissues. These results agree with those observed by Yu et al. [25], who showed that limonin had reduced radical scavenging capacity. On the other hand, the fractions rich in flavonoids (F) presented an antioxidant activity around 30% lower than that measured in the extracts, with the highest levels observed in lemon flavedo and mandarin and lime segments. Complementarily, the radical scavenging potential of this fraction was only reduced by around 10%. The maximum DPPH activity was found in flavedo from limes and mandarins and in lemon albedo, while minimum values were measured in juices. Finally, the carboxylic acids fraction (A) was particularly affected with respect to antioxidant capacity as determined in both assays. Thus, juice provided better values than those found in fruit tissues except for lime and lemon segments, which presented an antioxidant capacity similar to that obtained from juice.

5. Conclusions

This study revealed that the spatial distribution of bioactive compounds is constant in the three citrus fruits. Thus, flavonoids are mostly located in the citrus peel (in both the flavedo and albedo); on the contrary, carboxylic acids are mainly found in segments and, therefore, are extracted in the juice. Regarding limonoids, they are quantitatively distributed in the albedo and segments and, consequently, are also extracted in the juice. Additionally, the composition of bioactive compounds allows for the discrimination of both citrus tissues and fruits. Our determination of these fruits' antioxidant properties demonstrated that limonoid content can be correlated with the antioxidant activity measured by the β-carotene bleaching assay, for which there is a synergistic effect caused by other families. However, the radical scavenging activity was explained by flavonoids and ascorbic acid. Finally, these results do not enable us to draw plausible conclusions about the

contributions of individual compounds to the bioactive properties of the complex extracts. However, the fractionation of the extracts provided information about the antioxidant capacity of the three main chemical families.

Supplementary Materials: The following supporting information can be downloaded at: https://www.mdpi.com/article/10.3390/antiox12040781/s1, Figure S1: 3D PCA score plots obtained by considering all extracts grouped by fruit, tissue, and fruit × tissue. Figure S2: Relative concentrations of the monitored chemical families in the three fractions and crude extracts from citrus fruits. These results were obtained as mean results by considering the three citrus fruits in order to demonstrate their respective capacities after fractionation. Table S1: Parameters for identification of bioactive compounds in the studied citrus fruits. Table S2: Concentrations (μg/g) of flavonoids, limonoids, phenolic acids, and carboxylic acids found in citrus fruits.

Author Contributions: Conceptualization, C.A.L.-E. and F.P.-C.; methodology, M.G.-N., C.A.L.-E. and F.P.-C.; software, M.G.-N. and C.A.L.-E.; validation, M.G.-N. and C.A.L.-E.; formal analysis, M.G.-N. and C.A.L.-E.; investigation, M.G.-N., C.A.L.-E. and F.P.-C.; resources, F.P.-C.; data curation, M.G.-N. and C.A.L.-E.; writing—original draft preparation, M.G.-N., C.A.L.-E. and F.P.-C.; writing—review and editing, M.G.-N., C.A.L.-E. and F.P.-C.; visualization, M.G.-N., C.A.L.-E. and F.P.-C.; supervision, C.A.L.-E. and F.P.-C.; project administration, F.P.-C.; funding acquisition, F.P.-C. All authors have read and agreed to the published version of the manuscript.

Funding: This research was funded by the Spanish Ministerio de Ciencia e Innovación [PID2019-111373RB-I00 project]. Consortium for Biomedical Research in Frailty and Healthy Ageing (CIBERfes) is an initiative of Carlos III Institute of Health.

Institutional Review Board Statement: Not applicable.

Informed Consent Statement: Not applicable.

Data Availability Statement: The data presented in this study are available in this article and in the Supplementary Materials.

Acknowledgments: M. García-Nicolás acknowledge a fellowship 21464/FPI/20 from Fundación Séneca.

Conflicts of Interest: The authors declare no conflict of interest.

References

1. Ke, Z.; Pan, Y.; Xu, X.; Nie, C.; Zhou, Z. Citrus Flavonoids and Human Cancers. *J. Food Nutr. Res.* **2015**, *3*, 341–351. [CrossRef]
2. Tripoli, E.; la Guardia, M.; Giammanco, S.; Majo, D.d.; Giammanco, M. Citrus Flavonoids: Molecular Structure, Biological Activity and Nutritional Properties: A Review. *Food Chem.* **2007**, *104*, 466–479. [CrossRef]
3. Feng, S.; Wang, Y. Citrus Phytochemicals and Their Potential Effects on the Prevention and Treatment of Obesity: Review and Progress of the Past 10 Years. *J. Food Bioact.* **2018**, *4*, 99–106. [CrossRef]
4. Benavente-García, O.; Castillo, J. Update on Uses and Properties of Citrus Flavonoids: New Findings in Anticancer, Cardiovascular, and Anti-Inflammatory Activity. *J. Agric. Food Chem.* **2008**, *56*, 6185–6205. [CrossRef] [PubMed]
5. Rong, X.; Xu, J.; Jiang, Y.; Li, F.; Chen, Y.; Dou, Q.P.; Li, D. Citrus Peel Flavonoid Nobiletin Alleviates Lipopolysaccharide-Induced Inflammation by Activating IL-6/STAT3/FOXO3a-Mediated Autophagy. *Food Funct.* **2021**, *12*, 1305–1317. [CrossRef] [PubMed]
6. Zhang, M.; Zhu, J.; Zhang, X.; Zhao, D.G.; Ma, Y.Y.; Li, D.; Ho, C.T.; Huang, Q. Aged Citrus Peel (Chenpi) Extract Causes Dynamic Alteration of Colonic Microbiota in High-Fat Diet Induced Obese Mice. *Food Funct.* **2020**, *11*, 2667–2678. [CrossRef] [PubMed]
7. Song, M.; Lan, Y.; Wu, X.; Han, Y.; Wang, M.; Zheng, J.; Li, Z.; Li, F.; Zhou, J.; Xiao, J.; et al. The Chemopreventive Effect of 5-Demethylnobiletin, a Unique Citrus Flavonoid, on Colitis-Driven Colorectal Carcinogenesis in Mice Is Associated with Its Colonic Metabolites. *Food Funct.* **2020**, *11*, 4940–4952. [CrossRef]
8. Zhang, Y.; Wang, J.S.; Wang, X.B.; Gu, Y.C.; Wei, D.D.; Guo, C.; Yang, M.H.; Kong, L.Y. Limonoids from the Fruits of Aphanamixis Polystachya (Meliaceae) and Their Biological Activities. *J. Agric. Food Chem.* **2013**, *61*, 2171–2182. [CrossRef]
9. Shi, Y.S.; Zhang, Y.; Li, H.T.; Wu, C.H.; El-Seedi, H.R.; Ye, W.K.; Wang, Z.W.; Li, C.B.; Zhang, X.F.; Kai, G.Y. Limonoids from Citrus: Chemistry, Anti-Tumor Potential, and Other Bioactivities. *J. Funct. Foods* **2020**, *75*, 104213. [CrossRef]
10. Matheyambath, A.C.; Padmanabhan, P.; Paliyath, G. Citrus Fruits. In *Encyclopedia of Food and Health*; Elsevier Press: Oxford, UK, 2016; pp. 136–140, ISBN 9780123849533.
11. Zhou, Z.; Yan, Y.; Li, H.; Feng, Y.; Huang, C.; Fan, S. Nomilin and Its Analogues in Citrus Fruits: A Review of Its Health Promotion Effects and Potential Application in Medicine. *Molecules* **2023**, *28*, 269. [CrossRef]
12. Raspo, M.A.; Vignola, M.B.; Andreatta, A.E.; Juliani, H.R. Antioxidant and Antimicrobial Activities of Citrus Essential Oils from Argentina and the United States. *Food Biosci* **2020**, *36*, 100651. [CrossRef]

13. Gao, Z.; Zhong, W.; Chen, K.; Tang, P.; Guo, J. Chemical Composition and Anti-Biofilm Activity of Essential Oil from *Citrus medica* L. Var. *sarcodactylis* Swingle against *Listeria monocytogenes*. *Ind. Crop. Prod.* **2020**, *144*, 112036. [CrossRef]
14. Mahato, N.; Sharma, K.; Koteswararao, R.; Sinha, M.; Baral, E.R.; Cho, M.H. Citrus Essential Oils: Extraction, Authentication and Application in Food Preservation. *Crit. Rev. Food Sci. Nutr.* **2019**, *59*, 611–625. [CrossRef] [PubMed]
15. Vavoura, M.v.; Karabagias, I.K.; Kosma, I.S.; Badeka, A.v.; Kontominas, M.G. Characterization and Differentiation of Fresh Orange Juice Variety Based on Conventional Physicochemical Parameters, Flavonoids, and Volatile Compounds Using Chemometrics. *Molecules* **2022**, *27*, 6166. [CrossRef]
16. Rosa, A.; Petretto, G.L.; Maldini, M.; Tirillini, B.; Chessa, M.; Pintore, G.; Sarais, G. Chemical Characterization, Antioxidant and Cytotoxic Activity of Hydroalcoholic Extract from the Albedo and Flavedo of *Citrus limon* Var. *pompia* Camarda. *J. Food Meas. Charact.* **2022**, *17*, 627–635. [CrossRef]
17. Ledesma-Escobar, C.A.; Priego-Capote, F.; Luque De Castro, M.D. Characterization of Lemon (*Citrus limon*) Polar Extract by Liquid Chromatography-Tandem Mass Spectrometry in High Resolution Mode. *J. Mass Spectrom.* **2015**, *50*, 1196–1205. [CrossRef]
18. Liu, W.; Zheng, W.; Cheng, L.; Li, M.; Huang, J.; Bao, S.; Xu, Q.; Ma, Z. Citrus Fruits Are Rich in Flavonoids for Immunoregulation and Potential Targeting ACE2. *Nat. Prod. Bioprospect.* **2022**, *12*, 4. [CrossRef]
19. Ledesma-Escobar, C.A.; Priego-Capote, F.; Robles Olvera, V.J.; Luque De Castro, M.D. Targeted Analysis of the Concentration Changes of Phenolic Compounds in Persian Lime (*Citrus latifolia*) during Fruit Growth. *J. Agric. Food Chem.* **2018**, *66*, 1813–1820. [CrossRef]
20. Aznar, R.; Rodríguez-pérez, C.; Rai, D.K. Comprehensive Characterization and Quantification of Antioxidant Compounds in Finger Lime (*Citrus australasica* L.) by HPLC-QTof-MS and UPLC-MS/MS. *Appl. Sci.* **2022**, *12*, 1712. [CrossRef]
21. Mei, Z.; Zhang, R.; Zhao, Z.; Xu, X.; Chen, B.; Yang, D.; Zheng, G. Characterization of Antioxidant Compounds Extracted from Citrus Reticulata Cv. Chachiensis Using UPLC-Q-TOF-MS/MS, FT-IR and Scanning Electron Microscope. *J. Pharm. Biomed. Anal.* **2021**, *192*, 113683. [CrossRef]
22. Carlos, A.L.E.; Priego-Capote, F.; de Castro, M.D.L. Comparative Study of the Effect of Sample Pretreatment and Extraction on the Determination of Flavonoids from Lemon (*Citrus limon*). *PLoS ONE* **2016**, *11*, e0148056. [CrossRef]
23. Sadeer, N.B.; Montesano, D.; Albrizio, S.; Zengin, G.; Mahomoodally, M.F. The Versatility of Antioxidant Assays in Food Science and Safety—Chemistry, Applications, Strengths, and Limitations. *Antioxidants* **2020**, *9*, 709. [CrossRef]
24. Zou, Z.; Xi, W.; Hu, Y.; Nie, C.; Zhou, Z. Antioxidant Activity of Citrus Fruits. *Food Chem.* **2016**, *196*, 885–896. [CrossRef] [PubMed]
25. Yu, J.; Wang, L.; Walzem, R.L.; Miller, E.G.; Pike, L.M.; Patil, B.S. Antioxidant Activity of Citrus Limonoids, Flavonoids, and Coumarins. *J. Agric. Food Chem.* **2005**, *53*, 2009–2014. [CrossRef] [PubMed]
26. Olfa, T.; Gargouri, M.; Akrouti, A.; Brits, M.; Gargouri, M.; ben Ameur, R.; Pieters, L.; Foubert, K.; Magné, C.; Soussi, A.; et al. A Comparative Study of Phytochemical Investigation and Antioxidative Activities of Six Citrus Peel Species. *Flavour Fragr. J.* **2021**, *36*, 564–575. [CrossRef]
27. Yaqoob, M.; Aggarwal, P.; Babbar, N. Extraction and Screening of Kinnow (*Citrus reticulata* L.) Peel Phytochemicals, Grown in Punjab, India. *Biomass Convers. Biorefin.* **2022**, 1–13. [CrossRef]
28. Cebadera, L.; Dias, M.I.; Barros, L.; Fernández-Ruiz, V.; Cámara, R.M.; del Pino, Á.; Santos-Buelga, C.; Ferreira, I.C.F.R.; Morales, P.; Cámara, M. Characterization of Extra Early Spanish Clementine Varieties (*Citrus clementina* Hort Ex Tan) as a Relevant Source of Bioactive Compounds with Antioxidant Activity. *Foods* **2020**, *9*, 642. [CrossRef]
29. De Sun, C.; Chen, K.S.; Chen, Y.; Chen, Q.J. Contents and Antioxidant Capacity of Limonin and Nomilin in Different Tissues of Citrus Fruit of Four Cultivars during Fruit Growth and Maturation. *Food Chem.* **2005**, *93*, 599–605. [CrossRef]
30. di Majo, D.; Giammanco, M.; la Guardia, M.; Tripoli, E.; Giammanco, S.; Finotti, E. Flavanones in Citrus Fruit: Structure–Antioxidant Activity Relationships. *Food Res. Int.* **2005**, *38*, 1161–1166. [CrossRef]
31. Altunkaya, A.; Gökmen, V.; Skibsted, L.H. PH Dependent Antioxidant Activity of Lettuce (*L. Sativa*) and Synergism with Added Phenolic Antioxidants. *Food Chem.* **2016**, *190*, 25–32. [CrossRef]
32. Hidalgo, M.; Sánchez-Moreno, C.; de Pascual-Teresa, S. Flavonoid–Flavonoid Interaction and Its Effect on Their Antioxidant Activity. *Food Chem.* **2010**, *121*, 691–696. [CrossRef]
33. Capitani, C.D.; Carvalho, A.C.L.; Botelho, P.B.; Carrapeiro, M.M.; Castro, I.A. Synergism on Antioxidant Activity between Natural Compounds Optimized by Response Surface Methodology. *Eur. J. Lipid Sci. Technol.* **2009**, *111*, 1100–1110. [CrossRef]

antioxidants

MDPI

Article

Skin Improvement with Antioxidant Effect of Yuja (*Citrus junos*) Peel Fractions: Wrinkles, Moisturizing, and Whitening

Young Yun Jung [1,†], In Jin Ha [2,†], Mina Lee [3,*] and Kwang Seok Ahn [1,*]

[1] College of Korean Medicine, Kyung Hee University, 24 Kyungheedae-ro, Dongdaemun-gu, Seoul 02447, Republic of Korea
[2] Korean Medicine Clinical Trial Center (K-CTC), Korean Medicine Hospital, Kyung Hee University, Seoul 02447, Republic of Korea
[3] College of Pharmacy and Research Institute of Life and Pharmaceutical Sciences, Sunchon National University, 255 Jungangno, Suncheon 57922, Republic of Korea
* Correspondence: minalee@scnu.ac.kr (M.L.); ksahn@khu.ac.kr (K.S.A.)
† These authors contributed equally to this work.

Abstract: Yuja (*Citrus junos*) has been cultivated and used for food and medicinal purposes in China and Korea. Its antioxidant, anti-wrinkle, moisturizing, and whitening effects were evaluated in HaCaT, HDF, and B16F10 cells. UVB has been known to cause cellular stress and the production of reactive oxygen species (ROS). Ambivalence of oxidative stress has been reported; however, excessive levels of ROS contribute to skin aging through the loss of elasticity and collagen fibers of connective tissue in the dermis. Skin aging is one of the biological processes that is affected by various factors, including UVB. Pro-Collagen I and hyaluronic acid contents were measured in UVB-irradiated HaCaT and HDF cells to evaluate the anti-wrinkle and moisturizing effects of Yuja-peel (YJP) fractions in -EA (ethyl acetate), -Hex (hexane), and -BuOH (butanol). The expression of matrix metalloproteinases (MMPs) involved in collagen degradation was confirmed to be inhibited by YJP fractions at both the protein and mRNA levels. Filaggrin and serine palmitoyltransferase (SPT), which are moisturizing factors, were induced by YJP fractions. B16F10 cells were treated with α-MSH to induce hyperpigmentation, and then the whitening efficacy of YJP fractions was verified by observing a decrease in melanin content. Overall, our results contribute to the development of various novel skin-improving cosmetics and pharmaceuticals with YJP fractions as active ingredients.

Keywords: Yuja (*Citrus junos*); anti-wrinkle; moisturizing; whitening

1. Introduction

Yuja (*Citrus junos*) is an arboreal species belonging to the genus *Citrus* of Rutaceae. It is found in Sichuan, Hubei, Yunnan, and Tibet in China, and also in Korea [1]. Yuja is mainly prepared in the form of sugar pickles and is used as tea, dressing, and vinegar, and it is widely used for medicinal purposes [1]. Our study confirmed the anti-wrinkle, moisturizing, and whitening effects of the skin using a Yuja-peel (YJP) fraction that has been traditionally used for food and medicine through a molecular mechanism approach.

Skin is a barrier between the organism and the environment [2]. Skin aging reduces its effectiveness as a barrier, and there are intrinsic (cellular metabolism, metabolic processes, and hormones) and extrinsic (pollution, chronic light exposure, chemicals, and toxins) factors that cause aging [2,3]. Specifically, our study focused on skin damage from ultraviolet (UV) radiation. Long-term exposure to ultraviolet (UV) radiation is a major factor of extrinsic skin aging (photoaging), causing wrinkle formation, pigment accumulation, and inflammation reactions [2,4]. According to the wavelength, UV is classified into three types: UVA (320–400 nm), UVB (280–320 nm), and UVC (200–280 nm) [4,5]. UVB (280–320 nm)

causes more cellular stress and production of reactive oxygen species (ROS) on human skin than other types of UV cause [4]. UVB radiation can induce collagen degradation and generate inflammatory mediators [6,7].

The ambivalence of oxidative stress has been reported through various previous studies [8–11]. Excessive levels of reactive oxygen species (ROS) stocks are also known to contribute to tumorigenesis [11]. ROS can be caused by mitochondria and other cells intracellularly; however, it can also be caused by radiation, drugs, tobacco, pollutants, and ultraviolet light externally [12–14]. In particular, excessive levels of intracellular ROS lead to the loss of elasticity and collagen fibers of connective tissue in the dermis [15]. An imbalance between glutathione (GSH) and oxidized glutathione (GSSG) by the antioxidant defense system blocks ROS accumulation and prevents skin aging, inflammation, and cancer [16,17].

Matrix metalloproteinases (MMPs) are a family of zinc-containing peptide hydrolases that can lead to the degradation of extracellular matrix proteins (ECMs) [18]. UV-irradiation induces the production of reactive oxygen species (ROS) that can lead to the activation of MMPs, which degrade the collagen matrix system in the dermis [3]. MMP-1 has been reported to lead to collagen degradation due to oxidative stress [6,18].

Dehydration of the skin is closely related to skin aging [19]. Hyaluronic acid modulates hyaluronic acid synthase (HAS-1, 2, and 3) to increase and provide moisture to the skin [20,21]. Filaggrin and serine palmitoyltransferase (SPT) are known to be key factors of hydration [22]. Epidermal barrier protein plays an important role in maintaining skin moisture by forming a protein-lipid matrix, and filaggrin is known as an epidermal barrier protein [21]. SPT has been reported to be related to ceramide biosynthesis among intercellular lipids [23].

Melanin is composed of pigments synthesized in epidermal melanocytes; it prevents and protects the skin from UV rays [24]. However, pigmentation disorders including hyperpigmentation cause various skin diseases, such as freckles, chloasma, and melanoma, due to abnormal melanin production [25,26]. The biosynthesis of melanin can be caused by various stimuli; for example, stimulation by UV-irradiation releases α-melanocyte stimulating hormone (α-MSH) and stimulates melanin biosynthesis in epidermal melanocytes [26]. At this time, α-MSH activates the cAMP-PKA-CREB (cyclic adenosine monophosphate-protein kinase A-cAMP response element binding protein) axis, and the activated cAMP-PKA-CREB axis induces the micropthalmia-associated transcription factor (MITF). MITF lead to increased tyrosinase (TYR), tyrosinase-related protein 1 (TRP-1), and tyrosinase-related protein 2 (TRP-2) in melanocytes stimulated with α-MSH [26,27].

In our study, we demonstrated anti-wrinkle, moisturizing, and whitening effects through molecular pathways using the fractions of Yuja-peel (YJP-EA, -Hex, and BuOH). Our study contributed to expanding the field of the applications of Yuja-peel by proving various effects along with the value of traditional use of citron peel.

2. Materials and Methods

2.1. Reagents

The seeds of *C. junos*, cultivated in Goheung, Korea, were cold-pressed for the oil extraction. After the removal of the oil, the Yuja-peel (YJP) was extracted with 50% ethanol by sonication for 2 h. The extracted solution was concentrated at room temperature using an evaporator under a speed vacuum. The extract was suspended in distilled H_2O and partitioned by increasing polarity with *n*-hexane (YJP-Hex), EtOAc (YJP-EA), and *n*-butanol (YJP-BuOH) fractions and water-soluble residue. YJP fractions (YJP-EA, YJP-Hex, and YJP-BuOH) were obtained from the extract and isolated by Dr. In Jin Ha in the Korean Medicine Clinical Trial Center, Kyung Hee University. The fractions were classified into EA (ethyl acetate), Hex (hexane), and BuOH (butanol), according to their chemical properties. 3-(4,5-dimethylthiazol-2-yl)-2,5-diphenyltetrazolium bromide (MTT) and bovine serum albumin (BSA), α-melanocyte stimulating hormone (α-MSH), tyrosinase (from mushroom), and anti-MMP-1 antibody were purchased from Sigma-Aldrich (St. Louis, MO, USA). A

Human Pro-Collagen I α1 ELISA kit and a Hyaluronan ELISA kit were purchased from R&D Systems (Minneapolis, MN, USA). Anti-MMP-9, anti-MMP-13, anti-GR, anti-Collagen I, anti-TRP-1, anti-TRP-2, anti-tyrosinase, anti-MITF, and anti-β-actin antibodies were purchased from Santa Cruz Biotechnology (Dallas, TX, USA). Anti-filaggrin and anti-SPT antibodies were obtained from Abcam (Cambridge, UK).

2.2. Cell Lines and Culture Conditions

Human keratinocyte HaCaT cells were obtained from Dr. Norbert E. Fusenig (German Cancer Research Center, Heidelberg, Germany). Human dermal fibroblast (HDF) cells and mouse skin melanoma B16F10 cells were obtained from the American Type Culture Collection (Manassas, VA, USA). The HDF cells were cultured in RPMI 1640 and DMEM/F12 medium (1:1) containing 10% feral bovine serum (FBS) and 1% penicillin-streptomycin. The HaCaT and B16F10 cells were cultured in Dulbecco's Modified Eagle Medium (DMEM) with a low-glucose medium containing 10% feral bovine serum (FBS) and 1% penicillin-streptomycin. The cells' conditions were maintained at 37 °C in 5% CO_2.

2.3. ROS Production Measurement

The HaCaT cells were irradiated with 30 mJ/cm^2 of UVB, and the HDF cells were irradiated with 100 mJ/cm^2. Next, the cells were treated with NAC (3 mM) for 15 min or with YJP-EA, -Hex, and –BuOH (50 μg/mL) for 12 h. The cells were then incubated with cell-permeable fluorescent 2′,7′-dichlorofluorescin diacetate (H2DCF-DA) (10 μM) for 30 min at 37 °C. Finally, the cells were analyzed using a BD AccuriTM C6 Plus Flow Cytometer (BD Biosciences, Becton-Dickinson, Franklin Lakes, NJ, USA).

2.4. Glutathione Measurement

The HaCaT cells were irradiated with 30 mJ/cm^2 of UVB, and the HDF cells were irradiated with 100 mJ/cm^2. The cells were then treated with NAC (3 mM) for 15 min or with YJP-EA, -Hex, and –BuOH (50 μg/mL) for 12 h. Next, the supernatants were removed, and the glutathione levels were measured using a GSH/GSSG-Glo^{TM} Assay (Promega, Madison, WI, USA), according to the manufacturer's protocol [22].

2.5. MTT Assay

To evaluate the cell viability of the YJP-EA-, Hex-, and BuOH-treated cells, an MTT assay was used as described previously [28,29]. The cell viability was examined using a VARIOSKAN LUX (Thermo Fisher Scientific Inc., Waltham, MA, USA) at 570 nm.

2.6. UVB Irradiation

The HaCaT and HDF cells were seeded in a six-well plate (5×10^5 cells/well). The cells were washed with PBS and subjected to 30 or 100 mJ/cm^2 of UVB radiation using a CL-1000 Ultraviolet Crosslinker (Ultra-violet products Ltd., Cambridge, UK). After irradiation, the cells were treated with YJP-EA, Hex, and BuOH at the indicated concentrations for 24 h.

2.7. Western Blot Analysis

The protein expression levels were evaluated by Western blot analysis using specific antibodies as described previously [29]. The cells (5×10^5 cells/well) were seeded and treated with the various indicated conditions. Whole cell lysates were prepared with equal amounts of proteins, and then the protein expression levels were evaluated by Western blot analysis. The proteins were resolved using a sodium dodecyl sulfate-polyacrylamide gel electrophoresis (SDS-PAGE) and transferred to nitrocellulose membrane. The membrane was then blocked with 5% skimmed milk in 1 × TBST (1 × TBS with 0.1% Tween 20). The proteins were probed by specific antibodies, and the membranes were detected using an enhanced chemiluminescence (ECL) kit (EZ-Western Lumi Femto, DOGEN) (Guro, Seoul, Republic of Korea).

2.8. Reverse Transcription PCR

The total RNA was extracted from the cells. The desired RNA was reverse transcribed, and the transcripts were analyzed as indicated in our previous studies [30]. An equal amount of total RNA was reverse transcribed into cDNA, and then RT-PCR was performed to evaluate the expression of MMP-1, -9, -13, and Collagen I. The pairs of forward and reverse primer sets used were as follows: MMP-1, 5′-ATTCTACTGATATCGGGGCTTTGA-3′, and 5′-ATGTCCTTGGGGTGTCCGTGTAG-3′; MMP-9, 5′-TTGAGGAGCGGCTCTCCAAG-3′, and 5′-CGGTCCTGGCAGAAATAGGC-3′; MMP-13, 5′-GGAGCCTCTGAGTCATGGAG-3′, and 5′- TTGAGCTGGACRCATTGTCG-3′; Collagen I, 5′-GGTGGTGGTTATGACTTTGG-3′, and 5′-GTTCTTGGCTGGGATGTTTT-3′. MMP-1 was amplified at 94 °C for 5 min, at 94 °C for 30 s, at 57 °C for 30 s, at 72 °C for 30 s with 27 cycles, and an extension at 72 °C for 7 min. MMP-9 was amplified at 94 °C for 5 min, at 94 °C for 30 s, at 60 °C for 30 s, at 72 °C for 30 s with 30 cycles, and an extension at 72 °C for 7 min. MMP-13 was amplified at 94 °C for 5 min, at 94 °C for 30 s, at 56 °C for 30 s, at 72 °C for 30 s with 27 cycles, and an extension at 72 °C for 7 min. Collagen I was amplified at 94 °C for 5 min, at 94 °C for 30 s, at 50 °C for 30 s, at 72 °C for 30 s with 27 cycles, and an extension at 72 °C for 7 min. Glyceraldehyde-3-phosphate dehydrogenase (GAPDH) was used as the control.

2.9. Determination of Pro-Collagen I and Hyaluronic Acid Secretion

The HaCaT and HDF cells were irradiated and treated with YJP-EA, Hex, and BuOH. The culture medium was collected after 24 h of treatment. The Type I Pro-Collagen amount was determined using a Human Pro-Collagen I α1 ELISA kit from R&D Systems (Minneapolis, MN, USA). The hyaluronic acid was determined using a Hyaluronan ELISA kit from R&D Systems (Minneapolis, MN, USA).

2.10. Evaluation of Melanin Contents

The B16F10 cells were treated with α-MSH (200 nM) and YJP-EA, Hex, and BuOH for 48 h. The cells were dissolved in 1M NaOH for 2 h at 60 °C and then detected using VARIOSKAN LUX (Thermo Fisher Scientific Inc., Waltham, MA, USA) at 490 nm.

2.11. Intracellular Tyrosinase Activity

The B16F10 cells were treated with α-MSH (200 nM) and YJP-EA, Hex, and BuOH for 72 h. The cells were dissolved using a cell lysis buffer, and each lysate was prepared with 20 μL. We then added 80 μL of L-DOPA (2 mg/mL) and incubated the mixtures for 2 h at 37 °C. After 2 h, it was measured using VARIOSKAN LUX (Thermo Fisher Scientific Inc., Waltham, MA, USA) at 490 nm.

2.12. Mushroom Tyrosinase Activity

The B16F10 cells were treated with α-MSH (200 nM) and YJP-EA, Hex, and BuOH for 72 h. The supernatants were obtained and prepared with 10 μL. We added 170 μL of L-DOPA (2 mg/mL) and 20 μL of tyrosinase (250 unit) and then incubated the mixtures for 1 h at 37 °C. After 1 h, it was measured using VARIOSKAN LUX (Thermo Fisher Scientific Inc., Waltham, MA, USA) at 475 nm.

2.13. Statistical Analysis

All numeric values were represented as the mean ± SD. The statistical significance of the data compared with that of the untreated control was determined using the Student unpaired *t*-test. The significance was set at * $p < 0.05$, ** $p < 0.01$, and *** $p < 0.001$.

3. Results

3.1. YJP Fractions Inhibit Collagen I Degradation in UVB-Irradiated Human Keratinocyte HaCaT Cells

We evaluated the cell viability of HaCaT cells (1×10^4 c/w) under YJP-EA, Hex, and BuOH (0, 5, 10, 50, 100 μg/mL) for 24 h (Figure 1A). At the highest concentration of

100 μg/mL, the cell viability of YJP-EA was the lowest, and all cell viability was near or above 80%. After evaluating the cell viability, the anti-wrinkle effect was confirmed by selecting a concentration with a survival rate above 80%. The HaCaT cells (5×10^5 c/w) were irradiated with UVB (30 mJ/cm^2) and then treated with YJP-EA, Hex, and BuOH for 24 h. Whole cell lysates were analyzed by Western blot analysis and probed with MMP-1, -9, -13, and Collagen I (Figure 1B). Collagen degradation-related MMP-1, -9, and -13 were increased according to UVB irradiation; however, their expressions were decreased under YJP-EA, Hex, and BuOH treatments. The expression level of Collagen I was suppressed by UVB irradiation, while YJP-EA, Hex, and BuOH increased Collagen I expression. Under the same conditions, to investigate the RNA-level expression, we extracted the RNA from the cells and synthesized cDNA. Using cDNA, we performed a PCR on MMP-1, -9, -13, and Collagen I and then separated it on 1% agar gel (Figure 1C). Similar to that of the protein expression, MMP-1, -9, and -13 were induced by UVB irradiation and suppressed by YJP fractions. The RNA expression of Collagen I was suppressed by UVB irradiation; however, YJP fractions recovered it. Next, the type I Pro-Collagen was measured using the Human Pro-Collagen I α1 ELISA kit. The cells were irradiated with UVB (30 mJ/cm^2) first and then treated with YJP-EA, Hex, and BuOH for 24 h. As shown in Figure 1D, the type I Pro-Collagen was suppressed by UVB irradiation. However, YJP-EA, Hex, and BuOH recovered the Pro-Collagen content in HaCaT cells. The results show that YJP fractions have anti-wrinkle effects on UVB-irradiated HaCaT cells.

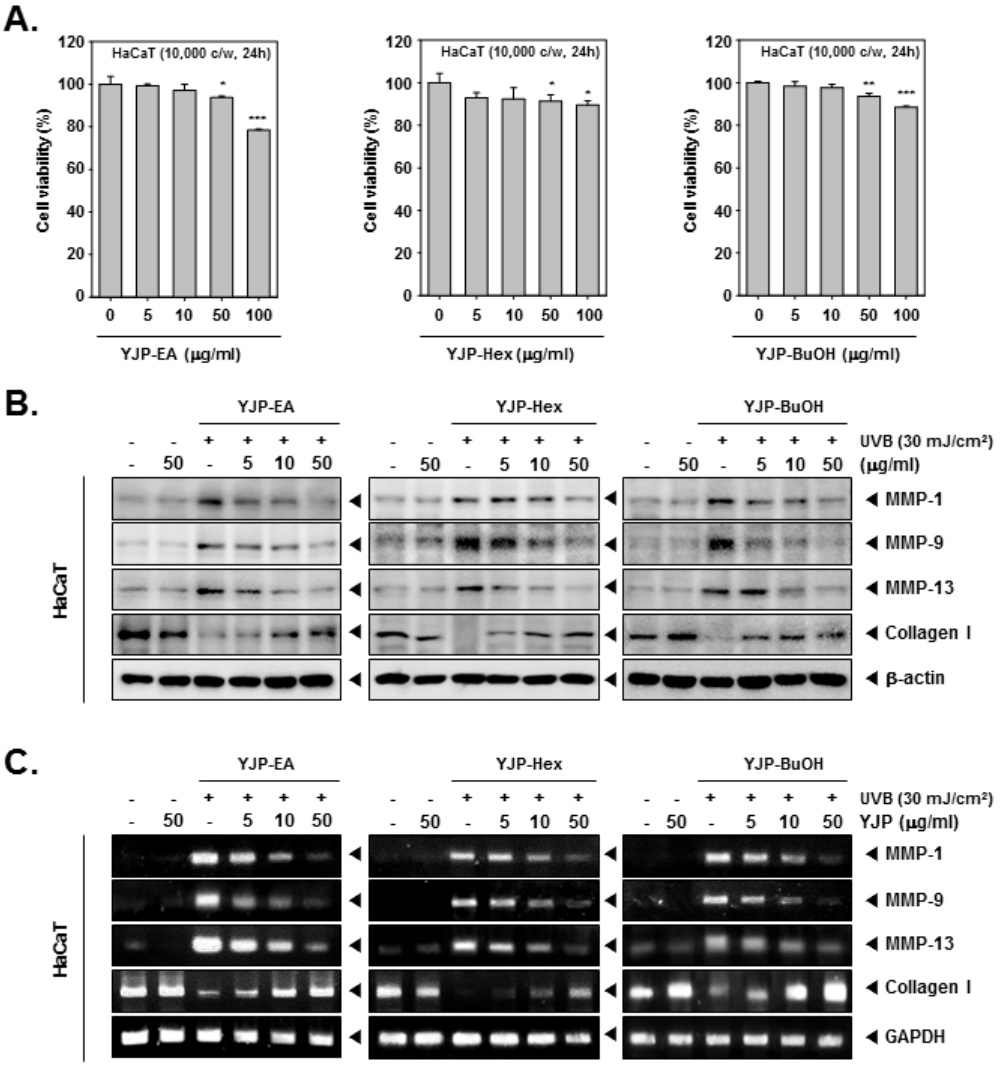

Figure 1. *Cont.*

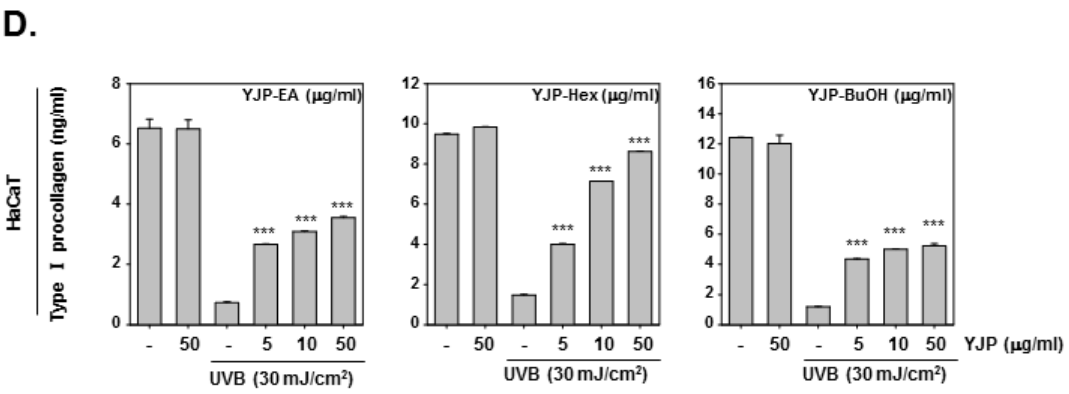

Figure 1. Anti-wrinkle effects of YJP-EA, Hex, and BuOH on UVB-irradiated human keratinocyte HaCaT cells. (**A**) HaCaT cells were treated with YJP-EA, Hex, and BuOH for 24 h. An MTT assay was performed to evaluate cell viability. (**B**) HaCaT cells were irradiated with UVB (30 mJ/cm^2) and then treated with YJP-EA, Hex, and BuOH for 24 h. Whole cell lysates were analyzed by Western blot analysis. (**C**) HaCaT cells were treated by YJP-EA, Hex, and BuOH for 24 h after UVB (30 mJ/cm^2) irradiation. The RNA level was evaluated using reverse transcription PCR. (**D**) The Pro-Collagen of HaCaT cells was measured using an ELISA kit, following the manufacturer's instructions, with 450 nm. All experiments were performed individually in triplicate. *** $p < 0.001$ vs. non-treated (NT) cells, ** $p < 0.01$ vs. non-treated (NT) cells, and * $p < 0.05$ vs. non-treated (NT) cells.

3.2. YJP Fractions Inhibit Collagen I Degradation in UVB-Irradiated Human Dermal Fibroblasts (HDF) Cells

Next, we investigated the anti-wrinkle effects of YJP fractions on human dermal fibroblasts (HDF) cells. To evaluate cell viability, the HDF cells were treated with YJP-EA, Hex, and BuOH for 24 h, and an MTT assay was examined (Figure 2A). Specifically, YJP-Hex-treated HDF cells showed the lowest cell viability among the YJP fractions. After the MTT assay, we selected the concentrations with a survival rate above 80%. Next, the HDF cells were irradiated with UVB (100 mJ/cm^2) and treated with YJP-EA, Hex, and BuOH (0, 5, 10, 50 μg/mL) for 24 h. The MMP-1, -9, -13, and Collagen I were analyzed by Western blot analysis with whole cell lysates (Figure 2B). MMP-1, -9, and 13 were induced under UVB irradiation and then suppressed by YJP-EA, Hex, and BuOH. In addition, the YJP fractions restored the expression of collagen, which had been suppressed by UVB. Next, the RNA levels of MMP-1, -9, -13, and Collagen I were investigated using reverse transcription PCR. After the PCR was done, the cDNA was synthesized from RNA, separated on 1% agar gel, and evaluated (Figure 2C). Similar to that of the protein's expression level, the RNA expressions of MMP-1, -9, and 13 were induced under UVB irradiation and suppressed by YJP-EA, Hex, and BuOH. Collagen I, however, was suppressed by UVB irradiation and recovered by YJP-EA, Hex, and BuOH. The contents of type I Pro-Collagen were decreased with UVB irradiation, and then YJP fractions increased the contents of Pro-Collagen in HDF cells (Figure 2D). The results show that the YJP fractions also have anti-wrinkle effects on UVB-irradiated HDF cells.

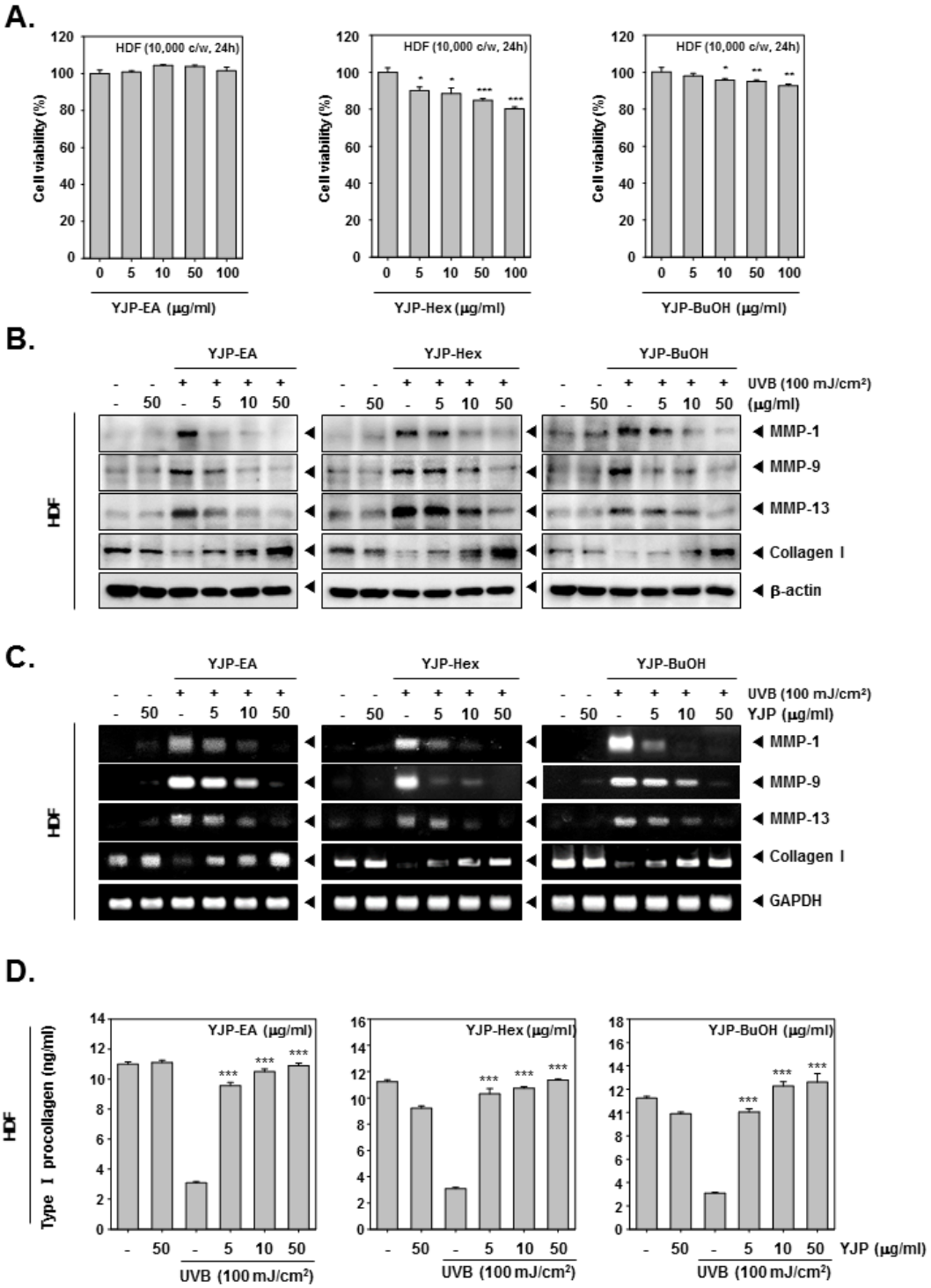

Figure 2. Anti-wrinkle effects of YJP-EA, Hex, and BuOH on UVB-irradiated human dermal fibroblast cells. (**A**) HDF cells were treated with YJP-EA, Hex, and BuOH for 24 h. An MTT assay was performed to evaluate cell viability. (**B**) HDF cells were irradiated with UVB (100 mJ/cm^2) and then treated with YJP-EA, Hex, and BuOH for 24 h. Whole cell lysates were analyzed by Western blot analysis. (**C**) HDF cells were treated by YJP-EA, Hex, and BuOH for 24 h after UVB (100 mJ/cm^2) irradiation. The RNA level was evaluated using reverse transcription PCR. (**D**) The Pro-Collagen of HDF cells was measured using an ELISA kit, following the manufacturer's instructions, with 450 nm. All experiments were performed individually in triplicate. *** $p < 0.001$ vs. non-treated (NT) cells, ** $p < 0.01$ vs. non-treated (NT) cells, and * $p < 0.05$ vs. non-treated (NT) cells.

3.3. YJP Fractions Restore Moisturizing Effects on HaCaT and HDF Cells under UVB-Irradiation

To investigate the moisturizing effects of YJP-EA, Hex, and BuOH, we stimulated HaCaT and HDF cells with UVB irradiation. After UVB irradiation, YJP-EA, Hex, and BuOH (0, 5, 10, 50 μg/mL) were treated for 24 h. The contents of the hyaluronic acid were measured using a Hyaluronan ELISA kit. As shown in Figure 3A,B, the contents of the hyaluronic acid were decreased with UVB irradiation in both HaCaT and HDF cells. However, the treatment of the YJP fraction restored the decreased hyaluronic acid with increasing concentration. Next, we investigated the protein expression of filaggrin and SPT by Western blot analysis to study the molecular mechanism of the moisturizing effect (Figure 3C,D). In both HaCaT and HDF cells, UVB irradiation inhibited the filaggrin and SPT expression. Despite the UVB irradiation, filaggrin and SPT were restored by YJP-EA, Hex, and BuOH. The results show that YJP fractions can recover moisturizing effects in UVB-irradiated HaCaT and HDF cells.

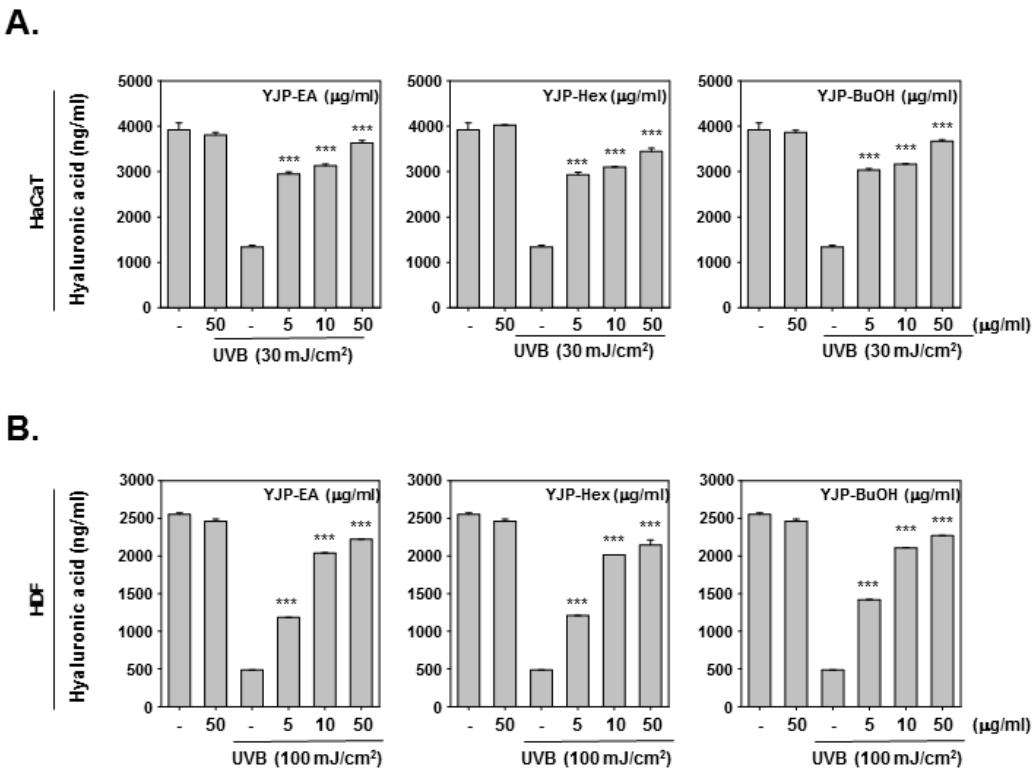

Figure 3. *Cont.*

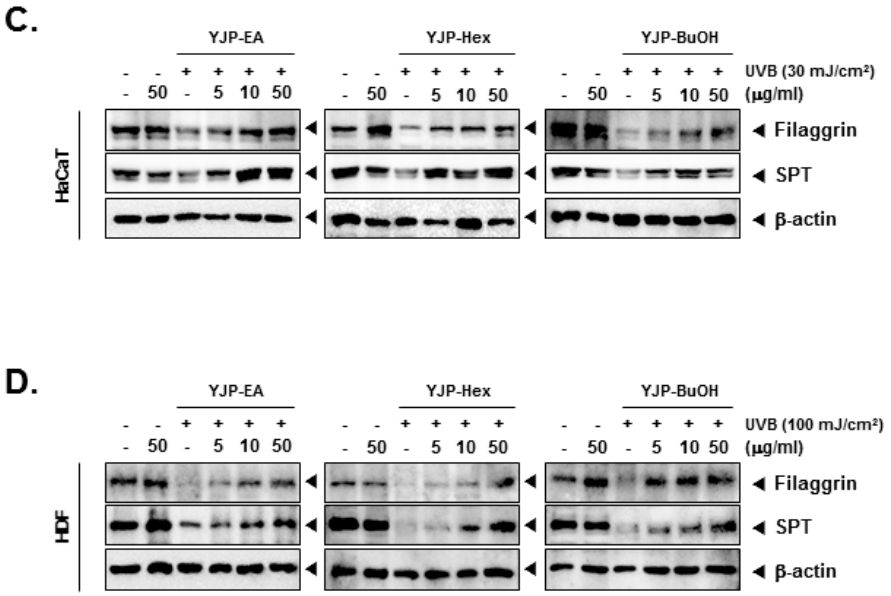

Figure 3. Moisture-recovery effects of YJP-EA, Hex, and BuOH on UVB-damaged HaCaT and HDF cells. (**A**,**B**) HaCaT and HDF cells were irradiated with UVB (30 or 100 mJ/cm^2) and treated with YJP-EA, Hex, and BuOH for 24 h. The hyaluronic acid was measured using a hyaluronan ELISA kit and detected with 450 nm. (**C**,**D**) The protein-expression levels of filaggrin and SPT were analyzed by Western blot analysis. All experiments were performed individually in triplicate. *** $p < 0.001$ vs. non-treated (NT) cells.

3.4. YJP Fractions Suppress Melanin Contents in Mouse Skin Melanoma B16F10 Cells

We first confirmed the cytotoxicity of YJP-EA, Hex, and BuOH on B16F10 cells using the MTT assay (Figure 4A). We confirmed that all YJP fractions had no cytotoxicity on B16F10 cells. Next, we measured the melanin contents from B16F10 cells treated with α-MSH (200 nM) and YJP-EA, Hex, and BuOH (0, 5, 10, 50 μg/mL) for 48 h. The cell lysates were measured using VARIOSKAN LUX (Thermo Fisher Scientific Inc., Waltham, MA, USA) at 490 nm. The melanin contents were increased by α-MSH, which is known to stimulate melanin synthesis, and then inhibited by YJP fractions. Next, the intracellular tyrosinase activity and mushroom tyrosinase activity were analyzed under the same conditions as that of the B16F10 cells (Figure 4C,D). α-MSH also induced both intracellular tyrosinase activity and mushroom tyrosinase activity. However, the YJP fractions significantly inhibited both activities in the B16F10 cells. From the whole cell lysate, we confirmed the protein-expression levels of TRP-1, -2, and tyrosinase and the microphthalmia-associated transcription factor (MITF), known as the enzymes and factors that promote melanin formation (Figure 4E). TRP-1, -2, tyrosinase, and MITF were induced by α-MSH; however, all YJP fractions reduced it. The results show that YJP-EA, Hex, and BuOH inhibit melanin contents and the related enzyme in mouse skin melanoma B16F10 cells.

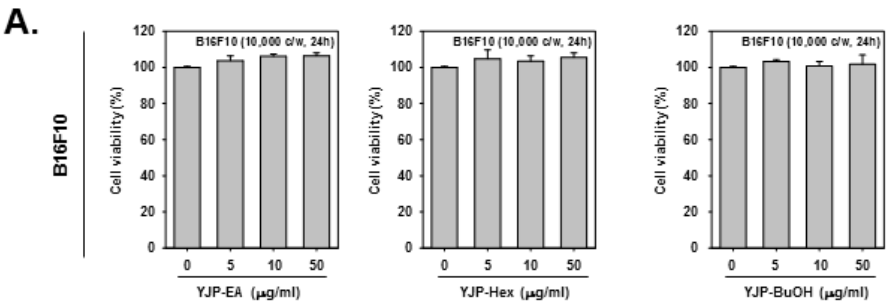

Figure 4. *Cont.*

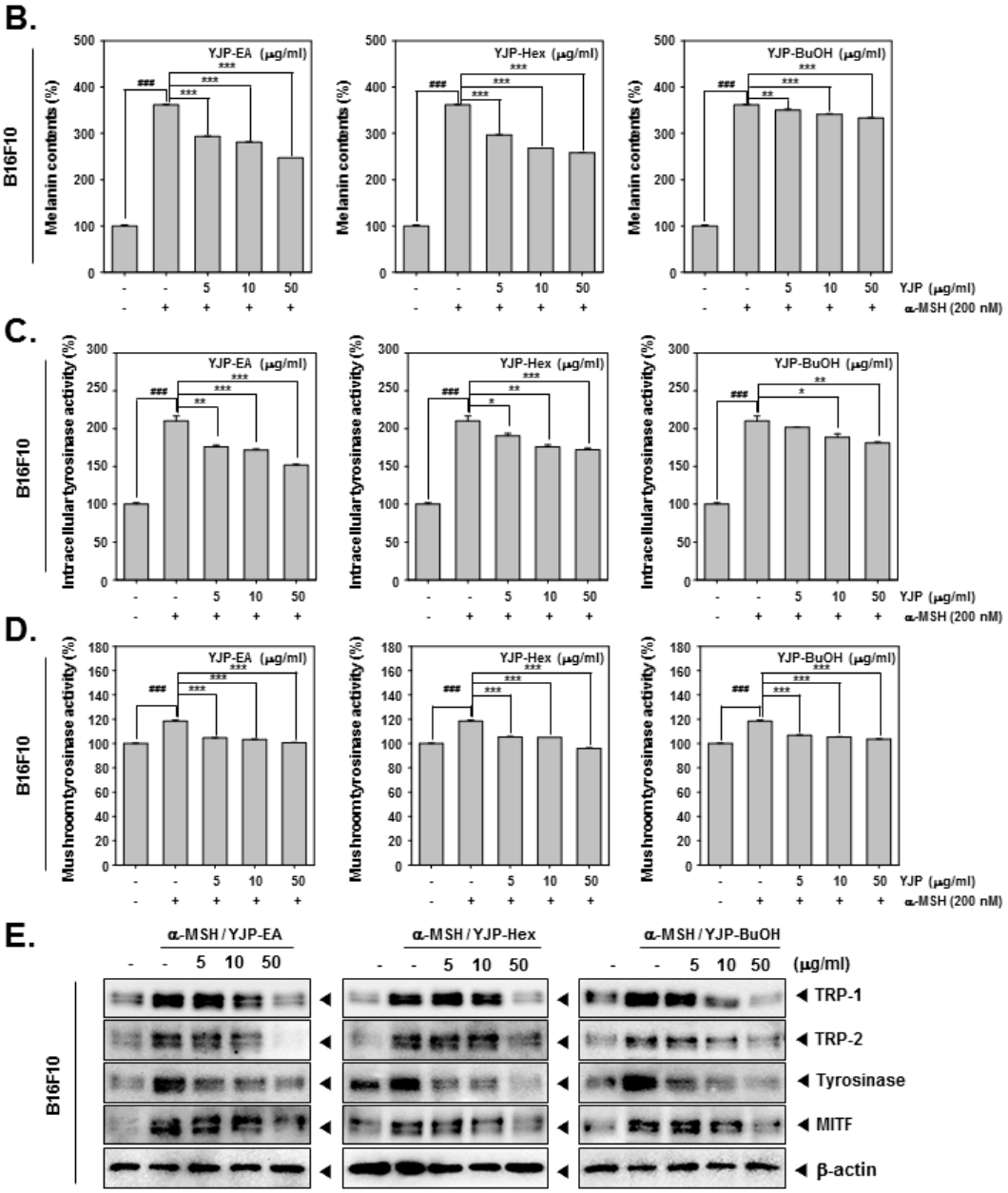

Figure 4. Melanin inhibition effects of YJP-EA, Hex, and BuOH on B16F10 cells. (**A**) B16F10 cells were treated with YJP-EA, Hex, and BuOH for 24 h. Next, the cell viability was measured using the MTT assay. (**B**) Melanin contents from α-MSH-stimulated B16F10 cell. The cells were treated with α-MSH (200 nM) and YJP-EA, Hex, and BuOH for 48 h. The cell lysates were measured at 490 nm. (**C**) To measure intracellular tyrosinase activity, the B16F10 cells were treated with -MSH (200 nM) and YJP-EA, Hex, and BuOH for 72 h. L-DOPA was added into the lysates and measured at 490 nm. (**D**) The mushroom tyrosinase activity was evaluated at -MSH (200 nM) and in YJP-EA-, Hex-, and BuOH-treated B16F10 cells. The supernatants with L-DOPA and tyrosinase were measured at 475 nm. (**E**) The whole cell lysates were analyzed by Western blot analysis. All experiments were performed individually in triplicate. *** $p < 0.001$ vs. α-MSH-treated cells, ** $p < 0.01$ vs. α-MSH-treated cells, and * $p < 0.05$ vs. α-MSH-treated cells. ### $p < 0.001$ vs. non-treated (NT) cells.

3.5. YJP Fractions Induce GSH/GSSG Imbalance and Inhibit ROS Production in HaCaT, HDF, and B16F10 Cells

Next, we investigated the antioxidant effects of YJP-EA, -Hex, and -BuOH in HaCaT, HDF, and B16F10 cells under UVB irradiation or α-MSH stimulation. In HaCaT and HDF cells, the ROS production and GSH/GSSG levels were measured with UVB-irradiated cells.

The B16F10 cells were stimulated by α-MSH. N-acetyl-l-cysteine (NAC) has been proven to prevent the development of oxidative stress and activate antioxidant enzymes [31]. We used NAC as a positive control. The HaCaT cells were irradiated with 30 mJ/cm^2 of UVB; the HDF cells were irradiated with 100 mJ/cm^2; and the B16F10 cells were stimulated with α-MSH (200 nM). The cells were then treated with NAC (3 mM) for 15 min or with YJP-EA, -Hex, and -BuOH (50 μg/mL) for 12 h. First, we evaluated the ROS production in HaCaT, HDF, and B16F10 cells. The cells were incubated with H_2DCF-DA and analyzed using a flow cytometer. Both UVB irradiation and α-MSH increased the ROS level in HaCaT, HDF, and B16F10 cells. However, YJP fractions reduced the increased-ROS production level (Figure 5A–C). Next, we evaluated the GSH and GSSG levels. The cells were treated the same as when the ROS production was measured. As shown in the results, in HaCaT, HDF, and B16F10 cells, both UVB irradiation and α-MSH reduced the GSH level and increased the GSSG level. As a result, it was confirmed that the GSSG/GSH ratio was increased by UVB irradiation and α-MSH. However, when the YJP fractions were treated, it was confirmed that the decreased GSH level recovered and the GSSG level decreased, despite UVB irradiation and α-MSH (Figure 5D–F).

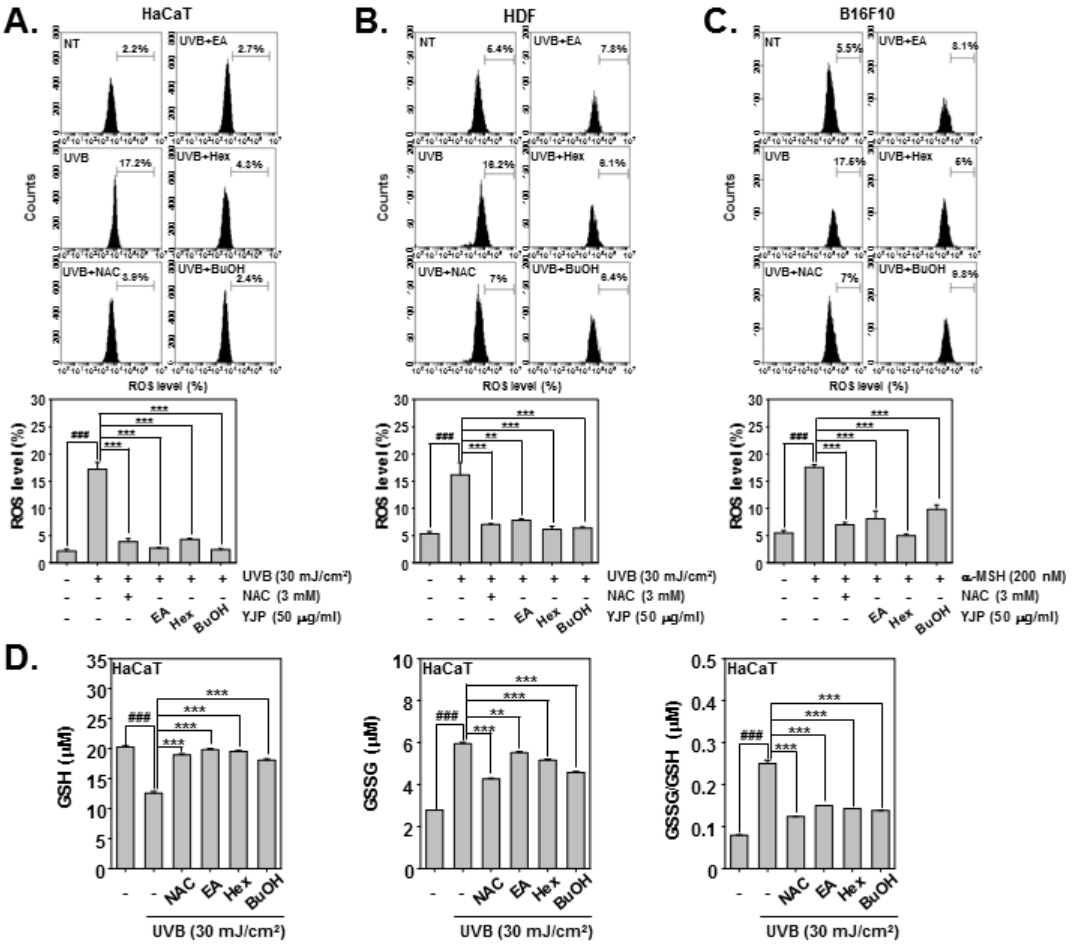

Figure 5. *Cont.*

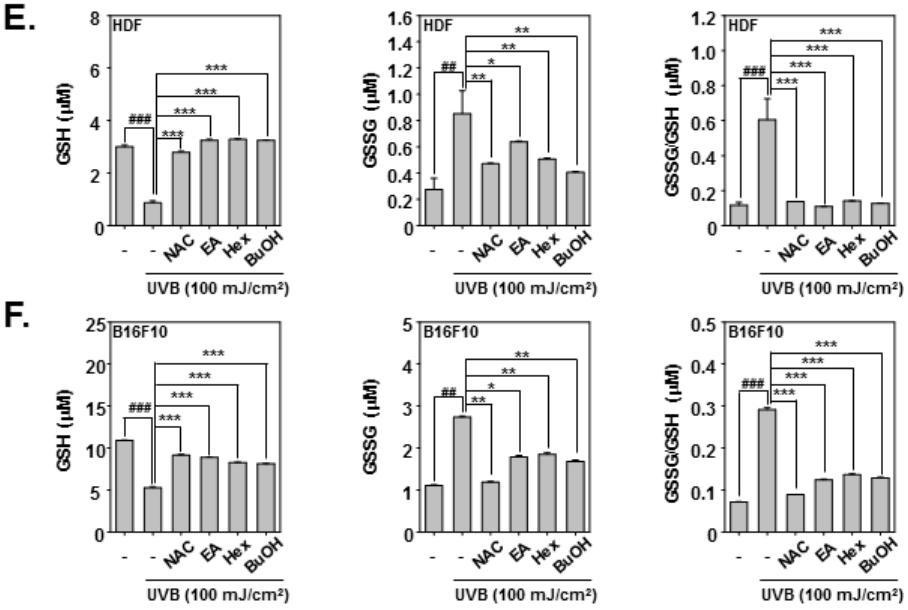

Figure 5. Antioxidant effects of YJP-EA, -Hex, and -BuOH on HaCaT, HDF, and B16F10 cells. HaCaT and HDF cells were irradiated with UVB; B16F10 cells were stimulated by α-MSH. We then treated them with NAC (3 mM) for 15 min or with YJP-EA, -Hex, and -BuOH (50 μg/mL) for 12 h. (**A**–**C**) The ROS production was analyzed by flow cytometer. (**D**–**F**) The GSH and GSSG levels were measured, and the GSSG/GSH ratio was evaluated in both cells. All experiments were performed individually in triplicate. ### $p < 0.001$ vs. non-treated (NT) cells, ## $p < 0.01$ vs. non-treated (NT) cells, *** $p < 0.001$ vs. UVB or α-MSH-stimulated cells, ** $p < 0.01$ vs. UVB or α-MSH-stimulated cells, and * $p < 0.05$ vs. UVB or α-MSH-stimulated cells.

4. Discussion

In our study, we analyzed and evaluated the anti-wrinkle, moisturizing, and whitening effects of Yuja-peel fractions (YJP-EA, -Hex, and -BuOH) in HaCaT, HDF, and B16F10 cells. Prior to the experiment, we first evaluated the toxicity of the three fractions on each cell, and we then conducted a sub-experiment by selecting a concentration with low toxicity. In addition, we stimulated HaCaT and HDF cells with UVB irradiation and B16F10 cells with α-MSH to create a hyperpigmented state [4,26,27].

To evaluate the antioxidant effects, we measured GSH and GSSG levels [16,17]. Under UVB irradiation, cells lost their antioxidant capacity. The ROS productions were increased by UVB; however, the YJP fractions reduced the ROS level in both HaCaT and HDF cells. In addition, the GSH level was reduced and GSSG level was increased by UVB irradiation. However, YJP-EA, -Hex, and –BuOH recovered the GSH level and reduced the GSSG level with N-acetyl-l-cysteine (NAC) [31]. These results demonstrate that YJP fractions have antioxidant effects on HaCaT and HDF cells.

The expression of MMPs (MMP-1, -9, -13), contributing to collagen degradation, were increased in UVB-irradiated HaCaT and HDF cells, while Collagen I was decreased [3,6,18]. However, YJP-EA, -Hex, and -BuOH inhibited MMP-1, -9, and -13 but restored Collagen I in the protein and mRNA levels. In addition, when the Pro-Collagen content was investigated, it was confirmed that the percentage of Type I Pro-Collagen, which had been reduced by UVB-irradiation, was restored by treatment with YJP-EA, -Hex, and -BuOH. These results demonstrate that YJP fractions have significant anti-wrinkle effects through regulating MMPs at low toxicity in both HaCaT and HDF cells.

Next, to confirm the moisturizing effect, we irradiated HaCaT and HDF cells with UVB [19]. We confirmed that the intracellular hyaluronic acid content from both cells were reduced by UVB irradiation and that the treatment of YJP fractions significantly increased the hyaluronic acid. To confirm this moisturizing effect, the protein expressions of filaggrin and SPT, which are key factors of hydration, were evaluated [21–23]. Both filaggrin and

SPT were suppressed under UVB irradiation; however, the YJP fractions induced their expression. These results show that YJP fractions can recover moisturization through regulating filaggrin and SPT in HaCaT and HDF cells.

In the B16F10 cells, we treated α-MSH to induce hyperpigmentation [25,26]. α-MSH induced hyperpigmentation, and as a result, it was confirmed that melanin content, intracellular tyrosinase activity, and mushroom tyrosinase activity were all increased in B16F10 cells [25,26]. Increased melanin content, intracellular tyrosinase activity, and mushroom tyrosinase activity were decreased by YJP-EA, -Hex, and -BuOH. Additionally, α-MSH-induced MITF, tyrosinase (TYR), tyrosinase-related protein 1 (TRP-1), and tyrosinase-related protein 2 (TRP-2) were all confirmed to have decreased protein expression levels after treatment with YJP fractions [26,27]. These results demonstrate that YJP fractions suppress hyperpigmentation through the modulation of MITF, TRP-1, TRP-2, and tyrosinase.

5. Conclusions

Our study demonstrated the potential effects of YJP fractions by confirming their anti-wrinkle, moisturizing, and whitening effects at low toxicity. Depending on the polarity and previous reports [32,33], it was assumed that YJP-BuOH includes flavonoid glycosides, YJP-EA contains limonoids and coumarins, and YJP-Hex is comprised of limonoids and some fatty acids. In particular, the yield of YJP-Hex from *C. junos* seed shells appears to be higher than that of other fractions, and thus there may be some economic advantages associated with product development. These results encourage a focus on the excellence of materials coming from nature.

Author Contributions: Conceptualization, Y.Y.J. and K.S.A.; methodology, Y.Y.J. and I.J.H.; writing—original draft preparation and writing—review and editing, M.L. and K.S.A. All authors have read and agreed to the published version of the manuscript.

Funding: This work was supported by a National Research Foundation of Korea (NRF) grant funded by the Korean government (MSIP) (NRF-2021R1I1A2060024, NRF-2022R1A5A8033794, NRF-2021R1F1A1049427, and NRF-2022R1I1A1A01071593).

Institutional Review Board Statement: Not applicable.

Informed Consent Statement: Not applicable.

Data Availability Statement: The data presented in this study are available on request from the corresponding author.

Conflicts of Interest: The authors declare no conflict of interest.

References

1. Jeong, J.W.; Lee, Y.C.; Kim, I.H.; Kim, J.H.; Lee, K.M. Manufacture condition of oleoresin using citrus peel. *Korean J. Food Sci. Technol.* **1998**, *30*, 139–145.
2. Zhang, S.; Duan, E. Fighting against Skin Aging: The Way from Bench to Bedside. *Cell Transplant.* **2018**, *27*, 729–738. [CrossRef] [PubMed]
3. Lee, J.E.; Lee, I.S.; Kim, K.C.; Yoo, I.D.; Yang, H.M. ROS Scavenging and Anti-Wrinkle Effects of Clitocybin A Isolated from the Mycelium of the Mushroom Clitocybe aurantiaca. *J. Microbiol. Biotechnol.* **2017**, *27*, 933–938. [CrossRef] [PubMed]
4. Wang, L.; Lee, W.; Oh, J.Y.; Cui, Y.R.; Ryu, B.; Jeon, Y.J. Protective Effect of Sulfated Polysaccharides from Celluclast-Assisted Extract of Hizikia fusiforme Against Ultraviolet B-Induced Skin Damage by Regulating NF-kappaB, AP-1, and MAPKs Signaling Pathways In Vitro in Human Dermal Fibroblasts. *Mar. Drugs* **2018**, *16*, 239. [CrossRef] [PubMed]
5. Cavinato, M.; Jansen-Durr, P. Molecular mechanisms of UVB-induced senescence of dermal fibroblasts and its relevance for photoaging of the human skin. *Exp. Gerontol.* **2017**, *94*, 78–82. [CrossRef]
6. Chae, S.; Piao, M.J.; Kang, K.A.; Zhang, R.; Kim, K.C.; Youn, U.J.; Nam, K.W.; Lee, J.H.; Hyun, J.W. Inhibition of matrix metalloproteinase-1 induced by oxidative stress in human keratinocytes by mangiferin isolated from Anemarrhena asphodeloides. *Biosci. Biotechnol. Biochem.* **2011**, *75*, 2321–2325. [CrossRef]
7. Lorz, L.R.; Yoo, B.C.; Kim, M.Y.; Cho, J.Y. Anti-Wrinkling and Anti-Melanogenic Effect of *Pradosia mutisii* Methanol Extract. *Int. J. Mol. Sci.* **2019**, *20*, 1043. [CrossRef]
8. Sies, H. Oxidative Stress: Concept and Some Practical Aspects. *Antioxidants* **2020**, *9*, 852. [CrossRef]

9. Jitca, G.; Osz, B.E.; Tero-Vescan, A.; Miklos, A.P.; Rusz, C.M.; Batrinu, M.G.; Vari, C.E. Positive Aspects of Oxidative Stress at Different Levels of the Human Body: A Review. *Antioxidants* **2022**, *11*, 572. [CrossRef]
10. Jung, Y.Y.; Ha, I.J.; Um, J.Y.; Sethi, G.; Ahn, K.S. Fangchinoline diminishes STAT3 activation by stimulating oxidative stress and targeting SHP-1 protein in multiple myeloma model. *J. Adv. Res.* **2022**, *35*, 245–257. [CrossRef]
11. Dai, X.; Wang, L.; Deivasigamni, A.; Looi, C.Y.; Karthikeyan, C.; Trivedi, P.; Chinnathambi, A.; Alharbi, S.A.; Arfuso, F.; Dharmarajan, A.; et al. A novel benzimidazole derivative, MBIC inhibits tumor growth and promotes apoptosis via activation of ROS-dependent JNK signaling pathway in hepatocellular carcinoma. *Oncotarget* **2017**, *8*, 12831–12842. [CrossRef] [PubMed]
12. Starkov, A.A. The role of mitochondria in reactive oxygen species metabolism and signaling. *Ann. N. Y. Acad. Sci.* **2008**, *1147*, 37–52. [CrossRef] [PubMed]
13. Caliri, A.W.; Tommasi, S.; Besaratinia, A. Relationships among smoking, oxidative stress, inflammation, macromolecular damage, and cancer. *Mutat. Res. Rev. Mutat. Res.* **2021**, *787*, 108365. [CrossRef] [PubMed]
14. de Jager, T.L.; Cockrell, A.E.; Du Plessis, S.S. Ultraviolet Light Induced Generation of Reactive Oxygen Species. *Adv. Exp. Med. Biol.* **2017**, *996*, 15–23. [CrossRef] [PubMed]
15. Masaki, H. Role of antioxidants in the skin: Anti-aging effects. *J. Derm. Sci.* **2010**, *58*, 85–90. [CrossRef] [PubMed]
16. Meng, Q.; Velalar, C.N.; Ruan, R. Effects of epigallocatechin-3-gallate on mitochondrial integrity and antioxidative enzyme activity in the aging process of human fibroblast. *Free Radic. Biol. Med.* **2008**, *44*, 1032–1041. [CrossRef]
17. Kim, S.Y.; Kang, H.T.; Choi, H.R.; Park, S.C. Biliverdin reductase A in the prevention of cellular senescence against oxidative stress. *Exp. Mol. Med.* **2011**, *43*, 15–23. [CrossRef]
18. Gao, W.; Wang, Y.S.; Hwang, E.; Lin, P.; Bae, J.; Seo, S.A.; Yan, Z.; Yi, T.H. *Rubus idaeus* L. (red raspberry) blocks UVB-induced MMP production and promotes type I procollagen synthesis via inhibition of MAPK/AP-1, NF-kappabeta and stimulation of TGF-beta/Smad, Nrf2 in normal human dermal fibroblasts. *J. Photochem. Photobiol. B Biol.* **2018**, *185*, 241–253. [CrossRef]
19. Papakonstantinou, E.; Roth, M.; Karakiulakis, G. Hyaluronic acid: A key molecule in skin aging. *Derm.-Endocrinol.* **2012**, *4*, 253–258. [CrossRef]
20. Kim, E.; Hwang, K.; Lee, J.; Han, S.Y.; Kim, E.M.; Park, J.; Cho, J.Y. Skin Protective Effect of Epigallocatechin Gallate. *Int. J. Mol. Sci.* **2018**, *19*, 173. [CrossRef]
21. Kim, E.; Kim, D.; Yoo, S.; Hong, Y.H.; Han, S.Y.; Jeong, S.; Jeong, D.; Kim, J.H.; Cho, J.Y.; Park, J. The skin protective effects of compound K, a metabolite of ginsenoside Rb1 from Panax ginseng. *J. Ginseng Res.* **2018**, *42*, 218–224. [CrossRef] [PubMed]
22. Kim, C.; Ji, J.; Ho Baek, S.; Lee, J.H.; Ha, I.J.; Lim, S.S.; Yoon, H.J.; Je Nam, Y.; Ahn, K.S. Fermented dried Citrus unshiu peel extracts exert anti-inflammatory activities in LPS-induced RAW264.7 macrophages and improve skin moisturizing efficacy in immortalized human HaCaT keratinocytes. *Pharm. Biol.* **2019**, *57*, 392–402. [CrossRef] [PubMed]
23. Takeda, S.; Shimoda, H.; Takarada, T.; Imokawa, G. Strawberry seed extract and its major component, tiliroside, promote ceramide synthesis in the stratum corneum of human epidermal equivalents. *PLoS ONE* **2018**, *13*, e0205061. [CrossRef] [PubMed]
24. Riley, P.A. Melanogenesis and melanoma. *Pigment Cell Res.* **2003**, *16*, 548–552. [CrossRef] [PubMed]
25. Bae, J.S.; Han, M.; Yao, C.; Chung, J.H. Chaetocin inhibits IBMX-induced melanogenesis in B16F10 mouse melanoma cells through activation of ERK. *Chem. Biol. Interact.* **2016**, *245*, 66–71. [CrossRef] [PubMed]
26. D'Mello, S.A.; Finlay, G.J.; Baguley, B.C.; Askarian-Amiri, M.E. Signaling Pathways in Melanogenesis. *Int. J. Mol. Sci.* **2016**, *17*, 1144. [CrossRef]
27. Kim, H.J.; Yonezawa, T.; Teruya, T.; Woo, J.T.; Cha, B.Y. Nobiletin, a polymethoxy flavonoid, reduced endothelin-1 plus SCF-induced pigmentation in human melanocytes. *Photochem. Photobiol.* **2015**, *91*, 379–386. [CrossRef]
28. Ahn, K.S.; Sethi, G.; Aggarwal, B.B. Simvastatin potentiates TNF-α-induced apoptosis through the down-regulation of NF-kappaB-dependent antiapoptotic gene products: Role of IkappaBα kinase and TGF-β-activated kinase-1. *J. Immunol.* **2007**, *178*, 2507–2516. [CrossRef]
29. Sethi, G.; Ahn, K.S.; Sandur, S.K.; Lin, X.; Chaturvedi, M.M.; Aggarwal, B.B. Indirubin enhances tumor necrosis factor-induced apoptosis through modulation of nuclear factor-kappa B signaling pathway. *J. Biol. Chem.* **2006**, *281*, 23425–23435. [CrossRef]
30. Lee, J.H.; Chinnathambi, A.; Alharbi, S.A.; Shair, O.H.M.; Sethi, G.; Ahn, K.S. Farnesol abrogates epithelial to mesenchymal transition process through regulating Akt/mTOR pathway. *Pharm. Res.* **2019**, *150*, 104504. [CrossRef]
31. Zukowski, P.; Maciejczyk, M.; Matczuk, J.; Kurek, K.; Waszkiel, D.; Zendzian-Piotrowska, M.; Zalewska, A. Effect of N-Acetylcysteine on Antioxidant Defense, Oxidative Modification, and Salivary Gland Function in a Rat Model of Insulin Resistance. *Oxid. Med. Cell Longev.* **2018**, *2018*, 6581970. [CrossRef] [PubMed]
32. Shin, J.; Song, H.Y.; Lee, M. Sudachinoid- and Ichangensin-Type Limonoids from *Citrus junos* Downregulate Pro-Inflammatory Cytokines. *Int. J. Mol. Sci.* **2020**, *21*, 6963. [CrossRef] [PubMed]
33. Song, H.Y.; Jo, A.; Shin, J.; Lim, E.H.; Lee, Y.E.; Jeong, D.E.; Lee, M. Anti-Inflammatory Activities of Isogosferol, a Furanocoumarin Isolated from *Citrus junos* Seed Shells through Bioactivity-Guided Fractionation. *Molecules* **2019**, *24*, 4088. [CrossRef] [PubMed]

antioxidants

MDPI

Article

Comparing Metabolomic and Essential Oil Fingerprints of *Citrus australasica* F. Muell (Finger Lime) Varieties and Their In Vitro Antioxidant Activity

Emily Cioni [1,†], Chiara Migone [1,†], Roberta Ascrizzi [1,2,3], Beatrice Muscatello [1,3], Marinella De Leo [1,2,3,*], Anna Maria Piras [1,3], Ylenia Zambito [1,2,3], Guido Flamini [1,2,3] and Luisa Pistelli [1,2,3]

1 Dipartimento di Farmacia, Università di Pisa, via Bonanno 33, 56126 Pisa, Italy
2 Centro Interdipartimentale di Ricerca "Nutraceutica e Alimentazione per la Salute", Via del Borghetto 80, Università di Pisa, 56124 Pisa, Italy
3 Centro per l'Integrazione della Strumentazione dell'Università di Pisa (CISUP), Lungarno Pacinotti 43, 56126 Pisa, Italy
* Correspondence: marinella.deleo@unipi.it
† These authors contributed equally to this work.

Abstract: Comparative chemical analyses among peel and pulp essential oils (EOs) and methanolic extracts of four *Citrus australasica* varieties (Red, Collette, Pink Ice, and Yellow Sunshine), and the hybrid *Faustrime*, were performed using GC-MS and UHPLC-DAD-HR-Orbitrap/ESI-MS. Peel and pulp extracts were also analysed for their in vitro antioxidant activity on a Balb/3T3 clone A31 mouse embryo fibroblast cell line. The results of peel and pulp EOs were mainly characterised by monoterpenes and sesquiterpenes, respectively. All peels displayed a higher total phenol content (TPC) than pulps, and consequently a greater antioxidant activity. Collette peels and Pink Ice pulps showed the highest amount of identified flavonoids (e.g., luteolin, isosakuranetin, and poncirin derivatives). Collette and Red peels were rich in anthocyanins (delphinidin and petunidin glycosides), exhibiting the maximum protective activity against induced oxidative damage. In conclusion, finger lime fruits are good sources of health-promoting phytocomplexes, with the Red, Collette, and Pink Ice varieties being the most promising.

Keywords: *Citrus australasica*; finger lime; phenols; volatiles; antioxidant; UHPLC-MS/Orbitrap; chemometrics

1. Introduction

The *Citrus* genus, belonging to the Rutaceae family, includes widely distributed, consumed, and studied species, such as *Citrus limon* (L.) Osbeck (lemon), *C. medica* L. (cedar), *C.* × *aurantium* L. (bitter orange), *C. paradisi* Macfad. (grapefruit), *C. reticulata* Blanco (tangerine), and *C. sinensis* (L.) Osbeck (orange), but also the lesser known *C. australasica* F. Muell [1,2]. *Citrus australasica* is a small tree native to Australia which is recently acquiring growing commercial interest in Italy and in Europe, in general, due to the uniqueness of its fruits that are used in gourmet culinary preparations. *Citrus australasica* is commonly called finger lime or lemon caviar, because its spindle-shaped fruits are finger-like, while the vesicles of its pulp are similar to pearls of caviar. There are several varieties and hybrids of *C. australasica* that differ macroscopically in peel and pulp color, and have more or less acidulous or floral odorous notes [3]. These differences reflect changes in qualitative and quantitative chemical composition, and may mean a greater or lesser content of bioactive compounds and/or secondary metabolites of therapeutic interest. Previous evidence reports that *Citrus* fruits are a source of both macronutrients (e.g., simple sugars, fibers, and water) and micronutrients (e.g., folic acid, thiamine, niacin, vitamin C, and vitamin B6). Their pulps, peels, and seeds contain minerals (potassium, calcium, phosphorus,

and magnesium), and are free of sodium and cholesterol; moreover, they are low in proteins and fats [4]. However, their secondary metabolites are the constituents of major interest, especially flavonoids (flavones, flavonols, flavanones, and flavanonols), phenolic acids (hydroxybenzoic acids and hydroxycinnamic acids), anthocyanins, coumarins, and limonoids, which have demonstrated antioxidant, anti-inflammatory, anti-cancer, and neuro-cardioprotective activities [5,6]. Among the flavonoids, the most common aglycones in the *Citrus* genus are naringenin, hesperetin, apigenin, nobiletin, tangeretin, and quercetin, often carrying saccharide chains that are composed of glucose, rhamnose, rutinose, and neohesperidose. Sinapic, *p*-coumaric, ferulic, caffeic, and gallic acids are the most common phenolic acids that have been identified in the fruits of this genus. Furthermore, among the bitter limonoid constituents, limonin, nomilin, obacunone, and limonexic acid are also present [7].

More than 170 molecules with antioxidant activity have been identified in the most common fruits of the *Citrus* genus. The antioxidant activity could be attributed to the whole phytocomplex, which is capable of ensuring the maintenance of healthy cell structure and function through the inactivation of free radicals, the inhibition of lipid peroxidation, and the prevention of harmful oxidative mechanisms [8]. Free radicals, or reactive oxygen species (ROS), by-products of the metabolism of aerobic cells, can generate other peroxidic and hydroperoxidic radicals that are capable of interacting with lipid molecules, or, in a cytotoxic manner, with nucleic acids and proteins essential for life, damaging them or altering their functionality. Therefore, the search for molecules that are capable of counteracting these free radicals is of great interest [7,9].

In this context, *C. australasica* fruits attract great attention as a potential source of bioactive molecules with antioxidant properties. To the best of our knowledge, few current studies have been reported in the literature, with most focused on volatile components of Alstonville, Judy's Everbearing, and Durham's Emerald varieties, along with *Faustrime* hybrid [10,11]; total phenolic content of four Florida-grown selections [3]; the phenolic composition of XiangBin and LiSiKe varieties [2]; and a Spanish cultivated plant [12].

Based on the previous promising studies and the growing economic, gastronomic, and health-related demands on this peculiar *Citrus* fruit, the aim of the present study was to carry out a full comparative chemical analysis on both volatile and non-volatile components of the peel and pulp of *C. australasica* varieties, with particular attention to phenolic compounds and anthocyanins, still lacking in the literature. To this purpose, four *C. australasica* varieties (Collette, Yellow Sunshine, Pink Ice, and Red), and the hybrid species *Faustrime* (*Monocitrus australasica* × *Fortunella* sp. × *Citrus aurantifolia*) (Figure 1A), were selected. The metabolomic profile of all varieties was investigated by means of ultra-high performance liquid chromatography (UHPLC), coupled with a diode array detector (DAD) and a high-resolution Orbitrap-based electrospray ionization source mass spectrometer (HR-Orbitrap/ESI-MS); meanwhile, the EO composition was established through gas chromatography coupled with mass spectrometry (GC/MS). All of the extracts were also investigated for their in vitro antioxidant activity on a Balb/3T3 clone A31 mouse embryo fibroblast cell line. This study is part of a larger project conducted by our research group, which is aimed at re-evaluating the beneficial properties of fruits of the genus *Citrus*, due to their high content of bioactive compounds belonging to the class of polyphenols and triterpenoids [13–17].

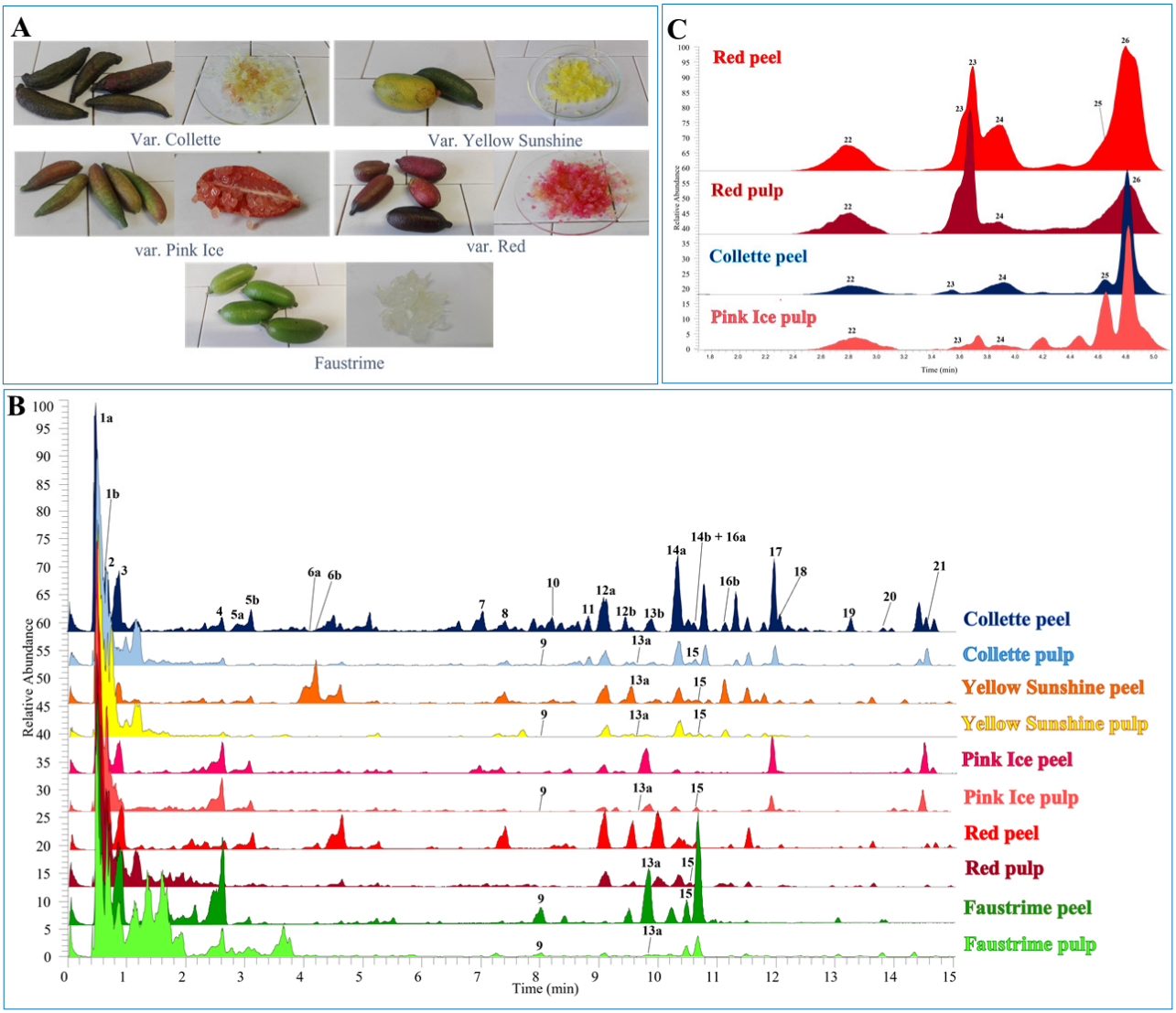

Figure 1. (**A**) *Citrus australasica* studied varieties; (**B**) comparison of chromatograms of *C. australasica* peels and pulps extracts, recorded by UHPLC-HR-Orbitrap/ESI-MS analyses in negative ion mode; (**C**) anthocyanin HR-Orbitrap/ESI-MS profiles of *C. australasica* peels and pulps, recorded in positive ion mode.

2. Materials and Methods

2.1. Chemicals and Reagents

UHPLC-grade *n*-hexane, acetonitrile, methanol, water, and formic acid Supelco® were purchased from Merck KGaA (Darmstadt, Germany). All analytical-grade solvents were purchased from VWR (Milano, Italy). Standards of rutin, hesperidin, and gallic acid were purchased from Merck KGaA (Darmstadt, Germany), cyanidin 3-*O*-glucoside chloride was purchased from Extrasynthese (Extrasynthese, France), and luteolin-4′-*O*-neohesperidoside was previously obtained in our laboratory by isolation from plant materials and characterised by 1D- and 2D-NMR techniques. Folin–Ciocâlteu reagent was purchased from Merck KGaA (Darmstadt, Germany). The Balb/3T3 clone A31 mouse embryo fibroblast cell line was purchased from the American Type Culture Collection LGC standards (ATCC CCL163, Milan, Italy) and propagated as indicated by the supplier. Dulbecco's Modified Eagle's medium (DMEM), 0.01 M pH 7.4 phosphate buffer saline without Ca^{2+} and Mg^{2+} (PBS), bovine calf serum (BCS), glutamine, and antibiotics (penicillin/streptomycin) were obtained from Merck KGaA (Darmstadt, Germany). Cell proliferation reagent WST-1 was provided by Roche Diagnostic (Milan, Italy).

2.2. Plant Materials and Non-Volatile Extract Preparation

The fruits of *C. australasica* varieties (Red, Collette, Pink Ice, and Yellow Sunshine), and the hybrid species *Faustrime* (Figure 1A), were provided by the Agrumi Lenzi Company (Pescia, Pistoia, Italy) in October 2019. Fruits (6 for each variety) were collected at the ripening stage from plants that were growing in pots. For each fruit, peels were separated from pulps. For the extraction of non-volatile compounds, peels were dried in an oven at 40 °C, while pulps were freeze-dried (Modulyo, Pirani 501, Edwards, UK). The dried material was stored at room temperature, and protected from light until extraction. A portion of fresh material was stored at −20 °C for essential oil preparation (see Section 2.5) and anthocyanin extraction.

For each variety, powdered peels and pulps were first defatted with *n*-hexane, then subjected to extraction with methanol (solid:liquid mg/mL ratio 1:20 w/v) via dynamic maceration (120 rpm) with a digital orbital shaker (IKA™ KS 501, Minerva S.r.l., Pisa, Italy) for three consecutive days at room temperature, renewing the solvent every 24 h. Finally, the solvent was removed under vacuum to obtain dry extracts, as reported in Table S1.

Anthocyanins were extracted from the peels of Red and Collette varieties, and from the pulps of Red and Pink Ice varieties, and characterised by visible pigmentation. For extraction, 500 mg of defrosted plant material were placed in 3 mL of a 2% methanol/hydrochloric acid mixture for 15 min under stirring, then centrifuged for 5 min at 4000 rpm. The supernatants were withdrawn using a syringe, and directly analysed in triplicate using UHPLC-HR-ESI-MS.

2.3. Determination of the Total Polyphenol Content

Total polyphenol content (TPC) was evaluated in the methanolic extracts of *C. australasica* peels and pulps following the colorimetric method of Folin–Ciocâlteu [18]. Methanol solutions (10 mg/mL) of peel and pulp extracts were diluted with water until a final concentration of 0.48 mg/mL was reached for peels and 0.70 mg/mL for pulps. Samples were prepared by adding 1 mL of distilled water, 100 µL of Folin–Ciocâlteu reagent, and 300 µL of Na_2CO_3 (20%) to 500 µL of the aqueous solutions; then, the samples were mixed and incubated in the dark at room temperature for 2 h. The absorbance was measured at 765 nm against a blank solution using a UV-VIS spectrophotometer (Lambda 25, Perkin-Elmer, Waltham, MA, USA). Gallic acid was employed as the standard in the concentration range 0.005–0.030 mg/mL (R^2 = 0.999). All of the samples were tested in quadruplicate, and the results were expressed as mg of gallic acid equivalents (GAE)/g of dry weight (DW) [19].

2.4. UHPLC-DAD-HR-Orbitrap/ESI-MS Analyses

2.4.1. Quali-Quantitative Analyses of Phenols

Quali-quantitative chemical analyses were performed via UHPLC using a Vanquish Flex Binary pump that was coupled with a DAD and an HR Q Exactive Plus MS, based on Orbitrap technology, equipped with an ESI source, a hybrid-quadrupole analyser and Xcalibur 3.1 software (Thermo Fischer Scientific Inc., Bremem, Germany). Elutions were conducted at a flow rate of 0.5 mL/min, using a splitting system of 1:1 to an MS detector (250 µL/min) and a DAD/UV detector (250 µL/min), respectively.

For each variety of *C. australasica*, methanol extracts were solubilized in methanol at concentrations of 2 and 10 mg/mL for the peels and the pulps, respectively. These solutions were prepared in triplicate, and centrifuged for 5 min at 4000 rpm in order to remove suspended particles. Volumes of 5 µL of the supernatants were injected into the LC-MS system. Chromatographic analyses were performed using a 2.1 × 100 mm, 2.6 µm, Kinetex® Biphenyl C-18 column provided from a Security Guard™ Ultra Cartridge (Phenomenex, Bologna, Italy), and a mixture of HCOOH in H_2O 0.1% v/v (solvent A) and acetonitrile in H_2O 0.1% v/v (solvent B) as the mobile phase. A linear gradient was used, increasing from 5 to 35% B in 15 min for both the methanol extracts of peels and pulps. DAD data were recorded in a 200–600 nm range, with the three preferential channels set at 254, 280, and 325 nm, which are typical absorbances for phenolic compounds. The HR-MS results were

acquired in a m/z scan range of 250–1200 in negative ion mode, operating in full (resolution 70,000 and maximum injection time of 220 ms) and data dependent-MS/MS (resolution 17,500 and maximum injection time of 60 ms). The used ionization parameters were the following: nebulization voltage of 3500 V, capillary temperature of 300 °C, sheath gas (N_2) 20 arbitrary units, auxiliary gas (N_2) 3 arbitrary units, and an HCD (higher-energy C- trap dissociation) of 18 eV.

In order to quantify the phenolic compounds that were identified in the five methanol extracts of *C. australasica* varieties, four calibration curves were constructed using rutin as the external standard for flavonol glycosides, hesperidin for flavanones glycosides, luteolin 4′-*O*-neohesperidoside for flavone glycosides, and chlorogenic acid for hydroxycinnamic acids and their esters. Stock solutions of 1 mg/mL of each standard were prepared, and then different concentrations were obtained using serial dilutions. Rutin, hesperidin, and luteolin 4′-*O*-neoesperidoside were prepared in triplicate acetonitrile solutions in a concentration range of 15.63–1.95 μg/mL, while concentrations of 200–20 μg/mL were used for the chlorogenic acid standard. Integration of the peak areas obtained for each standard in UHPLC-HR-MS was related to the respective concentration, and the equation of the resulting curve was used to quantify the phenolic compounds. The obtained curves showed a good linearity in the range of prepared concentrations and correlation coefficients (R^2) equal to 0.993 for rutin, 0.990 for hesperidin, 0.995 for luteolin 4′-*O*-neoesperidoside, and 0.999 for chlorogenic acid, were obtained. The amount of each compound was calculated using Microsoft® Office Excel, and expressed as μg/g of dried peel or freeze-dried pulp (DW) ± standard deviation.

2.4.2. Quali-Quantitative Analyses of Anthocyanins

The anthocyanin extracts were analysed in triplicate using UHPLC-DAD-HR-ESI-MS. The solutions (5 μL injection volume) were injected in a 2.1 × 100 mm, 2.6 μm, Kinetex® Biphenyl C-18 column provided by a Security Guard™ Ultra Cartridge (Phenomenex, Bologna, Italy), at a flow rate of 0.5 mL/min. A mixture of HCOOH in H_2O 0.1% v/v (solvent A) and acetonitrile in H_2O 0.1% v/v (solvent B) was used for the elution, according to a linear gradient from 5 to 20% B in 5 min. UV data were recorded using 515 nm as a detection wavelength, the typical absorbance of anthocyanins. The HR-MS data were acquired in a m/z scan range of 120–1200 in positive ion mode, operating in full and data dependent-MS/MS using the same ionization parameters as for phenols.

In order to quantify the anthocyanins in the peels of the Collette and Red varieties, as well as in the pulps of Red and Pink Ice varieties, a calibration curve was constructed with cyanidin 3-*O*-glucoside as an external standard. Triplicate acetonitrile solutions at the concentrations of 0.05, 0.025, and 0.0025 μg/mL were prepared, beginning from a stock 1 mg/mL solution. By correlating the integrations of the peak areas with the respective standard concentrations, a curve was obtained that showed good linearity in the selected concentration range, and an R^2 equal to 0.996. The amount of the anthocyanins identified in the plant material was obtained by Microsoft® Office Excel, and finally expressed as μg/g of dried peel or freeze-dried pulp (DW) ± standard deviation.

2.5. Essential Oils (EOs) Hydrodistillation and Analysis

For all of the samples, 15 g of defrosted peels and 30 g of fresh pulps (after removal of the seeds) were subjected to hydrodistillation in a standard Clevenger apparatus for 2 h. The hydrodistillation duration was experimentally determined as the time necessary for the complete EO volatilisation from the samples. For each sample, triplicates were performed. The hydrodistillation yields could not be evaluated, given the small material amount; thus, the volatile fraction was captured in HPLC-grade *n*-hexane in the Clevenger apparatus. The EOs in HPLC-grade *n*-hexane were stored in amber-glass vials and maintained at –20 °C until analysis.

The hydrodistilled samples were injected into a GC-MS apparatus. Gas chromatography–electron impact mass spectrometry (GC-EIMS) analyses were performed with an Agilent

7890B gas chromatograph (Agilent Technologies Inc., Santa Clara, CA, USA) that was equipped with an Agilent HP-5MS (Agilent Technologies Inc., Santa Clara, CA, USA) capillary column (30 m × 0.25 mm; coating thickness 0.25 μm) and an Agilent 5977B single quadrupole mass detector (Agilent Technologies Inc., Santa Clara, CA, USA). The analytical conditions used were as follows: injector and transfer line temperatures 220 and 240 °C, respectively; oven temperature programmed from 60 to 240 °C at 3 °C/min; carrier gas helium at 1 mL/min; injection of 1 μL (0.5% HPLC grade *n*-hexane solution); split ratio 1:25. The acquisition parameters used were as follows: full scan; scan range: 30–300 m/z; scan time: 1.0 sec. The identification of the constituents was based on a comparison of their retention times with those of authentic samples (when available), comparing their linear retention indices relative to the series of *n*-hydrocarbons. Computer matching was also used against a commercial [20] and a laboratory-developed mass spectra library that was built up from pure substances and components of commercial essential oils of known composition, and from MS literature data [21].

2.6. Cell Viability

Cell viability evaluations of *C. australasica* extracts were performed using the Balb/3T3 clone A31 cell line. Cells were grown in complete DMEM containing 10% bovine calf serum (BCS), 4 mM glutamine, and 100 U/mL:100 μg/mL penicillin:streptomycin. Balb/3T3 clone A31 fibroblast cells were seeded in 96-well culture plates at a concentration of 10^4 cells per well, incubated at 37 °C and 5% CO_2, and left to proliferate for 24 h prior to the incubation with the samples. The culture medium from each well was removed and replaced with a medium containing pre-dissolved sample in dimethyl sulfoxide (DMSO), and diluted with complete DMEM at different concentrations. Cells incubated with fresh growth medium were used as a control. The DMSO percentage in control and extract samples was kept at 1% v/v. With a view to the assessment of antioxidant effects, cytotoxicity ranges of peel and pulp extracts were set on GAE equivalents, resulting in 15–120 μg/mL for peels, and 30–300 μg/mL for pulps. After 2 h of incubation, cell viability was assessed using WST-1 tetrazolium salt reagent diluted to 1:10, and incubated for 4 h at 37 °C and 5% CO_2. Measurements of formazan dye absorbance were carried out at 450 nm, with the reference wavelength of 655 nm, using a microplate reader (BioTek 800/TS, Thermo Scientific).

2.7. Cell Treatment and Oxidative Stress

Adherent Balb/3T3 fibroblast cells, grown on 96-well culture plates, were incubated for 2 h with peel and pulp extracts that were diluted to polyphenol concentrations of 0.25, 0.50, and 1.00 μg/mL GAE in complete DMEM (Table S2). After the treatment, the cells were washed with phosphate buffered saline (PBS), and stressed with 1500 μM of commercial H_2O_2 for 1 h. Fibroblast cells incubated with H_2O_2 without sample treatment were considered as reference for the oxidative stress. The cells were evaluated for viability by means of WST-1 reagent. Cell viability percentages were referred to Balb/3T3 control cells, in the absence of treatment and without H_2O_2 incubation [22].

2.8. Statistical Analyses

All of the analyses were performed with JMP® Pro 14.0.0 (SAS Institute Inc., Cary, NC, USA) software.

For the statistical evaluation of all the EO compositions, an 89 × 10 correlation matrix (89 individual compounds × 10 samples = 890 data) was used, while for composition of phenols and anthocyanins, a 28 × 10 correlation matrix (28 individual compounds × 10 samples = 280 data) was applied. In order to perform the principal component analysis (PCA), linear regressions were operated on mean-centred, unscaled data to select the two highest principal components (PCs). This unsupervised method reduced the dimensionality of the multivariate data of the matrix, whilst preserving most of the variance [23]. For the essential oil analyses, the chosen PC1 and PC2 explained 58.5% and 20.0% of the variance, respectively, for a total explained variance of 78.5%. For the non-volatile components, the

chosen PC1 and PC2 explained 52.9% and 25.1% of the studied variance, respectively, for a total studied variance of 78.0%. A hierarchical cluster analysis (HCA) was performed using Ward's method, with Euclidean distances as a measure of similarity. The observations of the groups of samples performed with HCA and the PCA unsupervised methods can be applied even when there are no available reference samples that can be used as a training set to establish the model.

The significant difference (p value < 0.05) between groups of values was evaluated using a one-way ANOVA.

3. Results and Discussion

3.1. Polyphenol Content of Finger Lime Fruits

The TPC was determined for both peels and pulps of the four varieties of *C. australasica* (Red, Collette, Pink Ice, and Yellow Sunshine), and the hybrid species *Faustrime* (Table 1). In general, the results highlighted significantly different TPC among the varieties, but always a higher content of polyphenols in peels than pulps. Specifically, Red and Pink Ice peels had similar TPC values that were higher than the other varieties (9.1 ± 0.2 and 8.2 ± 0.2 mg of GAE/g of DW, respectively). Meanwhile, the hybrid species *Faustrime* was the most lacking in TPC, as shown by the quantitative datum 4.9 ± 0.1 mg of GAE/g DW. Regarding the pulps, Pink Ice and Collette were the two varieties that were most abundant in polyphenols (6.4 ± 0.2 and 5.6 ± 0.2 mg of GAE/g DW, respectively); *Faustrime* was confirmed to be poor in TPC, as was Yellow Sunshine variety (3.1 ± 0.2 and 2.6 ± 0.1 mg of GAE/g DW, respectively). Even though Yellow Sunshine peels had a TPC value that was comparable to the other *C. australasica* varieties, a significant decrease was observed in the pulps (Table 1). Compared to previous results reported by [12], all of the extracts showed higher TPC levels in both peels and pulps.

Table 1. Total polyphenol content (TPC) of *Citrus australasica* peel and pulp extracts, expressed as mg of gallic acid equivalents (mg GAE) for mass of dry weight (g DW) ± standard deviation (SD).

Finger Lime Varieties	Peel	Pulp
	mg GAE/g DW ± SD	**mg GAE/g DW ± SD**
Red	9.1 ± 0.2	5.0 ± 0.2
Collette	7.4 ± 0.2	5.6 ± 0.2
Pink Ice	8.2 ± 0.2	6.4 ± 0.2
Yellow Sunshine	6.8 ± 0.2	2.6 ± 0.1
Faustrime	4.9 ± 0.1	3.1 ± 0.2

3.2. Metabolomic Fingerprint and Quantitative Analysis of Non-Volatile Components

3.2.1. Phenol Composition

The quali-quantitative analyses of *C. australasica* fruits were performed using UHPLC-DAD-HR-Orbitrap/ESI-MS technique. The chromatographic profiles of all peels and pulps showed similarities and differences, both within the same variety and among different varieties (Figure 1B).

The tentative identification of constituents was performed by comparing their elution order, UV data, HR full mass spectra, and fragmentation patterns, with data that were reported in the literature [2,24]. The level of the identification led to the proposal of tentative candidates, since it was not possible to establish the position of substituents based only on full MS and MS/MS experiments. In addition, a mass error < 5 ppm on the experimental molecular formula was considered for the annotation. Following this approach, 7 hydroxycinnamic acid derivatives, 18 glycosylated flavonoids, and a limonoid, were tentatively identified from all of the analysed finger lime fruits (Table 2). Compounds **7**, **16**, and **24** were confirmed on the basis of injection of reference standards.

Table 2. Chromatographic data (retention time, t_R) and HR-ESI-MS/MS data of compounds **1–26**, detected in peels and pulps of *Citrus australasica* F. Muell. C = Collette; F = *Faustrime*; PI = Pink Ice; R = Red; YS = Yellow Sunshine. pe = only peel; pu = only pulp.

N. [a]	Compound	t_R(min)	[M-H]$^-$	Formula	Error (ppm)	-ESI-MS/MS (m/z) [b]	Extract
	Hydroxycinnamic acids						
1a	Caffeoylisocitric acid (isomer I)	0.50	353.0723	$C_{15}H_{14}O_{10}$	−0.8497	293.05; 191.02; 173.01; **111.01**	R; F; PI; C; YS
1b	Caffeoylisocitric acid (isomer II)	0.66	353.0723	$C_{15}H_{14}O_{10}$	−0.8497	173.01; 120.20; **111.01**; 87.01	R; F; PI; C; YS
2	Caffeoylmethylisocitric acid	0.7–2	367.0879	$C_{16}H_{16}O_{10}$	−0.8172	205.03, 191.02; 179.06; 169.01; 161.05; 143.03; **111.00**; 101.02; 89.02	R; F; PI; C; YS
3	Methylisocitric acid derivative	0.88	433.0596	-	-	401.04; 227.02; 205.03; 173.01; 143.03; **111.01**; 87.01	R; F; PI; C; YS
4	3-Hydroxy-3-methylglutaric acid derivative	2.62	365.1451	-	-	303.14; 263.11; 221.10; 161.04; 125.02; 99.04; 59.87; **57.03**	R; F; PI; C
5a	*p*-Coumaroylglucoside acid (isomer I)	2.87	325.0927	$C_{15}H_{18}O_8$	−0.9228	163.04; 159.05; **145.03**	R; F (pe); PI; C; YS
5b	*p*-Coumaroylglucoside acid (isomer II)	3.11	325.0927	$C_{15}H_{18}O_8$	−0.9228	163.04; 159.05; **145.03**	R; F(pe); PI; C; YS
6a	Feruloylglucoside acid (isomer I)	3.99	355.1034	$C_{16}H_{20}O_9$	−0.2816	193.05; **175.04**; 160.02	R; F(pe); PI; C; YS
6b	Feruloylglucoside acid (isomer II)	4.19	355.1034	$C_{16}H_{20}O_9$	−0.2816	193.05; **175.04**; 160.02	R; F(pe); PI; C; YS
	Flavonoids						
7	Rutin	7.02	609.1458	$C_{27}H_{30}O_{16}$	−0.4925	301.04; 300.03; 271.03	R; F; PI; C; YS
8	Quercetin glucoside	7.33	463.0880	$C_{21}H_{20}O_{12}$	−0.4319	301.04; **300.03**	R; F; PI; C; YS
9	Neoeriocitrin/eriocitrin	7.99	595.1666	$C_{27}H_{32}O_{15}$	−0.3360	459.11; **287.06**; 193.01; 161.02; 151.00; 135.04	F; PI(pu); C(pu); YS(pu)
10	Luteolin 7-*O*-neohesperidoside/rutinoside	8.19	593.1514	$C_{27}H_{30}O_{15}$	+0.3372	529.27; 474.31; **285.04**; 182.91	R; F (pu); PI; C; YS
11	Kaempferol glucoside	8.47	447.0933	$C_{21}H_{20}O_{11}$	0	327.05; 304.33; 285.04; **284.03**; 256.04; 255.03; 227.03	R; F(pe); PI; C; YS
12a	Isorhamnetin glucoside (isomer I)	9.07	477.1035	$C_{22}H_{22}O_{12}$	−0.8384	357.06; 327.06; 315.05; 314.04; 286.05; 285.04; 271.02; 257.05; 243.03	R; F; PI; C; YS
12b	Isorhamnetin glucoside (isomer II)	9.52	477.1035	$C_{22}H_{22}O_{12}$	−0.8384	449.11; 357.06; 333.73; 315.04; 299.02; 285.04; 271.02; 243.03	R; F; PI; C; YS
13a	Naringin/Naringenin rutinoside	9.50	579.1713	$C_{27}H_{32}O_{14}$	−1.0360	471.43; 397.56; 313.07; 295.06; 285.08; **271.06**; 151.00	F; PI(pu); C(pu); YS
13b	Naringin/Naringenin rutinoside	9.94	579.1713	$C_{27}H_{32}O_{14}$	−1.0360	313.07; **271.06**; 151.00	R; F; PI; C; YS
14a	3-Hydroxy-3-methylglutaryl isorhamnetin glucoside (isomer I)	10.30	621.1457	$C_{28}H_{30}O_{16}$	−0.6440	596.51; 559.15; 519.11; 477.10; **315.05**; 299.02; 285.04; 271.02; 243.03	R; F; PI; C; YS
14b	3-Hydroxy-3-methylglutaryl isorhamnetin glucoside (isomer II)	10.59	621.1458	$C_{28}H_{30}O_{16}$	−0.6440	559.15; 519.11; 477.10; **315.05**; 300.03; 271.03	R; F; C; PI; YS

Table 2. *Cont.*

N. [a]	Compound	t_R(min)	[M-H]$^-$	Formula	Error (ppm)	-ESI-MS/MS (*m*/*z*) [b]	Extract
15	Neodiosmin/diosmin	10.46	607.1666	$C_{28}H_{32}O_{15}$	−0.3294	341.07; 299.06; 284.03; 266.07; 255.03; 151.00	R(pu); F; PI(pu); C(pu); YS
16a	Neohesperidin/hesperidin	10.65	609.1820	$C_{28}H_{34}O_{15}$	−0.8208	418.95; 343.08; **301.07**; 286.05; 151.00	R; F; PI; C; YS
16b	Neohesperidin/hesperidin	11.01	609.1820	$C_{28}H_{34}O_{15}$	−0.8208	**301.07**; 286.05; 151.00	R; F; PI; C(pu); YS
17	Isosakuranetin rhamnosildiglucoside	11.93	755.2415	$C_{34}H_{44}O_{19}$	+1.4565	771.95; 755.24; 657.34; 490.63; **285.08**	R; F; PI; C; YS
18	Di-(3-hydroxy-3-methylglutaryl) isorhamnetin glucoside	12.03	765.1881	$C_{34}H_{38}O_{20}$	−0.3921	678.23; 642.82; 621.15; 519.12; 477.11; **315.05**; 299.02; 271.03; 187.04; 151.00	R; F; PI; C; YS
19	Kaempferol triglucoside	13.29	771.2354	$C_{34}H_{44}O_{20}$	+0.1297	527.23; 499.11; 408.51; **285.08**; 251.90	PI; C
21	Poncirin	14.47	593.1878	$C_{28}H_{34}O_{14}$	+0.1564	593.19; 427.38; 327.09; **285.08**	R; F; PI; C; YS
	Limonoids						
20	Limonexic acid	13.76	501.1763	$C_{26}H_{30}O_{10}$	−0.5986	**457.18**; 413.20; 271.89; 145.08	F; C; YS
	Anthocyanins						
N.[a]	**Compound**	**t_R(min)**	**[M]$^+$**	**Formula**	**Error (ppm)**	**+ESI-MS/MS (*m*/*z*)**	**Extract**
22	Cyanidin 3-*O*-glucoside	2.78	449.1068	$C_{21}H_{21}O_{11}^+$	−2.2266	**287.05**; 241.05; 213.05; 185.06; 157.06	R(pe, pu); C; PI
23	Petunidin rhamnosyldiglucoside	3.68	787.2272	$C_{34}H_{43}O_{21}^+$	−2.4135	625.17; 479.12; 427.10; **317.06**; 302.04	R(pe, pu)
24	Cyanidin 3-(6″-malonylglucoside)	3.87	535.1071	$C_{24}H_{23}O_{14}^+$	−2.0557	**287.05**; 241.05; 213.05; 171.04	R(pe, pu); C
25	Delfinidin rhamnosylglucoside	4.76	611.1593	$C_{27}H_{31}O_{16}^+$	−2.1271	366.30; **303.05**; 203.84; 173.85	R(pe); C; PI
26	Peonidin 3-(6″-malonylglucoside)	4.85	549.1227	$C_{25}H_{25}O_{14}^+$	−2.0032	517.09; 449.11; 301.07; **287.05**; 241.05; 213.05	R(pe, pu); C; PI

[a] Compounds are listed in ascending order of retention time; the numbering of the compounds corresponds to that used in Figure 1. All compounds were tentatively identified based on MS data, except for rutin (**7**), hesperidin (**16**), and cyanidin 3-*O*-glucoside (**24**), which were confirmed via injection of reference standards. [b] The base ion peak is indicated in bold.

In the first chromatographic region (0–5 min; Figure 1B), hydroxycinnamic acid derivatives were characterised. Compounds **1a** and **1b** (t_R = 0.50 and 0.66 min) are two caffeoylisocitric acid isomers, as indicated by HR mass data, showing the deprotonated ion [M-H]$^-$ at *m*/*z* 353.0723, the ion product [M-162-H]$^-$ at *m*/*z* 191.02 corresponding to isocitric acid that was generated by the loss of 162 u due to the cleavage of an ester bond with a caffeic acid residue. Compound **2** was annotated as caffeoylmethylisocitric acid, due to the deprotonated ion [M-H]$^-$ at *m*/*z* 367.0879, and the presence of a methylisocitric product ion at *m*/*z* 205.03 that was generated by the loss of a caffeoyl residue (−162 u). These hydroxycinnamic acid tricarboxylic acid esters are metabolites that are not commonly found in plants, especially isocitric acid derivatives [25]. Compounds **5a** and **5b** were identified as two *p*-coumaroylglucoside acid isomers. In the mass spectrum recorded in full scan, a parent ion at *m*/*z* 325.0927 was observed for both molecules, which under collision energy lost a hexose residue, and generated a *p*-coumaroyl fragment at *m*/*z* 163.04. Compounds **6a** and **6b** showed the same deprotonated ion [M-H]$^-$ at *m*/*z* 355.1034 in the full MS, while in the MS/MS experiment a feruloyl ion product at *m*/*z* 193.05 that was

generated by the cleavage of the glycosidic bond was observed; thus, the two compounds were tentatively attributed to feruloylglucoside acid isomers. Compounds **3** and **4** were not fully identified, but information about a portion of the molecule was deduced by the analyses of their MS fragmentation patterns. Compound **3** ($[M-H]^-$ at m/z 433.0596) showed product ions that were in common with compound **2** at m/z 205.03, 143.03, and 111.00, indicating the occurrence of a methylisocitric acid derivative. Compound **4** ($[M-H]^-$ at m/z 365.1451) showed the presence of typical product ions at m/z 303.14, 263.11, and 221.10, due to the loss of 62, 102, and 144 u, respectively, indicating the occurrence of a 3-hydroxy-3-methylglutaric acid derivative.

In the chromatographic region within 7–15 min, nine flavonol glycosides (compounds **7**, **8**, **11**, **12a**, **12b**, **14a**, **14b**, **18**, and **19**), seven flavanone glycosides (compounds **9**, **13a**, **13b**, **16a**, **16b**, **17**, and **21**), and two flavone glycosides (compounds **10** and **15**) were found. Both compounds **7** and **8** displayed the flavonol quercetin (m/z 301.04) as an aglycon portion. In particular, compound **7** was identified as rutin, as deduced by the parent ion at m/z 609.1458 and the observed loss of a rutinose residue (308 u); meanwhile, for compound **8** (deprotonated ion $[M-H]^-$ at m/z 463.0880), a loss of a hexose unit was observed, suggesting the occurrence of a quercetin glucoside. Compounds **11** and **19** were kaempferol derivatives, as indicated by the product ion at m/z 285.04 in the MS/MS. Compound **11** (deprotonated molecular ion $[M-H]^-$ at m/z 447.1035) was annotated as a kaempferol glucoside, due to the loss of a hexose residue (-162 u), while for compound **19** ($[M-H]^-$ at m/z 771.2354), a kaempferol triglucoside structure was suggested ([M-162-162-162-H] $^-$ at m/z 285.04). Compounds **12a**, **12b**, **14a**, **14b**, and **18** all exhibited a base ion peak at m/z 315.04 in the MS/MS, which was attributed to isorhamnetin. Compounds **12a** and **12b** ($[M-H]^-$ at m/z 477.1035) were assigned as isorhamnetin glucoside isomers, showing the loss of a hexose unit. Compounds **14a** and **14b** showed the same deprotonated ion at m/z 621.1457, and diagnostic fragments for a hexose unit (-162), and a 3-hydroxy-3-methylglutaryl residue (-62, -102, -144 u). Compound **18** ($[M-H]^-$ at m/z 765.1881) differed from **14a** and **14b,** only for having one more unit of 3-hydroxy-3-methylglutaric acid; thus, it was annotated as a di-(3-hydroxy-3-methylglutaryl) isorhamnetin glucoside. Compound **9** was revealed only in the fruits of the hybrid species *Faustrime*, and it could correspond to neoeriocitrin or eriocitrin, two flavanones glycosides that are commonly found in the genus *Citrus* [9]. In addition to the deprotonated ion $[M-H]^-$ at m/z 595.1666, a base ion peak at m/z 287.06 that corresponded to the aglycone portion of eriodictyol was observed, due to the loss of a disaccharide (308 u) which could be attributed to a rutinose or a neohesperidose, since they cannot be distinguished only on the basis of mass spectra. Peaks **13a** and **13b** displayed the same parent ion at m/z 579.1713 and the same base ion peak at m/z 271.02 attributed to naringenin. The loss of a disaccharide unit $[M-H-308]^-$ due to a rutinose or neohesperidose residue suggested the presence of two isomers, tentatively identified as naringin (naringenin neohesperidoside) and naringenin rutinoside. Compounds **16a** and **16b** were two isomeric forms of the same molecule, as deduced from the same deprotonated molecular ion $[M-H]^-$ at m/z 609.1029, and from the overlapping fragmentation mass spectra in which the base ion peak at m/z 301.07 was attributed to hesperetin. The two isomers were annotated as neohesperidin (hesperetin neohesperidoside) and hesperidin (hesperetin rutinoside). Peak **17** ($[M-H]^-$ at m/z 755.2415) was tentatively identified as isosakuranetin rhamnosyldiglucoside, since in the ESI-MS/MS, a base ion peak at m/z 285.08 ([M-162-162-146-H] $^-$) generated by the loss of two hexose residues (probably glucose) and a deoxyhexose (probably rhamnose) was observed. Poncirin (**21**, $[M-H]^-$ at m/z 593.1878) displayed a fragment ion at m/z 285.08 that was assigned to isosakuranetin, previously reported in *C. australasica* by Wang et al. (2019). The full MS ($[M-H]^-$ at m/z 593.1514) and MS/MS (base ion peak at m/z 285.04) suggested compound **10** as luteolin 7-*O*-neohesperidoside or luteolin 7-*O*-rutinoside, according to the aforementioned previous study (Wang et al., 2019). Compound **15** exhibited a parent ion at m/z 607.1666, and a diagnostic product ion at m/z 299.06, which was assigned to diosmetin. For its glycosidic portion, the option between two disaccharides (308 u), neohesperidose and rutinose, was

considered; therefore, **15** could be annotated as diosmin or neodiosmin. Compound **20** ([M-H]$^-$ at m/z 501.1763) was identified as limonexic acid, which belongs to the class of limonoids, typical terpenoids of the genus *Citrus* and responsible for their bitter taste [26]. The fragmentation peaks observed in the ESI-MS/MS at m/z 457.18 and 413.20 are in agreement with the data reported in the literature [27].

From a qualitative point of view, our results confirmed the presence of some components that were identified in *C. australasica* peel and pulp via UHPLC-MS/MS from a previous study [12]. To the best of our knowledge, the chemical composition of the hybrid species *Faustrime* has herein been reported for the first time. There are differences among the five varieties, especially in the case of the hybrid species *Faustrime* (Table 2), which showed several typical constituents of the *Citrus* genus, such as (neo)eriocitrin, (neo)diosmin, and naringenin rutinoside/naringin, that are rarely found in the other *C. australasica* varieties.

The quantitative estimation of all of the constituents (Table 3) that were obtained through UHPLC-MS highlighted greater differences among all studied fruits. Generally, it was confirmed that all phenol constituents are more abundant in peels than in pulps. The hydroxycinnamic acid derivatives were present in peels and the pulps of all varieties in very similar amounts, with the exception of Pink Ice, which was particularly rich in caffeoylisocitric acid. The largest amount of total flavonoids found among peels was in Collette (3432 $\pm$ 239 μg/g dry weight, DW), and in Pink Ice among pulps (897 $\pm$ 43 μg/g DW). Considering the whole fruit, among the identified compounds, the most abundant ones were rutin, luteolin 7-*O*-neohesperidoside/rutinoside, isosakuranetin rhamnosyldiglucoside, and poncirin, in Collette and Pink Ice; quercetin glucoside, isorhamnetin glucoside, and neohesperidin in Yellow Sunshine; quercetin glucoside, naringin, and poncirin in Red. The hybrid species *Faustrime* was distinguished by the significant presence, especially in the peels, of (neo)eriocitrin (316 $\pm$ 27 μg/g DW), (neo)diosmin (606 $\pm$ 41 μg/g DW), and naringenin rutinoside/naringin (145 $\pm$ 12 μg/g DW).

3.2.2. Anthocyanins Characterisation

Anthocyanins were identified in the extracts that were obtained from Red and Collette peels, and from Red and Pink Ice pulps, by comparing the data obtained through UHPLC-UV-ESI-MS/MS (Figure 1C) with those from a previous study on the *Citrus* fruits [28]. Five anthocyanins derived from cyanidin, delphinidin, petunidin, and peonidin were found (compounds **22–26**, Table 2).

Compound **22** (t_R = 2.78 min) was characterised as cyanidin 3-*O*-glucoside, as deduced by ESI-MS/MS data showing a molecular ion [M]$^+$ at m/z 449.1068, and a base ion peak at m/z 287.05 that corresponded to the aglycone portion of cyanidin, and generated by the loss of a hexose residue (−162 u). Compound **23** (t_R = 3.68 min) was assigned a molecular weight equal to 787.2272 u, on the basis of molecular ion [M]$^+$ recorded in full scan MS. In the fragmentation spectrum, a base ion peak at m/z 317.06 ([M-162-146-162]$^+$) was observed, corresponding to the aglycone portion, petunidin, generated by the loss of two hexose and one deoxyhexose residues; thus, **23** was tentatively identified as petunidin rhamnosyldiglucoside. Cyanidin 3-(6″-malonylglucoside) (**24**, t_R = 3.87 min) was characterised by a molecular ion [M]$^+$ at m/z 535.1071, and a base ion peak at m/z 287.05 that was attributed to the aglycone, cyanidin, generated by the loss of a malonyl residue and a hexose [M-162-86]$^+$. Peonidin 3-(6″-malonylglucoside) (**25**, t_R = 4.85 min) displayed a molecular ion [M]$^+$ at m/z 549.1227, a product ion at m/z 301 corresponding to peonidin, and similarly to compound **24**, the loss of 86 and 162 u residues. Compound **26** (t_R = 4.76 min, [M]$^+$ = 611.1593) was annotated as delphinidin rhamnosylglucoside. The analysis of the fragmentation pattern highlighted the aglycone portion at m/z 303.05, which was identified as delphinidin, and the loss of a disaccharide ([M-162-146]$^+$) was attributable to hexose and deoxyhexose residues.

Table 3. Content of phenolic compounds (μg/g of dried peel or pulp ± standard deviation) and anthocyanins (μg/g of fresh peel or pulp ± standard deviation) in *C. australasica* peel and pulp extracts. nd = not determined.

			Variety				
Peak [a]	**Compound**		**Collette**	**Yellow Sunshine**	**Pink Ice**	**Red**	***Faustrime***
1a	Caffeoylisocitric acid (isomer I)	Peel	1.18 ± 0.19 ^{C}	1.45 ± 0.05 ^{B}	2.01 ± 0.0 ^{A}	1.23 ± 0.0 ^{BC}	0.837 ± 0.026 ^{D}
		Pulp	0.911 ± 0.039 ^{D}	1.47 ± 0.06 ^{B}	2.23 ± 0.03 ^{A}	1.03 ± 0.03 ^{C}	0.919 ± 0.011 ^{D}
1b	Caffeoylisocitric acid (isomer II)	Peel	0.226 ± 0.031 ^{C}	0.283 ± 0.013 ^{B}	0.354 ± 0.012 ^{A}	0.212 ± 0.004 ^{C}	0.156 ± 0.014 ^{D}
		Pulp	0.215 ± 0.022 ^{C}	0.379 ± 0.029 ^{B}	0.451 ± 0.026 ^{A}	0.179 ± 0.008 ^{CD}	0.159 ± 0.004 ^{D}
2	Caffeoylmethylisocitric acid	Peel	0.179 ± 0.023 ^{A}	0.143 ± 0.002 ^{B}	0.167 ± 0.002 ^{A}	0.153 ± 0.006 ^{B}	0.172 ± 0.003 ^{A}
		Pulp	0.114 ± 0.006 ^{D}	0.143 ± 0.002 ^{C}	0.329 ± 0.000 ^{A}	0.071 ± 0.02 ^{C}	0.069 ± 0.001 ^{B}
5a	*p*-Coumaroylglucoside acid (isomer I)	Peel	0.105 ± 0.008 ^{A}	0.043 ± 0.007 ^{C}	0.092 ± 0.009 ^{AB}	0.080 ± 0.05 ^{B}	0.0066 ± 0.0003 ^{D}
		Pulp	0.0072 ± 0.0005 ^{BC}	0.0092 ± 0.001 ^{B}	0.059 ± 0.006 ^{A}	0.0083 ± 0.0004 ^{B}	Not detected ^{C}
5b	*p*-Coumaroylglucoside acid (isomer II)	Peel	0.187 ± 0.008 ^{A}	0.089 ± 0.005 ^{B}	0.189 ± 0.022 ^{A}	0.171 ± 0.004 ^{A}	0.012 ± 0.001 ^{D}
		Pulp	0.013 ± 0.001 ^{B}	0.016 ± 0.001 ^{B}	0.118 ± 0.006 ^{A}	0.018 ± 0.000 ^{B}	Not detected ^{C}
6a	Feruloylglucoside acid (isomer I)	Peel	0.011 ± 0.000 ^{C}	0.198 ± 0.018 ^{A}	0.013 ± 0.001 ^{C}	0.036 ± 0.002 ^{B}	0.0033 ± 0.0001 ^{C}
		Pulp	0.0015 ±0.0001 ^{D}	0.0031 ± 0.003 ^{C}	0.010 ± 0.000 ^{A}	0.0061 ± 0.0002 ^{B}	Not detected ^{E}
6b	Feruloylglucoside acid (isomer II)	Peel	0.064 ± 0.008 ^{B}	0.388 ± 0.032 ^{A}	0.021 ± 0.003 ^{B}	0.060 ± 0.003 ^{B}	0.017 ± 0.002 ^{B}
		Pulp	0.0030 ±0.0002 ^{CD}	0.0045 ± 0.0005 ^{BC}	0.025 ± 0.003 ^{A}	0.0068 ± 0.0001 ^{B}	Not detected ^{D}
7	Rutin	Peel	198 ± 13 ^{A}	18.7 ± 2.0 ^{C}	128 ± 12 ^{B}	5.69 ± 0.49 ^{C}	19.6 ± 1.3 ^{C}
		Pulp	7.50 ± 0.29 ^{B}	2.64 ± 0.21 ^{D}	21.1 ± 1.7 ^{A}	0.534 ± 0.136 ^{D}	4.72 ± 0.65 ^{C}
8	Quercetin glucoside	Peel	105 ± 5 ^{C}	145 ± 12 ^{B}	106 ± 10 ^{C}	245 ± 9 ^{A}	2.32 ± 0.03 ^{D}
		Pulp	28.6 ± 1.4 ^{A}	11.7 ± 0.8 ^{B}	32.0 ± 7.5 ^{A}	12.3 ± 0.2 ^{B}	0.775 ± 0.050 ^{C}
9	Neoeriocitrin/eriocitrin	Peel	Not detected ^{B}	Not detected ^{B}	Not detected ^{B}	Not detected ^{B}	316 ± 27 ^{A}
		Pulp	0.488 ± 0.109 ^{B}	1.38 ± 0.06 ^{B}	1.06 ± 0.05 ^{B}	Trace ^{B}	56.8 ± 2.8 ^{A}
10	Luteolin 7-*O*-neohesperidoside/rutinoside	Peel	660 ± 50 ^{A}	14.7 ± 1.2 ^{C}	224 ± 19 ^{B}	7.72 ± 0.35 ^{C}	Not detected ^{C}
		Pulp	19.1 ± 0.9 ^{B}	4.87 ± 0.25 ^{C}	35.7 ± 2.7 ^{A}	1.55 ± 0.06 ^{C}	38.0 ± 2.4 ^{A}
11	Kaempferol glucoside	Peel	11.8 ± 0.8 ^{C}	14.3 ± 1.4 ^{C}	76.0 ± 7.2 ^{A}	43.8 ± 2.2 ^{B}	2.55 ± 0.13 ^{D}
		Pulp	1.99 ± 0.12 ^{BC}	1.06 ± 0.06 ^{C}	10.7 ± 0.8 ^{A}	2.89 ± 0.05 ^{B}	Not detected ^{D}
12a	Isorhamnetin glucoside (isomer I)	Peel	288 ± 14 ^{B}	171 ± 11 ^{C}	47.8 ± 3.9 ^{D}	376 ± 21 ^{A}	5.15 ± 0.31 ^{E}
		Pulp	69.3 ± 2.3 ^{A}	32.2 ± 1.0 ^{C}	44.1 ± 2.6 ^{B}	65.0 ± 1.2 ^{A}	3.31 ± 0.09 ^{D}
12b	Isorhamnetin glucoside (isomer II)	Peel	37.6 ± 1.2 ^{C}	161 ± 10 ^{B}	15.5 ± 1.0 ^{D}	234 ± 4 ^{A}	1.04 ± 0.06 ^{E}
		Pulp	15.4 ± 0.9 ^{B}	20.9 ± 0.8 ^{A}	7.86 ± 0.57 ^{C}	20.5 ± 0.4 ^{A}	0.426 ± 0.031 ^{D}
13a	Naringin/naringenin rutinoside	Peel	Not detected ^{B}	9.65 ± 0.72 ^{B}	Not detected ^{B}	Trace ^{B}	145 ± 12 ^{A}
		Pulp	0.176 ± 0.049 ^{C}	4.60 ± 0.20 ^{B}	0.379 ± 0.050 ^{C}	Not detected ^{C}	13.6 ± 0.5 ^{A}
13b	Naringin/naringenin rutinoside	Peel	21.9 ± 1.9 ^{C}	146 ± 12 ^{B}	22.0 ± 2.4 ^{C}	1061 ± 63 ^{A}	2.26 ± 0.25 ^{C}
		Pulp	15.1 ± 0.5 ^{BC}	17.4 ± 1.1 ^{B}	13.5 ± 0.8 ^{C}	131 ± 1 ^{A}	Trace ^{D}

Table 3. *Cont.*

			Variety				
Peak [a]	**Compound**		**Collette**	**Yellow Sunshine**	**Pink Ice**	**Red**	***Faustrime***
14a	3-Hydroxy-3-methylglutaryl isorhamnetin glucoside (I)	Peel	573 ± 24 ^{A}	92.3 ± 5.8 ^{B}	36.1 ± 2.5 ^{C}	102 ± 2 ^{B}	7.53 ± 0.37 ^{C}
		Pulp	108 ± 6 ^{A}	31.4 ± 1.6 ^{C}	48.7 ± 3.2 ^{B}	22.9 ± 0.3 ^{C}	5.79 ± 0.25 ^{D}
14b	3-Hydroxy-3-methylglutaryl isorhamnetin glucoside (II)	Peel	67.0 ± 4.2 ^{A}	30.2 ± 1.8 ^{C}	4.02 ± 0.34 ^{D}	42.9 ± 2.2 ^{B}	1.39 ± 0.10 ^{D}
		Pulp	25.8 ± 1.5 ^{A}	9.53 ± 0.55 ^{B}	5.21 ± 0.46 ^{C}	10.3 ± 0.3 ^{B}	0.553 ± 0.008 ^{D}
15	Neodiosmin/diosmin	Peel	Not detected ^{C}	79.7 ± 7.5 ^{B}	Not detected ^{C}	Trace ^{C}	606 ± 41 ^{A}
		Pulp	1.70 ± 0.18 ^{C}	49.6 ± 3.1 ^{B}	4.41 ± 1.10 ^{C}	1.39 ± 0.07 ^{C}	198 ± 8 ^{A}
16a	Neohesperidin/hesperidin	Peel	2.11 ± 0.20 ^{B}	74.6 ± 7.4 ^{B}	2.61 ± 0.13 ^{B}	4.21 ± 1.03 ^{B}	1495 ± 107 ^{A}
		Pulp	4.72 ± 1.20 ^{C}	48.5 ± 1.7 ^{B}	6.52 ± 0.49 ^{C}	3.31 ± 0.14 ^{C}	174 ± 5 ^{A}
16b	Neohesperidin/hesperidin	Peel	Trace ^{B}	502 ± 43 ^{A}	2.92 ± 0.10 ^{B}	18.0 ± 1.9 ^{B}	10.5 ± 2.6 ^{B}
		Pulp	1.53 ± 0.43 ^{B}	107 ± 7 ^{A}	1.67 ± 0.11 ^{B}	4.43 ± 0.18 ^{B}	0.471 ± 0.149 ^{B}
17	Isosakuranetin rhamnosyldiglucoside	Peel	1119 ± 102 ^{A}	13.4 ± 1.2 ^{C}	911 ± 92 ^{B}	2.21 ± 0.00 ^{C}	4.09 ± 0.45 ^{C}
		Pulp	157 ± 4 ^{B}	2.17 ± 0.12 ^{C}	272 ± 13 ^{A}	1.49 ± 0.09 ^{C}	0.348 ± 0.029 ^{C}
18	Di-(3-hydroxy-3-methylglutaryl) isorhamnetin glucoside	Peel	114 ± 10 ^{A}	28.2 ± 2.2 ^{C}	4.11 ± 0.12 ^{D}	41.2 ± 1.1 ^{B}	11.6 ± 0.4 ^{D}
		Pulp	10.1 ± 0.6 ^{A}	9.61 ± 0.58 ^{A}	6.57 ± 0.53 ^{B}	6.20 ± 0.01 ^{B}	3.87 ± 0.22 ^{C}
19	Kaempferol triglucoside	Peel	11.8 ± 0.8 ^{A}	Trace ^{C}	9.85 ± 0.82 ^{B}	Not detected ^{C}	Trace ^{C}
		Pulp	2.09 ± 0.05 ^{B}	Not detected ^{C}	3.24 ± 0.12 ^{A}	Not detected ^{C}	Not detected ^{C}
21	Poncirin	Peel	221 ± 12 ^{B}	15.6 ± 1.3 ^{D}	767 ± 68 ^{A}	120 ± 9.0 ^{C}	3.68 ± 0.34 ^{D}
		Pulp	142 ± 5 ^{B}	4.82 ± 0.20 ^{D}	371 ± 6.6 ^{A}	15.8 ± 0.2 ^{C}	0.295 ± 0.006 ^{D}
	Total flavonoids and phenolic acids	Peel	3432 ± 239	1519 ± 121	2360 ± 220	2306 ± 117	2635 ± 193
		Pulp	612 ± 26	361 ± 19	896 ± 43	301 ± 4.0	502 ± 20
			Anthocyanins				
Peak	**Compound**		**Collette**	**Yellow Sunshine**	**Pink Ice**	**Red**	***Faustrime***
22	Cyanidin 3-*O*-glucoside	Peel	20.0 ± 0.5 ^{A}	nd	nd	12.3 ± 0.2 ^{B}	nd
		Pulp	nd	nd	0.925 ± 0.07 ^{B}	1.44 ± 0.09 ^{A}	nd
23	Petunidin rhamnosyldiglucoside	Peel	Trace ^{B}	nd	Nd	20.4 ± 0.3 ^{A}	nd
		Pulp	nd	nd	Trace ^{B}	3.41 ± 0.10 ^{A}	nd
24	Cyanidin 3-(6″-malonylglucoside)	Peel	20.3 ± 1.0 ^{A}	nd	nd	17.1 ± 0.3 ^{B}	nd
		Pulp	nd	nd	Trace ^{B}	0.62 ± 0.14 ^{A}	nd
25	Delfinidin rhamnosylglucoside	Peel	71.1 ± 1.0 ^{A}	nd	nd	3.80 ± 0.15 ^{B}	nd
		Pulp	nd	nd	1.98 ± 0.01 ^{A}	Not detected ^{B}	nd
26	Peonidin 3-(6″-malonylglucoside)	Peel	31.8 ± 0.7 ^{B}	nd	nd	42.6 ± 1.3 ^{A}	nd
		Pulp	nd	nd	1.47 ± 0.03 ^{B}	2.79 ± 0.23 ^{A}	nd

Table 3. *Cont.*

			Variety				
Peak	**Compound**		**Collette**	**Yellow Sunshine**	**Pink Ice**	**Red**	***Faustrime***
	Total anthocyanins	Peel	143.2 ± 3.2	nd	nd	96.2 ± 2.3	nd
		Pulp	nd	nd	4.38 ± 0.11	8.26 ± 0.56	nd
	Total phenols	Peel	3575 ± 242	1519 ± 121	2360 ± 220	2402 ± 119	2635 ± 193
		Pulp	612 ± 26	361 ± 19	900 ± 43	309 ± 4.6	502 ± 20

[a] Compound numbers correspond to the peak numbers in Figure 1. The superscript uppercase letters (A–E) indicate statistically significant differences among the varieties.

Based on the quantitative analysis (Table 3), cyanidin 3-*O*-glucoside was found to be the most representative anthocyanin, both in peels and pulps, of all of the investigated varieties. In agreement with our results, cyanidin 3-*O*-glucoside was found to be the most abundant anthocyanin from a previous study of red finger lime [29]. The peels of the Collette variety were the richest in anthocyanins (143.2 ± 3.2 μg/g DW), followed by the peels (96.2 ± 2.3 μg/g DW) and the pulps (8.26 ± 0.56 μg/g DW) of the Red variety.

3.2.3. Multivariate Statistical Analyses of the Non-Volatile Components

The dendrogram of the HCA (Figure 2A) shows a sample distribution into two macro-clusters: the first one (red samples) comprised Collette and Pink Ice peels, while the second one comprised two clusters (blue and green). The blue cluster is composed only of Red peel, while the green cluster includes the pulps of all of the varieties, as well as the *Faustrime* and Yellow Sunshine peels.

This organ-driven statistical distribution was confirmed through the PCA. Collette and Pink Ice peels were plotted on the right quadrants (PC1 > 0) of the score plot (Figure 2B). Red peels were plotted in the right area of the upper left quadrant (PC1 < 0, PC2 > 0) (score plot, Figure 2B), due to their high anthocyanin content (loadings plot, Figure 2C). The pulps of all of the varieties and of Yellow Sunshine peels were plotted on the left quadrants (PC1 < 0) of the score plot (Figure 2B), due to their content of neodiosmin/diosmin and neoeriocitrin/eriocitrin. Pink Ice and Yellow Sunshine varieties were plotted along the PC1 axis, and in the upper region of the bottom quadrants (PC2 < 0) (score plot, Figure 2B), due to their content of caffeoylisocitric acid (isomers I and II) and hydroxycinnamic acid derivatives (loadings plot, Figure 2C).

3.3. Essential Oil (EO) Composition of All of the Samples

The complete composition of all of the EOs that were hydrodistilled from both the peels and pulps of all the *C. australasica* varieties (Collette, Pink Ice, Red, and Yellow Sunshine), and the *Faustrime* hybrid, are reported in Table 4. Overall, 89 compounds were identified from the EO compositions.

Monoterpenes were the most abundant compounds found in all of the peel EOs, with the exception of the Yellow Sunshine variety, where sesquiterpenes prevailed. The Collette and Red varieties, as well as the *Faustrime* peel EOs, can be considered a limonene chemotype, whereas the Pink Ice and the Yellow Sunshine EOs exhibited a 4-terpineol/limonene and a limonene/bicyclogermacrene chemotype, respectively. This difference in peel EO chemotypes was found to be consistent with previous literature studies for other finger lime varieties [10,30,31], although the latter analysed a dichloromethane extract of the volatile peel constituents. Among the monoterpenes, their hydrocarbon form prevailed in all of the peel EOs, with the exception of the Pink Ice variety, where the oxygenated monoterpenes were more abundant. Among the monoterpene hydrocarbons, limonene was found to be the most quantitatively relevant in all of the samples, accounting for up to 73.6% in the Red variety. With the exception of the Red and Yellow Sunshine varieties, γ-terpinene and α-phellandrene followed, as relative concentrations. Among the peel EOs, oxygenated monoterpenes were more abundant in the Pink Ice variety and the *Faustrime* hybrid, exhibiting a relative presence of 48.0 and 35.5%, respectively. Among this class, 4-terpineol was observed to be the most abundant in the former, while citronellal and piperitone prevailed in the latter. This quantitatively relevant presence of citronellal and piperitone in the *Faustrime* hybrid EO is in accordance with [32], although their analysis was performed with an essential oil that was obtained by peel cold-pressing, and [11]. Bicyclogermacrene was the sesquiterpene hydrocarbon that exhibited the highest relative abundance in all of the peel EOs. Sesquiterpenes dominated all of the pulp EO compositions, with the only exception being the *Faustrime* hybrid, whose composition was mainly represented by monoterpenes. The Yellow Sunshine pulp EO was mainly composed of oxygenated sesquiterpenes, among which viridiflorol and globulol were the most represented; however, like the Red variety, the most characterising compound in its composition was

bicyclogermacrene, a sesquiterpene hydrocarbon. Among the latter chemical classes, β-caryophyllene was detected as the main relevant compound in the Collette variety, while it exhibited a comparable presence to its oxidized counterpart (caryophyllene oxide) in the leaf EO of the Pink Ice variety. α-Humulene and β-bisabolene followed within this class, reaching up to 12.7% in the Pink Ice pulp EO and 24.6% in the Red variety pulp EO, respectively. Viridiflorol, globulol, and guaiol were detected as the most abundant oxygenated sesquiterpenes in the pulp EOs of all of the analysed samples, with the exception of the *Faustrime* hybrid. The latter was, indeed, chiefly composed of monoterpene hydrocarbons, which represented over 70% of its complete composition, with limonene being the most abundant compound (48.3%), followed by γ-terpinene (10.8%), and α-phellandrene (7.2%).

Multivariate Statistical Analyses of the EO Compositions

The dendrogram of the HCA (Figure 2D) evidenced a distribution of the samples into two macro-clusters: the first comprised two clusters (red and green) and included all of the peel Eos, and the *Faustrime* pulp sample; the second macro-cluster was homogeneous (blue samples), and comprised all of the *C. australasica* pulp EOs, except the *Faustrime* pulp.

This organ-driven statistical distribution was confirmed with principal component analysis. All of the peel EOs were plotted on the left quadrants (PC1 < 0) of the score plot (Figure 2E), together with the *Faustrime* pulp sample. The Pink Ice peel EO was plotted in the right area of the upper left quadrant (PC1 < 0, PC2 > 0) (score plot, Figure 2E), due to its 4-terpineol content (loadings plot, Figure 2F). Collette and *Faustrime* peel EOs were closely grouped towards the center of the same quadrant, very close to the *Faustrime* pulp EO (score plot, Figure 2E): all of these samples were grouped in this area due to the contribution of γ-terpinene and α-phellandrene (loadings plot, Figure 2F). Both the Red and Yellow Sunshine peel EOs were plotted in the bottom right quadrant (PC1 and PC2 > 0) of the PCA score plot (Figure 2E): as evidenced in the loadings plot (Figure 2F), their position was due to their high relative content of limonene. With the exception of the *Faustrime* hybrid sample, all of the pulp EOs were plotted in the right quadrants (PC1 > 0) of the PCA score plot (Figure 2E). Collette and Pink Ice pulp EOs were grouped in the upper quadrant (PC2 > 0): the positioning of the former was mainly due to its high relative content of caryophyllene oxide, while β-caryophyllene and α-humulene showed a high relative presence in both samples. Finally, Yellow Sunshine and Red pulp EOs were plotted in the bottom right quadrant (PC1 > 0, PC2 < 0) of the PCA score plot (Figure 2E), due to the contributions of bicyclogermacrene, globulol, viridiflorol, and guaiol vectors (loadings plot, Figure 2F).

3.4. Cell Viability Assay and In Vitro Cellular Assessment of Antioxidant Properties

Before evaluating the extent of the protection they provided from oxidative stress, the cytotoxicity on Balb/3T3 of the peel and pulp extracts was assayed. The concentration ranges were set on the basis of relevant GAE equivalents, resulting in 15–120 μg/mL for peels, and 30–300 μg/mL for pulps. Neither the peel nor pulp extracts showed cytotoxic effects at any of the tested concentrations (Figure 3A,B).

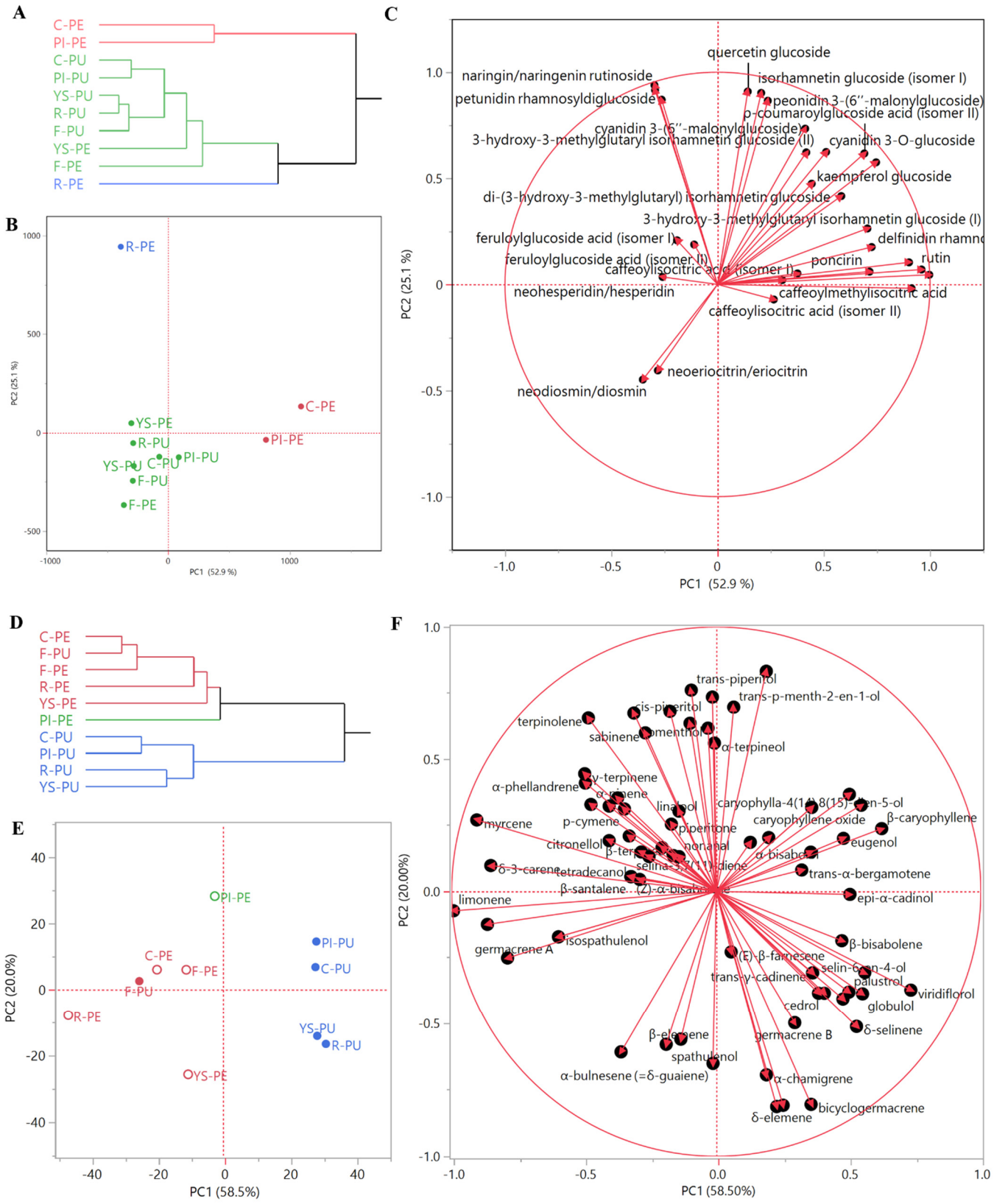

Figure 2. Non-volatile (**A**) and EO (**D**) dendrograms of the hierarchical cluster analysis (HCA), and respective score (**B**,**E**) and loadings (**C**,**F**) plots of the principal component analysis (PCA) performed on peels (PE) and pulps (PU) for essential oil and non-volatile compositions of all of the samples (C = Collette; F = Faustrime; PI = Pink Ice; R = Red; YS = Yellow Sunshine).

Table 4. Complete composition of the peel and pulp essential oils hydrodistilled from all of the analysed *Citrus australasica* varieties (Collette, Pink Ice, Red, and Yellow Sunshine), and for the *Faustrime* hybrid.

Compounds	l.r.i. [a]	Relative Abundance (%) ± SD									
		Collette		Pink Ice		Red		Yellow Sunshine		Faustrime	
		Peel	Pulp	Peel	Pulp	Peel	Pulp	Peel	Pulp	Peel	Pulp
α-Thujene	931	-	-	-	-	-	-	-	-	0.1 ± 0.01	-
α-Pinene	941	0.7 ± 0.02	-	0.4 ± 0.05	-	0.1 ± 0.00	0.2 ± 0.24	-	-	1.1 ± 0.08	1.0 ± 0.08
Sabinene	976	1.7 ± 0.04	-	1.7 ± 0.13	-	-	-	-	-	0.3 ± 0.02	0.2 ± 0.02
β-Pinene	982	0.4 ± 0.02	-	0.1 ± 0.01	-	-	-	-	-	0.5 ± 0.03	0.2 ± 0.02
Myrcene	993	1.0 ± 0.03	-	0.7 ± 0.04	-	1.0 ± 0.03	-	0.3 ± 0.08	-	1.0 ± 0.06	1.0 ± 0.03
Octanal	1001	-	-	-	-	-	-	-	-	0.6 ± 0.03	-
α-Phellandrene	1005	4.1 ± 0.57	-	3.1 ± 0.18	-	0.1 ± 0.01	-	-	-	5.2 ± 0.30	7.2 ± 0.41
δ-3-Carene	1011	0.2 ± 0.04	-	0.1 ± 0.01	-	0.5 ± 0.01	-	-	-	0.3 ± 0.02	0.2 ± 0.01
α-Terpinene	1018	1.3 ± 0.16	-	3.7 ± 0.21	-	-	-	-	-	0.8 ± 0.04	2.1 ± 0.09
p-Cymene	1027	0.3 ± 0.02	-	0.2 ± 0.01	-	-	-	-	-	1.0 ± 0.05	0.4 ± 0.04
Limonene	1032	42.4 ± 5.64	1.4 ± 0.48	26.5 ± 1.75	1.0 ± 0.54	73.6 ± 4.41	-	40.0 ± 2.47	0.4 ± 0.11	31.5 ± 1.86	48.3 ± 3.71
1,8-Cineole	1034	0.1 ± 0.01	-	-	-	-	-	-	-	-	-
(*Z*)-β-Ocimene	1042	0.3 ± 0.01	-	0.3 ± 0.01	-	1.2 ± 0.01	-	0.5 ± 0.05	-	0.7 ± 0.04	0.3 ± 0.01
(*E*)-β-Ocimene	1052	0.1 ± 0.01	-	0.2 ± 0.01	-	0.5 ± 0.00	-	0.4 ± 0.11	-	0.2 ± 0.01	0.1 ± 0.00
γ-Terpinene	1062	14.2 ± 1.96	-	7.3 ± 0.25	-	0.3 ± 0.01	-	0.4 ± 0.11	-	11.6 ± 0.5	10.8 ± 0.47
Terpinolene	1088	1.6 ± 0.24	-	2.0 ± 0.01	-	0.4 ± 0.01	-	-	-	1.2 ± 0.02	0.9 ± 0.01
Linalool	1101	0.9 ± 0.17	1.1 ± 0.11	0.3 ± 0.00	-	-	-	-	0.2 ± 0.04	2.6 ± 0.04	0.7 ± 0.01
Nonanal	1104	-	-	-	-	-	-	-	-	0.2 ± 0.01	-
cis-*p*-Menth-2-en-1-ol	1124	0.6 ± 0.03	1.2 ± 0.11	1.7 ± 0.05	-	-	-	-	-	1.1 ± 0.00	0.3 ± 0.00
trans-*p*-Menth-2-en-1-ol	1140	0.4 ± 0.03	1.2 ± 0.45	1.3 ± 0.04	-	-	-	-	-	0.8 ± 0.01	0.2 ± 0.01
β-Terpineol	1153	-	-	-	-	-	-	-	-	1.6 ± 0.02	0.1 ± 0.01
Menthone	1154	5.1 ± 0.14	1.0 ± 0.06	-	-	-	-	-	-	-	0.3 ± 0.01
Citronellal	1155	0.7 ± 0.04	-	-	-	1.7 ± 0.06	-	1.1 ± 0.12	-	9.4 ± 0.05	-
*iso*Borneol	1156	-	-	-	-	-	-	-	-	0.9 ± 0.03	-
*iso*Menthone	1164	-	-	2.6 ± 0.09	-	-	-	-	-	1.4 ± 0.03	-
4-Terpineol	1178	8.4 ± 0.23	12.0 ± 1.07	38.3 ± 0.81	19.3 ± 4.14	-	-	-	-	2.1 ± 0.06	0.4 ± 0.02
*iso*Menthol	1179	-	-	0.2 ± 0.01	-	-	-	-	-	-	-
Cryptone	1187	-	-	-	-	-	-	-	-	0.2 ± 0.01	-
α-Terpineol	1189	1.2 ± 0.06	2.5 ± 0.31	1.9 ± 0.11	-	-	-	-	0.3 ± 0.04	3.1 ± 0.11	0.7 ± 0.06
cis-Piperitol	1195	0.2 ± 0.02	-	0.6 ± 0.04	-	-	-	-	-	0.3 ± 0.02	-
Decanal	1204	-	-	0.3 ± 0.04	-	-	-	-	-	0.5 ± 0.02	0.7 ± 0.06
trans-Piperitol	1207	0.4 ± 0.05	0.5 ± 0.20	1.0 ± 0.05	-	-	-	-	-	0.6 ± 0.04	0.2 ± 0.01

Table 4. *Cont.*

Compounds	l.r.i. [a]	Relative Abundance (%) ± SD									
		Collette		Pink Ice		Red		Yellow Sunshine		Faustrime	
		Peel	Pulp	Peel	Pulp	Peel	Pulp	Peel	Pulp	Peel	Pulp
Citronellol	1230	1.1 ± 0.12	-	0.1 ± 0.08	-	0.4 ± 0.13	-	-	-	1.7 ± 0.11	-
Neral	1240	-	-	-	-	-	-	-	-	1.0 ± 0.07	-
Piperitone	1252	2.5 ± 0.15	2.7 ± 0.25	0.1 ± 0.07	-	-	-	-	-	6.9 ± 0.48	1.7 ± 0.16
(*E*)-2-Decenal	1260	-	-	-	-	-	-	-	-	0.1 ± 0.01	-
Phellandral	1272	-	-	-	-	-	-	-	-	0.1 ± 0.01	-
trans-Citral	1273	-	-	-	-	-	-	-	-	1.6 ± 0.13	-
n-Tridecane	1300	-	-	-	-	-	-	-	-	-	0.3 ± 0.04
Undecanal	1306	-	-	-	-	-	-	-	-	-	0.1 ± 0.01
δ-Elemene	1340	0.1 ± 0.01	0.4 ± 0.50	-	-	0.3 ± 0.07	1.8 ± 0.84	2.0 ± 0.00	0.6 ± 0.02	-	-
Citronellyl acetate	1354	-	-	-	-	-	-	-	-	0.2 ± 0.04	0.1 ± 0.02
Eugenol	1358	-	-	-	1.1 ± 0.04	-	-	-	0.4 ± 0.14	-	-
β-Elemene	1392	-	-	-	-	-	-	0.4 ± 0.00	-	-	-
1-Tetradecene	1392	-	-	-	-	-	-	-	-	-	0.1 ± 0.08
n-Tetradecane	1400	-	-	-	-	-	-	-	-	-	0.1 ± 0.09
Dodecanal	1408	-	-	0.1 ± 0.07	-	-	-	-	-	-	0.4 ± 0.11
cis-α-Bergamotene	1416	-	-	-	-	-	-	-	-	-	0.1 ± 0.02
β-Caryophyllene	1420	0.7 ± 0.11	21.3 ± 1.05	0.4 ± 0.09	14.1 ± 1.00	0.2 ± 0.04	6.9 ± 1.20	-	0.6 ± 0.22	0.8 ± 0.16	2.3 ± 0.39
trans-α-Bergamotene	1438	-	1.2 ± 0.37	-	2.3 ± 0.01	0.2 ± 0.04	1.9 ± 0.56	-	0.9 ± 0.25	1.5 ± 0.31	2.9 ± 0.48
α-Humulene	1456	-	8.4 ± 0.13	0.6 ± 0.14	12.7 ± 0.52	0.2 ± 0.06	4.0 ± 0.37	-	0.3 ± 0.06	1.0 ± 0.21	4.6 ± 0.69
(*E*)-β-Farnesene	1460	-	-	-	-	-	0.2 ± 0.23	-	-	-	0.2 ± 0.04
β-Santalene	1463	-	-	-	-	-	-	-	-	-	0.1 ± 0.02
γ-Gurjunene	1474	0.5 ± 0.72	0.9 ± 0.25	-	-	-	-	-	-	-	-
γ-Muurolene	1477	-	0.7 ± 0.25	-	-	-	-	-	-	-	-
Germacrene D	1478	0.3 ± 0.06	-	-	-	0.3 ± 0.07	2.7 ± 0.04	2.6 ± 0.05	1.0 ± 0.08	-	0.2 ± 0.01
β-Chamigrene	1485	-	-	-	-	-	-	-	-	-	0.1 ± 0.03
δ-Selinene	1490	-	-	-	-	0.1 ± 0.07	1.0 ± 0.11	-	1.2 ± 0.11	-	-
Bicyclogermacrene	1496	4.9 ± 0.62	10.9 ± 0.33	1.9 ± 0.40	9.8 ± 0.74	6.9 ± 1.10	28 ± 1.61	39.8 ± 2.24	20.3 ± 0.07	0.8 ± 0.20	1.0 ± 0.20
n-Pentadecane	1500	-	-	-	-	-	-	-	-	-	1.1 ± 0.25
(Z)-α-Bisabolene	1504	-	-	-	-	-	-	-	-	-	0.4 ± 0.09
α-Bulnesene	1505	-	-	-	-	-	-	0.9 ± 0.07	0.3 ± 0.03	-	-
Germacrene A	1506	-	-	-	-	0.2 ± 0.03	-	-	-	-	-
α-Chamigrene	1508	-	-	-	-	-	2.4 ± 0.36	2.5 ± 0.14	-	-	-
β-Bisabolene	1509	0.8 ± 0.12	4.8 ± 0.4	0.7 ± 0.18	9.2 ± 0.35	2.0 ± 0.42	24.6 ± 0.14	-	-	2.6 ± 0.57	5.6 ± 1.05

Table 4. *Cont.*

Compounds	l.r.i. [a]	Relative Abundance (%) ± SD									
		Collette		Pink Ice		Red		Yellow Sunshine		Faustrime	
		Peel	Pulp	Peel	Pulp	Peel	Pulp	Peel	Pulp	Peel	Pulp
trans-γ-Cadinene	1513	-	-	-	-	-	-	-	0.3 ± 0.06	-	-
(Z)-γ-Bisabolene	1515	-	-	-	-	-	-	-	-	-	0.1 ± 0.03
Selina-3,7(11)-diene	1542	-	-	-	-	-	-	-	-	-	0.1 ± 0.07
Germacrene B	1554	-	-	-	-	0.6 ± 0.15	5.2 ± 0.01	0.9 ± 0.02	0.2 ± 0.25	-	0.5 ± 0.11
Palustrol	1568	-	1.3 ± 0.06	0.2 ± 0.04	-	0.6 ± 0.12	1.7 ± 0.79	-	6.0 ± 0.00	-	-
Spathulenol	1576	-	-	-	-	0.1 ± 0.04	-	1.1 ± 0.15	-	-	-
Caryophyllene oxide	1581	-	-	-	15.6 ± 1.29	-	-	-	-	-	-
Globulol	1583	0.6 ± 0.12	9.5 ± 0.13	0.5 ± 0.13	-	1.8 ± 0.37	3.8 ± 0.99	2.9 ± 0.23	14.5± 0.15	-	0.1 ± 0.08
Viridiflorol	1590	0.7 ± 0.12	7.9 ± 0.30	0.4 ± 0.13	5.8 ± 1.58	1.7 ± 0.34	10.9 ± 0.21	1.2 ± 0.21	19.9 ± 0.01	-	-
Guaiol	1595	0.2 ± 0.03	1.1 ± 0.35	0.2 ± 0.03	-	0.5 ± 0.11	3.2 ± 0.05	0.3 ± 0.01	11.9 ± 0.71	-	-
Cedrol	1596	0.3 ± 0.12	1.4 ± 0.42	0.3 ± 0.08	-	0.8 ± 0.17	1.0 ± 1.45	0.8 ± 0.07	8.5 ± 0.08	-	-
n-Hexadecane	1600	-	-	-	-	-	-	-	-	-	0.6 ± 0.22
5-*epi*-7-*epi*-α-Eudesmol	1603	-	-	-	-	-	-	-	2.2 ± 0.06	-	-
Humulene epoxide II	1608	-	2.0 ± 0.20	-	4.1 ± 0.83	-	-	-	-	-	-
Selin-6-en-4-ol	1618	-	1.2 ± 0.25	-	-	0.2 ± 0.06	0.5 ± 0.66	-	2.2 ± 0.08	-	-
Caryophylla-4(14),8(15)-dien-5-ol	1637	-	-	-	1.9 ± 0.36	-	-	-	-	-	-
*iso*Spathulenol	1639	-	-	-	-	0.1 ± 0.11	-	-	-	-	-
epi-α-Cadinol	1641	-	-	-	3.2 ± 1.03	0.2 ± 0.10	-	0.4 ± 0.05	2.6 ± 0.49	-	-
Cubenol	1643	-	-	-	-	0.2 ± 0.07	-	0.5 ± 0.04	-	-	-
α-Cadinol	1654	-	0.8 ± 0.35	-	-	0.3 ± 0.08	-	0.4 ± 0.10	1.9 ± 0.09	-	-
β-Bisabolol	1672	-	-	-	-	-	-	-	-	0.2 ± 0.25	-
Tetradecanol	1676	-	-	-	-	-	-	-	-	-	0.2 ± 0.08
α-Bisabolol	1683	-	1.4 ± 0.08	-	-	0.2 ± 0.04	-	-	-	0.5 ± 0.18	0.4 ± 0.18
n-Heptadecane	1700	-	-	-	-	-	-	-	-	-	0.2 ± 0.08
Monoterpene hydrocarbons		68.2 ± 4.11	1.4 ± 0.48	46.1 ± 2.68	1.0 ± 0.54	77.7 ± 4.37	0.2 ± 0.24	41.6 ± 2.83	0.4 ± 0.11	55.5 ± 3.05	72.8 ± 4.91
Oxygenated monoterpenes		21.7 ± 1.05	22.2 ± 1.05	48.0 ± 1.34	19.3 ± 4.14	2.1 ± 0.18	-	1.1 ± 0.12	0.5 ± 0.08	35.5 ± 1.18	4.7 ± 0.27
Sesquiterpene hydrocarbons		7.3 ± 1.65	48.5 ± 0.41	3.6 ± 0.81	48.1 ± 0.45	10.9 ± 2.04	78.8 ± 3.97	49.2 ± 2.38	25.7 ± 0.03	6.7 ± 1.45	18.2 ± 3.22
Oxygenated sesquiterpenes		1.8 ± 0.39	26.6 ± 0.10	1.6 ± 0.41	30.5 ± 5.09	6.5 ± 1.60	21.1 ± 3.74	7.6 ± 0.60	69.8 ± 1.05	0.6 ± 0.43	0.5 ± 0.25
Phenylpropanoids		-	-	-	1.1 ± 0.04	-	-	-	0.4 ± 0.14	-	-
Non-terpene derivatives		-	-	0.3 ± 0.11	-	-	-	-	-	1.7 ± 0.00	3.7 ± 1.03
Total identified (%)		99.0 ± 1.02	98.6 ± 1.02	99.6 ± 0.01	100 ± 0.01	97.2 ± 0.54	100 ± 0.01	99.5 ± 0.04	96.8 ± 0.74	100 ± 0.01	99.9 ± 0.13

[a] Linear retention index calculated on a HP-5MS capillary column; - : Not detected.

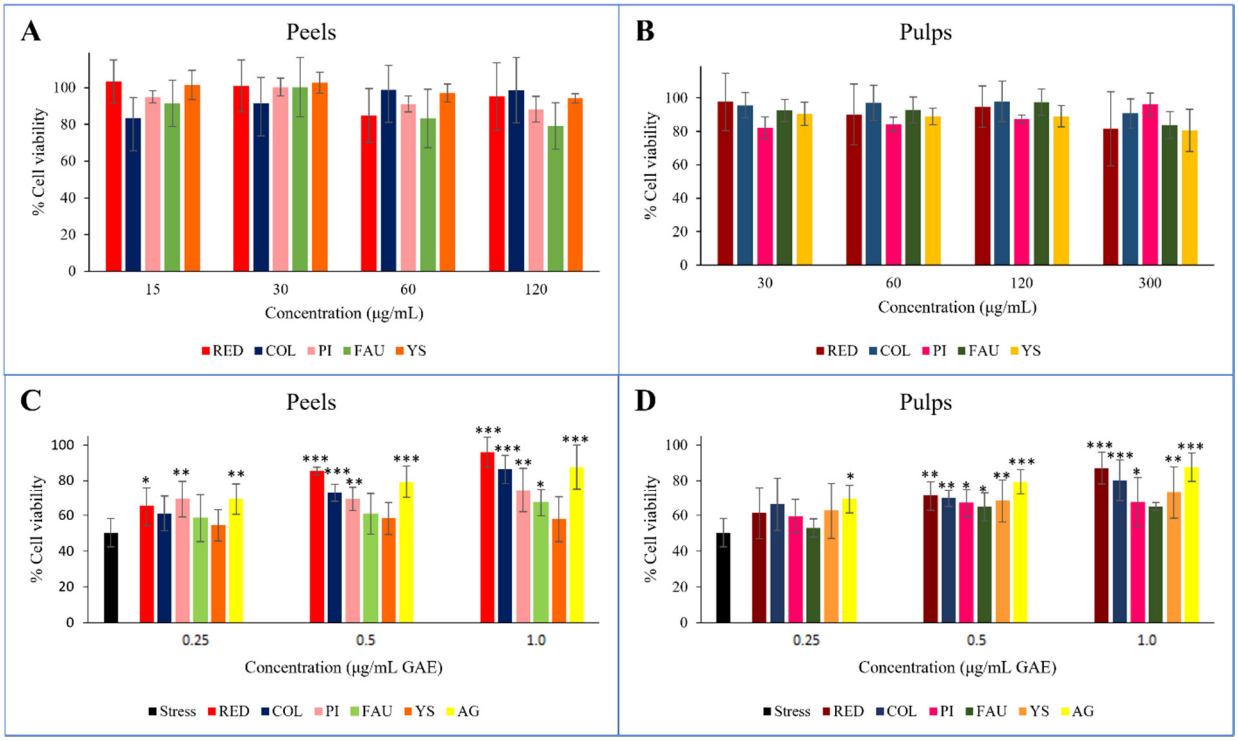

Figure 3. In vitro cell evaluation of the Balb/3T3 cell line. Cytotoxicity screening after 2-h treatments with peel (**A**) and pulp (**B**) extracts. Protective effects of peel (**C**) and pulp (**D**) extracts from H_2O_2-induced oxidative stress, reported as cell viability % after 2-h treatments with 1500 µM H_2O_2 of pre-treated Balb/3T3 cells. H_2O_2 = stressed control; C = Collette; F = *Faustrime*; GA = gallic acid; PI = Pink Ice; R = Red; YS = Yellow Sunshine; *** = p value < 0.0001; ** = p value < 0.005; * = p value < 0.05 vs. stress.

The antioxidant protective effect was assessed in vitro for all peel (Figure 3C) and pulp (Figure 3D) extracts. Three different concentrations were evaluated, namely 0.25, 0.50, and 1.0 µg/mL GAE, and compared to gallic acid that was used as a reference. The oxidative treatment with H_2O_2 resulted in a drastic decrease in cell viability (45%) with respect to untreated and unstressed control cells. Cell viability was increased with the pretreatment of all extracts, thus protecting cells from the induced oxidative stress. In general, the observed effects were directly proportional to the corresponding concentration of gallic acid, with greater accordance recorded for the Red and Collette extracts. In these cases, the effects on cell viability correlated with increasing GAE concentration treatments, incrementing from 65 to 96%, and from 61 to 87% for Red peel and pulp, respectively; and from 61 to 86%, and from 66 to 80% for Collette peel and pulp, respectively. Concerning the hybrid species *Faustrime*, a poor protection effect was detected for both its peel and pulp. This evidence could be explained on the basis of the higher polyphenol content in the Red and Collette varieties, and moreover, due to the valuable amounts of anthocyanins in these varieties.

4. Conclusions

The chemical investigation of the four finger lime varieties revealed an interesting profile of potentially health-promoting agents that were represented by hydroxycinnamic acids (ferulic, *p*-coumaric, and caffeic acid derivatives) and glycosylated flavonols (kaempferol, quercetin, and isorhamnetin derivatives), flavanones (naringenin, eriodictyol, and hesperetin derivatives), and flavones (luteolin and diosmetin derivatives). Furthermore, the glycosides of cyanidin, delfinidin, petunidin, and peonidin were the anthocyanins that were detected in the Red, Pink Ice, and Collette varieties. Among limonoids, triterpenoids typically found in *Citrus* fruits that are responsible for their bitter taste, only limonexic acid was revealed. For each variety, the peel and pulp showed similar qualitative profiles;

among all of the samples, the hybrid species *Faustrime* differed for the presence of neoeriocitrin, eriocitrin, neodiosmin, and diosmin, components that are usually predominant in other common *Citrus* fruits. All of the peels differed from their relative pulps in terms of phenol amount; they were richer in bioactive components, as confirmed by their higher antioxidant capacity observed in their provided protection from oxidative damage. Similarly, the volatile compositions of peel EOs of all of the samples were characterised mainly by monoterpenes, while pulp EOs were rich in sesquiterpenes.

The uniqueness of the organoleptic characteristics of these fruits, jointly with their composition that is rich in antioxidant metabolites, make them promising candidates for their use as fresh fruits, or for the development of nutraceutical products with beneficial properties.

Supplementary Materials: The following supporting information can be downloaded at: https://www.mdpi.com/article/10.3390/antiox11102047/s1, Table S1: Results of peel and pulp extraction from *Citrus australasica* varieties. Table S2: Concentrations of peel and pulp extracts from *Citrus australasica* varieties applied in the in vitro assay for protection from H_2O_2 oxidative stress on Balb/3T3.

Author Contributions: Conceptualization, A.M.P., M.D.L., L.P. and Y.Z.; methodology, A.M.P., G.F., M.D.L. and Y.Z.; validation, A.M.P., B.M. and E.C.; formal analysis, B.M., C.M., E.C. and R.A.; investigation, C.M., E.C., R.A. and M.D.L.; resources, M.D.L., L.P. and Y.Z; data curation, B.M., C.M., E.C. and R.A.; writing—original draft preparation, B.M., C.M., E.C. and R.A.; writing—review and editing, A.M.P., M.D.L., G.F., L.P. and Y.Z.; supervision, A.M.P., G.F., L.P. and M.D.L. All authors have read and agreed to the published version of the manuscript.

Funding: This research received no external funding.

Institutional Review Board Statement: Not applicable.

Informed Consent Statement: Not applicable.

Data Availability Statement: All of the data are contained within the article.

Acknowledgments: The authors are grateful to Agrumi Lenzi Company (Pescia, Pistoia, Italy) for kindly supplying the *C. australasica* fruits used in this study.

Conflicts of Interest: The authors declare no conflict of interest.

References

1. Favela-Hernández, J.M.J.; González-Santiago, O.; Ramírez-Cabrera, M.A.; Esquivel-Ferriño, P.C.; Camacho-Corona, M. Chemistry and pharmacology of *Citrus sinensis*. *Molecules* **2016**, *21*, 247. [CrossRef] [PubMed]
2. Wang, Y.; Ji, S.; Zang, W.; Wang, N.; Cao, J.; Li, X.; Sun, C. Identification of phenolic compounds from a unique *Citrus* species, finger lime (*Citrus australasica*) and their inhibition of LPS-induced NO-releasing in BV-2 cell line. *Food Chem. Toxicol.* **2019**, *129*, 54–63. [CrossRef] [PubMed]
3. Adhikari, B.; Dutt, M.; Vashisth, T. Comparative phytochemical analysis of the fruits offour Florida-grown finger lime (*Citrus australasica*) selections. *LWT-Food Sci.Technol.* **2020**, *135*, 110003. [CrossRef]
4. Liu, Y.Q.; Heying, E.; Tanumihardjo, S.A. History, global distribution, and nutritional importance of *Citrus* fruits. *Compr. Rev. Food Sci. Food Saf.* **2012**, *11*, 530–545. [CrossRef]
5. Alam, M.A.; Subhan, N.; Rahman, M.M.; Uddin, S.J.; Reza, H.M.; Sarker, S.D. Effect of *Citrus* flavonoids, naringin and naringenin, on metabolic syndrome and their mechanisms ofaction. *Adv. Nutr.* **2014**, *5*, 404417. [CrossRef]
6. Benavente-García, O.; Castillo, J. Update on uses and properties of *Citrus* flavonoids: New findings in anticancer, cardiovascular, and anti-inflammatory activity. *J. Agr. Food Chem.* **2008**, *56*, 6185–6205. [CrossRef]
7. Lv, X.; Zhao, S.; Ning, Z.; Zeng, H.; Shu, Y.; Tao, O.; Xiao, C.; Lu, C.; Liu, Y. *Citrus* fruits as a treasure trove of active natural metabolites that potentially provide benefits for human health. *Chem. Cent. J.* **2015**, *9*, 68. [CrossRef]
8. Zou, Z.; Xi, W.; Hu, Y.; Nie, C.; Zhou, Z. Antioxidant activity of *Citrus* fruits. *Food Chem.* **2016**, *196*, 885–896. [CrossRef]
9. Benavente-García, O.; Castillo, J.; Marin, F.R.; Ortuño, A.; Del Río, J.A. Uses and properties of *Citrus* flavonoids. *J. Agric. Food Chem.* **1997**, *45*, 4505–4515. [CrossRef]
10. Delort, E.; Jaquier, A.; Decorzant, E.; Chapuis, C.; Casilli, A.; Frérot, E. Comparative analysis of three australian finger lime (*Citrus australasica*) cultivars: Identification of unique citrus chemotypes and new volatile molecules. *Phytochemistry* **2015**, *109*, 111–124. [CrossRef]

11. Dugo, P.; Mondello, L.; Zappia, G.; Bonaccorsi, I.; Cotroneo, A.; Russo, M.T. The composition of the volatile fraction and the enantiomeric distribution of five volatile components of faustrime oil (*Monocitrus australatica* × *Fortunella* sp. × *Citrus aurantifolia*). *J. Essential Oil Res.* **2004**, *16*, 4. [CrossRef]
12. Aznar, R.; Rodríguez-Pérez, C.; Rai, D.K. Comprehensive characterization and quantification of antioxidant compounds in finger lime (*Citrus australasica* L.) by HPLC-QTof-MS and UPLC-MS/MS. *Appl. Sci.* **2022**, *12*, 1712. [CrossRef]
13. Da Pozzo, E.; De Leo, M.; Faraone, I.; Milella, L.; Cavallini, C.; Piragine, E.; Testai, L.; Calderone, V.; Pistelli, L.; Braca, A.; et al. Antioxidant and antisenescence effects of bergamot juice. *Ox. Med. Cell. Longev.* **2018**, *2018*, 9395804. [CrossRef] [PubMed]
14. De Leo, M.; Piragine, E.; Pirone, A.; Braca, A.; Pistelli, L.; Calderone, V.; Miragliotta, V.; Testai, L. Protective effects of bergamot (*Citrus bergamia* Risso & Poiteau) juice in rats fed with high-fat diet. *Planta Med.* **2020**, *86*, 180–189. [CrossRef]
15. Flamini, G.; Pistelli, L.; Nardoni, S.; Ebani, V.; Zinnai, A.; Mancianti, F.; Ascrizzi, R.; Pistelli, L. Essential oil composition and biological activity of "Pompia", a sardinian *Citrus* ecotype. *Molecules* **2019**, *24*, 908. [CrossRef]
16. Giovanelli, S.; Ciccarelli, D.; Giusti, G.; Mancianti, F.; Nardoni, S.; Pistelli, L. Comparative assessment of volatiles in juices and essential oils from minor *Citrus* fruits (Rutaceae). *Flavour Fragr. J.* **2020**, *35*, 639–652. [CrossRef]
17. Testai, L.; De Leo, M.; Flori, L.; Polini, B.; Braca, A.; Nieri, P.; Pistelli, L.; Calderone, V. Contribution of irisin pathway in protective effects of mandarin juice (*Citrus reticulata* Blanco) on metabolic syndrome in rats fed with high fat diet. *Pharmacol. Res.* **2021**, *35*, 4324–4333. [CrossRef]
18. Singleton, V.L.; Orthofer, R.; Lamuela-Raventós, R.M. Analysis of total phenols and other oxidation substrates and antioxidants by means of Folin-Ciocalteu reagent. *Methods Enzymol.* **1999**, *299*, 152–178. [CrossRef]
19. Felice, F.; Fabiano, A.; De Leo, M.; Piras, A.M.; Beconcini, D.; Cesare, M.M.; Braca, A.; Zambito, Y.; Di Stefano, R. Antioxidant effect of cocoa by-product and cherry polyphenol extracts: A comparative study. *Antioxidants* **2020**, *9*, 132. [CrossRef]
20. National Institute of Standards and Technology. NIST/EPA/NIH Mass Spectral Library. In *NIST Standard Reference Database Number 69*; (No. 2014); The NIST Mass Spectrometry Data Center: Gaithersburg, MD, USA, 2014.
21. Adams, R.P. *Identification of Essential Oil Components by Gas Chromatography/Mass Spectroscopy*, 4th ed.; Allured Pub. Corp.: Carol Stream, IL, USA, 2007.
22. Beconcini, D.; Fabiano, A.; Zambito, Y.; Berni, R.; Santoni, T.; Piras, A.M.; Di Stefano, R. Chitosan-based nanoparticles containing cherry extract from *Prunus avium* L. to improve the resistance of endothelial eells to oxidative stress. *Nutrients* **2018**, *10*, 1598. [CrossRef]
23. Ascrizzi, R.; Flamini, G.; Giusiani, M.; Stefanelli, F.; Deriu, V.; Chericoni, S. VOCs as fingerprints for the chemical profiling of hashish samples analyzed by HS-SPME/GC–MS and multivariate statistical tools. *Forensic Toxicol.* **2018**, *36*, 243–260. [CrossRef]
24. Parveen, I.; Winters, A.; Threadgill, M.D.; Hauck, B.; Morris, P. Extraction, structural characterisation and evaluation of hydroxycinnamate esters of orchard grass (*Dactylis glomerata*) as substrates for polyphenol oxidase. *Phytochemistry* **2008**, *69*, 2799–2806. [CrossRef] [PubMed]
25. Strack, D.; Leicht, P.; Bokern, M.; Wray, V.; Grotjahn, L. Hydroxycinnamic acid esters of isocitric acid: Accumulation and enzymatic synthesis in *Amaranthus cruentus*. *Phytochemistry* **1987**, *26*, 2919–2922. [CrossRef]
26. Russo, M.; Arigò, A.; Calabrò, M.L.; Farnetti, S.; Mondello, L.; Dugo, P. Bergamot (*Citrus bergamia* Risso) as a source of nutraceuticals: Limonoids and flavonoids. *J. Funct. Foods* **2016**, *20*, 10–19. [CrossRef]
27. Biavatti, M.W.; Vieira, P.C.; Da Silva, M.F.; Fernandes, J.B.; Albuquerque, S. Limonoids from the endemic brazilian species *Raulinoa echinata*. *Z. Naturforsch. C* **2001**, *56c*, 570–574. [CrossRef]
28. Fabroni, S.; Ballistreri, G.; Amenta, M.; Rapisarda, P. Anthocyanins in different *Citrus* species: An UHPLC-PDA-ESI/MS^n-assisted qualitative and quantitative investigation. *J. Sci. Food Agric.* **2016**, *96*, 4797–4808. [CrossRef]
29. Netzel, M.; Netzel, G.; Tian, Q.; Schwartz, S.; Konczak, I. Native Australian fruits—A novel source of antioxidants for food. *Innov. Food Sci. Emerg. Technol.* **2007**, *8*, 339–346. [CrossRef]
30. Johnson, J.B.; Batley, R.; Manson, D.; White, S.; Naiker, M. Volatile compounds, phenolic acid profiles and phytochemical content of five Australian finger lime (*Citrus australasica*) cultivars. *LWT* **2022**, *154*, 112640. [CrossRef]
31. Lota, M.-L.; de Rocca Serra, D.; Tomi, F.; Jacquemond, C.; Casanova, J. Volatile components of peel and leaf oils of lemon and lime species. *J. Agric. Food Chem.* **2002**, *50*, 796–805. [CrossRef]
32. Trozzi, A.; Verzera, A.; d'Alcontres, I.S. Constituents of the cold-pressed oil of Faustrime, a trigeneric hybrid of *Monocitrus australasica* × *Fortunella* sp. × *Citrus aurantifolia*. *J. Essent. Oil Res.* **1995**, *5*, 97–100. [CrossRef]

antioxidants

MDPI

Article

Variations of Bioactive Phytochemicals and Antioxidant Capacity of Navel Orange Peel in Response to Different Drying Methods

Chunling Lai [1], Yan Liang [1,*], Linyan Zhang [1], Jiangjiang Huang [1], Kumaravel Kaliaperumal [1], Yueming Jiang [1,2] and Jun Zhang [1,2,*]

[1] National Engineering Research Centre of Navel Orange, Gannan Normal University, Ganzhou 341000, China
[2] Key Laboratory of Plant Resources Conservation and Sustainable Utilization, South China Botanical Garden, Chinese Academy of Sciences, Guangzhou 510650, China
* Correspondence: zjhxy110@126.com (Y.L.); bri71527152@outlook.com (J.Z.)

Abstract: The effects of five different drying methods, namely, freeze drying (FD), shade drying (SD), hot-air oven drying at 50 °C (OD50), 70 °C (OD70), and microwave drying (MD) on the bioactive phytochemicals and antioxidant capacity of navel orange peel were assessed and comprehensively discussed in detail. Compared with other drying methods, MD-treated peel contained the lowest total phenolic content (TPC) and total flavonoid content (TFC). The peel subjected to OD70 treatment was superior in TPC relative to other treatments and the highest TFC was found in the peels treated with FD. HPLC analysis identified thirteen flavonoids involving three flavanone glycosides (FGs) and ten polymethoxyflavones (PMFs) in navel orange peel and revealed that PMFs in peel were stable under all these drying methods, whereas the three major FGs (narirutin, hesperidin, and didymin) in peel significantly degraded in response to MD treatment. The peels subjected to OD50/OD70 treatments had the most potent antioxidant capacity when compared to other drying methods. Furthermore, Pearson's correlation analysis was performed. The results revealed here allow us to recommend the use of OD50 or OD70 for the drying of orange peel, both of which help the maintenance of bioactive compounds in the peel and improve its antioxidant capacity.

Keywords: drying methods; orange peel; chemical composition; antioxidant activity

1. Introduction

Navel orange, one of the main varieties of citrus fruits, is widely grown in Ganzhou of Jiangxi Province, China. In 2021, the total planting area and the annual output of navel orange in Ganzhou reached over 100 thousand hectares, and over 1 million tons, respectively [1]. With the consumption of orange flesh, large quantities of peels were discarded, which caused the waste of resources and environmental pollution, thus raising concerns about the value-added utilization of this abundant resource [2]. Citrus peels contain large amounts of biologically active compounds, mainly phenolic acids and flavonoids, which exhibit pronounced antioxidant, neuroprotective, anti-inflammatory, antiproliferation, antiallergy, and antiviral properties [3–5]. Therefore, orange peel could be considered a valuable source of bioactive substances which may function as important ingredients in the production of cosmetics, pharmaceuticals, and nutraceuticals [6,7]. Fresh orange peel with a moisture content of over 70% is difficult to preserve due to the deterioration caused by microbes or enzymes [4]. Drying is one of the extensively used methods to extend the storage life of orange peel by removing water to inhibit spoilage as well as reduce the activity of enzymes [4,7]. In general practice, the drying process of the citrus peel should be conducted before carrying out further procedures, such as storage, transportation and extraction of bioactive components.

Several drying techniques have been applied to the dehydration of citrus byproducts, involving shade drying, sun drying, far-infrared radiation drying, hot-air drying, freezing drying, microwave drying, etc. [3,4,8]. Shade drying usually takes a long time and is generally applied to some traditional Chinese medicines containing volatile oils or mucus [3]. Freeze drying can prevent the degradation of heat or oxygen-sensitive bioactive compounds, but requires high energy consumption and lengthy processing time, making it much more suitable for some high-value products [8]. In contrast, hot-air drying is a relatively inexpensive and user-friendly method [9]. Microwave drying has been reported to efficiently transfer energy for the removal of moisture, thus decreasing the drying time and preserving the quality of the product, whereas it is hard to control the temperature to have a homogeneous treatment [10]. The effects of different drying methods on the chemical and biological properties of citrus products have been reported previously, but with some controversial results, suggesting that more influential factors such as citrus cultivar, the parameter of drying method, and extracting method, might influence the results as well. For example, the freeze-drying method resulted in the highest total phenolic content (TPC) and antioxidant effects in the immature citrus fruits of four citrus species (Ponkan, Gaocheng, Foyu, and Huyou), compared to the hot-air and sun drying methods [3]. However, Papoutsis et al. reported that the lemon pomace dried by hot air at 110 °C had the highest TPC, whereas the freeze-dried one had the lowest [8]. On the other hand, Ledesma-Escobar et al. reported that the lemon dried by freeze-drying had higher TPC than that dried by hot-air drying at 45 °C [11]. The total polyphenols, flavonoids, ascorbic acid, and antioxidant capacity of orange peel markedly decreased after drying processing [7]. In other studies, the highest antioxidant capacity for orange peel was obtained when the peel was dried in a hot-air oven at 60 °C [9], and the microwave drying at 450W significantly improved the extractible amounts of phenolics compared to the fresh orange peel [10]. Therefore, the selection of suitable drying methods for orange peel is challengeable and it plays an important role in realizing the optimal valorization of orange peel. To the best of our knowledge, the research about the drying methods of peel from navel orange planted in Ganzhou of China is largely unavailable yet.

Herein, the effects of five different drying methods, namely, freeze drying (FD), shade drying (SD), hot-air oven drying at 50 °C (OD50), 70 °C (OD70), and microwave drying (MD) on the chemical composition and antioxidant capacity of navel orange peel were evaluated for the first time. In the present study, the chemical compositions involving TPC, total flavonoid content (TFC) and thirteen individual flavonoids were comparatively analyzed, and three antioxidant assays as 2,2-diphenyl-1-picrylhydrazyl free radical (DPPH), 2,2′-azinobis-(3-ethylbenzthiazoline-6-sulphonate) free radical (ABTS), and ferric reducing antioxidant power (FRAP) assays were employed together for the antioxidant tests. Moreover, Pearson's correlation analysis was adopted to examine the relationships among all variables tested. The present results might provide useful information for the drying processing of orange peel, and contribute to the value-added utilization of this abundant side-product.

2. Materials and Methods

2.1. Chemicals

2,4,6-Tris(2-pyridyl)-s-triazine (TPTZ), 2,2-diphenyl-1-picryhydrazyl (DPPH, 97%), 2,2-azino-bis(3-ethylbenzothiazoline-6-sulfonic acid) diammonium salt (ABTS, 98%) and Folin–Ciocalteu reagent (1 M) were purchased from Solarbio Science and Technology Co., Ltd. (Beijing, China). Methanol, 95% ethanol, petroleum ether, ethyl acetate, dichloromethane, and N, N-Dimethylformamide (DMF) were of analytical grade and purchased from Damao Chemical Reagent Factory (Tianjin, China). The flavonoids involving narirutin, hesperidin, didymin, isosinensetin, 3,3′,4′,5,7,8-hexamethoxyflavone, sinensetin, 4′,5,7,8-tetramethoxyflavone, 3,3′,4′,5,6,7-hexamethoxyflavone, nobiletin, 4′,5,6,7-tetramethoxyflavone, 3,3′,4′,5,6,7,8-heptamethoxyflavone, 5-hydroxy-6,7,3′,4′-tetramethoxyflavone, and tangeretin were isolated from the orange peel by authors according to chromatographic methods [2] and each

had a purity of >95% (data shown in the supplement material). Acetonitrile (ACN) was of high-performance liquid chromatography (HPLC) grade (Anaqua Chemicals Supply, Houston, TX, USA). De-ionized water used for chromatography was obtained from a Milli-Q Gradient A10 system (Millipore, Billerica, MA, USA). All other chemicals were of analytical grade and purchased from Sigma-Aldrich (Shanghai, China).

2.2. Plant Materials

Newhall navel oranges (50 kg) at a commercial mature stage were harvested on 15 December 2020 from an orchard located in Ganzhou (23.1291° N, 113.2644° E) of Jiangxi Province, China. The orange trees were planted in red-yellow loam soil (pH 5.39 ± 0.3) and spaced at 4 m and 3 m between and along the rows, respectively. The freshly harvested fruits were transferred to the laboratory, washed and squeezed immediately. The peels were then collected from the pomace by hand and were cut into pieces of approximately 1 cm^2 each. The pieces of peel were pooled together and stored at −80 °C in sealed plastic bags until drying experiments.

2.3. Drying of Orange Peel

Orange peels were subjected to five different drying methods termed FD, SD, OD50, OD70, and MD. For each treatment, 1 kg of orange peel was used. The detailed procedures were described as follows: (1) For FD, the pieces of peel were spread out on trays to form a thin layer of about 0.5 cm thickness. The peels on trays were pre-frozen in the refrigerator at −80 °C overnight. The frozen peels were then dried to a constant weight for 48 h by using a freeze dryer (FD8-6 P, SIM International Group, Newark, NJ, USA). (2) For SD, the pieces of peel were spread out on trays to form a thin layer having a thickness of about 0.5 cm. The trays were kept in a well-ventilated and shady area at ambient temperature (approximate temperature 5–20 °C) and 60–80% relative humidity for 14 days to achieve a constant weight. (3) For both OD50 and OD70, the peels were distributed on a stainless steel wire mesh to form a thin layer (thickness of about 0.5 cm) and dried in a hot-air oven (DHG-9240A, Jinghong Co., Shanghai, China) at 50 or 70 °C with 2 m/s air flow rate and 5–10% relative humidity for 12 h (OD50) or 8 h (OD70) to achieve a constant weight. (4) The MD treatments were performed in a domestic microwave oven equipped with a glass turntable (M1-L204A, Midea, Guangdong, China) with the following features: 220 V (voltage), 1150 W (input power), 700 W (output power) and 2450 MHz (operating frequency). The peels were distributed on glass dishes to form a single layer (thickness of about 0.5 cm). The dishes containing peels were then placed on the turntable of a microwave oven and dried at 600 W for 12 min to achieve a constant weight.

After drying, samples were kept in a desiccator overnight to allow a homogeneous distribution of moisture, and the final moisture content was 10 ± 0.5% wet basis. The dried peels were ground to a powder by using an electric grinder (QE-100, Zhejiang YiLi Tool Co., Ltd., Jiaxing, China), followed by sieving through a 40-mesh sieve. The powders were packed in plastic bags, labeled and stored at −80 °C until extraction. The experiments were performed in triplicate for each drying method.

2.4. Extraction of Dried Orange Peel

Maceration extraction at room temperature was employed to extract bioactive compounds from the dried orange peel. Briefly, dried peel powders (5 g) were added into a 250 mL conical bottle, followed by the addition of 50 mL of 95% ethanol. The conical bottle was placed on the bench for 24 h with occasional shaking. After that, the mixture was filtered with Whatman filter paper (No 1) and the residue was collected and repeatedly extracted four times as described above. All filtrates were combined and concentrated by a vacuum rotary evaporator at 35 °C to give a brown residue, which was subjected to lyophilization for 48 h by using a freeze dryer (FD8-6 P, SIM International Group, Newark, NJ, USA) and stored at −80 °C until further analysis. The experiments were performed in triplicate for each dried sample.

2.5. TPC Analysis

TPC was determined spectrophotometrically with the Folin–Ciocalteu reagent according to one of our previous reports [2]. Briefly, the extract solution in methanol (20 μL), distilled water (60 μL), and Folin–Ciocalteu reagent (15 μL, pre-diluted from 1 M to 0.5 M with water at a volume ratio of 1:1) were sequentially added to a 96-well plate and mixed well by smoothly shaking for 3 min. After 4 min of static incubation at room temperature, 75 μL Na_2CO_3 aqueous solution (2% *w/v*) was added, followed by slightly shaking for 3 min. The optical density was measured at 750 nm using a microplate reader (Tecan Spark 10M, Männedorf, Switzerland) after 15 min of static incubation at room temperature. The methanol was used as a blank control. TPC was calculated from a linear calibration curve ($y = 0.0046x + 0.012$, $R^2 = 0.9998$, linear range from 6.25 to 100 mg/L) which was constructed by plotting the absorbance values against the concentrations of gallic acid, and expressed as micromole of gallic acid equivalent per gram dry weight of extract (μM GAE/g DW). Each measurement was conducted in triplicate.

2.6. TFC Analysis

TFC was estimated by the method described previously [2]. Briefly, 500 μL $NaNO_2$ (5% *w/v*), 500 μL $AlCl_3$ (10% *w/v*) and 500 μL NaOH (1.0 M) were sequentially added to a 10 mL volumetric flask containing 500 μL of extract solution in methanol at 0, 5 and 11 min, respectively. Each addition was followed by gentle shaking. Methanol was used as a blank control. The reaction mixture was kept at room temperature for 15 min with occasional shakings, distilled water was then added to achieve a final volume of 10 mL. The absorbance of the reaction mixture was measured at 415 nm by a UV-vis photospectrometer (Model 2450, Shimadzu Co., Ltd., Kyoto, Japan). TFC was calculated from a linear calibration curve ($y = 0.0013x + 0.0031$, $R^2 = 0.9996$, linear range from 31.25 to 500 μg) which was constructed by plotting the absorbance values against the amounts of quercetin, and expressed as micromole of quercetin equivalent per gram dry weight of extract (μM QE/g DW). Each measurement was conducted in triplicate.

2.7. HPLC Analysis

The individual flavonoids were analyzed according to the method reported previously with some minor modifications [12]. The peel extract was dissolved in 5% DMF/methanol solution (*v/v*) to form a clear solution with a concentration of 25 mg/mL, which was then filtered through a 0.22 μm Millipore filter. The flavonoids of the extract were analyzed by Agilent 1200 HPLC system coupled with an XBridge-C18 reverse phase column (150 mm length × 4.6 mm id, 5.0 μm particle size) at 340 nm detection wavelength. The mobile phase consisted of acetonitrile (A) and water (B) with a gradient elution: 10–25% A (0–15 min), 25–35% A (15–25 min), 35–50% A (25–50 min), 50–90% A (50–60 min), 90% A (60–70 min), 90–10% A (70–75 min). The injection volume was 20 μL with a flow rate of 1.0 mL/min. The identification of individual flavonoids in the extract was achieved by comparisons of retention time and UV absorption pattern with those of standard compound, and the calibration equation was used to quantify the amount of each flavonoid with the result being expressed as μg flavonoid per mg of the dry weight of peel extract (μg/mg DW). The retention time, regression parameters, and linear range of standard compounds analyzed by HPLC were reported in Table S1 (Supplementary File). Each measurement was conducted in triplicate.

2.8. DPPH Scavenging Assay

DPPH assay was performed according to the method reported previously with some modifications [13]. Briefly, DPPH was freshly prepared in methanol at a concentration of 0.1 mM. The peel extract was dissolved in methanol and subjected to two-fold dilution with methanol to prepare desired solutions with concentrations ranging from 0.625 to 10 mg/mL. In total, 50 μL of each solution was placed into a 96-well plate, followed by the addition of a freshly prepared DPPH reagent (150 μL). The plate was

incubated at 37 °C in dark for 20 min, then the absorption at 517 nm was detected by using a microplate reader (Tecan Spark 10M, Männedorf, Switzerland). Vitamin C (VC) was used as a positive control. The measurements were performed in triplicate with three replications. The inhibitory rate was calculated according to the formula: Inhibition (%) = $[1 - (A_{treated} - A_{blank})/A_{control}] \times 100$, where $A_{treated}$ represents the average absorption of wells adding both DPPH and extract solution, A_{blank} is the average absorption of wells only adding extract solution, and $A_{control}$ is the average absorption of wells only adding DPPH. The IC_{50} value represents the sample concentration scavenging 50% of the DPPH radical.

2.9. ABTS Scavenging Assay

ABTS radical scavenging ability was determined according to a previous method with some minor modifications [2]. The ABTS aqueous solution (7 mM) and ammonium persulfate aqueous solution (2.45 mM) were mixed at a volume ratio of 1:1 and reacted in dark at room temperature for 12 h to form a stable ABTS radical solution, which was then diluted with 70% ethanol/water to an absorbance of 0.70 ± 0.02 at 734 nm before use. The peel extract was dissolved and two-fold diluted with 70% ethanol/water to prepare test solutions. In total, 50 μL of each test solution was added to the wells of a 96-well plate, followed by the addition of freshly prepared ABTS radical solution (200 μL). A 70% ethanol/water and vitamin C mixture was employed as a blank and positive control, respectively. The plate was smoothly shaken for 10 min, then the absorbance was measured at 734 nm by using a microplate reader (Tecan Spark 10M, Männedorf, Switzerland). The scavenging capacity was calculated according to the formula: Inhibition (%) = $[1 - (A_{treated} - A_{blank})/A_{control}] \times 100$, where the $A_{treated}$ represented the average absorption of wells containing both ABTS and extract solution, A_{blank} was the average absorption of wells containing only extract solution, and $A_{control}$ was the average absorption of wells containing only ABTS. The measurements were performed in triplicate with three replications. The IC_{50} value was expressed as the concentration scavenging 50% of ABTS radical.

2.10. FRAP Assay

FRAP assay was carried out according to a previous method with minor modifications [14]. FRAP solution was prepared by mixing TPTZ (10 mM in 40 mM HCl aqueous solution), acetate buffer (0.1 mM, pH 3.6), and ferric chloride (20 mM in 40 mM HCl aqueous solution) at a volume ratio of 1:10:1. The peel extract was dissolved and two-fold diluted with 70% ethanol/water to give test solutions. In total, 50 μL of each test solution was added to the wells of a 96-well plate, followed by the addition of a freshly prepared FRAP reagent (200 μL). A 70% ethanol/water and vitamin C mixture was used as the blank and positive control, respectively. The plate was smoothly shaken for 10 min, and the absorbance was then measured at 593 nm by a microplate reader (Tecan Spark 10M, Männedorf, Switzerland). The measurements were performed in triplicate with three replications. FRAP value was calculated from a linear calibration curve ($y = 0.0345x - 0.0084$, $R^2 = 0.9997$, linear range from 1.56 to 50 mg/L) which was constructed by plotting the absorbance values against the concentrations of vitamin C (VC), and expressed as μg of VC equivalent antioxidant capacity per mg of the dry weight of the extract (μg VC/mg).

2.11. Statistical Analysis

Data were expressed as mean ± standard deviation (SD) of independent experiments performed in triplicate and were analyzed by using one-way analysis of variance (ANOVA) ($p < 0.05$) with SPSS 21 (IBM Corporation, Armonk, NY, USA). Pearson's correlation analysis was performed using SPSS 21 (IBM Corporation, Armonk, NY, USA) and the heatmap was obtained by the software TBtools (version 1.0692).

3. Results and Discussion

3.1. Effect of Different Drying Methods on the Extracting Yield, TPC, and TFC

The maceration extraction at room temperature was used to extract the dried peel in the present study since it had a minimum side effect on the chemical components compared to other extraction methods employing heat or sonication treatments which might cause degradation or decomposition of compounds. Therefore, the present result might give convincing results reflecting the effect of only different drying methods without the influence of extraction processing. The extracting yield was shown in Table 1. The peel treated with MD had the best extracting yield (35.63%) when compared to other treatments, followed in sequence by FD (34.59%), OD50 (33.33%), OD70 (32.08%), and SD (32.44%) treatments. Similarly, a previous study has reported that freeze drying has an obvious advantage in extracting yield compared with the hot-air drying method [15]. The microwave radiation might make the fiber matrix become larger and looser and promote the formation of a more porous structure in the peel, thus facilitating the extraction with solvent, which might account for the highest extracting yield for MD treatment in the present study. This assumption was supported by previous studies indicating that the pore size of the citrus peel dried by the microwave method was greater than that of the citrus peel dried by the hot-air method [16] and that the fiber structure in hot-air dried shiitake mushrooms was arranged tightly while the microwave-dried samples demonstrated a clear porous structure [17].

Table 1. Extracting yield, TPC and TFC of extracts from navel orange peel dried by different methods.

Drying Methods	Yield (%)	TPC (μM GAE/g DW)	TFC (μM QE/g DW)
FD	34.59 ± 0.27^{b}	75.42 ± 0.41^{c}	183.06 ± 1.57^{a}
SD	32.44 ± 0.31^{d}	77.75 ± 0.62^{b}	160.41 ± 1.22^{c}
OD50	33.33 ± 0.15^{c}	78.93 ± 1.04^{b}	182.57 ± 3.21^{a}
OD70	32.08 ± 0.11^{d}	81.36 ± 0.91^{a}	168.14 ± 0.92^{b}
MD	35.63 ± 0.12^{a}	71.72 ± 0.73^{d}	139.93 ± 3.28^{d}

The data are reported as average ± SD (three replicates). The different superscript lowercase letters within the same column indicate significant statistical difference ($p < 0.05$). GAE: Gallic acid equivalent. QE: Quercetin equivalent. DW: Dry weight. TPC: Total phenolic content. TFC: Total flavonoid content. FD: Freeze drying. SD: Shade drying. OD50: Hot-air oven drying at 50 °C. OD70: Hot-air oven drying at 70 °C. MD: Microwave drying.

The TPC in peel subjected to different drying methods was listed in the order OD70 > OD50 > SD > FD > MD. As shown in Table 1, the two highest TPC values were obtained both from the OD treatments, suggesting that the heat treatment might enhance the production of extractable phenolics in the peel. This suggestion was supported as well by the TPC results showing OD > SD > FD, where the drying temperature decreased in sequence. The phenolics in citrus were present in two forms—bound or free form—and the bound form was supposed to be liberated to the free form as the temperature increased [3]. The present result supported this assumption and suggested that the high drying temperature would liberate some bound phenolics to free form, thus resulting in more extractable phenolics in OD-treated peel than those in SD or FD-treated ones. Similarly, Papoutsis et al. reported that TPC was higher in lemon pomace dried by hot air than that dried by freeze drying and it increased as the drying temperature increased [8].

In addition, the TPC result in the present study could be attributed to the presence of polyphenol oxidase (PPO) in the peel as well. PPO is an enzyme responsible for the selective oxidation of polyphenols, and its activity tends to reduce as temperature increases [18]. In the present study, the PPO activity in OD70-treated peel should be lower than in other treatments since the drying temperature during OD70 processing is 70 °C, which might deactivate the enzymatic activity and cause less oxidative degradation of phenolics, thus resulting in the highest TPC value in the peel treated with OD70 compared to other treatments.

The TFC in dried peel was significantly affected by different drying methods ($p < 0.05$). As shown in Table 1, the peel treated with FD had the highest TFC value, followed by OD50, OD70, SD, and MD in sequence. The flavonoids could be degraded by thermal treatment and by some endogenous enzymes such as PPO and peroxidase (POD) [19]. The TFC in OD50 was slightly lower than that in FD (no significant difference at $p > 0.05$), suggesting that the heat temperature at 50 °C could be capable of deactivating the enzymes associated with the degradation of flavonoids, but not be high enough to significantly destroy flavonoids by thermal decomposition during drying processing. When the temperature is raised to 70 °C, some heat-sensitive flavonoids might be decomposed, thus resulting in lower TFC in OD70 relative to OD50 in the present study. The SD treatment was performed at ambient temperature which might be an appropriate temperature for the catalytic activity of some related enzymes such as PPO or POD, implying the flavonoids might be exposed to these high-activity enzymes for a long time, therefore, the TFC in SD treated peel was significantly lower than that in OD treated ones. It has been reported that the optimum temperature for the enzymatic activity of PPO and POD in *Rumex obtusifolius* L. is 30 and 25 °C, respectively [20], which is supportive of this assumption. In agreement with the present result, the TFC of physiologically dropped immature citrus fruit dried by hot air at 60 °C was not significantly different from that obtained from freeze drying, and both of them were higher than that treated with sun drying at a temperature around 25 °C [3]. Interestingly, the present result indicated that both the TPC and TFC values in the peel treated with MD were the smallest among all these five treatments. The microwave radiation with high energy can rapidly diffuse into the internal cells and be quickly absorbed by some molecules such as phenolics and flavonoids [21], thus causing their decomposition by breaking down covalent bonds, which might account for this observation. Similarly, Liu et al. reported that the microwave treatment contributed to the greatest losses of phenolics and antioxidant capacities in buckwheat samples relative to all other thermal treatments [22], and the microwave drying caused the greatest decrease in TPC of *Phyllanthus amarus* as compared to the sun and hot-air drying methods [23].

3.2. Effect of Different Drying Methods on the Contents of Individual Flavonoids

As shown in Figure 1, thirteen flavonoids involving three flavanone glycosides (FGs) and ten polymethoxyflavones (PMFs) were identified from the peel extract. The contents of these flavonoids were quantified by HPLC as shown in Table 2. The present study indicated that the most abundant FG in navel orange peel was hesperidin, followed by narirutin and didymin. The PMFs mainly consisted of sinensetin, nobiletin, 3,3′,4′,5,6,7,8-heptamethoxyflavone, 3,3′,4′,5,6,7-hexamethoxyflavone, and 4′,5,6,7-tetramethoxyflavone with a descending order in content, as revealed in Table 2. In line with the present result, previous phytochemical investigations have shown that hesperidin and narirutin are the two dominant flavanone glycosides present in the orange peel [6], and PMFs involving nobiletin, tangeretin, and sinesetin are abundant flavones in citrus peel [5]. The contents of these thirteen individual flavonoids from peels dried with different methods were compared in the present study. As shown in Table 2, the contents of PMFs were slightly influenced by different drying methods, which showed no significant statistical difference among all these different treatments. However, the MD treatment significantly reduced the content of all three FGs in peel extract compared with other treatments. The content of narirutin, hesperidin, and didymin was 6.22, 17.28, and 0.88 μg/mg DW, respectively, in the peel treated with MD, whereas it ranged from 8.17 to 9.57, 31.29 to 36.27, and 1.71 to 1.85, respectively, for other treatments.

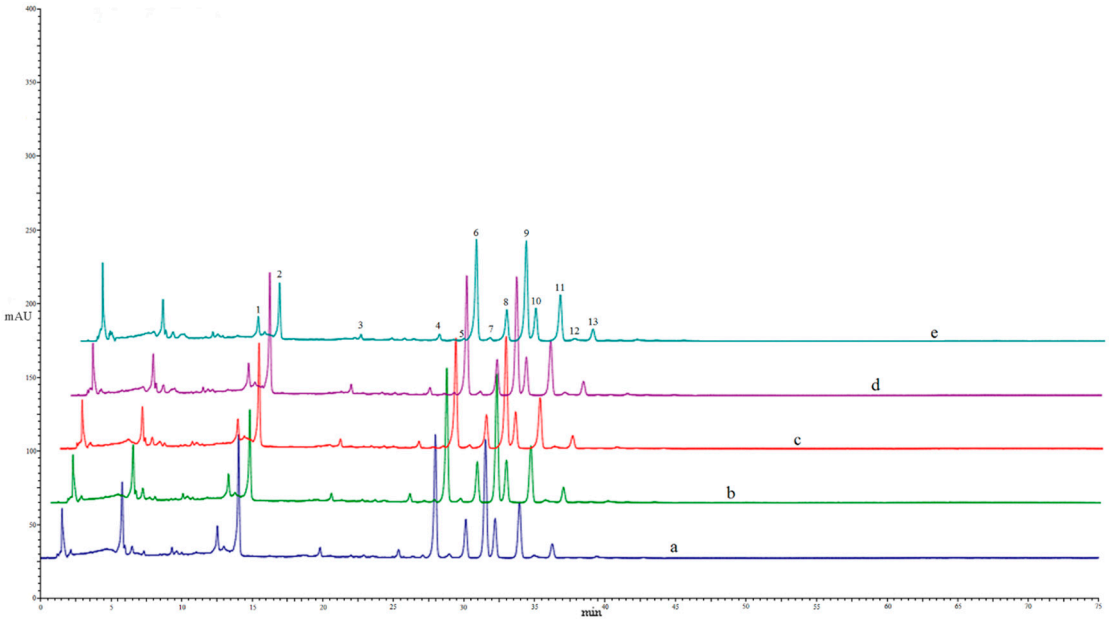

Figure 1. HPLC profiles of extracts from the navel orange peels dried by different drying methods. The letters from a to e, represent FD, SD, OD50, OD70, and MD, respectively. The number above the peak represent the following compounds: (1) narirutin, (2) hesperidin, (3) didymin, (4) isosinensetin, (5) 3,3′,4′,5,7,8-hexamethoxyflavone, (6) sinensetin, (7) 4′,5,7,8-tetramethoxyflavone, (8) 3,3′,4′,5,6,7-hexamethoxyflavone, (9) nobiletin, (10) 4′,5,6,7-tetramethoxyflavone, (11) 3,3′,4′,5,6,7,8-heptamethoxyflavone, (12) 5-hydroxy-6,7,3′,4′-tetramethoxyflavone, (13) tangeretin.

Table 2. HPLC quantification analysis of flavonoids (μg/mg DW) in extracts from the orange peels dried by different methods.

NO	Flavonoids	FD	SD	OD50	OD70	MD
1	narirutin	9.10 ± 0.32 ^{a}	8.17 ± 0.80 ^{a}	9.13 ± 0.70 ^{a}	9.57 ± 0.32 ^{a}	6.22 ± 1.11 ^{b}
2	hesperidin	36.27 ± 3.25 ^{a}	31.29 ± 1.19 ^{a}	32.79 ± 2.14 ^{a}	35.51 ± 1.22 ^{a}	17.28 ± 2.91 ^{b}
3	didymin	1.71 ± 0.05 ^{a}	1.72 ± 0.26 ^{a}	1.85 ± 0.35 ^{a}	1.82 ± 0.14 ^{a}	0.88 ± 0.25 ^{b}
4	isosinensetin	0.12 ± 0.01 ^{a}	0.12 ± 0.01 ^{a}	0.11 ± 0.02 ^{a}	0.12 ± 0.01 ^{a}	0.10 ± 0.01 ^{a}
5	3,3′,4′,5,7,8-hexamethoxyflavone	0.05 ± 0.01 ^{a}	0.04 ± 0.01 ^{a}	0.05 ± 0.01 ^{a}	0.06 ± 0.01 ^{a}	0.05 ± 0.01 ^{a}
6	sinensetin	1.59 ± 0.04 ^{a}	1.62 ± 0.01 ^{a}	1.59 ± 0.09 ^{a}	1.56 ± 0.05 ^{a}	1.56 ± 0.07 ^{a}
7	4′,5,7,8-tetramethoxyflavone	0.05 ± 0.01 ^{a}	0.04 ± 0.01 ^{a}	0.05 ± 0.01 ^{a}	0.05 ± 0.01 ^{a}	0.05 ± 0.01 ^{a}
8	3,3′,4′,5,6,7-hexamethoxyflavone	0.58 ± 0.01 ^{a}	0.59 ± 0.01 ^{a}	0.59 ± 0.03 ^{a}	0.59 ± 0.02 ^{a}	0.58 ± 0.02 ^{a}
9	nobiletin	1.09 ± 0.03 ^{a}	1.13 ± 0.04 ^{a}	1.12 ± 0.06 ^{a}	1.10 ± 0.04 ^{a}	1.09 ± 0.05 ^{a}
10	4′,5,6,7-tetramethoxyflavone	0.52 ± 0.01 ^{a}	0.56 ± 0.02 ^{a}	0.53 ± 0.03 ^{a}	0.51 ± 0.02 ^{a}	0.52 ± 0.04 ^{a}
11	3,3′,4′,5,6,7,8-heptamethoxyflavone	0.90 ± 0.01 ^{a}	0.93 ± 0.02 ^{a}	0.92 ± 0.05 ^{a}	0.92 ± 0.03 ^{a}	0.89 ± 0.04 ^{a}
12	5-hydroxy-6,7,3′,4′-tetramethoxyflavone	0.09 ± 0.01 ^{a}	0.08 ± 0.01 ^{a}	0.08 ± 0.01 ^{a}	0.11 ± 0.03 ^{a}	0.10 ± 0.01 ^{a}
13	tangeretin	0.13 ± 0.01 ^{a}	0.14 ± 0.01 ^{a}	0.15 ± 0.01 ^{a}	0.14 ± 0.02 ^{a}	0.14 ± 0.01 ^{a}

The data are reported as averages ± SD (three replicates). Different superscript lowercase letters within the same line indicate significant statistical difference ($p < 0.05$). FD: Freeze drying. SD: Shade drying. OD50: Hot-air oven drying at 50 °C. OD70: Hot-air oven drying at 70 °C. MD: Microwave drying.

Despite there being no significant difference in the content of FGs in peels treated with FD, SD, OD50, and OD70, the peel treated with SD contained the lowest amounts of both narirutin and hesperidin among them. This result was consistent with the TFC result showing that the peel treated with MD and SD contained the lowest and the second-lowest TFC, respectively. Previous studies indicated that microwave irradiation can cleave the ester and glycosidic bond of phenolics in citrus peel [24], and have the ability to hydrolyze rice starch by breaking down C-O-C covalent linkage between monosaccharides [25]. Therefore, we assumed that the glycosidic bond of FGs might be vulnerable to the MD treatment,

which might initially break down upon absorbing the microwave irradiation, then inducing the further degradation of FGs, thus making the peel treated with MD contain low amounts of FGs as shown in Table 2. Moreover, the PMFs' structural differences from FGs mainly by the absence of sugar moiety were slightly influenced by MD treatment, which further supported this assumption. However, more studies should be carried out to elucidate the degradation mechanisms of FGs. The present result also revealed that the PMFs were much more stable under all these drying conditions, which was in line with a previous study showing that the methylation treatments improved the stability of flavonoids [26].

3.3. Evaluation of Antioxidant Capacity

The antioxidant capacity of peels dried with different methods was evaluated by DPPH, ABTS, and FRAP assays. As shown in Table 3, the extract from peel treated with OD50 demonstrated the most potent capacity in scavenging both DPPH and ABTS radicals, and the extract from peel treated with OD70 was superior in FRAP assay when compared to other treatments. In contrast, the extract from the peel treated with FD had the highest IC_{50} value in both DPPH and ABTS assays, and the SD treatment made the peel extract less powerful in reducing ferric (III) to ferrous (II) ions as revealed in the FRAP assay relative to other treatments. Both DPPH and ABTS are stable free radicals, the scavenging of these two radicals is mainly based on the electron transfer and the hydrogen atom transfer reaction mechanisms [27]. Being different from the radical-scavenging assays, the FRAP assay is commonly used to evaluate the overall reducing ability of antioxidants by measuring the reduction of ferric (III) to ferrous (II) ions [28]. The antioxidant capacity evaluated by the DPPH assay is much more consistent with that by the ABTS assay but different from that obtained by the FRAP assay in the present study, which might be due to the discrepancy in the mechanisms of different antioxidant assays. The present result also supported that more than one antioxidant assay should be performed to comprehensively evaluate the antioxidant capacity because a single antioxidant assay is not sufficient to measure the various modes of action of antioxidants [29]. Similar to the present study, the extract from lemon pomace dried by hot air exhibited higher antioxidant capacity in scavenging DPPH radical than that dried by freeze drying [8]. However, Sun et al. reported that the antioxidant capacity of physiologically dropped immature citrus fruits dried by freeze drying was higher when compared to those dried by hot air or sun drying in both DPPH and FRAP assays [3], which was inconsistent with the present study. These differences could be attributed to the different drying conditions and the extraction methods applied, as well as the different citrus cultivars used.

Table 3. Antioxidant capacity of extracts from the navel orange peels dried by different methods via DPPH, ABTS, and FRAP assays.

Drying Methods	DPPH (IC_{50} mg/mL)	ABTS (IC_{50} mg/mL)	FRAP (μg VC/mg)
FD	1.37 ± 0.01^{a}	0.32 ± 0.01^{a}	4.03 ± 0.04^{b}
SD	1.23 ± 0.02^{b}	0.24 ± 0.01^{c}	3.39 ± 0.05^{d}
OD50	1.15 ± 0.04^{c}	0.23 ± 0.00^{c}	3.92 ± 0.03^{bc}
OD70	1.18 ± 0.01^{bc}	0.28 ± 0.01^{b}	4.27 ± 0.09^{a}
MD	1.34 ± 0.01^{a}	0.29 ± 0.01^{b}	3.86 ± 0.06^{c}
VC (positive control)	0.0033 ± 0.0003^{d}	0.0029 ± 0.0001^{d}	—

The data are reported as average ± SD (three replicates). The different superscript lowercase letters within the same column indicate significant statistical difference ($p < 0.05$). VC: Vitamin C. —: Not applicable. FD: Freeze drying. SD: Shade drying. OD50: Hot-air oven drying at 50 °C. OD70: Hot-air oven drying at 70 °C. MD: Microwave drying. DPPH: 2,2-Diphenyl-1-picrylhydrazyl free radical. ABTS: 2,2′-Azinobis-(3-ethylbenzthiazoline-6-sulphonate) free radical. FRAP: Ferric reducing antioxidant power.

3.4. Pearson's Correlation Analysis

Pearson's correlation analysis was used to evaluate the relationships among all variables in the present study. The result of Pearson's correlation analysis is usually expressed

as a correlation coefficient value, which is represented as *r*. The values of *r* range between −1.000 and 1.000. A correlation of −1.000 shows a perfect negative correlation, while a correlation of 1.000 shows a perfect positive correlation [30]. As shown in Figure 2, TFC was highly correlated with all three FGs involving narirutin ($r = 0.777$), hesperidin ($r = 0.843$) and didymin ($r = 0.795$) at $p < 0.01$, suggesting that these three FGs should be the major flavonoids present in peel extract. In addition, the consistent variation trend of DPPH and ABTS in response to different drying methods was found in the present study, which was supported by the strong positive correlation between DPPH and ABTS ($r = 0.770$, $p < 0.01$). Similarly, several previous studies reported a high positive correlation between them [13]. Moreover, DPPH was highly negatively correlated with TPC ($r = -0.793$, $p < 0.01$), and moderately negatively correlated with TFC ($r = -0.455$, $p < 0.01$), suggesting that the phenolics rather than flavonoids should be the main contributors in scavenging the DPPH radical in peel extract. DPPH was expressed as IC_{50} in the present study, the lower value of it representing the higher antioxidant capacity of extract, therefore, the negative correlation coefficient value was obtained. FRAP showed a weak correlation with both TPC ($r = 0.258$, $p < 0.01$) and TFC ($r = 0.313$, $p < 0.01$), indicating that the antioxidant capacity evaluated by FRAP assay could be ascribed to the synergistic effects among antioxidants, or come from other compounds such as polysaccharides, limonoids, and ascorbic acid. Consistent with the present study, a very weak correlation ($r = 0.118$) was observed between FRAP and TPC of extracts from the pomelo peel [14].

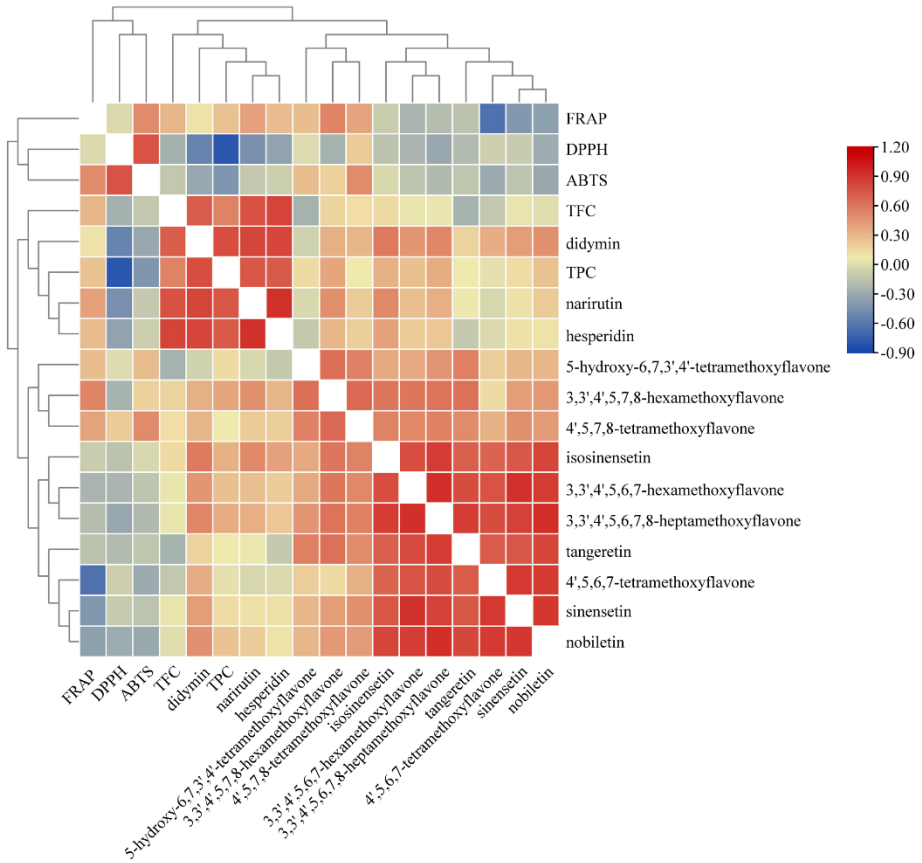

Figure 2. Pearson's correlation analysis among all variables under investigation.

Actually, the antioxidant activity might not always correlate with phenolic content, and the presence of other bioactive compounds such as terpenoids and limonoids in citrus peel could act as an antioxidant [5]. The high correlations between DPPH with didymin ($r = -0.529$, $p < 0.01$) and between FRAP with 3,3′,4′,5,6,7-hexamethoxyflavone were found in the present study, suggesting these two compounds might be potent antioxidants in

the orange peel. In line with our results, a high correlation between didymin and DPPH ($r = 0.83$, $p < 0.01$) was found in a recent report studying immature dropped *Citrus sinensis* L. Osbeck fruits [31].

4. Conclusions

This study comprehensively studied the effects of five different drying methods, namely FD, SD, OD50, OD70, and MD, on the chemical compositions and antioxidant capacity of navel orange peel. The peel treated with OD70 had the highest TPC and FRAP values, and the peel treated with OD50 exhibited the best antioxidant capacity in both DPPH and ABTS assays, when compared to other treatments. The highest TFC was obtained in peel dried by the FD method, which was slightly higher than that in the peel treated with OD50, but there was no significant difference between them ($p > 0.05$). The peel dried by the MD method had the highest extracting yield but contained the lowest TPC and TFC, as well as the lowest contents of three FGs involving narirutin, hesperidin, and didymin, relative to other drying methods. HPLC analysis identified thirteen flavonoids (three FGs and ten PMFs) in the peel extract, and all PMFs were stable during the drying process, showing slight variation in all five different drying methods applied. Pearson's correlation analysis was further employed to test the relationships among all variables. The results revealed here allow us to recommend the use of OD50 or OD70 for the drying of orange peel, both of which help the maintenance of bioactive compounds in the peel and improve its antioxidant capacity. This recommendation is supported as well since the OD drying method is a relatively inexpensive and user-friendly method.

Supplementary Materials: The following supporting information can be downloaded at: https://www.mdpi.com/article/10.3390/antiox11081543/s1. Table S1. The retention time, regression parameters, and linear range of standard compounds analyzed by HPLC. Figures S1–S13. HPLC profile (340 nm) of flavonids (**1**-**13**) obtained from the navel orange peel.

Author Contributions: Conceptualization, K.K. and Y.J.; methodology, C.L., L.Z. and J.Z.; software, Y.L. and J.H.; validation, Y.L., J.H. and K.K.; formal analysis, Y.L.; investigation, C.L. and L.Z.; resources, J.Z. and Y.J.; data curation, J.Z.; writing—original draft preparation, C.L. and Y.L.; writing—review and editing, J.Z. and K.K.; visualization, C.L.; supervision, J.Z. and Y.J.; project administration, J.Z. and Y.L.; funding acquisition, J.Z. and Y.J. All authors have read and agreed to the published version of the manuscript.

Funding: This research work was financially supported by the National Natural Science Foundation of China (No. 31860091), the Key Research Project of Jiangxi Province (No. 20203BBF63028), the "Double Thousand Talents Plan" of Jiangxi Province (jxsq2019102029), and the Foundation of Science and Technology Bureau of Ganzhou (Nos. 202101124704, 202060).

Institutional Review Board Statement: Not applicable.

Informed Consent Statement: Not applicable.

Data Availability Statement: Data are contained within the article and supplementary material.

Conflicts of Interest: The authors declare no conflict of interest.

References

1. Zhang, J.; Zhang, J.Y.; Shan, Y.X.; Guo, C.; He, L.; Zhang, L.Y.; Ling, W.; Liang, Y.; Zhong, B.L. Effect of harvest time on the chemical composition and antioxidant capacity of Gannan navel orange (*Citrus sinensis* L. Osbeck 'Newhall') juice. *J. Integr. Agr.* **2022**, *21*, 261–272. [CrossRef]
2. Guo, C.; Shan, Y.; Yang, Z.; Zhang, L.; Ling, W.; Liang, Y.; Ouyang, Z.; Zhong, B.; Zhang, J. Chemical composition, antioxidant, antibacterial, and tyrosinase inhibition activity of extracts from Newhall navel orange (*Citrus sinensis* Osbeck cv. Newhall) Peel. *J. Sci. Food Agric.* **2020**, *100*, 2664–2674. [CrossRef]
3. Sun, Y.; Shen, Y.; Liu, D.; Ye, X. Effects of drying methods on phytochemical compounds and antioxidant activity of physiologically dropped un-Matured citrus fruits. *LWT-Food Sci. Technol.* **2015**, *60*, 1269–1275. [CrossRef]
4. Ghanem Romdhane, N.; Bonazzi, C.; Kechaou, N.; Mihoubi, N.B. Effect of air-drying temperature on kinetics of quality attributes of lemon (*Citrus limon* cv. Lunari) peels. *Dry. Technol.* **2015**, *33*, 1581–1589. [CrossRef]

5. Saini, R.K.; Ranjit, A.; Sharma, K.; Prasad, P.; Shang, X.; Gowda, K.G.M.; Keum, Y.S. Bioactive compounds of citrus fruits: A review of composition and health benefits of carotenoids, flavonoids, limonoids, and terpenes. *Antioxidants* **2022**, *11*, 239. [CrossRef]
6. Pereira, R.M.; López, B.G.C.; Diniz, S.N.; Antunes, A.A.; Garcia, D.M.; Oliveira, C.R.; Marcucci, M.C. Quantification of flavonoids in Brazilian orange peels and industrial orange juice processing wastes. *Agric. Sci.* **2017**, *8*, 631–644. [CrossRef]
7. Deng, L.Z.; Mujumdar, A.S.; Yang, W.X.; Zhang, Q.; Zheng, Z.A.; Wu, M.; Xiao, H.W. Hot air impingement drying kinetics and quality attributes of orange peel. *J. Food Process. Pres.* **2020**, *44*, e14294. [CrossRef]
8. Papoutsis, K.; Pristijono, P.; Golding, J.B.; Stathopoulos, C.E.; Bowyer, M.C.; Scarlett, C.J.; Vuong, Q.V. Effect of vacuum-drying, hot air-drying and freeze-drying on polyphenols and antioxidant capacity of lemon (*Citrus limon*) pomace aqueous extracts. *Int. J. Food Sci. Technol.* **2017**, *52*, 880–887. [CrossRef]
9. Garau, M.C.; Simal, S.; Rossello, C.; Femenia, A. Effect of air-drying temperature on physico-chemical properties of dietary fibre and antioxidant capacity of orange (*Citrus aurantium* v. Canoneta) by-products. *Food Chem.* **2007**, *104*, 1014–1024. [CrossRef]
10. Kammoun Bejar, A.; Kechaou, N.; Boudhrioua Mihoubi, N. Effect of microwave treatment on physical and functional properties of orange (*Citrus Sinensis*) peel and leaves. *J. Food Process. Technol.* **2011**, *2*, 109–116. [CrossRef]
11. Ledesma-Escobar, C.A.; Priego-Capote, F.; Luque de Castro, M.D. Comparative study of the effect of sample pretreatment and extraction on the determination of flavonoids from lemon (*Citrus limon*). *PLoS ONE* **2016**, *11*, e0148056. [CrossRef] [PubMed]
12. Zhang, J.; Zhang, J.; Kaliaperumal, K.; Zhong, B. Variations of the chemical composition of *Citrus sinensis* Osbeck cv. Newhall fruit in relation to the symptom severity of Huanglongbing. *J. Food Compos. Anal.* **2022**, *105*, 104–269. [CrossRef]
13. Dudonne, S.; Vitrac, X.; Coutiere, P.; Woillez, M.; Mérillon, J.M. Comparative study of antioxidant properties and total phenolic content of 30 plant extracts of industrial interest using DPPH, ABTS, FRAP, SOD, and ORAC assays. *J. Agric. Food Chem.* **2009**, *57*, 1768–1774. [CrossRef] [PubMed]
14. Abd Rahman, N.F.; Shamsudin, R.; Ismail, A.; Shah, N.N.A.K.; Varith, J. Effects of drying methods on total phenolic contents and antioxidant capacity of the pomelo (*Citrus grandis* (L.) Osbeck) peels. *Innov. Food Sci. Emerg.* **2018**, *50*, 217–225. [CrossRef]
15. Jia, Y.; Khalifa, I.; Hu, L.; Zhu, W.; Li, J.; Li, K.; Li, C. Influence of three different drying techniques on persimmon chips' characteristics: A comparison study among hot-air, combined hot-air-microwave, and vacuum-freeze drying techniques. *Food Bioprod. Process.* **2019**, *118*, 67–76. [CrossRef]
16. Shu, B.; Wu, G.; Wang, Z.; Wang, J.; Huang, F.; Dong, L.; Zhang, R.; Wang, Y.; Su, D. the effect of microwave vacuum drying process on citrus: Drying kinetics, physicochemical composition and antioxidant activity of dried citrus (*Citrus reticulata* Blanco) peel. *J. Food Meas. Charact.* **2020**, *14*, 2443–2452. [CrossRef]
17. Tian, Y.; Zhao, Y.; Huang, J.; Zeng, H.; Zheng, B. Effects of different drying methods on the product quality and volatile compounds of whole Shiitake mushrooms. *Food Chem.* **2016**, *197*, 714–722. [CrossRef]
18. Krapfenbauer, G.; Kinner, M.; Gössinger, M.; Schönlechner, R.; Berghofer, E. Effect of thermal treatment on the quality of cloudy apple juice. *J. Agric. Food Chem.* **2006**, *54*, 5453–5460. [CrossRef]
19. Almeida, J.R.; D'Amico, E.; Preuss, A.; Carbone, F.; de Vos, C.R.; Deiml, B.; Mourgues, F.; Perrotta, G.; Fischer, T.C.; Bovy, A.G.; et al. Characterization of major enzymes and genes involved in flavonoid and proanthocyanidin biosynthesis during fruit development in strawberry (*Fragaria* × *ananassa*). *Arch. Biochem. Biophs.* **2007**, *465*, 61–71. [CrossRef]
20. Alici, E.H.; Arabaci, G. Determination of SOD, POD, PPO and cat enzyme activities in *Rumex obtusifolius* L. *Annu. Res. Rev. Biol.* **2016**, *11*, 1–7. [CrossRef]
21. Flórez, N.; Conde, E.; Domínguez, H. Microwave assisted water extraction of plant compounds. *J. Chem. Technol. Biot.* **2015**, *90*, 590–607. [CrossRef]
22. Liu, Y.; Cai, C.; Yao, Y.; Xu, B. Alteration of phenolic profiles and antioxidant capacities of common buckwheat and tartary buckwheat produced in China upon thermal processing. *J. Sci. Food Agric.* **2019**, *99*, 5565–5576. [CrossRef] [PubMed]
23. Lim, Y.Y.; Murtijaya, J. Antioxidant properties of *Phyllanthus amarus* extracts as affected by different drying methods. *LWT-Food Sci. Technol.* **2007**, *40*, 1664–1669. [CrossRef]
24. Hayat, K.; Zhang, X.; Chen, H.; Xia, S.; Jia, C.; Zhong, F. Liberation and separation of phenolic compounds from citrus mandarin peels by microwave heating and its effect on antioxidant activity. *Sep. Purif. Technol.* **2010**, *73*, 371–376. [CrossRef]
25. Iris, K.M.; Fan, J.; Budarin, V.L.; Bouxin, F.P.; Clark, J.H.; Tsang, D.C. NaCl-promoted phase transition and glycosidic bond cleavage under microwave heating for energy-efficient biorefinery of rice starch. *Green Chem.* **2020**, *22*, 7355–7365. [CrossRef]
26. Walle, T. Methylation of dietary flavones increases their metabolic stability and chemopreventive effects. *Int. J Mol. Sci.* **2009**, *10*, 5002–5019. [CrossRef] [PubMed]
27. Schaich, K.M.; Tian, X.; Xie, J. Hurdles and pitfalls in measuring antioxidant efficacy: A critical evaluation of ABTS, DPPH, and ORAC assays. *J. Funct. Foods* **2015**, *14*, 111–125. [CrossRef]
28. Li, H.B.; Wong, C.C.; Cheng, K.W.; Chen, F. Antioxidant properties in vitro and total phenolic contents in methanol extracts from medicinal plants. *LWT-Food Sci. Technol.* **2008**, *41*, 385–390. [CrossRef]
29. Rakholiya, K.; Kaneria, M.; Chanda, S. Vegetable and fruit peels as a novel source of antioxidants. *J. Med. Plants Res.* **2011**, *5*, 63–71. [CrossRef]
30. Mukaka, M.M. A guide to appropriate use of correlation coefficient in medical research. *Malawi Med. J.* **2012**, *24*, 69–71.
31. Kumar, D.; Ladaniya, M.S.; Gurjar, M.; Kumar, S. Impact of drying methods on natural antioxidants, phenols and flavanones of immature dropped *Citrus sinensis* L. Osbeck fruits. *Sci. Rep.* **2022**, *12*, 6684. [CrossRef] [PubMed]

antioxidants

MDPI

Article

The Flavonoid Hesperidin Methyl Chalcone Targets Cytokines and Oxidative Stress to Reduce Diclofenac-Induced Acute Renal Injury: Contribution of the Nrf2 Redox-Sensitive Pathway

Allan J. C. Bussmann [1], Tiago H. Zaninelli [1], Telma Saraiva-Santos [1], Victor Fattori [1], Carla F. S. Guazelli [1], Mariana M. Bertozzi [1], Ketlem C. Andrade [1], Camila R. Ferraz [1], Doumit Camilios-Neto [2], Antônio M. B. Casella [3], Rubia Casagrande [4], Sergio M. Borghi [1,5,*] and Waldiceu A. Verri, Jr. [1,*]

[1] Laboratory of Pain, Inflammation, Neuropathy, and Cancer, Department of Pathology, Londrina State University, Londrina 86057-970, Brazil; bussmann@uel.br (A.J.C.B.); tzaninelli@uel.br (T.H.Z.); telma.saraiva.santos@uel.br (T.S.-S.); vfattori@outlook.com (V.F.); carlafsg@yahoo.com.br (C.F.S.G.); marianambertozzi@gmail.com (M.M.B.); ketlemandrade94@gmail.com (K.C.A.); camila_ferraz96@hotmail.com (C.R.F.)

[2] Department of Biochemistry and Biotechnology, Center of Exact Sciences, Londrina State University, Londrina 86057-970, Brazil; camiliosneto@uel.br

[3] Department of Internal Medicine, Center of Health Sciences, Londrina State University, Londrina 86039-440, Brazil; casella@uel.br

[4] Department of Pharmaceutical Sciences, Center of Health Sciences, Londrina State University, Londrina 86039-440, Brazil; rubiacasa@uel.br

[5] Center for Research in Health Sciences, University of Northern Paraná, Londrina 86041-140, Brazil

* Correspondence: sergio.borghi@kroton.com.br (S.M.B.); waverri@uel.br (W.A.V.J.); Tel.: +55-43-3371-9848 (S.M.B.); +55-43-3371-4979 (W.A.V.J.)

Abstract: Hesperidin is derived from citrus fruits among other plants. Hesperidin was methylated to increase its solubility, generating hesperidin methyl chalcone (HMC), an emerging flavonoid that possess anti-inflammatory and antioxidant properties. The nuclear factor erythroid 2-related factor 2 (Nrf2) is a powerful regulator of cellular resistance to oxidant products. Previous data evidenced HMC can activate Nrf2 signaling, providing antioxidant protection against diverse pathological conditions. However, its effects on kidney damage caused by non-steroidal anti-inflammatory drugs (NSAIDs) have not been evaluated so far. Mice received a nephrotoxic dose of diclofenac (200 mg/kg) orally followed by intra-peritoneal (i.p.) administration of HMC (0.03–3 mg/kg) or vehicle. Plasmatic levels of urea, creatinine, oxidative stress, and cytokines were assessed. Regarding the kidneys, oxidative parameters, cytokine production, kidney swelling, urine NGAL, histopathology, and Nrf2 mRNA expression and downstream targets were evaluated. HMC dose-dependently targeted diclofenac systemic alterations by decreasing urea and creatinine levels, and lipid peroxidation, as well as IL-6, IFN-γ, and IL-33 production, and restored antioxidant properties in plasma samples. In kidney samples, HMC re-established antioxidant defenses, inhibited lipid peroxidation and pro-inflammatory cytokines and upregulated IL-10, reduced kidney swelling, urine NGAL, and histopathological alterations. Additionally, HMC induced mRNA expression of Nrf2 and its downstream effectors HO-1 and Nqo1, as well as reduced the levels of Keap1 protein detected in renal tissue. The present data demonstrate HMC is a potential compound for the treatment of acute renal damage caused by diclofenac, a routinely prescribed non-steroidal anti-inflammatory drug.

Keywords: citrus flavonoid; hesperidin methylchalcone; Nrf2; diclofenac; acute renal injury; oxidative stress

1. Introduction

The use of non-steroidal anti-inflammatory drugs (NSAIDs) is a common approach due to their analgesic, anti-inflammatory, and anti-pyretic effects [1]. Based on their recognized effectiveness for the treatment of inflammatory diseases and pain, their prescription is preferred in primary health care. However, NSAIDs can induce acute kidney injury (AKI) [2,3], a condition with potential health risks. Increased risk of AKI is observed in older individuals and in patients with chronic kidney disease [2]. Even in healthy patients, long term NSAID use may cause subclinical kidney dysfunction [4,5]. Diclofenac represents the most prescribed and used NSAID in low-, middle-, and high-income countries worldwide [6,7]. As a phenylacetic acid derivative, diclofenac is classified as a non-selective NSAID applied to treat pain, fever, and inflammation [1]. It is one of the main options for the treatment of acute and chronic pain, related mainly to the musculoskeletal system, including myalgia, lower back pain, osteoarthritis, rheumatoid arthritis, and ankylosing spondylitis [8–10]. Unfortunately, diclofenac has many adverse effects, such as gastrointestinal injury, hepatotoxicity, cardiovascular pathology, and AKI [1,3,9,11].

The main mechanism related to NSAID-induced AKI is prostaglandin inhibition, which in turn, has a fundamental role in the control of renin release, electrolytic dysfunction, and vasoconstriction [4,12]. At standard treatment doses, cyclooxygenase (COX)-2 selective and non-selective COX-2 NSAIDs induce a similar risk of AKI, depending on the study, and findings also suggest a higher risk upon the use of COX-2 NSAIDs with <5-fold selectivity compared to >5-fold selectivity [2]. Despite being considered as possessing equivalent inhibition of all COX enzymes, evidence also suggests diclofenac is more selective for COX-2 [7,13]. We previously demonstrated diclofenac does not alter COX-2 levels in renal tissue [9]. This particular aspect highlights the fact that diclofenac may induce AKI via a different primary pathological mechanism. It is postulated that a mechanism related to the induction of oxidative stress and/or reduction of antioxidant capacity may be determinant for diclofenac-induced nephrotoxicity [14,15]. In this sense, investigations have shown that through oxidative stress, increased cytokine release, and nuclear factor κB (NFκB) activation, diclofenac may induce AKI [1,9,16]. Therefore, the search for compounds that target these effector mechanisms, especially oxidative stress, is pertinent.

Hesperidin methyl chalcone (HMC; $C_{29}H_{36}O_{15}$; Figure 1) is a product of methylation of the flavanone hesperidin (hesperidin-7-rhamnoglucoside), a flavonoid found in plants and foods, for instance, Rutaceae and citrus fruits, respectively [17,18]. Hesperidin presents poor water solubility, resulting in unsatisfactory absorption in the small intestine; however, its solubility is improved after a methylation reaction under alkaline conditions, which promotes hesperidin isomerization, and the generation of the HMC. Thus, the higher solubility of HMC confers enriched bioavailability, metabolic stability, and tissue absorption [19,20]. Methods applied to obtain HMC from hesperidin include methylation with dimethylsulfate [21]. Chromatography analysis indicates HMC is composed of both fully and partially methoxylated hesperidin, generated from methylation of the hydroxyl substituents on aglycon and linked sugars, characterizing this compound as a mixture of chalcones and flavanones species [21]. HMC peaks in the blood 1–2 h after oral administration and is excreted in both urine and feces within the first 24 h after administration [20]. In models of inflammation and pain, the biological properties of HMC include vasoprotective, antioxidant, anti-inflammatory, and analgesic effects [19,22–25]. HMC can both inhibit the major pro-inflammatory transcription factor nuclear factor κB (NFκB) [19,22,24] as well as induce nuclear factor erythroid 2-related factor 2 (Nrf2) signaling [23]. After the release of the Kelch-like ECH-associated protein 1 (Keap1)-Nrf2 complex in the cytoplasm, Nrf2 translocates to the nucleus where it activates nuclear antioxidant responsive elements (ARE) that regulate the dynamic expression of phase II genes, triggering the transcription of several detoxification enzymes and cytoprotective genes [26,27]. In humans, the efficacy of HMC in combination with other molecules for the treatment of vascular dysfunction, including hemorrhoid and chronic venous insufficiency, is supported by clinical trials [25,28–30]. Importantly, experimental and clinical data demonstrated that HMC is safe, even during

long term use and high doses [31,32]. Thus, the eventual repurposing of HMC is feasible. Nevertheless, an investigation of its effects in kidney tissue stimulated with toxic doses of diclofenac, which mimics AKI induced by NSAIDs, has yet to be conducted. The present study aims to explore the beneficial therapeutic properties of HMC on experimental NSAID-induced AKI and the mechanisms underlying these effects.

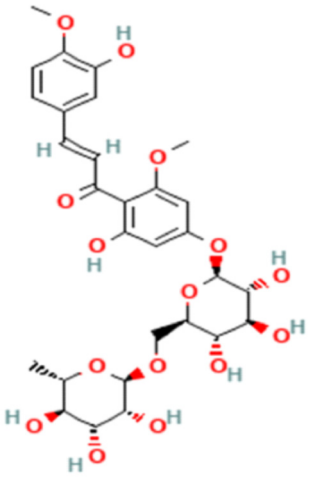

Figure 1. Chemical structure of HMC (compound CID: 6436550; https://pubchem.ncbi.nlm.nih.gov, accessed on 7 April 2022).

2. Materials and Methods

2.1. Animals and Experimental Design

The study was carried out on Swiss mice (male, 30–35 g, aged 6–8 weeks) obtained through the State University of Londrina (Paraná State, Brazil). The conditions of the facility in which mice were maintained were as follows: ad libitum feed, twelve/twelve hours light/dark cycle, regular thermal comfort (21 °C), and circulation of air (15–30 cubic feet per minute/square feet). Animals were maintained in pathogen-free conditions. During the process of euthanasia for sample collection, animals were exposed to a lethal dose of 5% isoflurane, followed by cervical dislocation, and subsequent decapitation. The experimental protocol was carried out according to previous studies by our group [1,9]. Mice received a standard toxic dose of diclofenac (200 mg/kg, 100 µL, per oral), and 30 min later, were administered HMC (0.03, 0.3, and 3 mg/kg; 200 µL) or vehicle (saline; 200 µL) via the intra-peritoneal (i.p.) route. Blood, kidney, and urine samples were analyzed 24 h after NSAID (sodium diclofenac, SDCF) administration. Blood samples were collected after a dose-response experiment for the assessment of urea and creatinine levels to determine the best dose of HMC, and a dose of 3 mg/kg of HMC was chosen for all subsequent experiments in the study. After this initial analysis, blood samples were collected for a new round of experiments that included evaluations of oxidative stress (antioxidant capacity parameters and lipid peroxidation) and cytokine production (both described in detail below). Renal tissue and urine samples were collected to evaluate the following parameters: oxidative stress (antioxidant capacity parameters and lipid peroxidation), cytokine production, swelling, histopathological changes, and mRNA expression of Nrf2 and its downstream effectors, as well as the concentration of a well-known urinary marker of AKI (NGAL). The experiments using kidney samples were conducted on the entire organ (one kidney per analysis).

2.2. Compounds Used in the Study

SDCF (Neutaren®) was purchased from Novartis (São Paulo, SP, Brazil); HMC was acquired from Santa Cruz Biotechnology (Santa Cruz, CA, USA); and saline was acquired from Gaspar Viana S/A (Fortaleza, CE, Brazil). The dilution of SDCF and HMC us-

ing saline was performed immediately before administration via the oral (p.o.) and i.p. routes, respectively.

2.3. Evaluation of Renal Function Markers

The evaluation of plasma concentrations of urea and creatinine were performed in blood samples after p.o. administration of SDCF (24 h). Samples were collected into heparinized tubes with posterior centrifugation (200× *g*, 10 min, 4 °C), and subsequently processed for determination of renal function markers using commercial kits (Labtest Diagnóstico S.A., Lagoa Santa, MG, Brazil). The data are shown as milligram per deciliter (mg/dL) of plasma.

2.4. Ferric-Reducing Ability Potential (FRAP), 2,2′-Azino-bis(3-ethylbenzothiazoline-6-sulfonic Acid) ($ABTS^{\bullet+}$) Radical Cation, and Reduced Glutathione (GSH) Assays

FRAP, ABTS and GSH assays were performed to evaluate antioxidant capacity during the protocols in the present model [1,9]. Kidney and blood samples (EDTA microtubes) were collected 24 h after SDCF administration and homogenized with 500 µL of 1.15% KCl, subsequently centrifuged (10 min × 200× *g* × 4 °C), and the ability of the sample to resist oxidative damage was determined by measuring ferric-reducing ability with the FRAP assay and free radical scavenging ability with the ABTS assay. FRAP determination used 50 µL of supernatant, together with 150 µL of deionized water and 1.5 mL of freshly prepared FRAP reagent. The reaction mixture was incubated at 37 °C for 30 min, and subsequently, the absorbance was measured at 595 nm. The ABTS test was conducted by using ABTS solution diluted with phosphate-buffered saline at pH 7.4 to an absorbance of 0.80 at 730 nm. After this step, 1.0 mL of diluted ABTS solution was mixed with 20 µL of supernatant (as prepared for the FRAP assay). After 6 min, the absorbance was measured at 730 nm. The results were equated against a Trolox standard curve (1.5–30 µmol/L, final concentrations). The results are expressed as nanomoles (nmol) of Trolox equivalents per milliliter (mL) or milligram (mg) of tissue for plasma and kidney, respectively, for both analyses. For the GSH assay, kidney samples were harvested 24 h after SDCF administration. Samples were homogenized in 0.02 M ethylenediamine tetraacetic acid (EDTA) reagent and treated with 2 mL of water plus 0.5 mL of 50% TCA (trichloroacetic acid). Next, homogenates underwent centrifugation (1500× *g*, 15 min, 4 °C) and the resultant supernatants were carefully removed for subsequent addition to 2 mL of Tris 0.4 M (pH 8.9) plus 50 mL of dithionitrobenzoic acid (DTNB) solution. After 5 min, spectrophotometric readings were carried out at 412 nm. Data are expressed as nmol of GSH per mg of tissue. For the three analyses, a Multiskan GO Microplate Spectrophotometer (Thermo Scientific, Vantaa, Finland) was used.

2.5. Assessment of Thiobarbituric Acid-Reactive Substances (TBARS)

Lipid peroxidation in kidney and blood samples (EDTA microtubes) was assessed 24 h after the administration of SDCF via TBARS determination using an adapted methodology described previously [9]. In brief, TCA (10%) was included in the tissue homogenate or plasma samples to precipitate the proteins. Subsequently, samples underwent centrifugation (1000× *g*, 3 min, 4 °C) and the supernatant was removed for the next step. The supernatants were then mixed with thiobarbituric acid (TBA; 0.67%), incubated for 15 min in a boiling water bath (100 °C), then transferred to an ice bath. Malondialdehyde (MDA) was then quantitated as an indicator of lipid peroxidation in kidney and plasma samples by measuring the absorbance by spectrophotometry (572–535 nm). Data are presented as TBARS (nmol of MDA per mL) for plasmatic samples, and as TBARS (nmol of MDA per mg of tissue) for renal samples.

2.6. Evaluation of Cytokines and Neutrophil Gelatinase-Associated Lipocalin (NGAL) Production

The following cytokines were assessed in blood and kidney samples 24 h after the administration of SDCF: interleukin (IL)-1β, IL-6, interferon (IFN)-γ, IL-33, and IL-10.

Considering plasmatic assay, after collection (EDTA microtubes), samples were centrifuged (800× *g*, 10 min, 4 °C), and the generated supernatants were used to assess the levels of cytokines. Kidney samples were homogenized in 500 µL of saline. Cytokine levels in both tissues were then measured using enzyme-linked immunosorbent assays (ELISA) according to the manufacturer's instructions (eBioscience, San Diego, CA, USA) and analyzed spectrophotometrically. Data are expressed as mg/dL for plasma samples and as picograms (pg) per 100 mg of tissue for kidney samples [1,9]. NGAL urine level was also evaluated by ELISA 24 h after the administration of SDCF. Urine samples were collected into EDTA microtubes after applying moderate compression of the pelvic region of mice. Samples were then transferred into anti-mouse NGAL pre-coated plates and processed according to the manufacturer's instructions (Cloud-Clone Corp., Katy, TX, USA). The levels of NGAL were analyzed by spectrophotometry at 450 nm, and the data are presented as nanogram (ng) per mL of urine [1].

2.7. Histopathological and Swelling Evaluations

For histopathological analysis, kidneys were collected 24 h after the administration of SDCF. Kidneys initially underwent a fixation process using 4% paraformaldehyde (PFA) in phosphate-buffered saline (PBS). Subsequently, the kidneys were dehydrated in a graded series of ethanol solutions and finally processed for paraffin embedding. The process of sectioning the cortical potions of the organs was carried out using a cryostat (CM1520, Leica Biosystem, Richmond, IL, USA) with a thickness of 5 µm. After this step, for the sections underwent hematoxylin and eosin (H&E) and periodic acid–Schiff (PAS) staining. Stained sections from the control group, model group (SDCF) treated with vehicle, and model group treated with HMC were analyzed in a blinded manner through the use of light microscopy at 40× magnification. A semi-quantitative assessment of kidney damage was carried out in 10 high-power fields randomly selected as described previously with modifications [1,9,33] with scoring for each animal. Summed histopathological scores of different experimental groups were determined by the morphological analysis of the following parameters: (1) glomerular pathology; (2) impairment of the cortical brush border; and (3) the presence of vacuoles in tubular cells. A four-point scale was used to describe the level of pathological change: 0, normal; 1, mild; 2, moderate; 3, severe. The score for each parameter were combined into a total histopathological score (9 maximum). Kidney swelling was also evaluated 24 h after SDCF administration by using the organ wet weight as an indicator. After collection, the kidneys were weighed on a precision balance and the results presented as mg of renal tissue per gram (g) bodyweight.

2.8. Reverse Transcription and Quantitative Polymerase Chain Reaction (RT-qPCR) Assay

RT-qPCR was performed as previously described [34]. Kidneys were collected 24 h after the administration of SDCF, homogenized in TRIzol™ Reagent (Thermo Fisher Scientific, Waltham, MA, USA), and total RNA was isolated according to the manufacturer's guidelines. The purity of total RNA was measured spectrophotometrically (Multiskan GO Microplate Spectrophotometer, Thermo Scientific, Vantaa, Finland), and the wavelength absorption ratio (260/280) was between 1.8 and 2.0 for all preparations. Reverse transcription of total RNA to cDNA and qPCR were performed using the GoTaq® 2-Step RT-qPCR System (Promega, Madison, WI, EUA) and target primers with the Step One Plus TM Real-Time PCR System (Applied Biosystems®, Waltham, MA, USA). The relative gene expression was measured using the comparative $2^{-(\Delta\Delta Cq)}$ method. The primers used in this study were as follows: Nrf2—forward, 5′-TCACACGAGATGAGCTTAGGGCAA-3′; reverse, 5′-TACAGTTCTGGGCGGCGACTTTAT-3′ (gene accession number 18024); heme-oxygenase-1 (Ho-1)—forward, 5′-CCCAAAACTGGCCTGTAAAA-3′; reverse, 5′-CGTGGTCAGTCAACATGGAT-3′ (gene accession number 15368); NAD(P)H dehydrogenase (quinone 1) (Nqo1)—forward, 5′-TGGCCGAACACAAGAAGCTG-3′; reverse, 5′-GCTACGAGCACTCTCTCAAACC-3′ (gene accession number 18104). The expression of β-actin (forward, 5′-AGCTGCGTTTTACACCCT TT-3′; reverse, 5′-AAGCCATGCCAATGTT-

GTCT-3′ (gene accession number 11461) mRNA was used as a control for tissue integrity in all samples.

2.9. Immunofluorescence Assay in Confocal Microscopy

Twenty-four hours after the administration of SDCF, animals underwent a perfusion process using 4% PFA in PBS injected via the ascending aorta artery. Next, the kidney was carefully removed and immersed in 4% PFA and remained in this solution for the next 24 h. After this period, samples were placed in 30% saccharose and incubated for 3 days. Once embedded (Tissue-Tek® reagent, Torrance, CA, USA), the kidneys were sectioned to a thickness of 10 μm using cryostat equipment (CM1520, Leica Biosystems, Wetzlar, Germany). Four samples per animal per slide and five animals per group were analyzed. Antigenic recovery was performed (exposure to 90 °C followed by immediate cooling until 30 °C) then the sections passed through a blocking stage (200 μL/slide; 0.5% tween 20 and 5% bovine serum albumin in PBS) for 2 h, followed by overnight incubation at 4 °C with the primary antibody (keap1, D6B12, rabbit IgG mAb, #8047, 1:100 dilution, Cell Signaling Technology, Danvers, MA, EUA). A solution containing the secondary antibody (anti-rabbit IgG Fab2 Alexa Fluor® 647, #4414S, 1:1000 dilution, Cell Signaling Technology, Danvers, MA, EUA) was applied to the slides the next day for 1 h. Treatment with secondary antibody alone was used to test for non-specific staining. For assembly of the slides, DAPI melting media reagent (ProLong™ Gold Antifade Mountant, #P36931, Thermo Fisher Scientific, Waltham, MA, USA) was used. Immunofluorescence analysis of aleatory fields using a confocal microscope (TSC SP8 Leica microsystem, Wetzlar, Germany) were performed on different portions of the cortical region of kidneys with a magnification of 40×. Representative images from each group are presented with a 50 μm scale. Keap1 fluorescence intensity were analyzed by a blinded experimenter and measured using confocal microscope software to provide quantitative data for the experiment.

2.10. Statistical Methodology

Statistical methods were applied to 6 animals per group (5 animals for immunofluorescence) in individual experiments. For histopathological evaluations, the final score considered 12 animals per group in individual experiments. The results are representative of two independent experiments. One-way analysis of variance with Tukey's post hoc test was used for the determination of statistical interpretations. Additionally, the non-parametric Kruskal–Wallis test with Dunn's post hoc tests was applied to the analysis of categorical variables. The analyses were carried out with GraphPad Prism 7.00 (GraphPad software Inc., La Jolla, CA, USA) software. All data are presented as the mean ± standard deviation (SD). Results with values of $p < 0.05$ were considered statistically significant.

3. Results

3.1. HMC Reduces SDCF-Triggered Renal Dysfunction: Urea and Creatinine Levels, and Oxidative Stress in Plasma

Our first approach was designed to determine the most effective dose of HMC to inhibit SDCF-induced renal dysfunction. SDCF was administrated to the mice orally, and after 30 min, they received i.p. treatment with HMC (0.03, 0.3, and 3 mg/kg). The plasmatic levels of urea and creatinine (Figure 2A,B, respectively) were determined 24 h later. HMC treatment inhibited the elevation of renal dysfunction markers induced by SDCF in a dose-dependent manner. For urea, it was observed that only a dose of 3 mg/kg inhibited the increase induced by SDCF. For creatinine, intermediate and high doses of HMC (0.3, and 3 mg/kg, respectively) inhibited the effect of SDCF. Since 3 mg/kg was the only dose able to inhibit both markers of impaired renal function, this dose was selected for the following experiments. Thereafter, we investigate the antioxidant properties of HMC upon SDFC-induced oxidative stress (Figure 2C–E). HMC treatment restored the impaired plasmatic antioxidant status induced by SDFC, seen as increased FRAP and ABTS levels compared to the vehicle control, and inhibited lipid peroxidation levels, seen as a reduced

concentration of TBARS. These results indicate HMC protects renal tissue from the toxic effects of SDFC. Further, HMC reduces systemic oxidative parameters in AKI mice, which reflects its potential antioxidant actions in response to increased free radical activity.

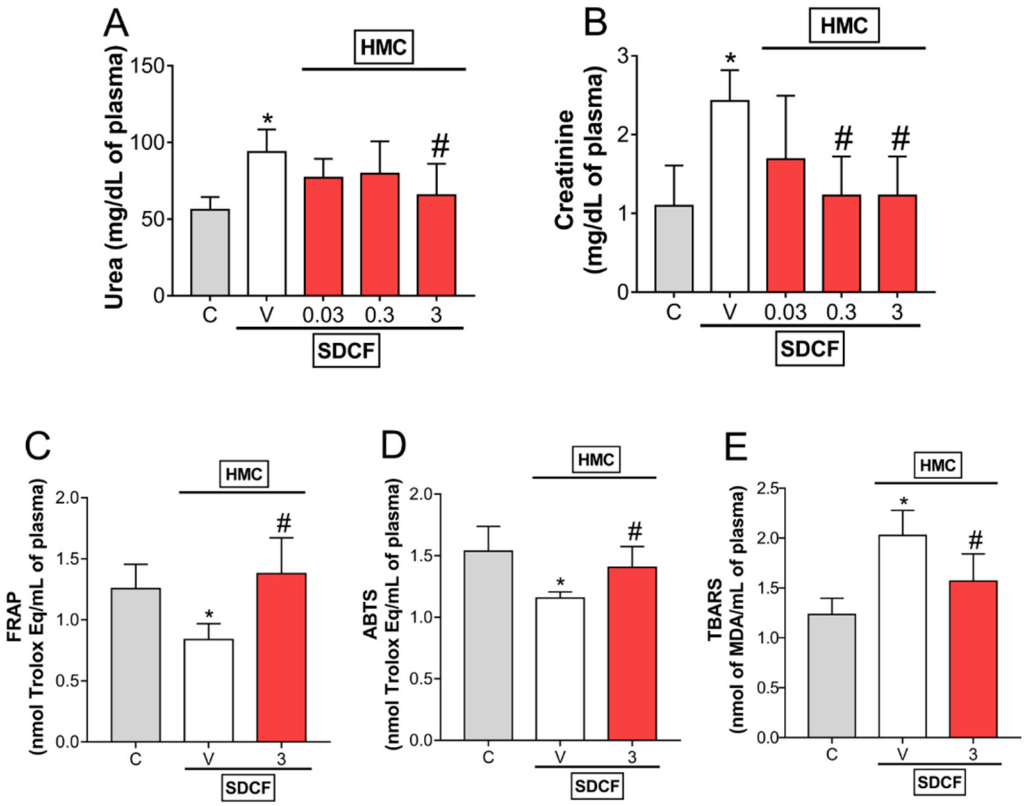

Figure 2. HMC inhibits SDCF-induced increase of plasmatic levels of urea, creatinine, and oxidative stress. Blood samples were collected 24 h after the administration of SDCF for the evaluation of urea (**A**), creatinine (**B**), FRAP (**C**), ABTS (**D**), and TBARS (**E**) levels. Results are expressed as mean ± SD, $n = 6$ mice per group per experiment, and are representative of two independent experiments. * $p < 0.05$ vs. control (C) group; # $p < 0.05$ vs. vehicle (V) treated group; one ANOVA followed by Tukey's post hoc test.

3.2. HMC Reduces IL-6, IFN-γ, and IL-33, but Does Not Modify IL-1β and IL-10 Levels in Plasma

The next investigation aimed to evaluate the levels of pro- and anti-inflammatory cytokines in plasma. For this approach, SDCF was administrated to the mice orally, and after 30 min, they received i.p. treatment with HMC (3 mg/kg) for the evaluation of plasmatic levels of IL-1β, IL-6, IFN-γ, IL-33, and IL-10 (Figure 3A–E). SDCF did not interfere with IL-1β and IL-10, however, it induced a significant increase in IL-6, IFN-γ, and IL-33 levels in plasma. HMC treatment did not affect IL-1β and IL-10, but inhibited SDCF-induced IL-6, IFN-γ, and IL-33 (Figure 3A–E). These data suggest HMC may modulate some pro-inflammatory cytokines systemically in AKI mice.

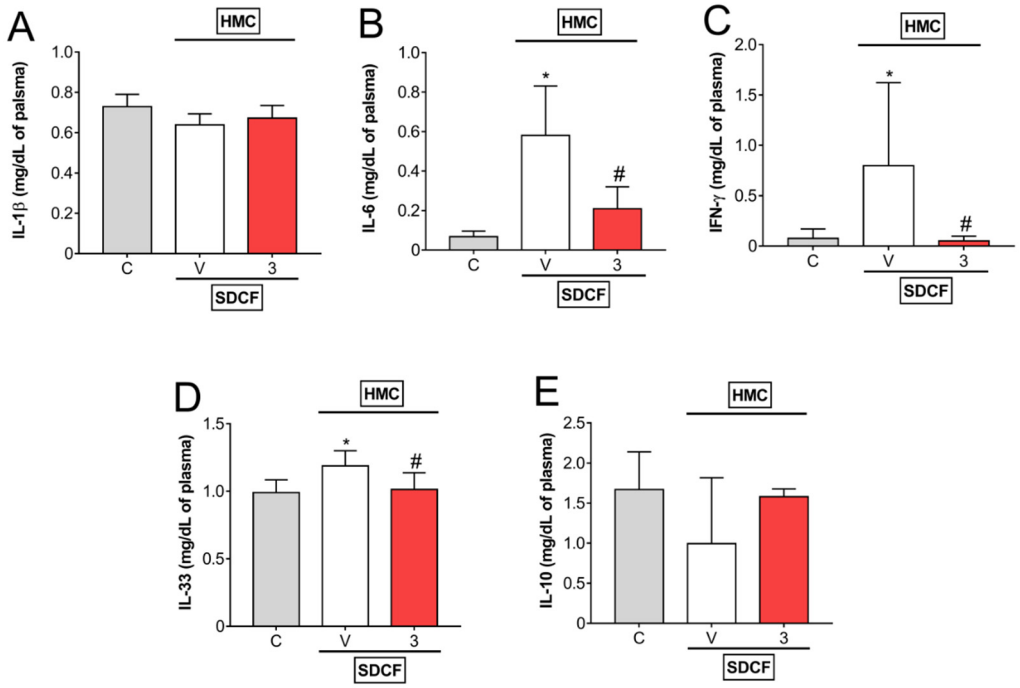

Figure 3. HMC inhibits SDCF-induced IL-6, IFN-γ, and IL-33, but does not change IL-1β and IL-10 plasmatic levels. Blood was collected 24 h after the administration of SDCF for the evaluation of IL-1β (**A**), IL-6 (**B**), IFN-γ (**C**), IL-33 (**D**), and IL-10 (**E**) levels. Results are expressed as mean ± SD, $n = 6$ mice per group per experiment, and are representative of two independent experiments. * $p < 0.05$ vs. control (C) group; # $p < 0.05$ vs. vehicle (V) treated group; one ANOVA followed by Tukey's post hoc test.

3.3. HMC Reduces Oxidative Stress in Renal Tissue

Antioxidant parameters and lipid peroxidation levels were measured in the kidneys, the target organ for oxidative stress induced by SDCF, to investigate the effects of HMC. SDCF was administrated to the mice orally, and after 30 min, they received i.p. treatment with HMC (3 mg/kg) for the evaluation of FRAP, ABTS, GSH, and TBARS levels (Figure 4A–D). The toxic dose of SDCF impaired antioxidant defenses, observed as reduced FRAP, ABTS, and GSH levels, and increased lipid peroxidation, observed as increased TBARS levels in renal tissue. HMC treatment re-established all antioxidant parameters, and even inhibited lipid peroxidation in kidneys (Figure 4A–C). These data demonstrate HMC can effectively counteract the oxidative stress induced by SDCF in renal tissue.

3.4. HMC Reduces IL-1β, IL-6, IFN-γ, and IL-33, as well as Increases IL-10 Levels in Renal Tissue

After determining the systemic modulation of cytokines by HMC in SDCF-induced AKI, our next objective was to evaluate the modulation of cytokines by HMC in renal tissue. Therefore, SDFC was administrated to the mice orally, and after 30 min, they received i.p. treatment with HMC (3 mg/kg) and IL-1β, IL-6, IFN-γ, IL-33, and IL-10 levels were determined in renal tissue (Figure 5A–E). SDCF increased the production of pro-inflammatory cytokines IL-1β, IL-6, IFN-γ, and IL-33, and reduced the production of the anti-inflammatory cytokine IL-10. Treatment with HMC efficiently inhibited the increased levels of IL-1β, IL-6, IFN-γ, and IL-33 induced by SDCF, and restored the levels of IL-10 significantly (Figure 5A–D). These results indicate that in addition to inhibiting oxidative stress, HMC acts by inhibiting pro-inflammatory and inducing anti-inflammatory cytokines to combat the toxic effects of SDCF in the kidney.

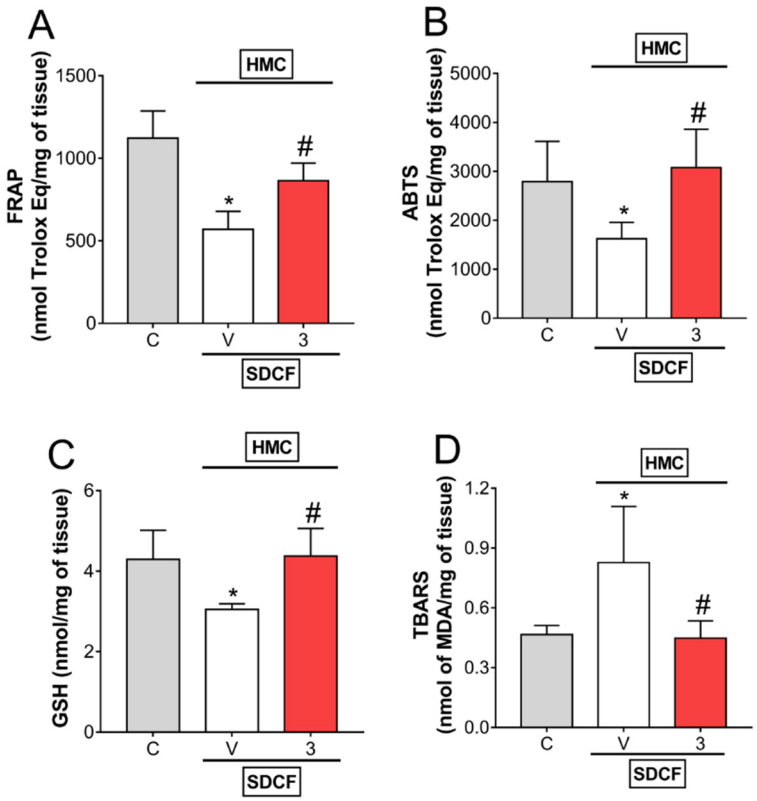

Figure 4. HMC inhibits SDCF-induced oxidative stress in renal tissue. Kidney was collected 24 h after the administration of SDCF for the evaluation of FRAP (**A**), ABTS (**B**), GSH (**C**), and TBARS (**D**) levels. Results are expressed as mean ± SD, $n = 6$ mice per group per experiment, and are representative of two independent experiments. * $p < 0.05$ vs. control (C) group; # $p < 0.05$ vs. vehicle (V) treated group; one ANOVA followed by Tukey's post hoc test.

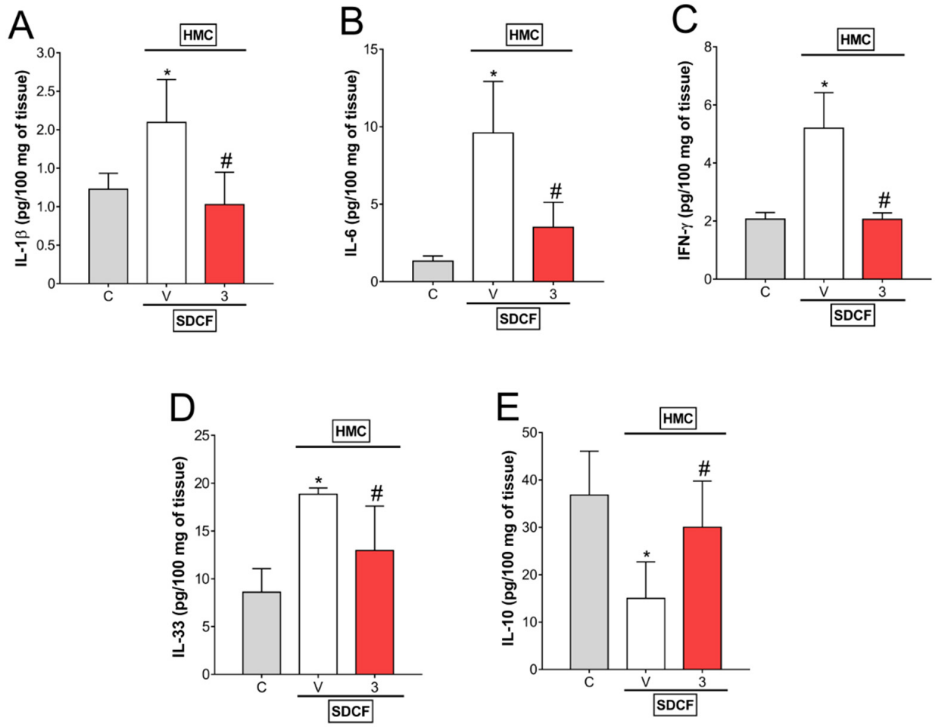

Figure 5. HMC inhibits SDCF-induced IL-1β, IL-6, IFN-γ, and IL-33, and reverses SDCF-induced depletion of IL-10 levels in renal tissue. Kidney was collected 24 h after the administration of SDCF for

the evaluation of IL-1β (**A**), IL-6 (**B**), IFN-γ (**C**), IL-33 (**D**), and IL-10 (**E**) levels. Results are expressed as mean ± SD, n = 6 mice per group per experiment, and are representative of two independent experiments. * $p < 0.05$ vs. control (C) group; # $p < 0.05$ vs. vehicle (V) treated group; one ANOVA followed by Tukey's post hoc test.

3.5. HMC Reduces SDCF-Induced Renal Histopathology, Swelling and Tubular Cells Cytotoxicity

Our next goal was to investigate the protective effects of HMC upon tissue inflammatory pathology induced by SDCF. For this approach, SDCF was administrated to the mice orally, and after 30 min, they received i.p. treatment with HMC (3 mg/kg) for the evaluation of renal histopathology and swelling, and NGAL urinary levels (Figure 6). SDCF altered the regular morphology of the cortical layer of renal tissue, observed as tubular cell dilatation together with flattening of the renal epithelium and disruption of the brush borders in the proximal convoluted tubes, as well as deformation in glomeruli shape and Bowman's capsule injury (Figure 6C,D, respectively), which were not observed in control mice (Figure 6A,B, respectively). HMC treatment reduced this altered morphology, conferring protection on the kidney (Figure 6E,F). Besides reducing the histopathology in renal tissue (Figure 6G), HMC treatment also inhibited kidney swelling and reduced NGAL levels in urine (Figure 6H,I, respectively), which denotes a reduction in organ inflammation and tubular cells damage. Altogether, these data show HMC can act as a powerful therapeutic compound for SDCF-induced AKI-related tissue pathology.

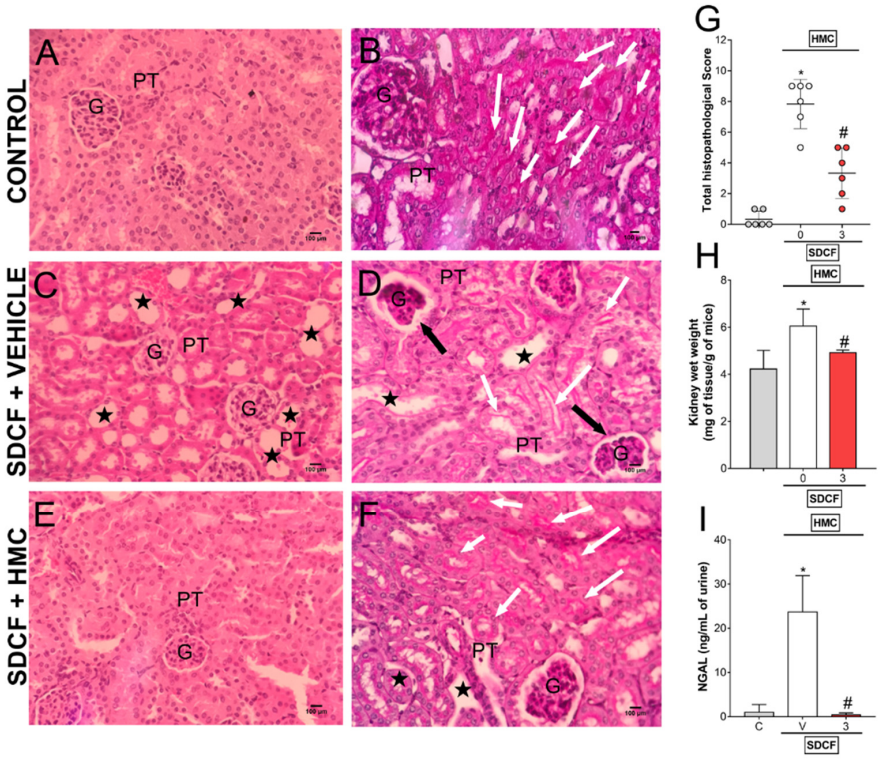

Figure 6. HMC inhibits SDCF-induced renal histopathology, swelling and tubular cells cytotoxicity. Kidney samples were collected 24 h after the administration of SDCF for the evaluation of histopathology with H&E (**A**,**C**,**E**), and PAS (**B**,**D**,**F**) staining, total histopathological score (**G**), swelling (**H**), and NGAL urinary levels (**I**). Original magnification 40×; 100 µm scale. Stars show tubular dilatation; black arrows show glomeruli/Bowman's capsule lesions; and white arrows show brush border differences in varied experimental groups. Data are shown as mean ± SD, n = 12 and n = 6 mice per group per experiment for histopathological analysis and swelling/NGAL, respectively, and are representative of two independent experiments. * $p < 0.05$ vs. control (C) group; # $p < 0.05$ vs. SDCF + vehicle (V) treated group; Kruskal-Wallis followed by Dunn's post hoc test (**G**) and one ANOVA followed by Tukey's post hoc test (**H**,**I**). G, glomerulus; PT, proximal tubule.

3.6. HMC induces Nrf2 Signaling to Reduce SDCF-Induced AKI

Considering the importance of oxidative stress to SDCF-triggered AKI and HMC activity, we investigated whether the HMC protective mechanism involves the activation of the major antioxidant pathway, Nrf2/ARE. Therefore, SDCF was administrated to the mice orally, and after 30 min, they received i.p. treatment with HMC (3 mg/kg) for the evaluation of Nrf2, HO-1, and Nqo1 mRNA expression (Figure 7). Nrf2 and Nqo1 mRNA expression were not altered by SDCF administration (Figure 7A,C, respectively), however Ho-1 expression was increased by SDCF (Figure 7B). Treatment with HMC significantly increased Nrf2 and Nqo1 mRNA expression compared to control mice, and more robustly, increased Ho-1 mRNA expression in comparison to both control and SDCF administered mice (Figure 7A–C). These results demonstrate the induction of the Nrf2 pathway by HMC, and consequently, its downstream signaling effectors, contributing to the mechanism that reduces SDCF-induced AKI.

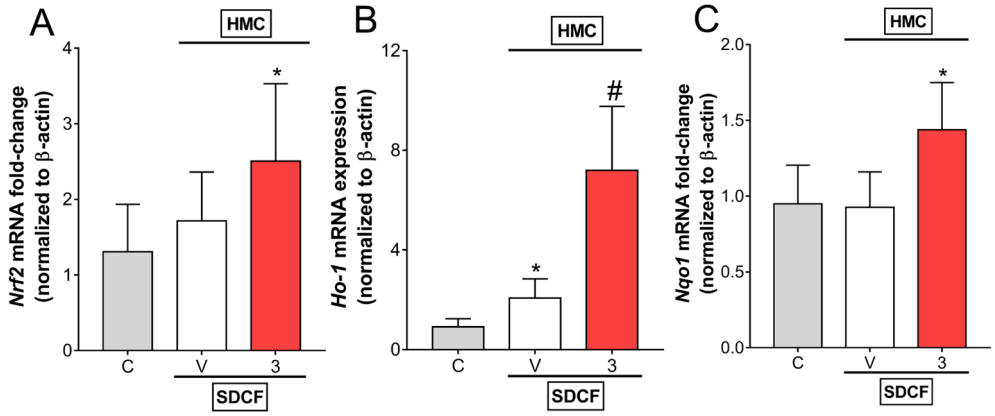

Figure 7. HMC induces Nrf2 signaling in renal tissue. Kidney samples were collected 24 h after the administration of SDCF for the evaluation of Nrf2 (**A**), Ho-1 (**B**), and Nqo1 (**C**) mRNA expression. Results are expressed as mean ± SD, $n = 6$ mice per group per experiment, and are representative of two independent experiments. * $p < 0.05$ vs. control (**C**) group; # $p < 0.05$ vs. vehicle (V) treated group; one ANOVA followed by Tukey's post hoc test.

3.7. HMC Reduces Keap1 in the Kidney

The results in Figure 7 indicate that the Nrf2 system is stimulated by HMC treatment. Keap1 is a negative regulator of Nrf2 present in the cytoplasm. Keap1 favors cullin-based E3 ubiquitin ligase-mediated ubiquitination of Nrf2 [26]. Control and SDCF + vehicle groups presented similar renal staining for Keap1 indicating that Nrf2 is under control (Figure 8A,B,D). HMC treatment reduced Keap1 fluorescence detection (Figure 8C,D), and Nrf2 would be able to translocate to the nucleus and activate ARE-dependent gene expression in these mice. Thus, these data line up with the previous results indicating HMC reduces oxidative stress and enhances endogenous antioxidant defenses as well as stimulating the Nrf2 pathway and its downstream targets.

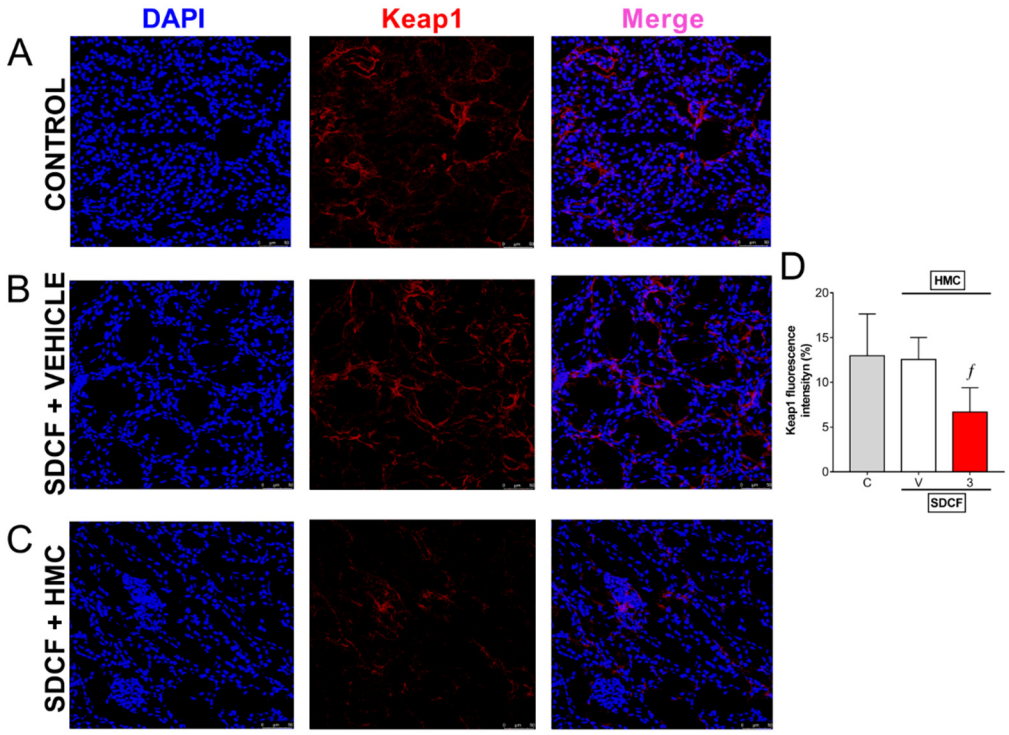

Figure 8. HMC reduces Keap1 protein expression in renal tissue. Kidney samples were collected 24 h after the administration of SDCF for the evaluation of immunofluorescence detection of Keap1 (**A**–**D**). Original magnification 40×; 50 µm scale. DAPI was used for nuclear detection in samples. Data are showed as mean ± SD, n = 5 mice per group per experiment, and are representative of two independent experiments. ^{f} $p < 0.05$ vs. control (C) and SDFC + vehicle treated (V) groups; one ANOVA followed by Tukey's post hoc test.

4. Discussion

Although considered an effective pharmacological tool for the treatment of fever, acute and chronic pain, and inflammatory diseases, the clinical applicability of diclofenac is frequently hampered by adverse effects related to its use [1,3,9,11]. Kidneys represent the master human organ related to diclofenac excretion [35]. For this reason, renal tissue is frequently exposed to diclofenac and its metabolites, such as diclofenac acyl glucuronide (diclofenac beta-D-glucosiduronic acid; $C_{20}H_{19}Cl_2NO_8$), and thus, is especially vulnerable to their toxic effects [36]. The nephrotoxic effects of diclofenac are dose-dependent, increasing concomitantly with higher doses [37]. Moreover, the interaction of diclofenac with other drugs, including the nucleotide analogue inhibitor of reverse transcriptase, tenofovir disoproxil, substantially boosts the risk of acute kidney injury [38]. Evidence also indicates that long-term use together with the analgesic drug paracetamol (acetaminophen) leads to drug-induced chronic kidney disease [39]. All these data highlight the need for new alternative therapies to treat AKI.

The present study demonstrates for the first time the nephroprotective effects of the flavonoid HMC in diclofenac-induced AKI in mice. HMC reversed the dysfunctional pathological aspects of AKI since we observed an improvement in the levels of the renal function markers urea and creatinine. The magnitude of inflammation in acute kidney injury may vary according to some aspects, including age and weight of animals [40,41]. Kidney inflammation caused by SDCF was also counteracted by HMC, reducing kidney swelling and modulating systemic and renal cytokine production. Mechanistically, we showed HMC presents a remarkable antioxidant effect in blood and kidney (restoration of antioxidant capacity and reduction of lipid peroxidation), with this effect being attributed to the structural antioxidant activity of HMC [23] and activation of the Nrf2 pathway. The outcomes observed in the present model indicated diminished damage to kidney

tissue after SDCF administration (attenuation of renal histopathological score and NGAL urinary levels in HMC treated mice). The HMC dose needed to achieve these effects in the present intoxication model was 3 mg/kg. In other models studied by our group, including those of inflammation and pain, treatment effects were obtained with higher doses [19,22,24,35,42]. The difference among these models is a major point for the difference in HMC action. Models in which an inflammatory stimulation activated tissue resident and recruited immune cells through receptors to cause inflammation and pain characterizes our previous studies. The current SDCF-induced AKI is a different condition because it is not related to the primary mechanism of action for SDCF, that is, the inhibition of COX isoforms. SDCF does not induce oxidative stress at therapeutic doses. However, there is overuse and intentional intoxication on some occasions. Thus, it is essential to note that in previous studies we adopted models based on pharmacology principles in which the recruitment and activation of leukocytes was higher, and consequently, oxidative stress was also higher. It is hypothesized that SDCF and its metabolites cause kidney damage via interaction with renal organic anion transporters (OATs) [36], a different mechanism to that induced by inflammatory stimuli. Furthermore, our previous studies were of arthritis, skin inflammation and colitis, thus, the targets tissues involved and the physiopathological mechanisms in each model were different, as were the stimuli. Additionally, the routes used for the administration of HMC varied between these studies (oral and i.p.), which modifies the pharmacokinetics of the drug, as well as its bioavailability. In addition to all these differences, it is important to highlight that HMC is excreted is the urine [20], likely allowing more abundant accumulation of the compound in the kidney. Thus, we speculate that it may reach higher concentrations in the kidney than in other organs, such as joints and skin, which were used in previous studies. Therefore, these variables (different stimuli, physiopathological mechanisms, affected tissues, disease duration, route of excretion, and routes of HMC administration of) may explain the different dosages needed for a treatment effect among these studies.

Acute renal failure is clinically observed as a rapid elevation in serum creatinine and urea concentrations above the limits considered normal. The main rationale characterizing the use of urea and creatinine levels as markers of AKI concerns glomerular filtration rate (GFR) status, a fundamental aspect for clinical diagnosis of AKI. As GFR declines, the excretion of urea and creatinine in urine decreases and blood concentrations increase [43]. We observed a clear glomerular architectural change after SDCF administration together with increased urea and creatinine levels in the blood, indicating glomerulus injury and reduced GFR, respectively. These changes were inhibited in mice that received HMC treatment, indicating this flavonoid targets SDCF toxicity to prevent functional deficits in renal tissue. Importantly, although frequently used, urea and creatinine serum levels may not be as sensitive for identifying AKI [1,43]. Thus, we are also concerned with evaluating the most reliable markers for kidney damage. Preclinical studies were very important for the discovery of more specific markers of kidney injury [44]. NGAL protein is considered a sensitive and predictive early molecule of AKI [45], and its urinary increase reflects damage, especially to the glomeruli and proximal tubules [46,47]. In a previous study by our group, we demonstrated for the first time that NGAL is also an important marker of SDCF-induced AKI [1]. In this sense, we evaluated the effects of HMC on SDCF-induced increased NGAL urinary levels. HMC treatment efficiently mitigated the rise in NGAL levels, which is consistent with the improvement in renal function (reduced urea and creatinine levels) and histopathological score (reduced glomerular and proximal tubular cells damage) observed in HMC-treated mice.

After observing that HMC leads to reduced SDCF toxicity in renal tissue, the mechanisms by which HMC confers such protection were investigated. As mentioned earlier, HMC is known for its anti-inflammatory and antioxidant effects. SDCF induces the activation of NFκB in the kidney [1,9,48] and leads to an increase in the production of inflammatory mediators, including cytokines [1,9]. In AKI, cytokines may be released by recruited and/or resident leukocytes as well as by renal tubular cells, promoting kidney inflamma-

tion (as observed by kidney swelling in the present study). Cytokines are also released into the blood, thus reflecting potential urine and blood biomarkers of AKI [1,9,49,50]. Their systemic release during AKI may even promote damage to distant organs, raising the importance of inhibiting cytokine production to avoid both kidney and distant organ injury [49]. We observed that HMC inhibited pro-inflammatory cytokine production and stimulated an anti-inflammatory cytokine after SDCF administration. In plasma samples, HMC inhibited IL-6, IFN-γ, and IL-33 levels, whereas it did not affect IL-1β and IL-10 levels since they were not altered in SDCF AKI. In the kidney, the inhibition detected after HMC treatment included IL-6, IFN-γ, IL-33, and IL-1β. The profile for IL-10 levels in plasma and renal tissue differed between the experimental groups. In the plasma, there was only a tendency for a reduction in IL-10 in the SDCF vehicle-treated group, and for an increase in the HMC-treated group, which contrasts with the significant changes observed in renal tissue. This apparent incongruence in the data may represent differences in the dynamics of cytokine production and release after SDCF stimulus. Regardless, HMC inhibited all evaluated pro-inflammatory cytokines altered by SDCF, and at the same time, it induced IL-10 in the kidney. In renal tissue, an increase in IL-10 production is interesting considering that besides being a fundamental cytokine for controlling excessive inflammation through inhibition of pro-inflammatory cytokines, IL-10 may positively regulate HO-1 [51]. In turn, HO-1 promotes adaptive antioxidant cellular response to reduce or prevent damage resulting from oxidative stress. In SDCF-induced AKI, we demonstrated that in addition to inducing IL-10 production, HMC also activated another decisive signaling cascade that mediates HO-1 production, the Nrf2/ARE antioxidant pathway, which is discussed below.

Mice that were treated with HMC presented increased antioxidant capacity in both plasma and renal samples, as indicated by FRAP and ABTS tests. Reduced levels of lipid peroxidation were also detected in both tissues in animals treated with HMC. Moreover, HMC induced increased production of the non-enzymatic antioxidant GSH in renal tissue. These data are extremely important, since oxidative stress accounts for the impairment in GFR [52,53]. In fact, in a reactive oxygen species-dependent manner, cytokines such as IL-1β and IL-6 may promote dysfunction of glomerular permeability to impair the GFR rate [53]. These latter data highlight the intimate link between cytokines and oxidative stress in renal damage caused by SDCF. The present results corroborate previous studies which demonstrated potential antioxidant effects of HMC in other models involving different pathological mechanisms [19,22–24,54]. For instance, in ultraviolet B (UVB)-irradiated mouse skin, HMC restored impaired GSH production and inhibited the expression of $gp91^{phox}$ subunit of nicotinamide adenine dinucleotide phosphate (NADPH) oxidase that generates superoxide anions [23,54]. Increased production of cellular superoxide anion is a contributing mechanism to the perpetuation of an oxidant cascade that ultimately leads to lipid peroxidation. The restoration of GSH levels and inhibition of oxidative stress by HMC were also demonstrated in models of zymosan-induced arthritis [22] and experimental ulcerative colitis [42]. In the present experimental model, HMC efficiently reduced lipid peroxidation in blood and renal tissues. HMC has the structural ability to act as an antioxidant [23]; however, the activation of the Nrf2/ARE signaling pathway might also account for the effects of HMC. HMC can induce Nrf2 signaling in inflamed skin [23], and here, we demonstrate this modulation can also occur in the kidney after suffering the toxic effects of SDCF. ARE-dependent gene expression drives the canonical expression of HO-1, NQO1, glutamatecysteine ligase (GCL), glutathione S-transferases (GSTs), catalase (CAT), superoxide dismutase (SOD), and thioredoxin, among others [26], which mediate powerful antioxidant effects. Through GCL induction, Nrf2 can upregulate GSH levels [55]. Therefore, the upregulation of GSH observed here after HMC treatment is consistent with an effect on Nrf2 activity. In addition to increasing GSH levels in renal tissue, HMC effectively enhanced mRNA expression for *Nrf2* and its downstream effectors *Nqo1* and *Ho-1* in the kidney, further contributing to the antioxidant effects observed. We also observed that Keap1 immunostaining was reduced in the kidneys after HMC treatment, which is also consistent with the notion that Nrf2 signaling was enhanced by

this flavonoid [26]. The inhibition of NFκB by HMC is possibly an additional mechanism for containing oxidative stress in SDCF-induced AKI, as this pro-inflammatory transcription factor is redox sensitive [1,9,26,34].

Besides being a potent inducer of antioxidant responses, Nrf2 can also contribute to reducing inflammation [26,56]. This concept is supported by several preclinical studies evaluating Nrf2 during the modulation of inflammatory states. For instance, Nrf2 activity may reduce the expression of pro-inflammatory cytokines (including tumor necrosis factor-α (TNF-α) and IL-6) in immune cells, such as neutrophils and macrophages. High Nrf2 expression counteracts the expression of pro-inflammatory genes by inhibiting NFκB and Nrf2 disruption aggravates the inflammatory response in models of sepsis, pleurisy, emphysema, and autoimmune diseases [56]. Through GATA binding protein-3 (GATA-3) induction, Nrf2 can simultaneously suppress the production of IFN-γ and increase the production of Th2 cytokines IL-4, IL-5, and IL-13 [57] and $CD4^+$ T cells from Nrf2 knockout mice produce more IFN-γ and less Th2 cytokines [57]. Finally, Nrf2 can promote the production of IL-10 and transforming growth factor-β (TGF-β) in FoxP3-expressing Treg cells [56]. Thus, this robust body of evidence indicates Nrf2 per se is crucial for the control of inflammation.

5. Conclusions

Although considered a drug of first choice for many clinical conditions related to pain and inflammation, SDCF may induce kidney toxicity. One relevant pathological mechanism of SDCF for the induction of renal damage involves the depletion of antioxidant defenses together with increased oxidative stress. Therefore, alternative pharmacological tools with antioxidant properties and no adverse reactions for renal tissue need to be validated to reduce the potential negative impacts of this condition. Data obtained from this study indicates HMC improves antioxidant status, as measured by total antioxidant capacity in blood and renal tissue, and GSH levels in the kidney. Reduced lipid peroxidation in kidney and blood was also observed after HMC treatment. The alleviation of SDCF-induced nephrotoxicity by HMC was not limited to redox state modulation since it also inhibited pro-inflammatory cytokines in blood and kidney and increased production of the anti-inflammatory cytokine IL-10 in the kidney. These antioxidant and anti-inflammatory properties of HMC in the present model reduced the damage in renal tissue caused by SDCF with a contribution from the activation of the Nrf2/ARE redox-sensitive pathway and a reduction in Keap1. Thus, the present study supports clinical investigation of HMC as an effective therapeutic option for the treatment of SDCF-induced AKI.

Author Contributions: Conceptualization, W.A.V.J.; formal analysis, A.J.C.B., T.H.Z., T.S.-S., V.F., C.F.S.G., M.M.B., K.C.A., C.R.F., D.C.-N., A.M.B.C., R.C. and S.M.B.; funding acquisition, A.M.B.C., R.C. and W.A.V.J.; investigation, A.J.C.B., T.H.Z., T.S.-S., V.F., C.F.S.G., M.M.B., K.C.A., C.R.F. and S.M.B.; resources, D.C.-N., A.M.B.C. and R.C.; supervision, W.A.V.J.; validation, W.A.V.J.; writing—review & editing, S.M.B. and W.A.V.J. All authors have read and agreed to the published version of the manuscript.

Funding: This research was funded by Coordenadoria de Aperfeiçoamento de Pessoal de Nível Superior (CAPES, finance code 001), Conselho Nacional de Desenvolvimento Científico e Tecnológico (CNPq), Programa de Apoio a Grupos de Excelência (PRONEX) grant supported by Araucária Foundation, SETI (Secretaria da Ciência, Tecnologia e Ensino Superior) and MCTI (Ministério da Ciência, Tecnologia e Inovação)/CNPq; Paraná State Government (agreement 014/2017, protocol 46.843), and Programa de Pesquisa para o Sistema Único de Saúde (PPSUS) grant supported by Araucária Foundation, MCTI, and SESA-PR. S.M.B. acknowledges Fundação Nacional de Desenvolvimento do Ensino Superior Particular (FUNADESP) research fellowship. R.C. and W.A.V.J. acknowledge CNPq productivity research fellowships.

Institutional Review Board Statement: The animal protocol used in this study was approved (protocol code 15236.2015.73) by the Institutional Ethics Committee on Animal Use (CEUA) of Universidade Estadual de Londrina (UEL) and all animal experiments were carried out in accordance with the Brazilian Council on Animal Experimentation (CONCEA).

Informed Consent Statement: Not applicable.

Data Availability Statement: Data is contained within the article.

Conflicts of Interest: The authors declare no conflict of interest.

References

1. Borghi, S.M.; Fattori, V.; Ruiz-Miyazawa, K.W.; Bertozzi, M.M.; Lourenco-Gonzalez, Y.; Tatakihara, R.I.; Bussmann, A.J.C.; Mazzuco, T.L.; Casagrande, R.; Verri, W.A., Jr. Pyrrolidine dithiocarbamate inhibits mouse acute kidney injury induced by diclofenac by targeting oxidative damage, cytokines and NF-kappaB activity. *Life Sci.* **2018**, *208*, 221–231. [CrossRef] [PubMed]
2. Zhang, X.; Donnan, P.T.; Bell, S.; Guthrie, B. Non-steroidal anti-inflammatory drug induced acute kidney injury in the community dwelling general population and people with chronic kidney disease: Systematic review and meta-analysis. *BMC Nephrol.* **2017**, *18*, 256. [CrossRef] [PubMed]
3. Ungprasert, P.; Cheungpasitporn, W.; Crowson, C.S.; Matteson, E.L. Individual non-steroidal anti-inflammatory drugs and risk of acute kidney injury: A systematic review and meta-analysis of observational studies. *Eur. J. Intern. Med.* **2015**, *26*, 285–291. [CrossRef]
4. Ejaz, P.; Bhojani, K.; Joshi, V.R. NSAIDs and kidney. *J. Assoc. Physicians India* **2004**, *52*, 632–640.
5. Lucas, G.N.C.; Leitao, A.C.C.; Alencar, R.L.; Xavier, R.M.F.; Daher, E.F.; Silva Junior, G.B.D. Pathophysiological aspects of nephropathy caused by non-steroidal anti-inflammatory drugs. *J. Bras. Nefrol.* **2019**, *41*, 124–130. [CrossRef]
6. McGettigan, P.; Henry, D. Use of non-steroidal anti-inflammatory drugs that elevate cardiovascular risk: An examination of sales and essential medicines lists in low-, middle-, and high-income countries. *PLoS Med.* **2013**, *10*, e1001388. [CrossRef]
7. Altman, R.; Bosch, B.; Brune, K.; Patrignani, P.; Young, C. Advances in NSAID development: Evolution of diclofenac products using pharmaceutical technology. *Drugs* **2015**, *75*, 859–877. [CrossRef] [PubMed]
8. Emery, P.; Koncz, T.; Pan, S.; Lowry, S. Analgesic effectiveness of celecoxib and diclofenac in patients with osteoarthritis of the hip requiring joint replacement surgery: A 12-week, multicenter, randomized, double-blind, parallel-group, double-dummy, noninferiority study. *Clin. Ther.* **2008**, *30*, 70–83. [CrossRef]
9. Fattori, V.; Borghi, S.M.; Guazelli, C.F.; Giroldo, A.C.; Crespigio, J.; Bussmann, A.J.; Coelho-Silva, L.; Ludwig, N.G.; Mazzuco, T.L.; Casagrande, R.; et al. Vinpocetine reduces diclofenac-induced acute kidney injury through inhibition of oxidative stress, apoptosis, cytokine production, and NF-kappaB activation in mice. *Pharmacol. Res.* **2017**, *120*, 10–22. [CrossRef]
10. Dreiser, R.L.; Marty, M.; Ionescu, E.; Gold, M.; Liu, J.H. Relief of acute low back pain with diclofenac-K 12.5 mg tablets: A flexible dose, ibuprofen 200 mg and placebo-controlled clinical trial. *Int. J. Clin. Pharmacol. Ther.* **2003**, *41*, 375–385. [CrossRef]
11. Schmidt, M.; Sorensen, H.T.; Pedersen, L. Diclofenac use and cardiovascular risks: Series of nationwide cohort studies. *BMJ* **2018**, *362*, k3426. [CrossRef] [PubMed]
12. Cheng, H.F.; Harris, R.C. Cyclooxygenases, the kidney, and hypertension. *Hypertension* **2004**, *43*, 525–530. [CrossRef] [PubMed]
13. Gan, T.J. Diclofenac: An update on its mechanism of action and safety profile. *Curr. Med. Res. Opin.* **2010**, *26*, 1715–1731. [CrossRef] [PubMed]
14. Abiola, T.S.; Adebayo, O.C.; Babalola, O.O. Diclofenac-Induced Kidney Damage in Wistar Rats: Involvement of Antioxidant Mechanism. *J. Biosci. Med.* **2019**, *7*, 44–57. [CrossRef]
15. Alkuraishy, H.M.; Al-Gareeb, A.I.; Hussien, N.R. Diclofenac-induced acute kidney injury is linked with oxidative stress and pro-inflammatory changes in sprague-dawley rats. *J. Contemp. Med. Sci.* **2019**, *5*, 140–144. [CrossRef]
16. Hickey, E.J.; Raje, R.R.; Reid, V.E.; Gross, S.M.; Ray, S.D. Diclofenac induced in vivo nephrotoxicity may involve oxidative stress-mediated massive genomic DNA fragmentation and apoptotic cell death. *Free Radic. Biol. Med.* **2001**, *31*, 139–152. [CrossRef]
17. Nizamutdinova, I.T.; Jeong, J.J.; Xu, G.H.; Lee, S.H.; Kang, S.S.; Kim, Y.S.; Chang, K.C.; Kim, H.J. Hesperidin, hesperidin methyl chalone and phellopterin from Poncirus trifoliata (Rutaceae) differentially regulate the expression of adhesion molecules in tumor necrosis factor-alpha-stimulated human umbilical vein endothelial cells. *Int. Immunopharmacol.* **2008**, *8*, 670–678. [CrossRef]
18. Ferraz, C.R.; Carvalho, T.T.; Manchope, M.F.; Artero, N.A.; Rasquel-Oliveira, F.S.; Fattori, V.; Casagrande, R.; Verri, W.A., Jr. Therapeutic Potential of Flavonoids in Pain and Inflammation: Mechanisms of Action, Pre-Clinical and Clinical Data, and Pharmaceutical Development. *Molecules* **2020**, *25*, 762. [CrossRef]
19. Pinho-Ribeiro, F.A.; Hohmann, M.S.; Borghi, S.M.; Zarpelon, A.C.; Guazelli, C.F.; Manchope, M.F.; Casagrande, R.; Verri, W.A., Jr. Protective effects of the flavonoid hesperidin methyl chalcone in inflammation and pain in mice: Role of TRPV1, oxidative stress, cytokines and NF-kappaB. *Chem. Biol. Interact.* **2015**, *228*, 88–99. [CrossRef]
20. Chanal, J.L.; Cousse, H.; Sicart, M.T.; Bonnaud, B.; Marignan, R. Absorption and elimination of (^{14}C) hesperidin methylchalcone in the rat. *Eur. J. Drug Metab. Pharmacokinet.* **1981**, *6*, 171–177. [CrossRef]
21. Gastillo, J.; Benavente, O.; Borrego, F. Analysis of commercial hesperidin methylchlcone by high performance liquid chromatography. *J. Chromatogr.* **1991**, *555*, 285–290. [CrossRef]
22. Rasquel-Oliveira, F.S.; Manchope, M.F.; Staurengo-Ferrari, L.; Ferraz, C.R.; Saraiva-Santos, T.; Zaninelli, T.H.; Fattori, V.; Artero, N.A.; Badaro-Garcia, S.; de Freitas, A.; et al. Hesperidin methyl chalcone interacts with NFkappaB Ser276 and inhibits zymosan-induced joint pain and inflammation, and RAW 264.7 macrophage activation. *Inflammopharmacology* **2020**, *28*, 979–992. [CrossRef] [PubMed]

23. Martinez, R.M.; Pinho-Ribeiro, F.A.; Steffen, V.S.; Caviglione, C.V.; Pala, D.; Baracat, M.M.; Georgetti, S.R.; Verri, W.A.; Casagrande, R. Topical formulation containing hesperidin methyl chalcone inhibits skin oxidative stress and inflammation induced by ultraviolet B irradiation. *Photochem. Photobiol. Sci.* **2016**, *15*, 554–563. [CrossRef]
24. Ruiz-Miyazawa, K.W.; Pinho-Ribeiro, F.A.; Borghi, S.M.; Staurengo-Ferrari, L.; Fattori, V.; Amaral, F.A.; Teixeira, M.M.; Alves-Filho, J.C.; Cunha, T.M.; Cunha, F.Q.; et al. Hesperidin Methylchalcone Suppresses Experimental Gout Arthritis in Mice by Inhibiting NF-kappaB Activation. *J. Agric. Food Chem.* **2018**, *66*, 6269–6280. [CrossRef]
25. Jawien, A.; Bouskela, E.; Allaert, F.A.; Nicolaides, A.N. The place of Ruscus extract, hesperidin methyl chalcone, and vitamin C in the management of chronic venous disease. *Int. Angiol.* **2017**, *36*, 31–41. [CrossRef]
26. Staurengo-Ferrari, L.; Badaro-Garcia, S.; Hohmann, M.S.N.; Manchope, M.F.; Zaninelli, T.H.; Casagrande, R.; Verri, W.A., Jr. Contribution of Nrf2 Modulation to the Mechanism of Action of Analgesic and Anti-inflammatory Drugs in Pre-clinical and Clinical Stages. *Front. Pharmacol.* **2018**, *9*, 1536. [CrossRef]
27. Raghunath, A.; Sundarraj, K.; Nagarajan, R.; Arfuso, F.; Bian, J.; Kumar, A.P.; Sethi, G.; Perumal, E. Antioxidant response elements: Discovery, classes, regulation and potential applications. *Redox Biol.* **2018**, *17*, 297–314. [CrossRef]
28. Kakkos, S.K.; Bouskela, E.; Jawien, A.; Nicolaides, A.N. New data on chronic venous disease: A new place for Cyclo 3® Fort. *Int. Angiol.* **2018**, *37*, 85–92. [CrossRef] [PubMed]
29. Allaert, F.A.; Hugue, C.; Cazaubon, M.; Renaudin, J.M.; Clavel, T.; Escourrou, P. Correlation between improvement in functional signs and plethysmographic parameters during venoactive treatment (Cyclo 3 Fort). *Int. Angiol.* **2011**, *30*, 272–277.
30. Stoianova, V. Cyclo 3 fort—Alternative in chronic venous insufficiency. *Akush. Ginekol. (Sofiia)* **2006**, *45* (Suppl. 3), 78–80.
31. Beltramino, R.; Penenory, A.; Buceta, A.M. An open-label, randomized multicenter study comparing the efficacy and safety of Cyclo 3 Fort versus hydroxyethyl rutoside in chronic venous lymphatic insufficiency. *Angiology* **2000**, *51*, 535–544. [CrossRef] [PubMed]
32. Kirtley, W.R.; Peck, F.B. Administration of massive doses of vitamin P hesperidin methyl chalcone. *Am. J. Med. Sci.* **1948**, *216*, 64–70. [CrossRef] [PubMed]
33. Wood, R.C., 3rd; Wyatt, J.E.; Bullins, K.W.; Hanley, A.V.; Hanley, G.A.; Denham, J.W.; Panus, P.C.; Harirforoosh, S. Effects of rebamipide on nephrotoxicity associated with selected NSAIDs in rats. *Eur. J. Pharmacol.* **2013**, *720*, 138–146. [CrossRef] [PubMed]
34. Borghi, S.M.; Domiciano, T.P.; Rasquel-Oliveira, F.S.; Ferraz, C.R.; Bussmann, A.J.C.; Vignoli, J.A.; Camilios-Neto, D.; Ambrosio, S.R.; Arakawa, N.S.; Casagrande, R.; et al. *Sphagneticola trilobata* (L.) Pruski-derived kaurenoic acid prevents ovalbumin-induced asthma in mice: Effect on Th2 cytokines, STAT6/GATA-3 signaling, NFkappaB/Nrf2 redox sensitive pathways, and regulatory T cell phenotype markers. *J. Ethnopharmacol.* **2022**, *283*, 114708. [CrossRef] [PubMed]
35. Davies, N.M.; Anderson, K.E. Clinical pharmacokinetics of diclofenac. Therapeutic insights and pitfalls. *Clin. Pharmacokinet.* **1997**, *33*, 184–213. [CrossRef]
36. Huo, X.; Meng, Q.; Wang, C.; Wu, J.; Wang, C.; Zhu, Y.; Ma, X.; Sun, H.; Liu, K. Protective effect of cilastatin against diclofenac-induced nephrotoxicity through interaction with diclofenac acyl glucuronide via organic anion transporters. *Br. J. Pharmacol.* **2020**, *177*, 1933–1948. [CrossRef]
37. Sivaraj, R.; Umarani, S. Diclofenac-induced biochemical changes in nephrotoxicity among male Albino rats. *Int. J. Basic Clin. Pharmacol.* **2018**, *7*, 640–643.
38. Bickel, M.; Khaykin, P.; Stephan, C.; Schmidt, K.; Buettner, M.; Amann, K.; Lutz, T.; Gute, P.; Haberl, A.; Geiger, H.; et al. Acute kidney injury caused by tenofovir disoproxil fumarate and diclofenac co-administration. *HIV Med.* **2013**, *14*, 633–638. [CrossRef]
39. Babladi, V.P.; Patil, N.; Manjunath, G.; Salimath, P.V.; Ninne, S.R.; Chary, K.M. A Case Report on Diclofenac Induced Chronic Kidney Disease. *Indian J. Pharm. Pract.* **2019**, *12*, 129–132. [CrossRef]
40. Mohammad, R.S.; Lokhandwala, M.F.; Banday, A.A. Age-Related Mitochondrial Impairment and Renal Injury Is Ameliorated by Sulforaphane via Activation of Transcription Factor NRF2. *Antioxidants* **2022**, *11*, 156. [CrossRef]
41. Van der Heijden, R.A.; Bijzet, J.; Meijers, W.C.; Yakala, G.K.; Kleemann, R.; Nguyen, T.Q.; de Boer, R.A.; Schalkwijk, C.G.; Hazenberg, B.P.; Tietge, U.J.; et al. Obesity-induced chronic inflammation in high fat diet challenged C57BL/6J mice is associated with acceleration of age-dependent renal amyloidosis. *Sci. Rep.* **2015**, *5*, 16474. [CrossRef]
42. Guazelli, C.F.S.; Fattori, V.; Ferraz, C.R.; Borghi, S.M.; Casagrande, R.; Baracat, M.M.; Verri, W.A., Jr. Antioxidant and anti-inflammatory effects of hesperidin methyl chalcone in experimental ulcerative colitis. *Chem. Biol. Interact.* **2021**, *333*, 109315. [CrossRef] [PubMed]
43. Basile, D.P.; Anderson, M.D.; Sutton, T.A. Pathophysiology of acute kidney injury. *Compr. Physiol.* **2012**, *2*, 1303–1353. [PubMed]
44. Edelstein, C.L. Biomarkers of acute kidney injury. *Adv. Chronic Kidney Dis.* **2008**, *15*, 222–234. [CrossRef] [PubMed]
45. Devarajan, P. Neutrophil gelatinase-associated lipocalin (NGAL): A new marker of kidney disease. *Scand. J. Clin. Lab. Investig. Suppl.* **2008**, *241*, 89–94. [CrossRef]
46. Liu, F.; Yang, H.; Chen, H.; Zhang, M.; Ma, Q. High expression of neutrophil gelatinase-associated lipocalin (NGAL) in the kidney proximal tubules of diabetic rats. *Adv. Med. Sci.* **2015**, *60*, 133–138. [CrossRef]
47. Kuwabara, T.; Mori, K.; Mukoyama, M.; Kasahara, M.; Yokoi, H.; Saito, Y.; Yoshioka, T.; Ogawa, Y.; Imamaki, H.; Kusakabe, T.; et al. Urinary neutrophil gelatinase-associated lipocalin levels reflect damage to glomeruli, proximal tubules, and distal nephrons. *Kidney Int.* **2009**, *75*, 285–294. [CrossRef]

48. Abdou, R.M.; El-Maadawy, W.H.; Hassan, M.; El-Dine, R.S.; Aboushousha, T.; El-Tanbouly, N.D.; El-Sayed, A.M. Nephroprotective activity of Aframomum melegueta seeds extract against diclofenac-induced acute kidney injury: A mechanistic study. *J. Ethnopharmacol.* **2021**, *273*, 113939. [CrossRef]
49. Lee, D.W.; Faubel, S.; Edelstein, C.L. Cytokines in acute kidney injury (AKI). *Clin. Nephrol.* **2011**, *76*, 165–173. [CrossRef]
50. Kinsey, G.R.; Okusa, M.D. Role of leukocytes in the pathogenesis of acute kidney injury. *Crit. Care* **2012**, *16*, 214. [CrossRef]
51. Naito, Y.; Takagi, T.; Higashimura, Y. Heme oxygenase-1 and anti-inflammatory M2 macrophages. *Arch. Biochem. Biophys.* **2014**, *564*, 83–88. [CrossRef] [PubMed]
52. Ratliff, B.B.; Abdulmahdi, W.; Pawar, R.; Wolin, M.S. Oxidant Mechanisms in Renal Injury and Disease. *Antioxid. Redox Signal.* **2016**, *25*, 119–146. [CrossRef] [PubMed]
53. Sverrisson, K.; Axelsson, J.; Rippe, A.; Asgeirsson, D.; Rippe, B. Acute reactive oxygen species (ROS)-dependent effects of IL-1beta, TNF-alpha, and IL-6 on the glomerular filtration barrier (GFB) in vivo. *Am. J. Physiol. Renal. Physiol.* **2015**, *309*, F800–F806. [CrossRef] [PubMed]
54. Martinez, R.M.; Pinho-Ribeiro, F.A.; Steffen, V.S.; Caviglione, C.V.; Vignoli, J.A.; Baracat, M.M.; Georgetti, S.R.; Verri, W.A., Jr.; Casagrande, R. Hesperidin methyl chalcone inhibits oxidative stress and inflammation in a mouse model of ultraviolet B irradiation-induced skin damage. *J. Photochem. Photobiol. B* **2015**, *148*, 145–153. [CrossRef] [PubMed]
55. Suh, J.H.; Shenvi, S.V.; Dixon, B.M.; Liu, H.; Jaiswal, A.K.; Liu, R.M.; Hagen, T.M. Decline in transcriptional activity of Nrf2 causes age-related loss of glutathione synthesis, which is reversible with lipoic acid. *Proc. Natl. Acad. Sci. USA* **2004**, *101*, 3381–3386. [CrossRef]
56. Hohmann, M.S.; Zaninelli, T.H.; Staurengo-Ferrari, L.; Manchope, M.F.; Badaro-Garcia, S.; de Freitas, A.; Casagrande, R.; Verri, W.A.J. Nrf2 in Immune Responses during Inflammation. In *Nrf2 and Its Modulation in Inflammation*; Deng, H., Ed.; Springer: Cham, Switzerland, 2020; pp. 23–50.
57. Rockwell, C.E.; Zhang, M.; Fields, P.E.; Klaassen, C.D. Th2 skewing by activation of Nrf2 in $CD4^+$ T cells. *J. Immunol.* **2012**, *188*, 1630–1637.

antioxidants

MDPI

Review

Naringenin and Hesperidin as Promising Alternatives for Prevention and Co-Adjuvant Therapy for Breast Cancer

Maria Beatriz Madureira [1,*], Virginia Marcia Concato [1], Ellen Mayara Souza Cruz [1], Juliana Maria Bitencourt de Morais [1,2], Fabricio Seidy Ribeiro Inoue [1], Natália Concimo Santos [1], Manoela Daniele Gonçalves [3], Milena Cremer de Souza [2,4], Thalita Basso Scandolara [5,6], Mariane Fontana Mezoni [5], Murilo Galvani [5], Fábio Rodrigues Ferreira Seiva [2], Carolina Panis [5], Milena Menegazzo Miranda-Sapla [7] and Wander Rogério Pavanelli [1,*]

[1] Laboratory of Immunoparasitology of Neglected Diseases and Cancer, State University of Londrina, Londrina 86057-970, Brazil
[2] Department of Biology, Biological Sciences Center, State University of Northern Paraná—UENP, Luiz Meneghel Campus, Bandeirantes 86360-000, Brazil
[3] Laboratory of Biotransformation and Phytochemical, State University of Londrina, Londrina 86057-970, Brazil
[4] Department of Pathological Sciences, State University of Londrina, Londrina 86057-970, Brazil
[5] Laboratory of Tumor Biology, State University of West Paraná, Unioeste, Francisco Beltrão 85601-080, Brazil
[6] Department of Genetics, Federal University of Rio de Janeiro—UFRJ, Rio de Janeiro 21941-901, Brazil
[7] Postgraduate Program in Pharmaceutical Science, University of Vale do Itajaí, Itajaí 88302-901, Brazil
* Correspondence: maria.madureira@uel.br (M.B.M.); wanderpavanelli@uel.br (W.R.P.)

Abstract: Citrus (genus *Citrus* L.) fruits are essential sources of bioactive compounds with antioxidant properties, such as flavonoids. These polyphenolic compounds are divided into subclasses, in which flavanones are the most prominent. Among them, naringenin and hesperidin are emerging compounds with anticancer potential, especially for breast cancer (BC). Several mechanisms have been proposed, including the modulation of epigenetics, estrogen signaling, induction of cell death via regulation of apoptotic signaling pathways, and inhibition of tumor invasion and metastasis. However, this information is sparse in the literature and needs to be brought together to provide an overview of how naringenin and hesperidin can serve as therapeutic tools for drug development and as a successful co-adjuvant strategy against BC. This review detailed such mechanisms in this context and highlighted how naringenin and hesperidin could interfere in BC carcinogenesis and be helpful as potential alternative therapeutic sources for breast cancer treatment.

Keywords: citrus fruits; bioactive compounds; breast cancer; flavanones; naringenin; hesperidin; antioxidants; anticancer activity

1. Introduction

Breast cancer (BC) is the most common malignancy in women worldwide and the leading cause of cancer-related deaths in the population [1]. BC cases are expected to increase by 4.4 million annually by 2070 [2]. Based on the expression of hormonal receptors (estrogen—ER and progesterone—PR) and the human epidermal growth factor receptor 2 (HER2) amplification, BC is classified as luminal (ER and/or PR+), HER2-amplified (any ER/PR status), or triple-negative (ER and PR -). These molecular subtypes are pivotal for clinical management and chosen therapeutic strategies [3,4]. BC is a multifactorial disease, and despite advances in screening and treatment, the underlying mechanisms and treatment alternatives are under continuous investigation [5].

Oxidative stress has been implicated as a mechanism involved in breast cancer development [6,7]. This type of stress can result from various factors, including menopause, aging, exposure to estrogen, or even genetic predisposition, and occurs when there is an imbalance between the production and neutralization of reactive species (RS). Normal

cells continuously generate RS from the incomplete oxygen reduction that occurs during respiratory chain reactions. Thus, complex antioxidant systems are essential to protect the organism and are composed of a range of enzymatic (such as superoxide dismutase (SOD), glutathione peroxidase (GPx), glutathione reductase, catalase), and nonenzymatic antioxidants (e.g., glutathione (GSH), vitamins C and D), which help to reduce or inhibit oxidative damage caused by RS [6,8–10]. These systems act as scavengers or quenchers of RS, converting these reactive species into less reactive intermediates and preventing cell damage [11,12]. Antioxidants significantly prevent or delay the oxidation of sensitive substrates, such as lipids, proteins, and DNA, even at low concentrations, thereby maintaining cellular homeostasis [13].

However, when the oxidant-antioxidant balance is disrupted due to excessive RS production or insufficient antioxidants, the accumulation of RS can cause oxidative stress. This condition is directly linked to the physiopathology of numerous diseases, including chronic inflammation and cancer. Despite significant redundancy in the antioxidant systems, they all neutralize RS to preserve redox stability and protect lipids, proteins, and DNA from oxidative stress damage [14,15]. Under sustained environmental stress, RS can cause significant damage to cell structures, including DNA damage, which can contribute to abnormal cell growth and promote metastasis, angiogenesis, and hypoxia adaptation [16]. DNA damage can lead to genomic instability, which is a necessary step for cancer initiation, promotion, and progression [10,17,18].

Nonenzymatic antioxidants can be obtained from the diet and are indispensable for proper defense against widespread oxidation [19]. Therefore, they play a crucial role in maintaining cellular health, and maintaining an antioxidant-rich diet has been shown to prevent more than two-thirds of human cancers [14,20]. It is widely accepted that fruits and vegetables rich in antioxidants are pivotal components of a healthy diet and can reduce the incidence of numerous malignancies [14]. Phytochemicals appear to contribute to cancer prevention by reversing the malignant transformation caused by oxidative stress, indicating their chemopreventive potential [21]. It is worth noting that phytochemicals are great sources of oncological drugs and are usually cost-effective [22].

Investigating natural compounds derived from vegetables and fruits has the potential to provide new insights into both prevention and complementary therapeutics, thereby strengthening the field of "green chemistry." Among the fruits commonly consumed worldwide, citrus fruits belong to the *Citrus* genus, which encompasses some of the most widely cultivated fruit crops worldwide and stands out as a rich source of phenolic compounds that have been linked to reducing oxidative stress-related disorders [16,23]. The phenolic compounds found in citrus fruits have been shown to have several positive impacts on the body, including reducing inflammation [24], improving cardiovascular health [25], and protecting against oxidative stress-related disorders [26,27]. Several in vitro and in vivo studies have shown that flavonoids, especially flavanones, the main class of flavonoids in citrus extracts, such as naringin and naringenin [22,28], possess antiproliferative, anti-inflammatory, and pro-apoptotic properties [29–34]. Other compounds found in citrus fruits that have demonstrated potential anticancer effects include quercetin [15,35–41], hesperidin [42–44], hesperetin [45,46], polymethoxyflavones [47–49], eriodyctiol [50,51], bergapten [52,53], tangeretin [54,55], auraptene [56–58], limonin [59], naringenin [60–65], and naringin [66–68], as shown in (Table 1). These findings suggest a potential role for flavonoids in cancer therapy, including breast cancer.

Table 1. Activities of several citrus-derived natural bioactive compounds.

Compounds	Classification	Review Highlights
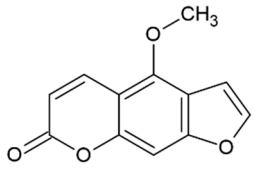 Bergapten 5-Methoxypsoralen	Polyphenol class: Other polyphenols Polyphenol sub-class: Furanocoumarins Family: Furanocoumarins	Anti-inflammatory, antimicrobial, antifungal, antiviral, anticancer, and antiosteoporosis [52]. Neuroprotection activity, effect on vitiligo and psoriasis, analgesic activity, immunosuppressive properties, and antidiabetics [53].
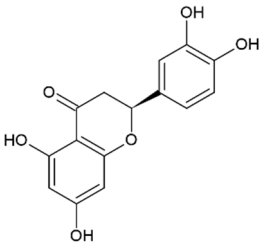 Eriodictyol 5,7,3′,4′-Tetrahydroxyflavanone	Polyphenol class: Flavonoids Polyphenol sub-class: Flavanones Family: Flavanones	Antioxidant, anti-inflammatory, anticancer, neuroprotective, cardioprotective, hepatoprotective, anti-diabetic, and anti-obesity activity [50]. Skin protection, immunomodulatory, analgesic, antipyretic, antinociceptive, and miscellaneous activities [51].
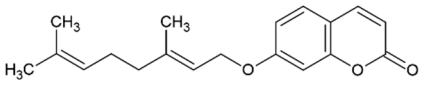 Auraptene 7-geranyloxycoumarin	Class: Phenol lipids Sub-class: Terpene Lactones Family: Terpene Lactones	Antitumor activity against BC, colorectal, ovarian, skin, gastric, esophageal, hepatic, and prostate cancer [56]. Cardioprotective, gastrointestinal protective, immune protective, and miscellaneous effects [57]. Effects on neurodegenerative diseases, periodontal disease, oncogenesis, cystic fibrosis, hypertension, and lipid profile [58].
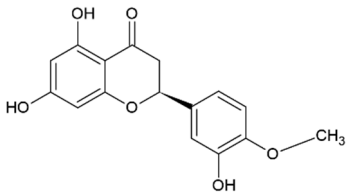 Hesperetin 5,7,3′-Trihydroxy-4′-methoxyflavanone	Polyphenol class: Flavonoids Polyphenol sub-class: Flavanones Family: Methoxyflavanones	Antioxidant and anti-inflammatory effects [45]. Anticancer activities against glioblastoma, breast, lung, prostate, colon, liver, pancreatic, kidney, gastric, oral, ovarian, and leukemia [46].
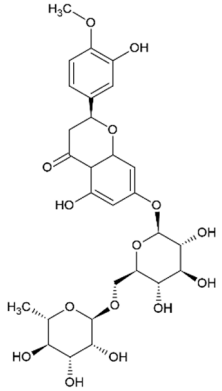 Hesperidin Hesperetin 7-*O*-rutinoside	Polyphenol class: Flavonoids Polyphenol sub-class: Flavanones Family: Flavanones	Effects on cardiovascular, neurological, psychiatric disorders, and antitumor activity [42]. Lipid metabolism, glucose metabolism, and inflammation activity [43]. Improvements in epidermal permeability barrier function, protection against UV irradiation, melanogenesis, acceleration of cutaneous wound healing, antioxidant [44].

Table 1. *Cont.*

Compounds	Classification	Review Highlights
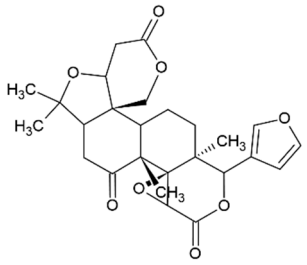 Limonin	Class: Prenol lipids Sub-class: Triterpenoids	Anticancer, anti-inflammatory, analgesic, antibacterial, antiviral, anti-insect, antioxidant, liver protection, neuroprotection, anti-osteoporosis, anti-obesity, and anti-allergy activities [59].
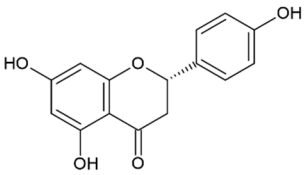 Naringenin 5,7,4′-Trihydroxyflavanone	Polyphenol class: Flavonoids Polyphenol sub-class: Flavanones Family: Flavanones	Immunomodulator [60], neuroprotective effects [61], anticancer activity against breast, colorectal, lung, liver, brain, leukemia, lymphoma, skin, cervical, prostate, pancreatic, gastric, oral, osteosarcoma, bladder, and ovarian cancer [62]. Effects on atherosclerosis, coronary artery disease, hypertension, cardiac hypertrophy, myocardial infarction, ischemic stroke [63], and fibrosis [64]. Antioxidant, antiviral, and antidiabetic [65].
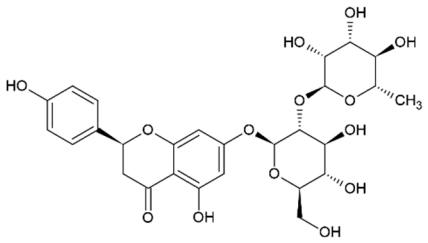 Naringin Naringenin 7-*O*-neohesperidoside	Polyphenol class: Flavonoids Polyphenol sub-class: Flavanones Family: Flavanones	Effect on obesity, diabetes, hypertension, cardiac toxicity, hypertrophy, remodeling, steatosis, hepatic protection, atherosclerosis, oxidative stress [66], metabolic syndrome, bone regeneration, genetic damage, central nervous system (CNS) diseases, anticancer and anti-inflammatory activity [67,68].
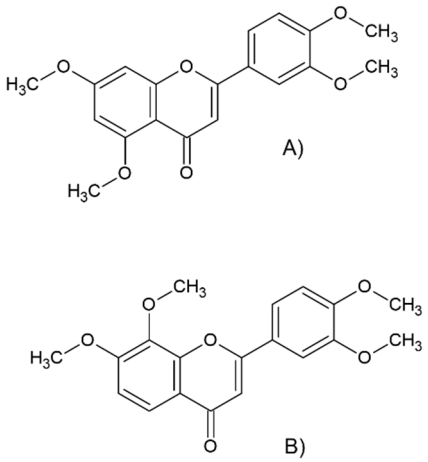 (A) 5,7,3′,4′-Tetra-methoxyflavone (B) 7,8,3′,4′-Tetra-methoxyflavone	Polyphenol class: Other polyphenols Polyphenol sub-class: Polymethoxyflavones Family: Polymethoxyflavones	Effects on circadian rhythm and metabolism [47] and neurodegenerative diseases [48]. Induces apoptosis via modulating the anti-tumor immunity, endoplasmic reticulum (ER) stress-mediated apoptosis, epigenetics modulators, protective autophagy, pyroptosis, ferroptosis, and anoikis cell death [49].

Table 1. *Cont.*

Compounds	Classification	Review Highlights
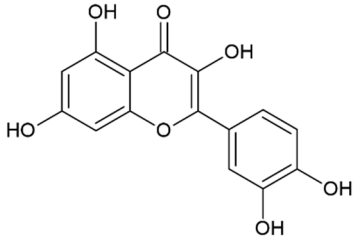 Quercetin 3,5,7,3′,4′-Pentahydroxyflavone	Polyphenol class: Flavonoids Polyphenol sub-class: Flavanols Family: Flavonols	Anti-cancer properties in BC, prostate cancer, ovarian cancer, lung cancer, colon cancer, hepatocellular carcinoma, lymphoma, and pancreatic cancer [15]. Effects on autoimmune diseases [35], metabolic syndrome [36], oxidative stress, and autophagy [37]. Anti-allergic [38], anti-inflammatory, anti-hypertensive [39], antiviral [40], and neuroprotective efficacy [41].
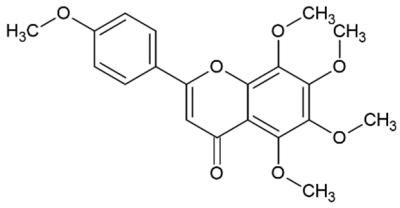 Tangeretin 5,6,7,8,4′-Pentamethoxyflavone	Polyphenol class: Flavonoids Polyphenol sub-class: Flavanes Family: methoxyflavones	Antitumor, neuroprotective, antidiabetic, hepatoprotective, immunomodulatory, melanogenesis, and antioxidant activities [54]. Induces apoptosis and autophagy and suppresses migration, invasion, and angiogenesis [55].

Structures presented in Table 1 were obtained from the ACD/ChemSketch software (Freeware) based on those presented in the original articles.

Citrus fruits are an important source of phenolic compounds that have the properties and the potential to be co-administered in chemotherapeutic regimens, but their mechanism of action is complex and requires further research. While there is evidence suggesting that citrus flavones may have a protective effect against breast cancer, more research is needed to fully evaluate the potential for their use in breast cancer prevention or treatment. In this context, the present review focuses on the current understanding of the anti-breast cancer effects of naringenin and hesperidin to investigate potential insights for co-adjuvant treatment strategies.

2. Data Analysis Methodology

This review focuses on research considering the composition, function, and anti-cancer properties of two citrus flavanones, naringenin and hesperidin, for BC. PubMed, ScienceDirect, and Google Scholar databases were searched using the keywords "citrus fruits/naringenin/anti-breast cancer", "Citrus fruits/hesperidin/anti-breast cancer", "naringenin/anti-breast cancer", and "hesperidin/anti-breast cancer". The studies selected were published between 2012 and 2022, and a total of 1.861 articles were analyzed thoroughly, examining the titles and abstracts to verify their relevance. We selected 162 original articles that specifically analyzed the bioactivity of naringenin and hesperidin concerning BC. Articles that did not fit these criteria were excluded.

3. Naringenin and Hesperidin: An Overview

3.1. Citrus Fruits and Flavanones

The genus *Citrus*, a member of the Rutaceae family and the Aurantioidae subfamily, is one of the most widely cultivated and consumed plant species globally [23,69]. Originating in the Himalayan region of southwestern China, northeastern India, and northern Burma, it has since been grown in over 140 countries [70]. The taxonomy of the genus *Citrus* is complex and controversial, mainly because of sexual compatibility between species and genera, the high frequency of bud mutations, and the long history of cultivation and wide

dispersion, making the quantification of species uncertain, but it is known that this genus contains numerous species that differ in their fruit, flower, leaf, and twig characteristics [71].

Some of the most commercially important species of *Citrus* include the sweet orange (*Citrus sinensis*), sour orange (*C. aurantium*), mandarin (*C. reticulata*), grapefruit (*C. paradisi*), pummelo (*C. grandis*), lemon (*C. limon*), citron (*C. medica*), lime (*C. aurantifolia*), kumquat (*C. japonica*), and hybrids [70]. Citrus fruits are rich in secondary metabolites such as polyphenols and terpenoids [71]. A hundred polyphenols have been detected in citrus, with flavonoids being the most important bioactive components with a wide variety and distribution present in almost all the parts of citrus fruits in different species [72].

Flavonoids, responsible for the flavor and color of fruits and flowers, are involved in metabolic processes and chemical signaling. They are further divided into subclasses such as flavanones, flavonols, anthocyanins, flavones, and polymethoxyflavones [73,74]. Although the content and types of flavonoids vary among *Citrus* species and fruit parts, flavanones are the most important in *Citrus* species, which are represented by two main categories, further classified into glycoside (hesperidin and narirutin) or aglycone (hesperetin and naringenin) (Figure 1) [69,71,73]. They can be found in all plant parts, such as stems, branches, bark, flowers, leaves, roots, and seeds [71].

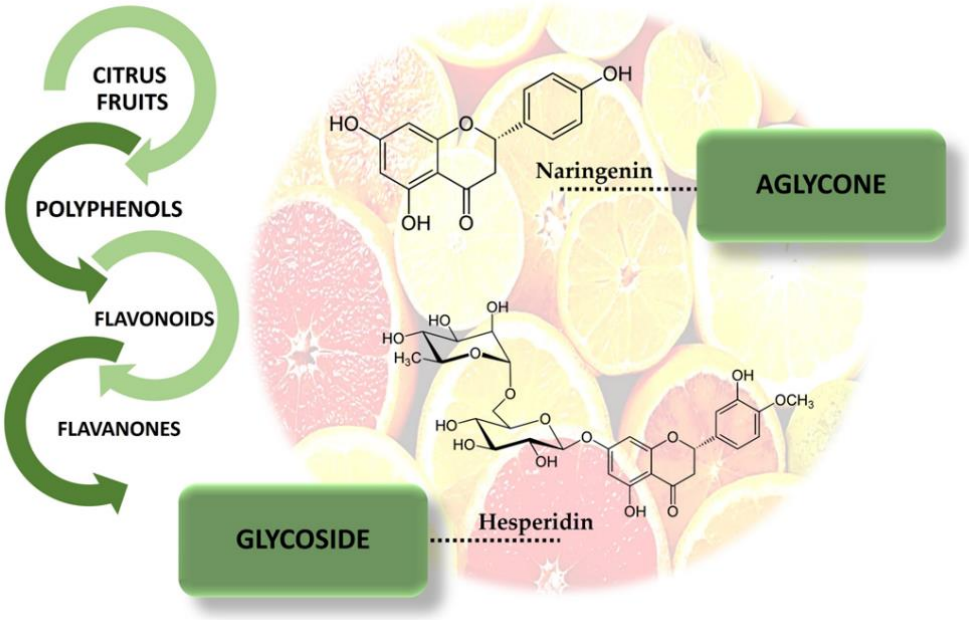

Figure 1. Naringenin and hesperidin derived from citrus fruits. Schematic representation of the sequential distribution of the major functional bioactive compounds (polyphenols, flavonoids, and flavanones) found in *Citrus* species and characterization of the molecular structure of the flavanone subclasses aglycone (naringenin) and glycoside (hesperidin).

Of all the flavanone varieties, hesperidin (3,5,7-trihydroxyflavanone 7-rhamnoglucoside) and naringenin (4′,5,7-trihydroxyflavanone) are the predominant flavanones in citrus fruits [75,76] and can be found in all parts of the plant, including stem, branches, bark, flowers, leaves, roots, rhizomes, seeds, fruits, and peels [71]. These flavones have well-established beneficial effects on human health and, in addition to citrus fruits, can also be found in other natural sources such as honey, mint, and tomatoes [76].

Hesperidin is a flavanone glycoside consisting of hesperetin (aglycone) and rutinose disaccharide (glucose-related rhamnose) (Table 1). It is most abundant in clementines, sweet oranges, mandarin oranges, and lemons. Studies have shown that hesperidin is most abundant in the peel and membranous sections of citrus fruits [72]. Naringenin is the predominant flavanone found mainly in grapefruit. It is an aglycone flavanone, and it can exist in different forms depending on the sugar molecule attached to it. Naringenin

can be found as glycoside forms naringenin-7-*O*-rutinoside (narirutin) and naringenin-7-*O*-glucoside (naringin), both occurring naturally as aglycone and glycoside forms [72,77].

In general, the biological properties of hesperidin and naringenin include antioxidant, anti-inflammatory, inhibitory effects against obesity-associated diseases, and anti-cancer properties. They also act in cardiovascular protection and analgesic manner [30,43,78–81]. Moreover, studies have demonstrated that these compounds can modulate molecular targets and signaling pathways involved in cell survival, proliferation, differentiation, migration, angiogenesis, and hormonal activity [82].

3.2. Sites of Interaction and Structure-Activity Relationship by Naringenin and Hesperidin

Secondary metabolites are generated during the biosynthesis process, which, for naringenin and hesperidin, follow a common pathway through the phenylpropanoid pathway. First, the phenylalanine is transformed into *p*-coumaronyl-CoA through the action of the enzymes phenylalanine ammonia-lyase (FAL), cinnamate 4-hydroxylase (C4H), and 4-coumaronyl-CoA ligase (4CL). Then, three malonyl-CoA molecules combine with one *p*-coumaronyl-CoA to form an aromatic ketone converted to naringenin (Figure 2). Subsequent events of hydroxylation and methylation result produce hesperidin [74]. Actinomycetes can also make naringenin. The bacterium *Streptomyces clavuligerus* synthesizes naringenin using *p*-coumaric acid and the P450 monooxygenase enzyme as pathway initiators rather than the general phenylpropanoid pathway seen in plants. Other bacteria in the genus *Streptomyces* can produce naringenin by the same principle, using *p*-coumaric acid or other pathway initiators, such as caffeic acid and benzoic acid [83].

The basic structure of phenolic compounds is based on two benzene rings and fifteen carbon atoms linked by a short chain of three carbon atoms, which in turn form a pyran ring. Structural variations are currently used to classify different types of flavonoids, such as the content of hydroxyl and methoxyl groups [84]. This is the case for flavanones, a phenolic class including naringenin and hesperidin. These compounds have a saturated C ring, and due to this fact, the double bonds present on carbons 1 and 2 are also saturated [73].

Naringenin is a solid compound with dissociation constants (pKa) values of 7.05 and 8.84, with a melting point of 208–251 °C, and basic nature. The compound is soluble in ethanol, dimethylformaldehyde dimethylsulfoxide, but poorly soluble in water (4.38 μg/mL). In a similar way, hesperidin also shows a low solubility (4.95 μg/mL) [85]. This characteristic of the two flavanones means that their biological activities are reduced when used alone. Therefore, the use of other compounds complexed to naringenin and hesperidin may be an alternative to increase their solubility in an aqueous medium and their biological activity. Cyclodextrin and its derivatives are the most used compounds for the formation of this type of complex. For example, naringenin complexed with hydroxylpropyl-β-cyclodextrin (P-β-CD) achieves a solubility of >500 g/L at 20 °C [73,86].

A study examined the complexation of naringenin with different cyclodextrin derivatives, including β-cyclodextrin (β-CD), 2,6-di-O-methyl-β-cyclodextrin (DM-β-CD), and randomly methylated β-CD (RAMEB). The study found that the naringenin/RAMEB complex had increased stability and solubility in aqueous solutions, with stability constants of 1015.5 Kc (M-1). The main type of force involved in binding the complexes was found to be van der Waals, which had a binding energy six times higher than electrostatic forces in all of the complexes. Additionally, the naringenin/DM-β-CD complex was found to have a stronger cytotoxic effect on MCF-7 and HeLa cells than on free naringenin. The study also showed that hesperetin, the compound from which hesperidin is derived, had improved stability and solubility after complex formation, as well as increased cytotoxicity, similar to naringenin [86].

Studies exploring the molecular interactions of naringenin and hesperidin are limited. Those examining the molecular interactions of hesperidin are even more scarce. In our search, we found a few papers that evaluated derivatives of this compound. One interaction that has been discovered for naringenin is with lysozyme, where it acts as a non-competitive inhibitor of the enzyme by binding to its active site through the remnants of the amino

acids tryptophan (Trp) 62, 63, and 108. This binding uses hydrophobic interactions, and positive entropy change (ΔS°) values contribute to the binding reaction. These findings, in a model using *Micrococcus lysodeikticus*, suggest that naringenin may act as an inhibitor of the lysozyme molecule [87]. Hesperidin has also shown the ability to spontaneously interact with the active site of trypsin to form a flavonoid-trypsin complex. This type of interaction influences the hydrophobicity of the microenvironment of tryptophan (Trp) residues, leading to a decrease in the enzymatic activity of trypsin [88].

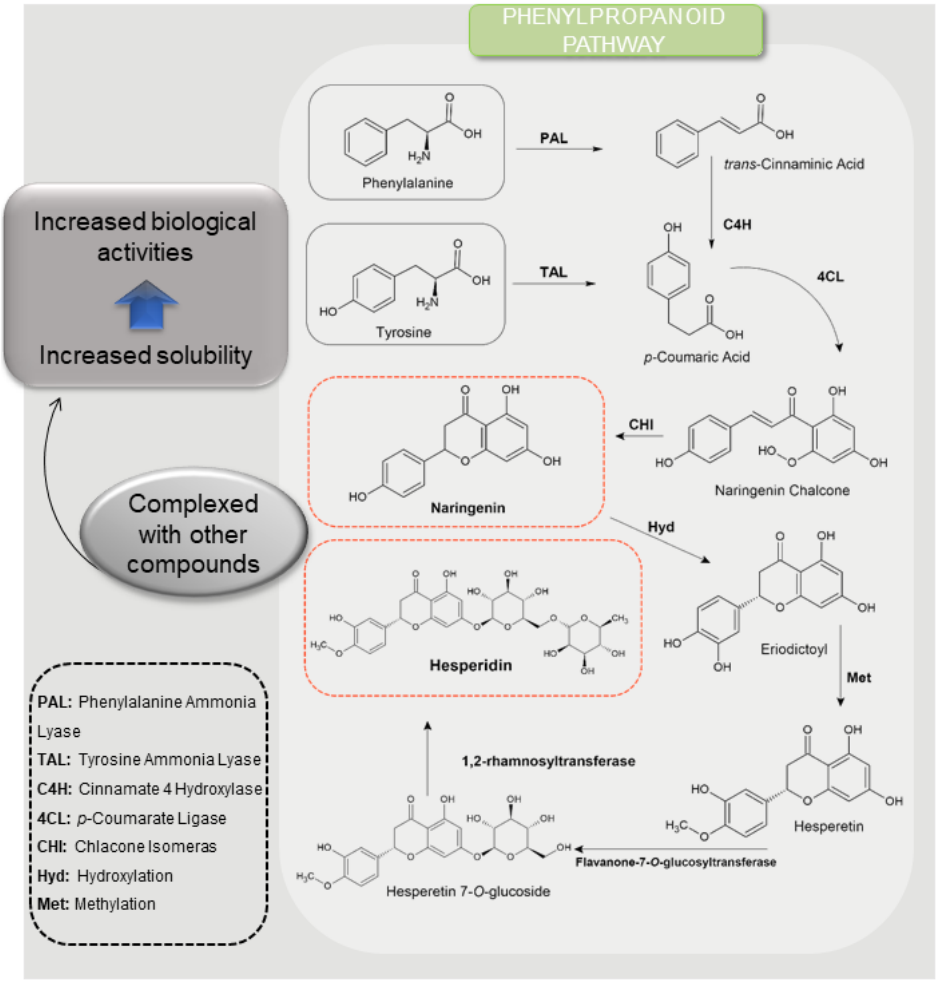

Figure 2. Naringenin and hesperidin follow a common pathway through the phenylpropanoid pathway.

Similarly, hesperidin is also able to inhibit the enzyme xanthine oxidase (XO), an essential enzyme of the purine catabolism pathway indirectly associated with pathological conditions such as cancer. Six products selected based on docking simulation studies were synthesized as aniline and hydrazine derivatives 3HDa 1–3 and 4HDb 1–3. The compounds showed potential antioxidant activity in vitro and an inhibitory effect on XO capacity in a competitive manner, with IC_{50} ranging from 0.263 µM–14.870 µM. The molecular simulation verified that the compounds showed interaction with the amino acid residues phenylalanine 798 (Phe798), glutamine 1194 (Gln1194), arginine 912 (Arg912), threonine 585 (Thr585), serine 1080 (Ser1080), and methionine 1038 (Met1038) positioned within the XO binding site [89].

The pharmacological mechanisms of neohesperidin dihydrochalcone (NHDC), a commercially synthesized by the catalytic alkali hydrogenation of hesperidin [90], were evaluated in vivo and identified 19 metabolites, with 18 being characterized for the first time. The metabolic reactions were evaluated using an optimized liquid chromatography method. The study also used network pharmacology to determine the targets of the

NHDC metabolites and found they were involved in various pathways related to cancer, ovarian steroidogenesis, proteoglycans in cancer, PI3K/protein kinase B (Akt) signaling pathway, and progesterone-mediated oocyte maturation, providing new insights into the pharmacological antitumoral potential mechanisms of NHDC [91].

The antioxidant properties of phytochemicals are particularly well-studied in cancer, as exacerbated free radical production is directly associated with developing malignant tumors [84]. The flavonoid antioxidant activity is linked to their chemical structure, i.e., the neutralizing free radicals' properties are influenced by the arrangement, number, and shape of hydroxyl groups and the presence of glycosides. The higher the number of hydroxyl groups, the greater the compound's antioxidant activity [74]. In this context, the loss of the hydroxyl group on carbon 5 of the naringenin (liquiritigenin) molecule increases its IC_{50} from 1.97 μM to 6.55 μM, and the presence of C(2)=C(3) double bond in the C ring of the (apigenin) molecule decreases the antioxidant capacity of the molecule when compared to naringenin (C(2)–C(3)) [92].

These findings show that naringenin and hesperidin have relevant properties. These compounds act on key enzymes in signaling pathways linked to inflammation and have evidence of potent antioxidant action. However, studies on naringenin and hesperidin and their molecular interactions still need to be made available. Still, these interactions are directly linked to their chemical structure and the type of bond between them. Even though it lacks further studies on their interaction and action mechanisms, naringenin and hesperidin may be an option for treating diseases such as cancers.

3.3. Anti-Breast Cancer Role of the Citrus-Derivated Compounds Naringenin and Hesperidin

Breast cancer, like other types of cancer, can be initiated and progressed by endogenous or exogenous oxidative stress, which can also increase therapy resistance, angiogenesis, and metastasis [7,93]. In this context, several studies have shown the anti-breast cancer role of naringenin. Naringenin cytotoxic effects were evaluated against three cell lines, including MDA-MB-231 and MDA-MB-468, both of which are triple-negative breast cancer cell lines, and CHO, a Chinese hamster ovary cell line, in comparison to kaempferol. Naringenin showed cytotoxicity against MDA-MB-468 and MDA-MB-231, obtaining IC_{50} values of 238 μg/mL and 70 μg/mL, respectively, without causing toxicity to CHO cells. The combination of kaempferol and naringenin resulted in higher IC_{50} values of 43 μg/mL and 44 μg/mL against MDA-MB-468 and MDA-MB-231, respectively. Additionally, naringenin induced morphological changes in tumor cells while being non-toxic to normal cells [94].

The breast cancer resistance protein (BCRP), a critical ATP-binding cassette (ABC) efflux transporter, acts in drug and xenotoxin disposition; its overexpression in tumors can result in multidrug resistance (MDR). The antiproliferative activity of 99 flavonoids, which are major components of traditional Chinese medicine (TCM), vegetables, and fruits, were evaluated in the BCRP-MDCKII cell line (canine kidney cell line containing breast cancer resistance protein) in the presence of mitoxantrone. Of the 99 compounds tested, 11 showed more than 50% inhibition of cell viability, including naringenin. In the same study, it was suggested that naringenin might have potential as an adjunctive therapy for brain tumors since it increased the concentration of mitoxantrone and increased the cytotoxicity of doxorubicin and temozolomide in several cell lines of human brain tumors after rats received a single dose of 30 mg/kg naringenin [95].

Another study investigated whether naringenin would act on the E0771 (mammary adipose tissue carcinoma) cell line. Naringenin treatment inhibited cell proliferation, increased phosphorylation of AMP-activated protein kinase (AMPK), negatively regulated cyclin D1 expression, and induced cell death. To confirm these data, obese ovariectomized C57BL/6 mice were fed a high-fat (HF), high-fat low-naringenin diet (LN; 1% naringenin), or high-fat high-naringenin diet (HN; 3% naringenin) and xenografted with E0771 cells for three weeks. The authors observed more significant naringenin accumulation in the tumor than in the mammary adipose tissue in HN mice. Furthermore, NH decreased body weight, fat mass, adipocyte size, smooth muscle actin mRNA in mammary adipose tissue, and

inflammatory cytokine. Also, compared to mice fed a HF diet, HN slowed tumor growth early but did not alter the final tumor weight, suggesting that naringenin exhibits beneficial effects on metabolic health and tumor origin [96].

In a study, ethanol extracts were obtained from the peels of several citrus fruits (*Citrus sinensis*, *C. aurantifolia*, *C. tangerine*, *C. aurantium*, *C. aurantium*, and *C. paradisi*), and their main components were isolated and tested for cytotoxicity against human breast cancer (MCF-7 and T47D) and normal human melanocytes (HFB4) cell lines. The results showed that the extracts and isolated compounds reduced cell viability without causing toxicity to normal cells, with naringenin being one of the most potent. The authors concluded that the effect of naringenin was not related to the modulation of the estrogen receptor or inhibition of aromatase. Furthermore, treatment with naringenin showed no uterotrophic activity and no changes in uterine weight or cornification, indicating that it does not have estrogenic activity. The treatment also reduced tumor volume and aromatase levels in mice with Ehrlich ascites carcinoma, suggesting that naringenin may have a potential role in breast cancer treatment before and after menopause. In contrast, hesperidin did not show significant anticancer activity at the tested concentration (0–50 μg/mL) in both cell lines [31].

Hesperidin also has pharmacological activity on breast cancer due to its anti-inflammatory and antioxidant properties [42]. Thus, the protective effect against oxidative stress and inflammation of hesperidin was evaluated in a study using MCF-7 cells and male Balb/c mice. The authors demonstrated that hesperidin can reduce cell proliferation starting at 40 μM. There was also reduced colony formation, increased nuclear condensation, and formation of apoptotic features. In the same study, mice treated with hesperidin showed an increased anti-inflammatory response, reducing IL-33 and TNF-α after stimulation with lipopolysaccharide (LPS). In addition, hesperidin treatment reduced lipid peroxidation and increased antioxidant capacity, where levels of the enzymes CAT and GSH increased in mice co-treated with LPS and hesperidin. They suggested that hesperidin may be a promising treatment for cancer [97].

In a case-control study, associations were made between serum concentrations of flavonols (quercetin, isorhamnetin, and kaempferol), flavones (apigenin and luteolin), flavanones (naringenin and hesperidin), and flavan-3-ols (catechin, epicatechin (EC), epigallocatechin (EGC), epicatechin-3-gallate (ECG), and epigallocatechin-3-gallate (EGCG)) and the risk of breast cancer in 792 female patients. It was demonstrated that higher blood levels of isorhamnetin, kaempferol, flavanones, and naringenin were associated with a lower risk of breast cancer (Figure 3) [98].

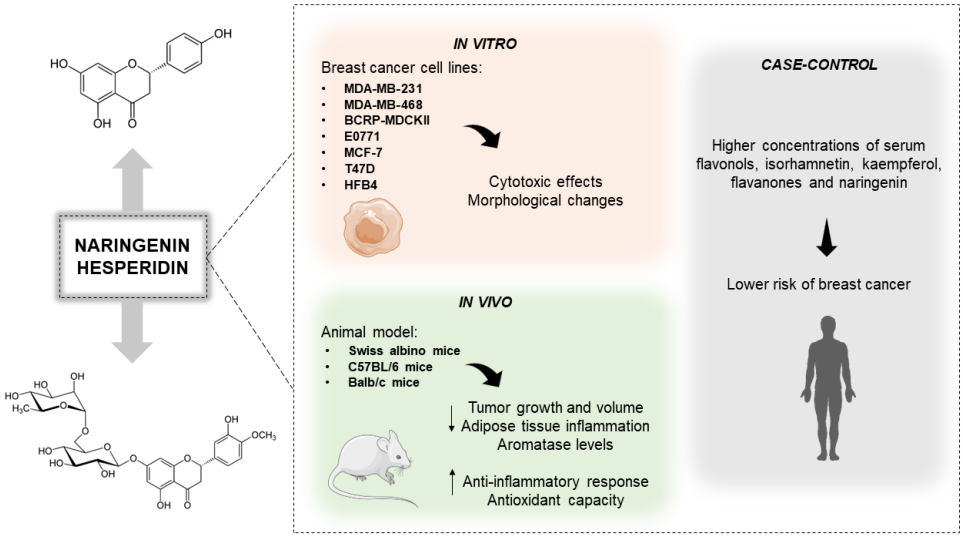

Figure 3. Schematic depiction of antitumor activity of naringenin and hesperidin.

3.4. Naringenin and Hesperidin on Modulation of Epigenetics and Estrogens Mechanisms

Epigenetic modifications coordinate gene expression and interfere with hormonal signaling pathways, triggering multistep breast carcinogenesis [99]. Flavanones are involved in the epigenetic regulation of cancer pathogenesis by interfering with DNA methylation, histone modification, and expression of non-coding RNAs, events that influence tumor progression and drug resistance [100–103]. Both transcriptional receptor α (Erα or ER66), which stimulates cell proliferation, and transcriptional receptor β (Erβ), which facilitates cytostatic and differentiation processes, are involved in breast cancer progression [104,105]. Some of these epigenetic mechanisms lead to this abnormal ER activity, resulting in the upregulation of oncogenes, gene suppression, or the silencing of DNA repair genes [105].

One of the most described processes of DNA methylation in breast cancer occurs through the silencing of Wnt antagonist genes, leading to the constitutive activation of β-catenin and promoting stem cell renewal and proliferation [106]. The Wnt/β-catenin signaling pathway such as PI3K/AKT, p53, and MAPK have frequently altered signaling pathways in resistant tumor cells and transmit extracellular and intracellular signals involved in cell growth, proliferation, survival, differentiation, migration, metabolism, and apoptosis.

Flavonoids are a promising group of compounds with potential therapeutic applications for breast cancer. Their ability to regulate epigenetic modifications and interfere with hormonal signaling pathways makes them attractive candidates for the development of new treatments or the enhancement of existing therapies. Several studies have demonstrated the effectiveness of various flavonoids in inhibiting breast cancer cell proliferation, inducing apoptosis, and inhibiting the activity of estrogen receptors. Flavonoids have been reported to activate proapoptotic proteins such as the Bcl2-associated X protein (Bax), bH3-interacting death domain (Bid), and Bcl-2-interacting protein (Bim), and inhibit the anti-apoptotic members Bcl-2, Bcl2-like protein (Bcl2L), and the long isoform of Bcl-2-related protein (BclXL), making them potentially useful anticancer agents [107].

Breast cancer subtypes expressing hormone receptors (ER and/or progesterone receptor (PR)) are the most prevalent [93]. Interestingly, co-exposure to tamoxifen and naringenin was able to modulate four ER subtypes, downregulating mRNA transcription of ER66, ER36, and GPR30 but upregulating Erβ expression, suggesting an apoptosis induction process [108]. While targeting the ER with drugs like tamoxifen (Tam) is a common treatment approach, long-term use can lead to resistance. In combination with tamoxifen, naringenin (Nar-Tam) was found to be more effective at impairing the cell viability of MCF-7 than either treatment alone [109]. This is because naringenin inhibits proliferation pathways PI3K and MAPK activated in breast cancer cells, blocks the activation of ER, and prevents MCF-7 proliferation [109]. Even in the absence of estrogen, naringenin was shown to inhibit ERK1/2 phosphorylation and alter ERα localization, confirming that it affects signaling pathways other than those dependent on estrogen [110].

Due to their structural similarity to estrogen, they can also be referred to as phytoestrogens because they can modulate estrogen function. These compounds have the potential to act as selective estrogen receptor modulators (SERMs) and act as ERα antagonists, impacting hormone signaling and synthesis [111]. Naringenin has also been identified as a potential therapeutic target for inhibiting breast cancer stem cells (BCSC). Bioinformatics analysis and in vitro modeling showed that naringenin upregulates ERα and p53, which regulate transforming growth factor-β (TGF-β) and Wnt/β-catenin pathways, resulting in BCSC inhibition [112]. Reinforcing this study, Pang et al. [113] also showed a virtual screening descriptor model that investigated, through a luciferase reporter gene assay on the MCF-7 cell line, the effects of naringenin as a potential ERα antagonist [113].

In another study, the effect of naringenin, 17-estradiol (E2), and genistein on the activity of estrogen receptor (ER) in T47D-KBluc (cells containing the triplet reporter gene ERE (estrogen-responsive elements)-promoter-luciferase) and ER-negative MDA-MB-231 breast cancer cell lines was investigated. Naringenin was found to be a partial agonist (functioning as a competitive antagonist in the presence of a full agonist such as E2 or

genistein) and not an efficient antagonist of the ER [114]. Additionally, in co-exposure with bisphenol A (BPA), naringenin was found to have a proapoptotic effect, which reduced the number of cells in both MCF-7 and T47D cell lines. On the other hand, BPA and E2 increased the number of cells in both cell lines by activating the Akt signaling pathway through Erα, leading to impaired cell proliferation and survival. However, naringenin prevented the proliferative effects of BPA by impairing Erα-mediated signals (Akt phosphorylation and Bcl-2 accumulation) and inducing persistent activation of p38, which initiated a proapoptotic cascade. Consequently, this study suggested that natural xenoestrogens, like naringenin, act as selective ER modulators by functioning on extranuclear Erα signaling pathways and providing critical information to develop tissue-specific E2 agonists and antagonists for breast cancer treatment [115].

The combination of hesperidin and chlorogenic acid also showed promising results for adjunctive therapies in breast cancer. The association enhanced toxicity towards MCF-7 cells but did not cause a cytotoxic effect on MCF-10A (non-tumorigenic epithelial). The synergistic effects of hesperidin and chlorogenic acid, which regulate multiple biochemical pathways, disrupt oxidative phosphorylation, mitochondrial dysfunction, and down-regulated synthesis of ATP and lipid functions by the ER pathway. The combined treatment significantly reduced gene expression of cytochrome-C (CYC1), mitochondrial transcription factor A (TFAM), mitochondrial membrane ATP synthase (mtATP6), ATP synthase subunit B (ATP5PB), mitochondrial DNA (mtDNA), and caused a slight reduction in nuclear respiratory factor 1 (NRF-1), but no change in ERα. Furthermore, the synergistic treatment did not induce RS production, which may be appropriate for chemotherapy [116].

The molecular interactions of hesperidin extracted from *C. limetta* with the Bcl-2, Bcl-W, myeloid cell leukemia 1 (MCL-1), and ERα receptors overexpressed in breast cancer were investigated. Hesperidin was found to have strong binding energy with BCL-W, MCL-1, and ERα proteins, and the hesperidin-MCL-1 complex was more stable. Following these analyses, hesperidin-loaded nanoliposomes were used to test cytotoxicity in MDA-MB-231 and MCF-10A cell lines. Both encapsulated and isolated hesperidin decreased tumor cell proliferation without causing toxicity to healthy cells. These findings suggest that hesperidin may be a promising target for breast cancer treatment [117].

3.5. Induction of Cell Death via Regulation of Apoptotic Signaling Pathways by Naringenin and Hesperidin

Apoptosis is programmed cell death responsible for the balance between proliferation and induction of death. This biological phenomenon replaces senescent, injured, or disease-derived cells. Disrupting the machinery that promotes this cellular control can allow genomic-damaged cells to survive, allowing their uncontrolled proliferation and initiating carcinogenesis. Cancer therapy is based on inhibiting cell proliferation and blocking or stimulating the signaling pathways that lead to the death of these aberrant cells [118]. Therefore, compounds that selectively induce cancer cell death are potential candidates for treating the disease. However, cancer's high clinical, morphological, and biological heterogeneity makes developing new therapies challenging and time-consuming. Thus, it is critical to understand how new compounds, such as naringenin and hesperidin, interact with cell signaling and how they induce cell death [119–122].

Anti-cancer activity of naringenin is related to apoptosis, cell cycle signaling and proliferation, and DNA repair mechanisms of cancer cells. Naringenin was tested against the MDA-MB-231 and MCF-10A cell lines and inhibited cell proliferation in a time and concentration-dependent manner in the MDA-MB-231 cell line. Moreover, naringenin was able to promote cell cycle arrest in the G0/G1 phase and increase in sub-G1 (indicative of apoptosis and DNA fragmentation), in addition to inducing apoptosis, with increased caspase 3/7, DNA fragmentation, and reduction of nuclear factor-kB (NF-kB) binding to DNA. To prove these findings, female Wistar rats that received dimethylbenz[α]anthracene (DMBA) (an immunosuppressive agent and inducer of mammary gland tumors) were treated with naringenin for eight days. Naringenin reduced tumor incidence and tumor

burden, reduced thiobarbituric acid reactive substances (TBARS), protein carbonyl and nitrate levels, down-regulated superoxide dismutase (SOD) and catalase expression, and up-regulated glutathione reductase (GR) and glutathione peroxidase (GPx) expression. Naringenin also increased markers of mitochondria-mediated apoptosis, including voltage-dependent anion channel (VDAC) and cytochrome-C (Cyt-C), increasing apoptosis in animals with breast cancer [123].

In another study, pure naringenin and its cyclic aminoethyl derivatives (ND): 4-methyl piperidine (3a), piperidine (3b), morpholine (3c), pyrrolidine (3d), 4 hydroxy piperidine (6-membered ring with -OH group on carbon 4) (3e), 3-methyl piperidine (6-membered ring with methyl group on carbon 3) (3f), thiomorpholine (6-membered ring with sulfur) (3g) and piperazine (6-membered ring with nitrogen) (3h)) were tested against several cell lines, including MCF-7, to assess viability and toxicity. The authors observed that 3a–3d reduced the proliferation of the tumor cell lines without causing damage to healthy cells. The compounds 3e–3h were highly cytotoxic. From these data, pure naringenin and ND 3a–3d were tested for their anticarcinogenic effects. After treatment, induction of selective apoptotic cell death was observed in MCF-7 by targeting intrinsic apoptosis signaling pathways and increased expression of p53, which was related to increased expression of Bax and suppression of Bcl-2 gene expression. There is a relationship between Bax/Bcl-2, in which Bax is favored due to Cyt-C and Apaf-1 (apoptotic protease activation factor 1). An increase in these factors was demonstrated when compared to the control group. The overexpression of these proteins forms the apoptosome (protein complex) in the cytosol, leading to an increase in caspase 3, which is responsible for apoptosis [124].

Naringenin was found to decrease the metabolic activity and the number of colony formations in MDA-MB-231 and MCF-7 breast cancer cells, as well as increase cytoplasmic membrane permeability and induce morphological changes indicating apoptotic cell death [125,126]. It also led to cell cycle arrest and reduced cellular capacity for migration and invasion. In MDA-MB-231 cells, naringenin increased the quantification of caspases 3, 8, 9, and Bax, while Bcl-2 was decreased [125]. In MCF-7 cells, naringenin reduced the phosphorylation of histone H3 (pH3), resulting in G2/M cell cycle arrest and increased the activities of poly (ADP-ribose) polymerase (PARP) and caspases 3 and 9, leading to an increase in the number of apoptotic cells [126].

Cyclin-dependent protein kinase 6 (CDK6) is overexpressed in many types of cancer and is responsible for regulating multiple pathways that maintain cell growth and development. Naringenin was also described to be strongly bound to CDK6, thereby preventing tumor development and progression in A549 and MCF-7 cells. Naringenin interacts with CDK6, leading to decreased viability of MCF-7 cells, inducing apoptosis, and reducing the ability to form colonies. This suggests that naringenin may act as a CDK6 inhibitor and can further direct future therapeutic approaches [127].

Naringenin also acts as an adjuvant in breast cancer [108,128]. MDA-MB-231 and MCF-10A treated with pure naringenin (NGEN) and naringenin complexed with copper (Cu(II)) and 2,2′-bipyridine (NGENCuB) were tested. The study exhibited its antiproliferative effect on MDA-MB-231 cells treated with NGEN and NGENCuB. Moreover, the co-treatment was also able to alter morphology, decrease wound closure and the number of colonies, and, in addition, showed apoptotic nuclei with up-regulation of caspase-9 expression. However, NGEN and NGENCuB reduced the viability of the normal lineage by 10% and 30%, respectively [129].

Similarly, the association of naringenin with doxorubicin and metformin affected the cell proliferation of MDA-MB-231 and 4T1 (mammary gland cancer) cell lines, being more effective in reducing cell proliferation, particularly in the 4T1 cell line. In the same study, breast carcinoma was chemically induced and treated with naringenin, liposomal doxorubicin (lipo-dox), and metformin separately or in combination for 28 days. The treatments led to a reduction in tumor weight and an increase in the necrotic area without any effect on blood glucose levels, body weight, or survival. The same results were

observed when mice with orthotopic 4T1-induced breast carcinoma were treated with naringenin, metformin, and lipo-dox [128].

The effects of the flavonoids naringenin, quercetin, and naringin, alone or in combination with the type 1 ribosome-inactivating protein, balsamin, on HepG2 (human hepatocarcinoma) and MCF-7 cell lines were evaluated. Treatment with naringenin, quercetin, and naringin together with balsamin reduced the viability of HepG2 and MCF-7 cells, increased caspase-3 and -8 activation, and induced apoptosis through the up-regulation of Bax (BCL-2 associated X protein), Bid (BH3 interacting domain death agonist), Bad (BCL2 associated agonist of cell death), and p53 gene and down-regulation of Bcl-2 and Bcl-XL. These effects were most effective in both cells' balsamin-naringenin and balsamin-quercetin combinations. Furthermore, the co-treatments were also able to increase the expression of the glucose-regulated protein (GRP) 78 and C/-EBP homologous protein (CHOP) (markers of endoplasmic reticulum stress (ERS)) in HepG2 and MCF-7. Therefore, combining flavonoids with balsamin can be a promising therapeutic approach to sensitize cells and enhance efficacy in breast and liver cancer therapy [130].

Hesperidin also shows proven cytotoxic activity in the literature. A study conducted on the synergism of the natural bioflavonoid compound hesperidin ((2S)-3′,5-dihydroxy-4′-methoxy-7-[α-L-rhamnopyrano-syl-(1→6)-β-D-glucopyranosyloxy]flavan-4-one, HSP) found in oranges and lemons with a synthetic derivative (3,5,7,8-tetrahydro-2-4-(trifluoromethyl)phenyl-4H-thiopyrano-4,3-dpyrimidin-4-one, XAV939), to evaluate the cytotoxic potential obtained in molecular and pathological profiles against HepG2 and MDA-MB-231 cell lines, revealed that the cytotoxicity was cell type- and concentration-dependent. HSP-XAV showed IC_{50} 10.25 μg/mL and 17.1 μg /mL for MDA-MB-231 and HepG2 cells, respectively. There was significant upregulation of the phosphoprotein 53 (p53) and pro-apoptotic genes, such as the X protein associated with B-cell lymphoma (Bax, creatine kinase (CK), and Caspase-3). In B-cell lymphoma, the anti-apoptotic gene (Bcl-2) was significantly down-regulated. In addition, the treatment increased RS levels, accompanied by higher DNA accumulation during the G2/M phase in both cell lines. According to the results, the authors suggest that the synergism promoted between HSP and XAV may be promising as an alternative in the therapy of human liver and breast cancer [131].

Changes in the proliferation, apoptosis, and cell cycle of MDA-MB-231 and MCF-7 breast carcinoma cells were compared concerning the effects of flavonoids hesperidin, apigenin, genistein, naringin, and quercetin. Their cytotoxic activity showed that only hesperidin at a lower dose (5 μM) significantly reduced the cell viability of MDA-MB-231 cells and presented the highest cytotoxic activity with a 100 μM dose in MCF-7 cells. Further analysis revealed that unlike all flavonoids tested, hesperidin did not reduce the percentage of live cancer cells or stimulate apoptosis, although increasing the dosage resulted in an increased number of dead cells. Therefore, the cell cycle progression of MDA-MB-231 and MCF-7 changed significantly after treatment with hesperidin, increasing the percentage of cells in phase G0/G1 [132].

The administration of hesperidin and luteolin demonstrated anti-cancer activity against the MCF-7 cell line. It was reported that in a dose-dependent manner, treatment with 100 or 140 mg/mL effectively reduced cell viability in MCF-7 cells to approximately 36% for hesperidin and 15% for luteolin after 48 h, increasing apoptotic cell populations. From these data, treatment with both compounds resulted in cell cycle arrest, accumulating cell population in the sub-G1 phase or the G0/G1 phase. Hesperidin and luteolin-induced apoptosis in MCF-7 cells led to caspase-3 and -9 expression in hesperidin-treated cells and increased expression of both caspase-9 and -8 in luteolin-treated cells, with the expression of miRNA (miR-16, -34a and -21). In contrast, an increase in the expression of pro-apoptotic proteins Bax was observed [133].

P-glycoprotein (P-gp) transporter is one of the main proteins that contribute significantly to the development of MDR [134]. Interestingly, hesperidin has been investigated to overcome doxorubicin resistance in MCF-7-resistant doxorubicin cells (MCF-7/Dox). In response to treatment, hesperidin increased MCF-7/Dox cells' sensitivity to doxorubicin

(IC_{50} value of 11 μmol/L) compared to MCF-7 cells. Thus, combining hesperidin with doxorubicin inhibits cancer cell growth and prevents resistance by suppressing P-gp expression [135]. Another study also investigated the influence of hesperidin and apigenin (API) on doxorubicin-treated MCF-7 breast cancer cells. First, an optimal concentration of apigenin and hesperidin (50 M) was used to sensitize cells in DOX treatment, and the synergistic effects on MCF-7 viability were confirmed.

Moreover, the combination treatment did not inhibit the cell cycle but showed an increase in cells in the subG1 phase, which corresponds to the dead cell population. It was also confirmed that a co-administration of hesperidin and apigenin with doxorubicin reduced the expression of genes involved in DNA repair, which API + Dox reduced the expression of genes (ERCC11, MSH2, MGMT, and XPC) in 70%, and hesperidin + Dox reduced expression of genes (ERCC1, ATM, OGG1) in over 80%. In summary, these flavonoids have shown an ability to enhance the effectiveness of classical anti-cancer drugs [136].

As discussed above, the search for potential targets to inhibit BCSCs using bioinformatics is also related to hesperidin. In one study, a functional network analysis was performed, and 75 likely therapeutic target proteins correlated with hesperidin were identified, with p53 emerging as a critical gene for the inhibition of BCSCs. In vitro experiments showed that hesperidin was cytotoxic to MCF-7 cells, decreased colony formation and migration ability, and induced cell cycle arrest in G0/G1 phase. In addition, hesperidin treatment significantly downregulated MMP-9 and aldehyde dehydrogenase 1 (ALDH1) while upregulating cyclin D1. Thus hesperidin can be used to develop drugs for BCSCs [137].

A recent study demonstrated the chemopreventive potential of hesperidin alone and in combination with doxorubicin against DMBA-induced breast cancer in female Wistar rats. Animals pretreated with hesperidin showed a decrease in tumor volume and incidence and a significant improvement in survival rate compared with the control group. In this study, an association between antioxidant and anti-inflammatory effects was found, resulting in a substantial decrease in malondialdehyde (MDA) and an increase in the concentration of GSH in the pretreated animals. Also, improvement in the inflammatory response and reduced organ damage and toxicity was found when compared to doxorubicin alone. The expression of the cell proliferation indicator Ki67 was analyzed. It showed that hesperidin is associated with attenuated Ki67 expression, resulting in a slight improvement in tumor spread and invasion [138].

In another study, the pretreatment of male Wistar rats with hesperidin before cisplatin administration resulted in less liver damage when compared to cisplatin alone. Animals with hesperidin pretreatment showed a significant reduction of known parameters induced by cisplatin, such as serum AST and ALT activity, as well as decreased triglycerides and total cholesterol. Oxidative stress markers resultant of cisplatin in the liver, such as MDA and NO metabolites, were also reduced, as opposed to GSH content, which was significantly higher. Cisplatin also activates a proinflammatory cascade, leading to tissue damage. However, prior administration of hesperidin resulted in NF-kB downregulation, ameliorating this inflammatory response and up-regulating p-Akt, a serine/threonine kinase that promotes cell survival and apoptosis blockade. Furthermore, co-administered cisplatin and hesperidin in several concentrations on MCF-7 cells did not differ from the cytotoxic activity of cisplatin alone. Thus, hesperidin demonstrated a protective effect against cisplatin toxicity in rats without affecting cisplatin's antitumoral effect [139].

Indeed, under in silico, in vitro, and in vivo approaches, naringenin and hesperidin can interfere with or target distinct cellular pathways in breast cancer cells (Table 2). However, many of these mechanisms still need to be fully understood, which may influence clinical outcomes. Because of this, it is interesting to consider further investigations for possible therapeutic applications.

Table 2. Summary of the mechanisms of naringenin and hesperidin in different analyses.

Compounds	Type of Study	Experimental Aspects	Proposed Mechanism	Reference
Naringenin	In vitro and in vivo	MDA-MB-231 and MCF-10A cell lines and female Wistar rats (120–160 g)	↓cell proliferation, tumor incidence and weight, TBARS, SOD, catalase, protein carbonyl, nitrate, GSH, vitamin C, vitamin E, GR, Bax, and Bad, ↑body weight (DMBA group) ↑G0/G1 and sub-G1 cell cycle, ↑caspase-3/-7, Apaf-1, VDAC, Bcl-2, cytochrome c, Bcl-xl, and procaspase-9	[123]
	In vitro	MCF-7, HT29, HeLa, DU145, and C8-D1A cell lines	For MCF-7: ↓cell proliferation, ↑expression P53 gene, Bax, cytochrome c, Apaf-1, and caspase-3	[124]
	In vitro	MDA-MB-231 cell line	↓cell proliferation, migration, invasion, and colony formation, ↑apoptosis, caspases-3/-8/-9, Bax, and ↓Bcl-2, ↑G2/M cell cycle	[125]
	In vitro	MDA-MB-231 cell line	↓cell viability, colony formation, percentage of pH3-positive cells, and ↑apoptosis, caspase-3/-9, anti-PARP levels, LDH release and G2/M cell cycle	[126]
	In silico and in vitro	MCF-7 and A549 cell lines	↓cell viability and colony formation, ↑apoptosis and binding affinity to CDK6	[127]
	In vitro	MDA-MB-231 and MCF-10A cell lines	↓cell proliferation, migration, colony number and size, pro-MMP9 activity, and ↑induce apoptosis/necrosis	[129]
	In vivo	Female Sprague Dawley rats (80–120 g) and female Balb/c mice (18–22 g)	↓tumor weight, volume, and ↑tumor necrosis	[128]
	In vitro	MCF-7 and HepG2 cell lines	↓cell viability, ↑apoptosis, caspase-3/-8, Bax, Bid, Bad, p53, ↑GRP78 and CHOP	[130]
Hesperidin	In vitro	MDA-MB-231 and HepG2 cell lines	↓cell viability, ↑caspase-3, Bax, and p53, ↓Bcl-2, ↓MMP1, ↑ROS, ↑G2/M cell cycle, apoptotic and nuclear fragmentation	[131]
	In vitro	MCF-7 and MDA-MB-231 cell lines	↓cell viability, cell cycle arrest, and ↑apoptosis	[132]
	In vitro	MCF-7 and HEK 293 cell lines	↓cell viability, ↑number of apoptotic cells, ↑G0/G1 and sub-G1 cell cycle, ↑caspase-3/-9, ↑miR-16 and -34a, ↓miR-21, ↑Bax and ↓Bcl-2	[133]
	In vitro	MCF-7-resistant doxorubicin cells (MCF-7/Dox)	↓cell viability and expression of Pgp	[135]
	In vitro	MCF-7 cell line	↓cell viability, ↑cells in sub-G1 phase, ↑early apoptosis, ↓GSH, ↑DNA damage, ↓expression of DNA repair genes	[136]
	In vitro	MCF-7 breast cancer cell line	↓cell viability, mammosphere formation, colony formation, cell migration, ↑G0/G1 cell cycle, ↓p21, ↑cyclin D1, ↓*ALDH1*, ↓*MMP9*, ↑p53, and ↓Bcl-2	[137]
	In vivo	Female Wistar rats	↑Survival rate, ↑body weight, ↓tumor volume, tumor spread and invasion, ↓MDA, ↑GSH, ↑IL-1β, ↓IL-6, NF-κB, TNF-α, and Ki67 expression	[138]
	In vivo	Adult male Wistar rats (120–150 g)	↓ALT, AST, TG, TC and MDA, ↑GSH, ↓hepatic NO, ↓NF-κB, ↑p-Akt expression	[139]

Abbreviations: DMBA: 7,12-dimethylbenz[a] anthracene; TBARS: thiobarbituric acid-reactive substances; SOD: superoxide dismutase; GSH: reduced glutathione; GR: glutathione reductase; Apaf-1: apoptotic protease activating factor-1; VDAC: voltage-dependent anion channel; Bcl-2: B-cell lymphoma 2; Bcl-xl: B-cell lymphoma-extra large; Bax: Bcl-2 associated X-protein; Bad: Bcl-2 associated agonist of cell death; HT29: colorectal adenocarcinoma; HeLa: cervix carcinoma; DU145: prostate carcinoma; C8-D1A: normal brain astrocyte; LDH: lactate dehydrogenase; pH3: phospho-histone H3; PARP: poli ADP-ribose polymerase; A549: lung adenocarcinoma; NAG: naringenin; CDK6: cyclin dependent kinase 6; pro-MMP9: pro-matrix metallopeptidase 9; HepG2: human hepatocellular carcinoma; GRP78: glucose-regulated protein 78; CHOP: CCAAT/enhancer-binding protein homologous protein; MMP1: matrix metallopeptidase 1; ROS: reactive oxygen species; HEK293: human embryotic kidney 293; miR-16,-34a,-21: microRNAs; Pgp: P-glycoprotein; ALDH1: aldehyde dehydrogenase 1; MDA: malondialdehyde; IL-1β: interleukin 1 beta; IL-6: interleukin 6; NF-κB: nuclear factor kappa-light-chain-enhancer of activated B cells; TNF-α: tumor necrosis factor alpha; Ki67: nuclear antigen; ALT: alanine aminotransferase; AST: aspartate aminotransferase; TG: triglycerides; TC: total cholesterol; NO: nitrate/nitrite; p-Akt: protein kinase B. The arrows represent up-regulated (↑) or down-regulated (↓).

3.6. Inhibition of Tumor Invasion and Metastasis by Naringenin and Hesperidin

Metastasis is considered one of the main problems for breast cancer patients, resulting in more than 90% of cancer-related deaths. During the metastatic process, cancer cells escape from the primary tumor, promote migration, adhesion, and invasion in a different location, and may settle predominantly in the bones, lungs, liver, brain, and lymph nodes [140,141].

The signaling transducer and activator of transcription 3 (STAT3) are activated in various types of cancer and are related to cell proliferation, migration, and invasion [142]. Thus, treatment with naringenin in MDA-MB-231 cells showed a decrease in cellular metabolic activity and an increase in apoptosis and its markers, such as Bax, caspase 3, and 9, decreasing the Bcl-2 protein. However, the co-administration of naringenin with cyclophosphamide enhanced the antitumor effect against this cell line. In addition, naringenin also inhibited the IL-6 effect on the Janus-kinase 2/signaling transducer and activator of the transcription 3 (JAK2/STAT3) pathway by blocking STAT3 phosphorylation, consequently decreasing cell proliferation capacity [143].

As mentioned earlier, estrogen metabolism plays a significant role in mediating breast cancer initiation and development; higher plasma levels and more prolonged exposure to estrogen increase the risk for this disease. To examine the modulatory mechanism and effects of naringenin in estrogen metabolism, chronic psychological stresses, which increase circulating estradiol concentration and promote breast cancer growth, were experimentally induced. In zebrafish (WT AB staining) and C57BL/6 female mice models, naringenin decreased psychological stress, reducing estradiol levels, thus limiting breast cancer growth and metastasis [144].

The control of breast cancer invasiveness and growth is also explained by abnormal signaling by TGF-β cytokines. In advanced-stage tumors, TGF-β activity is upregulated, stimulating the secretion of pro-angiogenic factors, extracellular matrix proteins, and suppression of the immune response culminating in epithelial-mesenchymal transition (EMT), reducing cell adhesion and increased motility [145,146]. Interestingly, naringenin as a treatment prevented TGF-β1 secretion from the 4T1 cell line and suppressed pulmonary metastasis. In this study, the role of protein kinase C (PKC) in regulating the intracellular trafficking machinery of TGF-β cytokines from the trans-Golgi network (TGN) compartment to the cell membrane was analyzed. The proposed mechanism was that naringenin decreased TGF-β1 trafficking from the trans-Golgi network via inhibiting PKC phosphorylation or activity, leading to the accumulation of intracellular TGF-β1, which suppressed tumor cell migration. These results suggest that naringenin can achieve antimetastatic activity by developing anti-cytokine therapies [147].

Dietary phytochemicals, such as hesperidin, allicin, and astragalus polysaccharides present in citrus fruits combined with an optimal diet, have inhibitory effects on breast cancer metastasis. For this, Balb/c mice were xenografted with 4T1 (mammary gland cancer) cells to evaluate the development of primary tumors and detect circulating tumor cells (CTCs) on days 7, 14, 21, and 28. The authors observed that the diet interventions inhibited primary tumor growth and metastasis to the lung. When they were combined with the phytochemicals tested, this effect was enhanced. Furthermore, the inhibitory effect of hesperidin on breast cancer metastasis occurred before day 14 and after day 21. Thus, these dietary compounds and dietary patterns can be evaluated as adjuvant therapies in cancer patients [148].

The overexpression of programmed death ligand 1 (PD-L1) is associated with triple-negative breast cancer (TNBC) (highly metastatic). The EMT process mediated PD-L1 upregulation through PI3K/Akt, mothers against decapentaplegic (SMAD), NF-κB, and ERK/MAPK signaling pathways, with consequent cell migration. Moreover, PD-L1 expression is accompanied by immune evasion modulation, resulting in tumor growth [149]. In this sense, hesperidin exhibited in vitro activity against MDA-MB231 cells by decreasing mRNA levels and PD-L1 protein expression by suppressing Akt and NF-κB signaling pathways. In addition, hesperidin reduced the secretion of the matrix metalloproteinases

(MMP-9 and MMP-2), inhibiting migration in MDA-MB-231 cells with high PD-L1 expression. Overall, hesperidin acts as an antitumor agent, and immunotherapy targeting PD-L1 can improve treatment efficacy [150].

Doxorubicin is essential to breast cancer chemotherapy; however, long-term use causes EMT and initiates invasion through lamellipodia formation, a fundamental first stage of the metastatic process [151]. Thus, the effect of *Citrus sinensis* (L.) peel extract (CSP) in combination with doxorubicin on the MDA-MB-231 cell line was examined. The CSP extract containing hesperidin and naringenin increased cytotoxicity and inhibited the induction of metastasis in these cell lines, suggesting that CSP is a potential co-chemotherapy agent to be developed (Figure 4) [152].

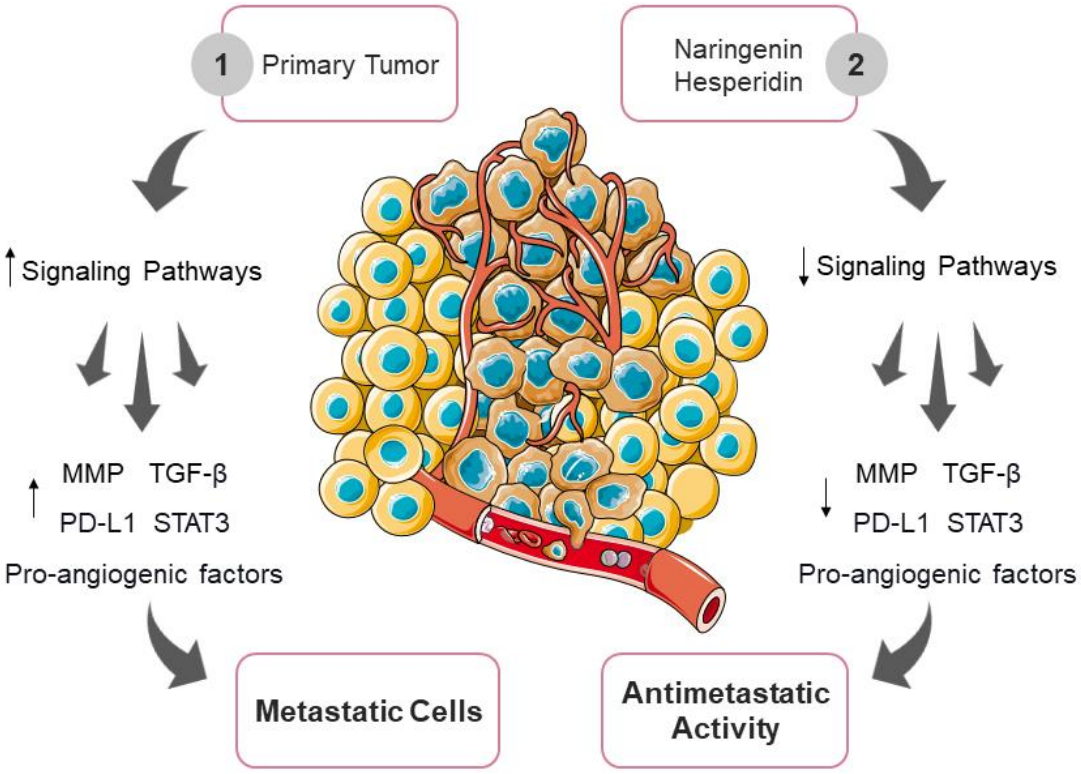

Figure 4. Antimetastatic potential of naringenin and hesperidin. (1) The primary tumor is capable of metastasis under the influence of abnormal signaling pathways, such as increased expression of activator of transcription 3 (STAT3), transforming growth factor-β (TGF-β), pro-angiogenic factors, matrix metalloproteinases, and programmed death ligand 1 (PD-L1); (2) Administration of naringenin and hesperidin inhibited tumor cell migration by blocking these activated signals, which reverse the epithelial-mesenchymal transition (EMT) process and consequent loss of ability to disseminate.

3.7. Nanotechnology as a Potentiator of Naringenin and Hesperidin Activity

Nanotechnology has been increasingly used in drug development as it improves bioavailability and produces co-delivery of two or more drugs. There are several nanoparticle delivery systems that can be employed for this purpose. Polymeric nanoparticles, such as polymeric micelles, dendrimers, nanogels, and nanocapsules, are considered to be nanocarriers made of biodegradable polymers. Their preparation can be done in nanospheres or nanocapsules, where the nanosphere is encapsulated uniformly within the polymer chains, and in the nanosphere, the drug is placed in the center and surrounded by a polymeric membrane. Lipid-based nanoparticles can be made of solid lipids or solid and liquid lipids. The main lipids in the nanoparticle are free fatty acids, phospholipids, glycolipids and sphingolipids, steroids, waxes, and triglycerides. Nanosuspensions cause the appearance of particles with a size <1 μm, which are drug-release systems that contain a pure therapeutic agent and a stabilizer. It can be a good choice to solve the low bioavailabil-

ity and pharmacokinetics of insoluble drugs. Nanoemulsions are prepared by combining surfactants, oils, hydrophilic solvents, and co-solvents that have the unique ability to form fine colloidal dispersions of oil in water [153–157]. Therefore, the use of nanotechnology offers a considerable advantage to the pharmacological potential of flavonoids, which have low solubility, rapid metabolism, and poor absorption in the gastrointestinal tract [156]. In this regard, the citrus compounds naringenin and hesperidin were nano-encapsulated and studied for their potential for successful drug delivery and promising results.

Hesperidin was synthesized by a nanoprecipitation technique using Poly (D, L-lactic-co-glycolic acid) (PLGA) polymers and Poloxamer 407 (a stabilizer) and tested on the MCF-7 cell line to increase stability and bioactive potentials. After treatment, nanohesperidin reduced proliferation and colony formation and induced apoptotic cell death, with increased expression of p53 and caspase-3, compared to native hesperidin. Moreover, nanohesperidin promoted DNA fragmentation. Finally, when tested against human erythrocytes, the modified hesperidin did not cause hemolysis. Therefore, hesperidin nanoparticles have the potential to be developed as a chemotherapeutic agent for human breast cancer, but further investigation is required [158].

In another study, hesperidin was synthesized using a chemical synthesis technique, loaded onto gold nanoparticles (Hsp-AuNPs), and tested on MDA-MB-231 and HBL-100 (normal human breast epithelial) cell lines. It was observed that the synthesized Hsp-AuNPs exhibited higher anti-cancer activity compared to hesperidin or AuNPs separately, without causing damage to normal cells. In the crystal violet assay (also used in cytotoxicity evaluation), Hsp-AuNPs induced morphological changes in tumor cells, including impaired cell-cell communication and reduced cell clusters. Normal cells maintained their full morphology. Furthermore, Hsp-AuNPs promoted the induction of cell death through apoptotic mechanisms. To confirm these data, male Balb/c mice were treated with a Hsp-AuNP dose ranging from 20–200 μg kg for 14 days and then their body weight and cytotoxicity in the kidney and liver were analyzed. Hsp-AuNPs did not alter serum concentrations of alanine transaminase (ALT), aspartate transaminase (AST), or alkaline phosphatase (ALP). In assessing tumor growth in Ehrlich tumor-bearing mice, it was observed that Hsp-AuNPs inhibited growth by inducing functional macrophage activity. In addition, pro-inflammatory cytokines (IL-1β, IL-6, and TNF-*A*) derived from bone marrow macrophages were inhibited after treatment with Hsp-AuNPs, demonstrating its antioxidant activity. Finally, in the human erythrocyte hemolysis assay, it was shown that synthesized Hsp-AuNPs are potentially biocompatible and can be safely used within the body [159]. Thus, Hsp-AuNPs may be effectively used in clinical cancer therapy and explored for drug delivery applications.

Although exhibiting therapeutic effects, naringenin is a hydrophobic compound with low oral bioavailability [160]. Thus, dextran-coated magnetic nanoparticles loaded with curcumin-naringenin (CUR-NAR-D-MNPs) were prepared by chemical coprecipitation and tested on MCF-7 cells. It was observed that MCF-7 cells treated with CUR-NAR-D-MNPs had reduced proliferation and were induced to die by apoptosis after 48 h of incubation. The co-treatment, using CUR-NAR-D-MNPs and single dose 6 Gy radiotherapy (represents the amount of ionizing radiation energy absorbed) on the tumor cells, caused apoptotic and necrotic cell death and increased RS levels. However, cells incubated with CUR-NAR-D-MNPs 48 h before radiotherapy had exacerbated apoptosis and necrosis percentages compared to those that received radiotherapy, indicating this compound's antiproliferative and radiosensitizing activity. When evaluating the effect of CUR-NAR-D-MNPs in female Sprague Dawley rats, the treatment reduced tumor volume, leading to cell cycle arrest and induction of apoptosis through modulation of signaling, high p53, high p21, low TNF-α, low CD44, and high RS [161].

Naringenin nanosuspension (NARNS) was prepared using a high-pressure homogenization method with polyethylene glycol D-α-tocopheryl succinate 1000 (TPGS) as a co-stabilizer. This study evaluated the ability of TPGS-coated NARNS to reverse drug resistance in the MCF-7 cell line and human breast adenocarcinoma animal model. In vitro,

NARNS demonstrated greater cytotoxic efficacy when compared to free NARNS. The treatment reduced GSH levels and increased mitochondrial membrane potential, intracellular RS, lipid peroxidation (TBARS), and caspase-3 activity, also showing apoptotic index (membrane blebs and nuclear fragmentation). In the animal model of breast adenocarcinoma, mice treated with NARNS exhibited a decrease in the number of tumor cells and a longer life expectancy. Therefore, NARNS can be considered a good chemotherapeutic agent [162].

Flavonoids such as naringenin and hesperidin have already demonstrated health benefits and positive results against cancer, but poor absorption is still a problem. Nanoparticles in this scenario are a promising target as they are a technology that improves the delivery of compounds.

4. Conclusions

Citrus fruits commonly present in the human diet are one of the most important dietary sources of flavonoids, and naringenin and hesperidin have significant impacts on many biological processes. The rising prevalence of breast cancer, whose primary therapeutic approach is represented by chemotherapy with side effects and resistance, brings to light the discussion of the role of natural antioxidants as possible co-adjuvant therapeutic agents. Managing cancer therapy to improve efficacy involves a more detailed explanation of molecular targets and signaling pathways by increasing the selectivity for cancer cells. The main mechanisms of hesperidin and naringenin in breast cancer are linked to their ability to interfere with cell survival by inhibiting proliferation and reducing tumor growth, volume, and incidence. These compounds also play a direct role in modulating epigenetic and estrogen receptor activity. In the case of cell death and metastasis, administration of these flavanones may induce apoptosis and impair the ability to metastasize. Based on the anticancer effects of flavanones, it is clear that further efforts are needed to treat patients and that many important aspects still need to be explored to improve our understanding of these compounds in cancer.

Author Contributions: Conceptualization, methodology, data curation, writing—original draft preparation, writing—review and editing, M.B.M. and V.M.C.; methodology and writing—original draft preparation, writing—review and editing, M.D.G.; writing—original draft preparation, E.M.S.C., J.M.B.d.M., F.S.R.I., N.C.S., M.C.d.S., T.B.S., M.F.M. and M.G.; writing—original draft preparation, writing—review and editing, supervision, project administration, F.R.F.S., C.P., M.M.M.-S. and W.R.P. All authors have read and agreed to the published version of the manuscript.

Funding: This research received no external funding.

Institutional Review Board Statement: Not applicable.

Informed Consent Statement: Not applicable.

Data Availability Statement: Not applicable.

Acknowledgments: This work was carried out with the support of the Coordenação de Aperfeiçoamento de Pessoal de Nível Superior (CAPES, Brazil), Conselho Nacional de Pesquisa (CNPq, Brazil), Universidade Estadual de Londrina (UEL, Brazil). All authors agree to be accountable for all aspects of work ensuring integrity and accuracy.

Conflicts of Interest: The authors declare no conflict of interest.

References

1. Sung, H.; Ferlay, J.; Siegel, R.L.; Laversanne, M.; Soerjomataram, I.; Jemal, A.; Bray, F. Global Cancer Statistics 2020: GLOBOCAN Estimates of Incidence and Mortality Worldwide for 36 Cancers in 185 Countries. *CA Cancer J. Clin.* **2021**, *71*, 209–249. [CrossRef] [PubMed]
2. Soerjomataram, I.; Bray, F. Planning for tomorrow: Global cancer incidence and the role of prevention 2020–2070. *Nat. Rev. Clin. Oncol.* **2021**, *18*, 663–672. [CrossRef] [PubMed]
3. Akram, M.; Iqbal, M.; Daniyal, M.; Khan, A.U. Awareness and current knowledge of breast cancer. *Biol. Res.* **2017**, *50*, 33. [CrossRef] [PubMed]
4. Waks, A.G.; Winer, E.P. Breast Cancer Treatment: A Review. *JAMA* **2019**, *321*, 288–300. [CrossRef] [PubMed]

5. Britt, K.L.; Cuzick, J.; Phillips, K.-A. Key Steps for Effective Breast Cancer Prevention. *Nat. Rev. Cancer* **2020**, *20*, 417–436. [CrossRef] [PubMed]
6. Hecht, F.; Pessoa, C.F.; Gentile, L.B.; Rosenthal, D.; Carvalho, D.P.; Fortunato, R.S. The Role of Oxidative Stress on Breast Cancer Development and Therapy. *Tumour Biol.* **2016**, *37*, 4281–4291. [CrossRef] [PubMed]
7. Lee, J.D.; Cai, Q.; Shu, X.O.; Nechuta, S.J. The Role of Biomarkers of Oxidative Stress in Breast Cancer Risk and Prognosis: A Systematic Review of the Epidemiologic Literature. *J. Women's Health* **2017**, *26*, 467–482. [CrossRef]
8. Sies, H. Oxidative Stress: A Concept in Redox Biology and Medicine. *Redox Biol.* **2015**, *4*, 180–183. [CrossRef]
9. Liguori, I.; Russo, G.; Curcio, F.; Bulli, G.; Aran, L.; Della-Morte, D.; Gargiulo, G.; Testa, G.; Cacciatore, F.; Bonaduce, D.; et al. Oxidative Stress, Aging, and Diseases. *Clin. Interv. Aging* **2018**, *13*, 757–772. [CrossRef]
10. Hęś, M.; Dziedzic, K.; Górecka, D.; Jędrusek-Golińska, A.; Gujska, E. Aloe Vera (L.) Webb.: Natural Sources of Antioxidants—A Review. *Plant Foods Hum. Nutr.* **2019**, *74*, 255–265. [CrossRef]
11. Forman, H.J.; Zhang, H. Targeting Oxidative Stress in Disease: Promise and Limitations of Antioxidant Therapy. *Nat. Rev. Drug Discov.* **2021**, *20*, 689–709. [CrossRef] [PubMed]
12. Embuscado, M.E. Spices and Herbs: Natural Sources of Antioxidants—A Mini Review. *J. Funct. Foods* **2015**, *18*, 811–819. [CrossRef]
13. Ramana, K.V.; Reddy, A.B.M.; Majeti, N.V.R.K.; Singhal, S.S. Therapeutic Potential of Natural Antioxidants. *Oxid. Med. Cell. Longev.* **2018**, *2018*, 9471051. [CrossRef] [PubMed]
14. Wang, Y.; Qi, H.; Liu, Y.; Duan, C.; Liu, X.; Xia, T.; Chen, D.; Piao, H.-L.; Liu, H.-X. The Double-Edged Roles of ROS in Cancer Prevention and Therapy. *Theranostics* **2021**, *11*, 4839–4857. [CrossRef]
15. Asgharian, P.; Tazekand, A.P.; Hosseini, K.; Forouhandeh, H.; Ghasemnejad, T.; Ranjbar, M.; Hasan, M.; Kumar, M.; Beirami, S.M.; Tarhriz, V.; et al. Potential Mechanisms of Quercetin in Cancer Prevention: Focus on Cellular and Molecular Targets. *Cancer Cell Int.* **2022**, *22*, 257. [CrossRef]
16. Sanches, V.L.; de Souza Mesquita, L.M.; Viganó, J.; Contieri, L.S.; Pizani, R.; Chaves, J.; da Silva, L.C.; de Souza, M.C.; Breitkreitz, M.C.; Rostagno, M.A. Insights on the Extraction and Analysis of Phenolic Compounds from Citrus Fruits: Green Perspectives and Current Status. *Crit. Rev. Anal. Chem.* **2022**, 1–27. [CrossRef]
17. Griñan-Lison, C.; Blaya-Cánovas, J.L.; López-Tejada, A.; Ávalos-Moreno, M.; Navarro-Ocón, A.; Cara, F.E.; González-González, A.; Lorente, J.A.; Marchal, J.A.; Granados-Principal, S. Antioxidants for the Treatment of Breast Cancer: Are We There Yet? *Antioxidants* **2021**, *10*, 205. [CrossRef]
18. Jelic, M.D.; Mandic, A.D.; Maricic, S.M.; Srdjenovic, B.U. Oxidative Stress and Its Role in Cancer. *J. Cancer Res. Ther.* **2021**, *17*, 22–28. [CrossRef]
19. Lourenço, S.C.; Moldão-Martins, M.; Alves, V.D. Antioxidants of Natural Plant Origins: From Sources to Food Industry Applications. *Molecules* **2019**, *24*, 4132. [CrossRef]
20. Zhang, Y.-J.; Gan, R.-Y.; Li, S.; Zhou, Y.; Li, A.-N.; Xu, D.-P.; Li, H.-B. Antioxidant Phytochemicals for the Prevention and Treatment of Chronic Diseases. *Molecules* **2015**, *20*, 21138–21156. [CrossRef]
21. Chikara, S.; Nagaprashantha, L.D.; Singhal, J.; Horne, D.; Awasthi, S.; Singhal, S.S. Oxidative Stress and Dietary Phytochemicals: Role in Cancer Chemoprevention and Treatment. *Cancer Lett.* **2018**, *413*, 122–134. [CrossRef]
22. Younas, M.; Hano, C.; Giglioli-Guivarc'h, N.; Abbasi, B.H. Mechanistic Evaluation of Phytochemicals in Breast Cancer Remedy: Current Understanding and Future Perspectives. *RSC Adv.* **2018**, *8*, 29714–29744. [CrossRef]
23. Wu, G.A.; Terol, J.; Ibanez, V.; López-García, A.; Pérez-Román, E.; Borredá, C.; Domingo, C.; Tadeo, F.R.; Carbonell-Caballero, J.; Alonso, R.; et al. Genomics of the Origin and Evolution of Citrus. *Nature* **2018**, *554*, 311–316. [CrossRef]
24. Miles, E.A.; Calder, P.C. Effects of Citrus Fruit Juices and Their Bioactive Components on Inflammation and Immunity: A Narrative Review. *Front. Immunol.* **2021**, *12*, 712608. [CrossRef]
25. Mahmoud, A.M.; Hernández Bautista, R.J.; Sandhu, M.A.; Hussein, O.E. Beneficial Effects of Citrus Flavonoids on Cardiovascular and Metabolic Health. *Oxid. Med. Cell. Longev.* **2019**, *2019*, 5484138. [CrossRef] [PubMed]
26. Musumeci, L.; Maugeri, A.; Cirmi, S.; Lombardo, G.E.; Russo, C.; Gangemi, S.; Calapai, G.; Navarra, M. Citrus Fruits and Their Flavonoids in Inflammatory Bowel Disease: An Overview. *Nat. Prod. Res.* **2020**, *34*, 122–136. [CrossRef] [PubMed]
27. Wang, Y.; Liu, X.-J.; Chen, J.-B.; Cao, J.-P.; Li, X.; Sun, C.-D. Citrus Flavonoids and Their Antioxidant Evaluation. *Crit. Rev. Food Sci. Nutr.* **2022**, *62*, 3833–3854. [CrossRef] [PubMed]
28. Rauf, A.; Shariati, M.A.; Imran, M.; Bashir, K.; Khan, S.A.; Mitra, S.; Emran, T.B.; Badalova, K.; Uddin, M.S.; Mubarak, M.S.; et al. Comprehensive Review on Naringenin and Naringin Polyphenols as a Potent Anticancer Agent. *Environ. Sci. Pollut. Res. Int.* **2022**, *29*, 31025–31041. [CrossRef]
29. Liskova, A.; Samec, M.; Koklesova, L.; Brockmueller, A.; Zhai, K.; Abdellatif, B.; Siddiqui, M.; Biringer, K.; Kudela, E.; Pec, M.; et al. Flavonoids as an Effective Sensitizer for Anti-Cancer Therapy: Insights into Multi-Faceted Mechanisms and Applicability towards Individualized Patient Profiles. *EPMA J.* **2021**, *12*, 155–176. [CrossRef]
30. Pandey, P.; Khan, F. A Mechanistic Review of the Anticancer Potential of Hesperidin, a Natural Flavonoid from Citrus Fruits. *Nutr. Res.* **2021**, *92*, 21–31. [CrossRef]
31. El-Kersh, D.M.; Ezzat, S.M.; Salama, M.M.; Mahrous, E.A.; Attia, Y.M.; Ahmed, M.S.; Elmazar, M.M. Anti-Estrogenic and Anti-Aromatase Activities of Citrus Peels Major Compounds in Breast Cancer. *Sci. Rep.* **2021**, *11*, 7121. [CrossRef] [PubMed]

32. Koolaji, N.; Shammugasamy, B.; Schindeler, A.; Dong, Q.; Dehghani, F.; Valtchev, P. Citrus Peel Flavonoids as Potential Cancer Prevention Agents. *Curr. Dev. Nutr.* **2020**, *4*, nzaa025. [CrossRef] [PubMed]
33. Lu, K.; Yip, Y.M. Therapeutic Potential of Bioactive Flavonoids from Citrus Fruit Peels toward Obesity and Diabetes Mellitus. *Future Pharmacol.* **2023**, *3*, 14–37. [CrossRef]
34. Alam, F.; Mohammadin, K.; Shafique, Z.; Amjad, S.T.; Asad, M.H.H.B. Citrus Flavonoids as Potential Therapeutic Agents: A Review. *Phytother. Res.* **2022**, *36*, 1417–1441. [CrossRef]
35. Shen, P.; Lin, W.; Deng, X.; Ba, X.; Han, L.; Chen, Z.; Qin, K.; Huang, Y.; Tu, S. Potential Implications of Quercetin in Autoimmune Diseases. *Front. Immunol.* **2021**, *12*, 689044. [CrossRef]
36. Hosseini, A.; Razavi, B.M.; Banach, M.; Hosseinzadeh, H. Quercetin and Metabolic Syndrome: A Review. *Phytother. Res.* **2021**, *35*, 5352–5364. [CrossRef]
37. Reyes-Farias, M.; Carrasco-Pozo, C. The Anti-Cancer Effect of Quercetin: Molecular Implications in Cancer Metabolism. *Int. J. Mol. Sci.* **2019**, *20*, 3177. [CrossRef]
38. Mlcek, J.; Jurikova, T.; Skrovankova, S.; Sochor, J. Quercetin and Its Anti-Allergic Immune Response. *Molecules* **2016**, *21*, 623. [CrossRef]
39. Marunaka, Y.; Marunaka, R.; Sun, H.; Yamamoto, T.; Kanamura, N.; Inui, T.; Taruno, A. Actions of Quercetin, a Polyphenol, on Blood Pressure. *Molecules* **2017**, *22*, 209. [CrossRef]
40. Di Petrillo, A.; Orrù, G.; Fais, A.; Fantini, M.C. Quercetin and Its Derivates as Antiviral Potentials: A Comprehensive Review. *Phytother. Res.* **2022**, *36*, 266–278. [CrossRef]
41. Khan, H.; Ullah, H.; Aschner, M.; Cheang, W.S.; Akkol, E.K. Neuroprotective Effects of Quercetin in Alzheimer's Disease. *Biomolecules* **2019**, *10*, 59. [CrossRef] [PubMed]
42. Li, C.; Schluesener, H. Health-Promoting Effects of the Citrus Flavanone Hesperidin. *Crit. Rev. Food Sci. Nutr.* **2017**, *57*, 613–631. [CrossRef] [PubMed]
43. Xiong, H.; Wang, J.; Ran, Q.; Lou, G.; Peng, C.; Gan, Q.; Hu, J.; Sun, J.; Yao, R.; Huang, Q. Hesperidin: A Therapeutic Agent for Obesity. *Drug Des. Devel. Ther.* **2019**, *13*, 3855–3866. [CrossRef]
44. Man, M.-Q.; Yang, B.; Elias, P.M. Benefits of Hesperidin for Cutaneous Functions. Evid. Based. Complement. *Alternat. Med.* **2019**, *2019*, 2676307. [CrossRef]
45. Parhiz, H.; Roohbakhsh, A.; Soltani, F.; Rezaee, R.; Iranshahi, M. Antioxidant and Anti-Inflammatory Properties of the Citrus Flavonoids Hesperidin and Hesperetin: An Updated Review of Their Molecular Mechanisms and Experimental Models: Hesperidin and Hesperetin as Antioxidant and Anti-Inflammatory Agents. *Phytother. Res.* **2015**, *29*, 323–331. [CrossRef] [PubMed]
46. Sohel, M.; Sultana, H.; Sultana, T.; Al Amin, M.; Aktar, S.; Ali, M.C.; Rahim, Z.B.; Hossain, M.A.; Al Mamun, A.; Amin, M.N.; et al. Chemotherapeutic Potential of Hesperetin for Cancer Treatment, with Mechanistic Insights: A Comprehensive Review. *Heliyon* **2022**, *8*, e08815. [CrossRef]
47. Neba Ambe, G.N.N.; Breda, C.; Bhambra, A.S.; Arroo, R.R.J. Effect of the Citrus Flavone Nobiletin on Circadian Rhythms and Metabolic Syndrome. *Molecules* **2022**, *27*, 7727. [CrossRef]
48. Nakajima, A.; Ohizumi, Y. Potential Benefits of Nobiletin, A Citrus Flavonoid, against Alzheimer's Disease and Parkinson's Disease. *Int. J. Mol. Sci.* **2019**, *20*, 3380. [CrossRef]
49. Huang, J.; Chang, Z.; Lu, Q.; Chen, X.; Najafi, M. Nobiletin as an Inducer of Programmed Cell Death in Cancer: A Review. *Apoptosis* **2022**, *27*, 297–310. [CrossRef]
50. Islam, A.; Islam, M.S.; Rahman, M.K.; Uddin, M.N.; Akanda, M.R. The Pharmacological and Biological Roles of Eriodictyol. *Arch. Pharm. Res.* **2020**, *43*, 582–592. [CrossRef]
51. Deng, Z.; Hassan, S.; Rafiq, M.; Li, H.; He, Y.; Cai, Y.; Kang, X.; Liu, Z.; Yan, T. Pharmacological Activity of Eriodictyol: The Major Natural Polyphenolic Flavanone. *Evid. Based. Complement. Alternat. Med.* **2020**, *2020*, 6681352. [CrossRef] [PubMed]
52. Quetglas-Llabrés, M.M.; Quispe, C.; Herrera-Bravo, J.; Catarino, M.D.; Pereira, O.R.; Cardoso, S.M.; Dua, K.; Chellappan, D.K.; Pabreja, K.; Satija, S.; et al. Pharmacological Properties of Bergapten: Mechanistic and Therapeutic Aspects. *Oxid. Med. Cell. Longev.* **2022**, *2022*, 8615242. [CrossRef] [PubMed]
53. Liang, Y.; Xie, L.; Liu, K.; Cao, Y.; Dai, X.; Wang, X.; Lu, J.; Zhang, X.; Li, X. Bergapten: A Review of Its Pharmacology, Pharmacokinetics, and Toxicity. *Phytother. Res.* **2021**, *35*, 6131–6147. [CrossRef] [PubMed]
54. Ashrafizadeh, M.; Ahmadi, Z.; Mohammadinejad, R.; Ghasemipour Afshar, E. Tangeretin: A Mechanistic Review of Its Pharmacological and Therapeutic Effects. *J. Basic Clin. Physiol. Pharmacol.* **2020**, *31*. [CrossRef] [PubMed]
55. Raza, W.; Luqman, S.; Meena, A. Prospects of Tangeretin as a Modulator of Cancer Targets/Pathways. *Pharmacol. Res.* **2020**, *161*, 105202. [CrossRef] [PubMed]
56. Tayarani-Najaran, Z.; Tayarani-Najaran, N.; Eghbali, S. A Review of Auraptene as an Anticancer Agent. *Front. Pharmacol.* **2021**, *12*, 698352. [CrossRef]
57. Bibak, B.; Shakeri, F.; Barreto, G.E.; Keshavarzi, Z.; Sathyapalan, T.; Sahebkar, A. A Review of the Pharmacological and Therapeutic Effects of Auraptene. *Biofactors* **2019**, *45*, 867–879. [CrossRef]
58. Derosa, G.; Maffioli, P.; Sahebkar, A. Auraptene and Its Role in Chronic Diseases. *Adv. Exp. Med. Biol.* **2016**, *929*, 399–407. [CrossRef]
59. Fan, S.; Zhang, C.; Luo, T.; Wang, J.; Tang, Y.; Chen, Z.; Yu, L. Limonin: A Review of Its Pharmacology, Toxicity, and Pharmacokinetics. *Molecules* **2019**, *24*, 3679. [CrossRef]

60. Zeng, W.; Jin, L.; Zhang, F.; Zhang, C.; Liang, W. Naringenin as a Potential Immunomodulator in Therapeutics. *Pharmacol. Res.* **2018**, *135*, 122–126. [CrossRef]
61. Goyal, A.; Verma, A.; Dubey, N.; Raghav, J.; Agrawal, A. Naringenin: A Prospective Therapeutic Agent for Alzheimer's and Parkinson's Disease. *J. Food Biochem.* **2022**, *46*, e14415. [CrossRef] [PubMed]
62. Motallebi, M.; Bhia, M.; Rajani, H.F.; Bhia, I.; Tabarraei, H.; Mohammadkhani, N.; Pereira-Silva, M.; Kasaii, M.S.; Nouri-Majd, S.; Mueller, A.-L.; et al. Naringenin: A Potential Flavonoid Phytochemical for Cancer Therapy. *Life Sci.* **2022**, *305*, 120752. [CrossRef] [PubMed]
63. Heidary Moghaddam, R.; Samimi, Z.; Moradi, S.Z.; Little, P.J.; Xu, S.; Farzaei, M.H. Naringenin and Naringin in Cardiovascular Disease Prevention: A Preclinical Review. *Eur. J. Pharmacol.* **2020**, *887*, 173535. [CrossRef] [PubMed]
64. Du, Y.; Ma, J.; Fan, Y.; Wang, X.; Zheng, S.; Feng, J.; Li, J.; Fan, Z.; Li, G.; Ye, Q. Naringenin: A Promising Therapeutic Agent against Organ Fibrosis. *Oxid. Med. Cell. Longev.* **2021**, *2021*, 1210675. [CrossRef]
65. Hernández-Aquino, E.; Muriel, P. Beneficial Effects of Naringenin in Liver Diseases: Molecular Mechanisms. *World J. Gastroenterol.* **2018**, *24*, 1679–1707. [CrossRef]
66. Alam, M.A.; Subhan, N.; Rahman, M.M.; Uddin, S.J.; Reza, H.M.; Sarker, S.D. Effect of Citrus Flavonoids, Naringin and Naringenin, on Metabolic Syndrome and Their Mechanisms of Action. *Adv. Nutr.* **2014**, *5*, 404–417. [CrossRef]
67. Chen, R.; Qi, Q.-L.; Wang, M.-T.; Li, Q.-Y. Therapeutic Potential of Naringin: An Overview. *Pharm. Biol.* **2016**, *54*, 3203–3210. [CrossRef]
68. Ghanbari-Movahed, M.; Jackson, G.; Farzaei, M.H.; Bishayee, A. A Systematic Review of the Preventive and Therapeutic Effects of Naringin against Human Malignancies. *Front. Pharmacol.* **2021**, *12*, 639840. [CrossRef]
69. Singh, B.; Singh, J.P.; Kaur, A.; Singh, N. Phenolic Composition, Antioxidant Potential and Health Benefits of Citrus Peel. *Food Res. Int.* **2020**, *132*, 109114. [CrossRef]
70. Liu, S.; Lou, Y.; Li, Y.; Zhang, J.; Li, P.; Yang, B.; Gu, Q. Review of Phytochemical and Nutritional Characteristics and Food Applications of *Citrus* L. Fruits. *Front. Nutr.* **2022**, *9*, 968604. [CrossRef]
71. Addi, M.; Elbouzidi, A.; Abid, M.; Tungmunnithum, D.; Elamrani, A.; Hano, C. An Overview of Bioactive Flavonoids from Citrus Fruits. *Appl. Sci.* **2021**, *12*, 29. [CrossRef]
72. Rehman, M.F.; Batool, A.I.; Qadir, R.; Aslam, M. Hesperidin and Naringenin. In *A Centum of Valuable Plant Bioactives*; Elsevier: Amsterdam, The Netherlands, 2021; pp. 403–444.
73. Joshi, R.; Kulkarni, Y.A.; Wairkar, S. Pharmacokinetic, Pharmacodynamic and Formulations Aspects of Naringenin: An Update. *Life Sci.* **2018**, *215*, 43–56. [CrossRef] [PubMed]
74. Zhao, C.; Wang, F.; Lian, Y.; Xiao, H.; Zheng, J. Biosynthesis of Citrus Flavonoids and Their Health Effects. *Crit. Rev. Food Sci. Nutr.* **2020**, *60*, 566–583. [CrossRef] [PubMed]
75. Pyrzynska, K. Hesperidin: A Review on Extraction Methods, Stability and Biological Activities. *Nutrients* **2022**, *14*, 2387. [CrossRef]
76. Lucas-Abellán, C.; Pérez-Abril, M.; Castillo, J.; Serrano, A.; Mercader, M.T.; Fortea, M.I.; Gabaldón, J.A.; Núñez-Delicado, E. Effect of Temperature, PH, β- and HP-β-Cds on the Solubility and Stability of Flavanones: Naringenin and Hesperetin. Lebenson. *Wiss. Technol.* **2019**, *108*, 233–239. [CrossRef]
77. Venkateswara Rao, P.; Kiran, S.; Rohini, P.; Bhagyasree, P. Flavonoid: A Review on Naringenin. *J. Pharmacogn. Phytochem.* **2017**, *6*, 27.
78. Aalikhani, M.; Safdari, Y.; Jahanshahi, M.; Alikhani, M.; Khalili, M. Comparison between Hesperidin, Coumarin, and Deferoxamine Iron Chelation and Antioxidant Activity against Excessive Iron in the Iron Overloaded Mice. *Front. Neurosci.* **2021**, *15*, 811080. [CrossRef]
79. Tejada, S.; Pinya, S.; Martorell, M.; Capó, X.; Tur, J.A.; Pons, A.; Sureda, A. Potential Anti-Inflammatory Effects of Hesperidin from the Genus Citrus. *Curr. Med. Chem.* **2018**, *25*, 4929–4945. [CrossRef]
80. Pla-Pagà, L.; Companys, J.; Calderón-Pérez, L.; Llauradó, E.; Solà, R.; Valls, R.M.; Pedret, A. Effects of Hesperidin Consumption on Cardiovascular Risk Biomarkers: A Systematic Review of Animal Studies and Human Randomized Clinical Trials. *Nutr. Rev.* **2019**, *77*, 845–864. [CrossRef]
81. Albuquerque de Oliveira Mendes, L.; Ponciano, C.S.; Depieri Cataneo, A.H.; Wowk, P.F.; Bordignon, J.; Silva, H.; Vieira de Almeida, M.; Ávila, E.P. The Anti-Zika Virus and Anti-Tumoral Activity of the Citrus Flavanone Lipophilic Naringenin-Based Compounds. *Chem. Biol. Interact.* **2020**, *331*, 109218. [CrossRef]
82. Hosseinzadeh, E.; Hassanzadeh, A.; Marofi, F.; Alivand, M.R.; Solali, S. Flavonoid-Based Cancer Therapy: An Updated Review. *Anticancer Agents Med. Chem.* **2020**, *20*, 1398–1414. [CrossRef] [PubMed]
83. Martín, J.F.; Liras, P. Comparative Molecular Mechanisms of Biosynthesis of Naringenin and Related Chalcones in Actinobacteria and Plants: Relevance for the Obtention of Potent Bioactive Metabolites. *Antibiotics* **2022**, *11*, 82. [CrossRef] [PubMed]
84. Sordon, S.; Popłoński, J.; Milczarek, M.; Stachowicz, M.; Tronina, T.; Kucharska, A.Z.; Wietrzyk, J.; Huszcza, E. Structure-Antioxidant-Antiproliferative Activity Relationships of Natural C7 and C7-C8 Hydroxylated Flavones and Flavanones. *Antioxidants* **2019**, *8*, 210. [CrossRef] [PubMed]
85. Zhang, L.; Song, L.; Zhang, P.; Liu, T.; Zhou, L.; Yang, G.; Lin, R.; Zhang, J. Solubilities of Naringin and Naringenin in Different Solvents and Dissociation Constants of Naringenin. *J. Chem. Eng. Data* **2015**, *60*, 932–940. [CrossRef]

86. Sangpheak, W.; Kicuntod, J.; Schuster, R.; Rungrotmongkol, T.; Wolschann, P.; Kungwan, N.; Viernstein, H.; Mueller, M.; Pongsawasdi, P. Physical Properties and Biological Activities of Hesperetin and Naringenin in Complex with Methylated β-Cyclodextrin. *Beilstein J. Org. Chem.* **2015**, *11*, 2763–2773. [CrossRef] [PubMed]
87. Ashrafi, N.; Shareghi, B.; Farhadian, S.; Hosseini-Koupaei, M. A Comparative Study of the Interaction of Naringenin with Lysozyme by Multi-Spectroscopic Methods, Activity Comparisons, and Molecular Modeling Procedures. *Spectrochim. Acta A Mol. Biomol. Spectrosc.* **2022**, *271*, 120931. [CrossRef] [PubMed]
88. Li, X.; Peng, Y.; Liu, H.; Xu, Y.; Wang, X.; Zhang, C.; Ma, X. Comparative Studies on the Interaction of Nine Flavonoids with Trypsin. Spectrochim. *Acta A Mol. Biomol. Spectrosc.* **2020**, *238*, 118440. [CrossRef]
89. Malik, N.; Dhiman, P.; Khatkar, A. Mechanistic Approach towards Interaction of Newly Synthesized Hesperidin Derivatives against Xanthine Oxidase. *Int. J. Biol. Macromol.* **2019**, *135*, 864–876. [CrossRef]
90. Choi, S.; Yu, S.; Lee, J.; Kim, W. Effects of Neohesperidin Dihydrochalcone (NHDC) on Oxidative Phosphorylation, Cytokine Production, and Lipid Deposition. *Foods* **2021**, *10*, 1408. [CrossRef]
91. Zhang, F.-X.; Yuan, Y.-L.-L.; Cui, S.-S.; Li, M.; Tan, X.; Qiu, Z.-C.; Li, R.-M. Dissection of the Potential Pharmacological Function of Neohesperidin Dihydrochalcone—A Food Additive—By in Vivo Substances Profiling and Network Pharmacology. *Food Funct.* **2021**, *12*, 4325–4336. [CrossRef]
92. Yang, X.; Wang, T.; Guo, J.; Sun, M.; Wong, M.W.; Huang, D. Dietary Flavonoids Scavenge Hypochlorous Acid via Chlorination on A- and C-Rings as Primary Reaction Sites: Structure and Reactivity Relationship. *J. Agric. Food Chem.* **2019**, *67*, 4346–4354. [CrossRef]
93. Harbeck, N.; Penault-Llorca, F.; Cortes, J.; Gnant, M.; Houssami, N.; Poortmans, P.; Ruddy, K.; Tsang, J.; Cardoso, F. Breast Cancer. *Nat. Rev. Dis. Primers* **2019**, *5*, 66. [CrossRef] [PubMed]
94. Ayob, Z.; Mohd Bohari, S.P.; Abd Samad, A.; Jamil, S. Cytotoxic Activities against Breast Cancer Cells of Local Justicia Gendarussa Crude Extracts. *Evid. Based. Complement. Alternat. Med.* **2014**, *2014*, 732980. [CrossRef]
95. Fan, X.; Bai, J.; Zhao, S.; Hu, M.; Sun, Y.; Wang, B.; Ji, M.; Jin, J.; Wang, X.; Hu, J.; et al. Evaluation of Inhibitory Effects of Flavonoids on Breast Cancer Resistance Protein (BCRP): From Library Screening to Biological Evaluation to Structure-Activity Relationship. *Toxicol. In Vitro* **2019**, *61*, 104642. [CrossRef]
96. Ke, J.-Y.; Banh, T.; Hsiao, Y.-H.; Cole, R.M.; Straka, S.R.; Yee, L.D.; Belury, M.A. Citrus Flavonoid Naringenin Reduces Mammary Tumor Cell Viability, Adipose Mass, and Adipose Inflammation in Obese Ovariectomized Mice. *Mol. Nutr. Food Res.* **2017**, *61*, 1600934. [CrossRef] [PubMed]
97. Al-Rikabi, R.; Al-Shmgani, H.; Dewir, Y.H.; El-Hendawy, S. In Vivo and in Vitro Evaluation of the Protective Effects of Hesperidin in Lipopolysaccharide-Induced Inflammation and Cytotoxicity of Cell. *Molecules* **2020**, *25*, 478. [CrossRef] [PubMed]
98. Feng, X.-L.; Zhan, X.-X.; Zuo, L.-S.-Y.; Mo, X.-F.; Zhang, X.; Liu, K.-Y.; Li, L.; Zhang, C.-X. Associations between Serum Concentration of Flavonoids and Breast Cancer Risk among Chinese Women. *Eur. J. Nutr.* **2021**, *60*, 1347–1362. [CrossRef]
99. Vo, A.T.; Millis, R.M. Epigenetics and Breast Cancers. *Obstet. Gynecol. Int.* **2012**, *2012*, 602720. [CrossRef] [PubMed]
100. Khan, H.; Belwal, T.; Efferth, T.; Farooqi, A.A.; Sanches-Silva, A.; Vacca, R.A.; Nabavi, S.F.; Khan, F.; Prasad Devkota, H.; Barreca, D.; et al. Targeting Epigenetics in Cancer: Therapeutic Potential of Flavonoids. *Crit. Rev. Food Sci. Nutr.* **2021**, *61*, 1616–1639. [CrossRef]
101. Jiang, W.; Xia, T.; Liu, C.; Li, J.; Zhang, W.; Sun, C. Remodeling the Epigenetic Landscape of Cancer-Application Potential of Flavonoids in the Prevention and Treatment of Cancer. *Front. Oncol.* **2021**, *11*, 705903. [CrossRef]
102. Lee, H.-S.; Herceg, Z. The Epigenome and Cancer Prevention: A Complex Story of Dietary Supplementation. *Cancer Lett.* **2014**, *342*, 275–284. [CrossRef] [PubMed]
103. Pan, M.-H.; Chiou, Y.-S.; Chen, L.-H.; Ho, C.-T. Breast Cancer Chemoprevention by Dietary Natural Phenolic Compounds: Specific Epigenetic Related Molecular Targets. *Mol. Nutr. Food Res.* **2015**, *59*, 21–35. [CrossRef] [PubMed]
104. Saha Roy, S.; Vadlamudi, R.K. Role of Estrogen Receptor Signaling in Breast Cancer Metastasis. *Int. J. Breast Cancer* **2012**, *2012*, 654698. [CrossRef] [PubMed]
105. Hervouet, E.; Cartron, P.-F.; Jouvenot, M.; Delage-Mourroux, R. Epigenetic Regulation of Estrogen Signaling in Breast Cancer. *Epigenetics* **2013**, *8*, 237–245. [CrossRef] [PubMed]
106. Garcia-Martinez, L.; Zhang, Y.; Nakata, Y.; Chan, H.L.; Morey, L. Epigenetic Mechanisms in Breast Cancer Therapy and Resistance. *Nat. Commun.* **2021**, *12*, 1786. [CrossRef]
107. Yuan, L.; Cai, Y.; Zhang, L.; Liu, S.; Li, P.; Li, X. Promoting Apoptosis, a Promising Way to Treat Breast Cancer with Natural Products: A Comprehensive Review. *Front. Pharmacol.* **2021**, *12*, 801662. [CrossRef]
108. Xu, Z.; Huang, B.; Liu, J.; Wu, X.; Luo, N.; Wang, X.; Zheng, X.; Pan, X. Combinatorial Anti-Proliferative Effects of Tamoxifen and Naringenin: The Role of Four Estrogen Receptor Subtypes. *Toxicology* **2018**, *410*, 231–246. [CrossRef]
109. Hatkevich, T.; Ramos, J.; Santos-Sanchez, I.; Patel, Y.M. A Naringenin-Tamoxifen Combination Impairs Cell Proliferation and Survival of MCF-7 Breast Cancer Cells. *Exp. Cell Res.* **2014**, *327*, 331–339. [CrossRef]
110. Eanes, L.; Patel, Y.M. Inhibition of the MAPK Pathway Alone Is Insufficient to Account for All of the Cytotoxic Effects of Naringenin in MCF-7 Breast Cancer Cells. *Biochim. Open* **2016**, *3*, 64–71. [CrossRef]
111. van Duursen, M.B.M. Modulation of Estrogen Synthesis and Metabolism by Phytoestrogensin Vitroand the Implications for Women's Health. *Toxicol. Res.* **2017**, *6*, 772–794. [CrossRef]

112. Hermawan, A.; Ikawati, M.; Jenie, R.I.; Khumaira, A.; Putri, H.; Nurhayati, I.P.; Angraini, S.M.; Muflikhasari, H.A. Identification of Potential Therapeutic Target of Naringenin in Breast Cancer Stem Cells Inhibition by Bioinformatics and in Vitro Studies. *Saudi Pharm. J.* **2021**, *29*, 12–26. [CrossRef] [PubMed]
113. Pang, X.; Fu, W.; Wang, J.; Kang, D.; Xu, L.; Zhao, Y.; Liu, A.-L.; Du, G.-H. Identification of Estrogen Receptor α Antagonists from Natural Products via in Vitro and in Silico Approaches. *Oxid. Med. Cell. Longev.* **2018**, *2018*, 1–11. [CrossRef]
114. Kim, S.; Park, T.I. Naringenin: A Partial Agonist on Estrogen Receptor in T47D-KBluc Breast Cancer Cells. *Int. J. Clin. Exp. Med.* **2013**, *6*, 890–899. [PubMed]
115. Bulzomi, P.; Bolli, A.; Galluzzo, P.; Acconcia, F.; Ascenzi, P.; Marino, M. The Naringenin-Induced Proapoptotic Effect in Breast Cancer Cell Lines Holds out against a High Bisphenol a Background. *IUBMB Life* **2012**, *64*, 690–696. [CrossRef] [PubMed]
116. Hsu, P.-H.; Chen, W.-H.; Juan-Lu, C.; Hsieh, S.-C.; Lin, S.-C.; Mai, R.-T.; Chen, S.-Y. Hesperidin and Chlorogenic Acid Synergistically Inhibit the Growth of Breast Cancer Cells via Estrogen Receptor/Mitochondrial Pathway. *Life* **2021**, *11*, 950. [CrossRef] [PubMed]
117. Taghizadeh, M.S.; Niazi, A.; Moghadam, A.; Afsharifar, A. Experimental, Molecular Docking and Molecular Dynamic Studies of Natural Products Targeting Overexpressed Receptors in Breast Cancer. *PLoS ONE* **2022**, *17*, e0267961. [CrossRef] [PubMed]
118. Strasser, A.; Vaux, D.L. Cell Death in the Origin and Treatment of Cancer. *Mol. Cell* **2020**, *78*, 1045–1054. [CrossRef]
119. Hossain, R.; Jain, D.; Khan, R.A.; Islam, M.T.; Mubarak, M.S.; Saikat, A.S.M. Natural-Derived Molecules as a Potential Adjuvant in Chemotherapy: Normal Cell Protectors and Cancer Cell Sensitizers. *Anticancer. Agents Med. Chem.* **2022**, *22*, 836–850. [CrossRef]
120. Hashem, S.; Ali, T.A.; Akhtar, S.; Nisar, S.; Sageena, G.; Ali, S.; Al-Mannai, S.; Therachiyil, L.; Mir, R.; Elfaki, I.; et al. Targeting Cancer Signaling Pathways by Natural Products: Exploring Promising Anti-Cancer Agents. *Biomed. Pharmacother.* **2022**, *150*, 113054. [CrossRef]
121. Roohbakhsh, A.; Parhiz, H.; Soltani, F.; Rezaee, R.; Iranshahi, M. Molecular Mechanisms behind the Biological Effects of Hesperidin and Hesperetin for the Prevention of Cancer and Cardiovascular Diseases. *Life Sci.* **2015**, *124*, 64–74. [CrossRef]
122. Mir, I.A.; Tiku, A.B. Chemopreventive and Therapeutic Potential of "Naringenin", a Flavanone Present in Citrus Fruits. *Nutr. Cancer* **2015**, *67*, 27–42. [CrossRef] [PubMed]
123. Zhao, Z.; Jin, G.; Ge, Y.; Guo, Z. Naringenin Inhibits Migration of Breast Cancer Cells via Inflammatory and Apoptosis Cell Signaling Pathways. *Inflammopharmacology* **2019**, *27*, 1021–1036. [CrossRef] [PubMed]
124. Zaim, Ö.; Doğanlar, O.; Zreigh, M.M.; Doğanlar, Z.B.; Özcan, H. Synthesis, Cancer-Selective Antiproliferative and Apoptotic Effects of Some (±)-Naringenin Cycloaminoethyl Derivatives. *Chem. Biodivers.* **2018**, *15*, e1800016. [CrossRef] [PubMed]
125. Qi, Z.; Kong, S.; Zhao, S.; Tang, Q. Naringenin Inhibits Human Breast Cancer Cells (MDA-MB-231) by Inducing Programmed Cell Death, Caspase Stimulation, G2/M Phase Cell Cycle Arrest and Suppresses Cancer Metastasis. *Cell. Mol. Biol.* **2021**, *67*, 8–13. [CrossRef]
126. Wang, R.; Wang, J.; Dong, T.; Shen, J.; Gao, X.; Zhou, J. Naringenin Has a Chemoprotective Effect in MDA-MB-231 Breast Cancer Cells via Inhibition of Caspase-3 and -9 Activities. *Oncol. Lett.* **2018**, *17*, 1217–1222. [CrossRef]
127. Yousuf, M.; Shamsi, A.; Khan, S.; Khan, P.; Shahwan, M.; Elasbali, A.M.; Haque, Q.M.R.; Hassan, M.I. Naringenin as a Potential Inhibitor of Human Cyclin-Dependent Kinase 6: Molecular and Structural Insights into Anti-Cancer Therapeutics. *Int. J. Biol. Macromol.* **2022**, *213*, 944–954. [CrossRef]
128. Pateliya, B.; Burade, V.; Goswami, S. Enhanced Antitumor Activity of Doxorubicin by Naringenin and Metformin in Breast Carcinoma: An Experimental Study. *Naunyn-Schmiedeberg's Arch. Pharmacol.* **2021**, *394*, 1949–1961. [CrossRef]
129. Filho, J.C.C.; Sarria, A.L.F.; Becceneri, A.B.; Fuzer, A.M.; Batalhão, J.R.; da Silva, C.M.P.; Carlos, R.M.; Vieira, P.C.; Fernandes, J.B.; Cominetti, M.R. Copper (II) and 2,2′-Bipyridine Complexation Improves Chemopreventive Effects of Naringenin against Breast Tumor Cells. *PLoS ONE* **2014**, *9*, e107058. [CrossRef]
130. Ajji, P.K.; Walder, K.; Puri, M. Combination of Balsamin and Flavonoids Induce Apoptotic Effects in Liver and Breast Cancer Cells. *Front. Pharmacol.* **2020**, *11*, 574496. [CrossRef]
131. Fazary, A.E.; Alfaifi, M.Y.; Elbehairi, S.E.I.; Amer, M.E.; Nasr, M.S.M.; Abuamara, T.M.M.; Badr, D.A.; Ju, Y.-H.; Mohamed, A.F. Bioactivity Studies of Hesperidin and XAV939. *ACS Omega* **2021**, *6*, 20042–20052. [CrossRef]
132. Kabała-Dzik, A.; Rzepecka-Stojko, A.; Kubina, R.; Iriti, M.; Wojtyczka, R.D.; Buszman, E.; Stojko, J. Flavonoids, Bioactive Components of Propolis, Exhibit Cytotoxic Activity and Induce Cell Cycle Arrest and Apoptosis in Human Breast Cancer Cells MDA-MB-231 and MCF-7—A Comparative Study. *Cell. Mol. Biol.* **2018**, *64*, 1–10. [CrossRef] [PubMed]
133. Magura, J.; Moodley, R.; Mackraj, I. The Effect of Hesperidin and Luteolin Isolated from Eriocephalus Africanus on Apoptosis, Cell Cycle and MiRNA Expression in MCF-7. *J. Biomol. Struct. Dyn.* **2022**, *40*, 1791–1800. [CrossRef] [PubMed]
134. Robinson, K.; Tiriveedhi, V. Perplexing Role of P-Glycoprotein in Tumor Microenvironment. *Front. Oncol.* **2020**, *10*, 265. [CrossRef] [PubMed]
135. Febriansah, R.; Dyaningtyas, D.P.; Nurulita, N.A.; Meiyanto, E.; Nugroho, A.E. Hesperidin as a Preventive Resistance Agent in MCF-7 Breast Cancer Cells Line Resistance to Doxorubicin. *Asian Pac. J. Trop. Biomed.* **2014**, *4*, 228–233. [CrossRef]
136. Korga-Plewko, A.; Michalczyk, M.; Adamczuk, G.; Humeniuk, E.; Ostrowska-Lesko, M.; Jozefczyk, A.; Iwan, M.; Wojcik, M.; Dudka, J. Apigenin and Hesperidin Downregulate DNA Repair Genes in MCF-7 Breast Cancer Cells and Augment Doxorubicin Toxicity. *Molecules* **2020**, *25*, 4421. [CrossRef]

137. Hermawan, A.; Khumaira, A.; Ikawati, M.; Putri, H.; Jenie, R.I.; Angraini, S.M.; Muflikhasari, H.A. Identification of Key Genes of Hesperidin in Inhibition of Breast Cancer Stem Cells by Functional Network Analysis. *Comput. Biol. Chem.* **2021**, *90*, 107427. [CrossRef]
138. Patel, P.; Shah, J. Protective Effects of Hesperidin through Attenuation of Ki67 Expression against DMBA-Induced Breast Cancer in Female Rats. *Life Sci.* **2021**, *285*, 119957. [CrossRef]
139. Omar, H.A.; Mohamed, W.R.; Arafa, E.-S.A.; Shehata, B.A.; El Sherbiny, G.A.; Arab, H.H.; Elgendy, A.N.A.M. Hesperidin Alleviates Cisplatin-Induced Hepatotoxicity in Rats without Inhibiting Its Antitumor Activity. *Pharmacol. Rep.* **2016**, *68*, 349–356. [CrossRef]
140. Riggio, A.I.; Varley, K.E.; Welm, A.L. The Lingering Mysteries of Metastatic Recurrence in Breast Cancer. *Br. J. Cancer* **2021**, *124*, 13–26. [CrossRef]
141. Farooqi, A.A.; Tahir, F.; Fakhar, M.; Butt, G.; Colombo Pimentel, T.; Wu, N.; Yulaevna, I.M.; Attar, R. Antimetastatic Effects of Citrus-Derived Bioactive Ingredients: Mechanistic Insights. *Cell. Mol. Biol.* **2021**, *67*, 178–186. [CrossRef]
142. Casey, S.C.; Amedei, A.; Aquilano, K.; Azmi, A.S.; Benencia, F.; Bhakta, D.; Bilsland, A.E.; Boosani, C.S.; Chen, S.; Ciriolo, M.R.; et al. Cancer Prevention and Therapy through the Modulation of the Tumor Microenvironment. *Semin. Cancer Biol.* **2015**, *35*, S199–S223. [CrossRef] [PubMed]
143. Noori, S.; Rezaei Tavirani, M.; Deravi, N.; Mahboobi Rabbani, M.I.; Zarghi, A. Naringenin Enhances the Anti-Cancer Effect of Cyclophosphamide against MDA-MB-231 Breast Cancer Cells via Targeting the STAT3 Signaling Pathway. *Iran. J. Pharm. Res.* **2020**, *19*, 122–133. [CrossRef] [PubMed]
144. Zhang, J.; Wang, N.; Zheng, Y.; Yang, B.; Wang, S.; Wang, X.; Pan, B.; Wang, Z. Naringenin in Si-Ni-San Formula Inhibits Chronic Psychological Stress-Induced Breast Cancer Growth and Metastasis by Modulating Estrogen Metabolism through FXR/EST Pathway. *J. Adv. Res.* **2022**. [CrossRef] [PubMed]
145. Daroqui, M.C.; Vazquez, P.; Bal de Kier Joffé, E.; Bakin, A.V.; Puricelli, L.I. TGF-β Autocrine Pathway and MAPK Signaling Promote Cell Invasiveness and in Vivo Mammary Adenocarcinoma Tumor Progression. *Oncol. Rep.* **2012**, *28*, 567–575. [CrossRef] [PubMed]
146. Goto, N.; Hiyoshi, H.; Ito, I.; Iida, K.; Nakajima, Y.; Nagasawa, K.; Yanagisawa, J. Identification of a Novel Compound That Suppresses Breast Cancer Invasiveness by Inhibiting Transforming Growth Factor-β Signaling via Estrogen Receptor α. *J. Cancer* **2014**, *5*, 336–343. [CrossRef] [PubMed]
147. Zhang, F.; Dong, W.; Zeng, W.; Zhang, L.; Zhang, C.; Qiu, Y.; Wang, L.; Yin, X.; Zhang, C.; Liang, W. Naringenin Prevents TGF-B1 Secretion from Breast Cancer and Suppresses Pulmonary Metastasis by In-Hibiting PKC Activation. *Breast Cancer Res.* **2016**, *18*, 1–16. [CrossRef] [PubMed]
148. Pang, S.; Jia, M.; Gao, J.; Liu, X.; Guo, W.; Zhang, H. Effects of Dietary Patterns Combined with Dietary Phytochemicals on Breast Cancer Metastasis. *Life Sci.* **2021**, *264*, 118720. [CrossRef] [PubMed]
149. Alsuliman, A.; Colak, D.; Al-Harazi, O.; Fitwi, H.; Tulbah, A.; Al-Tweigeri, T.; Al-Alwan, M.; Ghebeh, H. Bidirectional Crosstalk between PD-L1 Expression and Epithelial to Mesenchymal Transition: Significance in Claudin-Low Breast Cancer Cells. *Mol. Cancer* **2015**, *14*, 149. [CrossRef]
150. Kongtawelert, P.; Wudtiwai, B.; Shwe, T.H.; Pothacharoen, P.; Phitak, T. Inhibitory Effect of Hesperidin on the Expression of Programmed Death Ligand (PD-L1) in Breast Cancer. *Molecules* **2020**, *25*, 252. [CrossRef]
151. Amalina, N.; Nurhayati, I.P.; Meiyanto, E. Doxorubicin Induces Lamellipodia Formation and Cell Migration. *Indones. J. Cancer Chemoprevention* **2017**, *8*, 61. [CrossRef]
152. Suzery, M.; Cahyono, B.; Amalina, N.D. Citrus Sinensis (L) Peels Extract Inhibits Metastasis of Breast Cancer Cells by Targeting the Downregulation Matrix Metalloproteinases-9. *Open Access Maced. J. Med. Sci.* **2021**, *9*, 464–469. [CrossRef]
153. Barani, M.; Bilal, M.; Sabir, F.; Rahdar, A.; Kyzas, G.Z. Nanotechnology in Ovarian Cancer: Diagnosis and Treatment. *Life Sci.* **2021**, *266*, 118914. [CrossRef] [PubMed]
154. Aiello, P.; Consalvi, S.; Poce, G.; Raguzzini, A.; Toti, E.; Palmery, M.; Biava, M.; Bernardi, M.; Kamal, M.A.; Perry, G.; et al. Dietary Flavonoids: Nano Delivery and Nanoparticles for Cancer Therapy. *Semin. Cancer Biol.* **2021**, *69*, 150–165. [CrossRef]
155. Liu, C.H.; Grodzinski, P. Nanotechnology for Cancer Imaging: Advances, Challenges, and Clinical Op-Portunities. *Radiol. Imaging Cancer* **2021**, *3*, e200052. [CrossRef] [PubMed]
156. Khan, H.; Ullah, H.; Martorell, M.; Valdes, S.E.; Belwal, T.; Tejada, S.; Sureda, A.; Kamal, M.A. Flavonoids Nanoparticles in Cancer: Treatment, Prevention and Clinical Prospects. *Semin. Cancer Biol.* **2021**, *69*, 200–211. [CrossRef] [PubMed]
157. Bhia, M.; Motallebi, M.; Abadi, B.; Zarepour, A.; Pereira-Silva, M.; Saremnejad, F.; Santos, A.C.; Zarrabi, A.; Melero, A.; Jafari, S.M.; et al. Naringenin Nano-Delivery Systems and Their Therapeutic Applications. *Pharmaceutics* **2021**, *13*, 291. [CrossRef]
158. Ali, S.H.; Sulaiman, G.M.; Al-Halbosiy, M.M.F.; Jabir, M.S.; Hameed, A.H. Fabrication of Hesperidin Nanoparticles Loaded by Poly Lactic Co-Glycolic Acid for Improved Therapeutic Efficiency and Cytotoxicity. *Artif. Cells Nanomed. Biotechnol.* **2019**, *47*, 378–394. [CrossRef]
159. Sulaiman, G.M.; Waheeb, H.M.; Jabir, M.S.; Khazaal, S.H.; Dewir, Y.H.; Naidoo, Y. Hesperidin Loaded on Gold Nanoparticles as a Drug Delivery System for a Successful Biocompatible, Anti-Cancer, Anti-Inflammatory and Phagocytosis Inducer Model. *Sci. Rep.* **2020**, *10*, 9362. [CrossRef]

160. Wadhwa, R.; Paudel, K.R.; Chin, L.H.; Hon, C.M.; Madheswaran, T.; Gupta, G.; Panneerselvam, J.; Lakshmi, T.; Singh, S.K.; Gulati, M.; et al. Anti-Inflammatory and Anticancer Activities of Naringenin-Loaded Liquid Crystalline Nanoparticles in Vitro. *J. Food Biochem.* **2021**, *45*, e13572. [CrossRef]
161. Askar, M.A.; El Shawi, O.E.; Abou Zaid, O.A.R.; Mansour, N.A.; Hanafy, A.M. Breast Cancer Suppression by Curcumin-Naringenin-Magnetic-Nano-Particles: In Vitro and in Vivo Studies. *Tumour Biol.* **2021**, *43*, 225–247. [CrossRef]
162. Rajamani, S.; Radhakrishnan, A.; Sengodan, T.; Thangavelu, S. Augmented Anticancer Activity of Naringenin-Loaded TPGS Polymeric Nanosuspension for Drug Resistive MCF-7 Human Breast Cancer Cells. *Drug Dev. Ind. Pharm.* **2018**, *44*, 1752–1761. [CrossRef] [PubMed]

antioxidants

Review

Influence of the Neuroprotective Properties of Quercetin on Regeneration and Functional Recovery of the Nervous System

Simone Ortiz Moura Fideles [1], Adriana de Cássia Ortiz [1], Daniela Vieira Buchaim [2,3], Eliana de Souza Bastos Mazuqueli Pereira [2], Maria Júlia Bento Martins Parreira [1], Jéssica de Oliveira Rossi [4,5], Marcelo Rodrigues da Cunha [6,7], Alexandre Teixeira de Souza [8], Wendel Cleber Soares [9] and Rogerio Leone Buchaim [1,4,*]

[1] Department of Biological Sciences, Bauru School of Dentistry (FOB/USP), University of Sao Paulo, Bauru 17012-901, Brazil
[2] Postgraduate Program in Structural and Functional Interactions in Rehabilitation, University of Marilia (UNIMAR), Marília 17525-902, Brazil
[3] Teaching and Research Coordination of the Medical School, University Center of Adamantina (UNIFAI), Adamantina 17800-000, Brazil
[4] Graduate Program in Anatomy of Domestic and Wild Animals, Faculty of Veterinary Medicine and Animal Science, University of Sao Paulo, Sao Paulo 05508-270, Brazil
[5] Medical Bill Audit, Holy House of Mercy (Santa Casa de Misericórdia), Marília 17515-900, Brazil
[6] Anatomy Department, Padre Anchieta University Center (UniAnchieta), Jundiai 13210-795, Brazil
[7] Department of Morphology and Pathology, Jundiaí Medical School, Jundiai 13202-550, Brazil
[8] Department of Medicine, University Center of Adamantina (UNIFAI), Adamantina 17800-000, Brazil
[9] Department of Exact Sciences, University Center of Adamantina (UNIFAI), Adamantina 17800-000, Brazil
* Correspondence: rogerio@fob.usp.br; Tel.: +55-14-3235-8220

Abstract: Quercetin is a dietary flavonoid present in vegetables, fruits, and beverages, such as onions, apples, broccoli, berries, citrus fruits, tea, and red wine. Flavonoids have antioxidant and anti-inflammatory effects, acting in the prevention of several diseases. Quercetin also has neuroprotective properties and may exert a beneficial effect on nervous tissue. In this literature review, we compiled in vivo studies that investigated the effect of quercetin on regeneration and functional recovery of the central and peripheral nervous system. In spinal cord injuries (SCI), quercetin administration favored axonal regeneration and recovery of locomotor capacity, significantly improving electrophysiological parameters. Quercetin reduced edema, neutrophil infiltration, cystic cavity formation, reactive oxygen species production, and pro-inflammatory cytokine synthesis, while favoring an increase in levels of anti-inflammatory cytokines, minimizing tissue damage in SCI models. In addition, the association of quercetin with mesenchymal stromal cells transplantation had a synergistic neuroprotective effect on spinal cord injury. Similarly, in sciatic nerve injuries, quercetin favored and accelerated sensory and motor recovery, reducing muscle atrophy. In these models, quercetin significantly inhibited oxidative stress and cell apoptosis, favoring Schwann cell proliferation and nerve fiber remyelination, thus promoting a significant increase in the number and diameter of myelinated fibers. Although there is still a lack of clinical research, in vivo studies have shown that quercetin contributed to the recovery of neurological functions, exerting a beneficial effect on the regeneration of the central and peripheral nervous system.

Keywords: quercetin; nerve regeneration; nervous system; spinal cord; peripheral nerves

1. Introduction

Neurological disorders affect millions of people and can lead to complications that compromise quality of life [1,2]. Several factors may be associated with the etiology of neurological disorders, such as neurodegenerative and metabolic diseases, injuries, trauma, ischemia, and tumors. Among them, injuries and traumatic lesions have become a public health problem, considering the sequelae commonly associated with trauma [3]. Depending

on the severity and the affected site, injury to the nervous system can lead to different degrees of functional disability and not always a satisfactory recovery can be achieved. Although nervous tissue has a certain regenerative capacity, several neurological functions can be impaired as a result of injuries to the central or peripheral nervous system. Spinal cord injuries can lead to partial or total loss of functional capacity [1,4]. Traumatic brain injury, in turn, is one of the main causes of death or disability and has been considered a risk factor for the development of neurodegenerative pathologies, such as Parkinson's disease [5,6]. Similarly, peripheral nerve injuries can lead to neuropathies, sensory and motor deficits, muscle atrophy and neuritic pain [4,7,8].

In this regard, nerve regeneration and the recovery of neurological functions are influenced by events resulting from the imbalance in the homeostasis of the injured tissue [1]. Injuries in the nervous system cause several physiopathological changes in the microenvironment that impair the regenerative process, such as increased cellular oxidative stress and elevated synthesis of pro-inflammatory cytokines, like interleukin-1 (IL-1), interleukin-6 (IL-6), and tumor necrosis factor alpha (TNF-α) [8]. Increased concentrations of these cytokines activate the expression of other factors, such as cyclooxygenase-2 (COX-2) and inducible nitric oxide synthase (iNOS). Additionally, abnormalities that lead to mitochondrial dysfunction also promote increased oxidative stress, predisposing to alterations in neurotransmitters and neuronal activity [9]. Oxidative stress results from the accumulation of reactive oxygen species (ROS) or reactive nitrogen species (RNS) in cells and constitutes one of the main factors associated with neurodegenerative disorders [9–11]. The excessive production of free radicals can lead to alterations in macromolecules, such as DNA, proteins, and lipids, causing significant cellular damage and leading to cell death [9,12]. Therefore, an exacerbated and prolonged inflammatory response, increased oxidative stress, and cellular apoptosis are the main events associated with the neurodegeneration process [8]. These events favor axonal degeneration and demyelination, while inducing necrosis and apoptosis of nervous cells, such as neurons and oligodendrocytes. These physiopathological alterations can also favor the formation of a scar at the injury site, which is another factor that impairs axonal growth and tissue regeneration (Figure 1) [1].

Thus, considering the challenges encountered to obtain adequate regeneration and a satisfactory recovery of functional capacity, therapeutic strategies have been searched that can act as adjuvants to the resources available for the treatment of injured nervous tissue [3]. Therefore, the use of some bioactive agents with therapeutic potential, such as flavonoids, has been investigated as a strategy to promote tissue regeneration. Flavonoids are dietary phytochemicals, from the polyphenol class, found in a variety of fruits, vegetables, and beverages, including citrus fruits, strawberries, raspberries, apples, grapes, cocoa, legumes, grains, coffee, green tea, and red wine [13]. According to their chemical characteristics, flavonoids are classified into subgroups, such as flavonols, flavones, isoflavones, flavanones, flavanols, and anthocyanidins [14]. In general, flavonoid subgroups have nutritional properties and therapeutic potential on different pathologies, such as cancer, cardiovascular, neurological, inflammatory, and metabolic diseases [14–16]. Due to their antioxidant, anti-inflammatory, antiallergic, antimicrobial, antitumor, and antiviral properties, flavonoids can exert significant beneficial effect, modulating various biological processes [17]. Flavonoids exhibit the ability to scavenge ROS, activate antioxidant enzymes and inhibit enzymes related to the production of free radicals, as well as downregulate the expression and synthesis of factors related to oxidative stress, such as iNOS and nitric oxide (NO) [18,19]. Thus, the main mechanisms of action by which flavonoids exert their effect are related to their ability to inhibit ROS production and reduce the synthesis of inflammatory mediators, such as TNF-α, IL-6, interleukin-1 beta (IL-1β), COX-2, and prostaglandin E2 (PGE2) [16,20].

Considering the nutritional value and therapeutic potential of flavonoids, and with diet as a source of a wide variety of phytochemicals, studies have investigated the effect of the use of these bioactive agents in the control and progression of several pathologies. Among the various types of dietary flavonoids, quercetin is a flavonoid that is highlighted for having neuroprotective properties and biological effect on nervous tissue [10]. Thus,

this literature review compiled in vivo studies that investigated the effect of quercetin administration on regeneration and recovery of functional capacity in spinal cord injury (SCI) or peripheral nerve injury models.

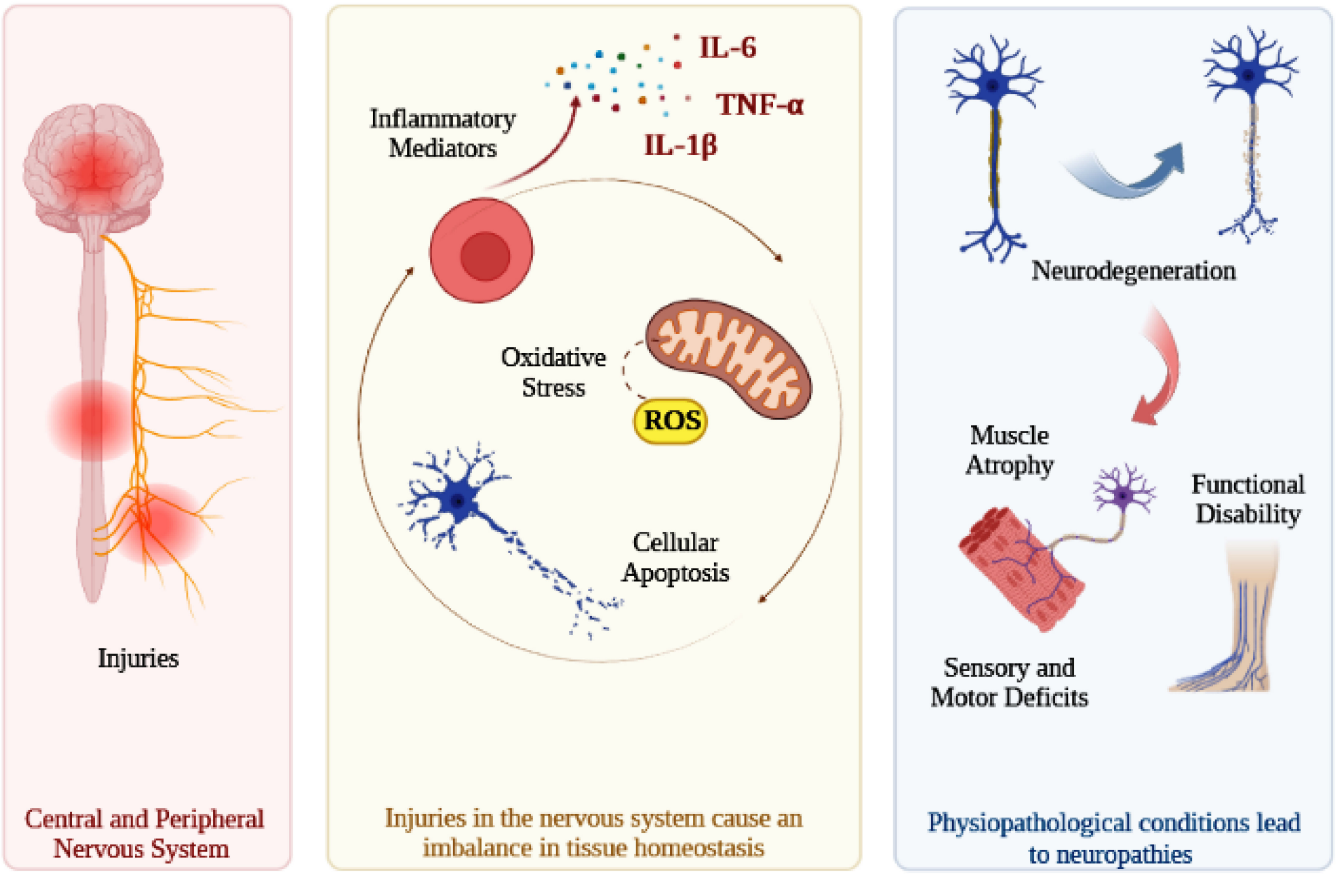

Figure 1. Injuries in the central or peripheral nervous system can lead to an increase in the synthesis of inflammatory cytokines, in the production of reactive oxygen species, and in cell apoptosis. These physiopathological alterations favor the degeneration of nervous cells, impair tissue regeneration, and compromise the recovery of neurological functions. Consequently, lesions in nervous tissue can cause complications of different degrees of severity, such as muscle atrophy, sensory and motor deficits, partial or total functional disability, and neuropathic pain. Interleukin-6 (IL-6); Tumor Necrosis Factor alpha (TNF-α); Interleukin-1 beta (IL-1β); Reactive Oxygen Species (ROS).

2. Flavonoid Quercetin

Biological Properties

The term quercetin is derived from the Latin "*quercetum*", commonly referred to as "oak forest" [12,21]. Quercetin is a bioactive agent that is widely distributed among a diversity of vegetable species and medicinal plants, such as *Ginkgo biloba, Hypericum perforatum,* and *Sambucus canadensis* [21]. Structurally, quercetin (3,3′,4′,5,7-pentahydroxyflavone) has two benzene rings linked by a heterocyclic pyran or pyrone ring and five hydroxyl groups [22], with the molecular formula $C_{15}H_{10}O_7$ [9,12,21]. Considering the chemical aspect, quercetin has a greenish-yellow crystalline solid appearance, being responsible for the pigmentation of various fruits, flowers, and vegetables [12,23,24]. Quercetin has an important nutritional value, constituting one of the most abundant flavonoids in the diet [21–24]. The main dietary sources of quercetin are onions and apples, in addition to other foods, such as cherries, grapes, blueberries, citrus fruits, red leaf lettuce, cabbage, broccoli, tomatoes, peppers, asparagus, wine, and tea [21,22,25,26].

In fruits and vegetables, quercetin is usually present in the form of glycosides, conjugated to carbohydrate residues, such as glucose and rutinose [12,22,25,27]. After ingestion,

quercetin glycosides are hydrolyzed by β-glycosidases in the intestine. Most of the aglycone form is absorbed in the gastrointestinal tract and metabolized in the liver [9,12,21,22,25]. Thus, the microbial of the gastrointestinal tract plays an important role in the degradation and metabolism of this bioactive agent [22]. Quercetin, therefore, has a rapid and extensive metabolism, being efficiently eliminated by the intestine and kidneys [9,19]. One of the important issues in this process refers to its bioavailability. In addition to the intestinal flora, some factors, such as diet, can alter the bioavailability of quercetin and its metabolites. Certain dietary elements can interfere to increase the plasmatic concentration of these molecules. Quercetin, however, has a short half-life and relatively low bioavailability, which may influence its biological effect [9,12,23,25]. Considering these issues, some studies have investigated different delivery systems that could increase the bioavailability and facilitate the access of quercetin in the target tissues, such as the use of loaded quercetin in hydrogels, nanoparticles, nanofibers, polymeric micelles, or mucoadhesive nanoemulsions [9,28–32]. Thus, research has advanced in the use of these technologies since the therapeutic effect of a bioactive agent depends largely on its bioavailability.

As with the other flavonoids, quercetin has several biological properties that are responsible for its therapeutic potential. Quercetin has anti-inflammatory, antioxidant, anticancer, neuroprotective, immunoprotective, antiviral, and antibacterial properties [21,22,33–36]. Studies report that quercetin can act in the prevention of several pathologies, such as cancer, bacterial and viral infections, cardiovascular, neurodegenerative, inflammatory, immunological, and metabolic diseases, like asthma and diabetes mellitus (Figure 2) [12,19,21,22,24,36]. Therefore, regular consumption of a diet rich in quercetin may provide health benefits, contributing to the prevention of diseases related to aging and lifestyle [12,27]. Thus, considering that quercetin is already part of the diet and considering the scientific evidence from in vivo studies and clinical trials that did not indicate adverse toxicological effects, in 2010, high purity quercetin was recognized by the Food and Drug Administration (FDA) as GRAS (Generally Recognized as Safe) for use as a food ingredient [22]. In addition to its recognized nutritional properties, the effects of quercetin as a therapeutic agent have also been investigated in various pathological conditions, such as in the rehabilitation of neurological functions.

There is evidence in the literature that quercetin has a neuroprotective effect and the potential to favor neurogenesis and regeneration of nervous tissue [9,12]. One of the characteristics that contributes to the neuroprotective action of quercetin concerns its solubility. Despite being relatively insoluble in water, quercetin is lipophilic [9,12,21]. The lipophilic nature of quercetin facilitates its passage through the blood-brain barrier. Then, quercetin absorbed and available in the plasma can easily access the brain tissue to exert its biological activity [10,12]. In the nervous system, quercetin can act in injured areas to minimize or reverse the dysfunctions resulting from neurodegenerative disorders, as well as to delay the advance of neurological alterations [9,12]. The neuroprotective effect of quercetin is mainly related to its anti-inflammatory and antioxidant potential, since quercetin acts by protecting the tissue against oxidative stress induced or resulting from physiological metabolism [10]. In addition to physiopathological changes, physiological conditions, such as aging, can compromise the antioxidant capacity of the tissue, resulting in increased oxidative damage [9]. Overall, the antioxidant action of quercetin occurs through several mechanisms, such as free radical scavenging, chelating action on metal ions, acting on mitochondrial function, on gene expression and on the synthesis of antioxidant factors [10]. In addition to reducing ROS formation and lipid peroxidation, quercetin also acts by modulating the inflammatory response, inhibiting the synthesis of pro-inflammatory cytokines, such as TNF-α, IL-1β, and IL-6, and favoring the synthesis of anti-inflammatory cytokines, such as interleukin-10 (IL-10) [19].

The anti-inflammatory and antioxidant properties of quercetin have been reported in several studies. In vitro studies showed that quercetin reduced the production of NO and ROS, inhibited the activation of nuclear factor-kappa B (NF-kB), and downregulated the expression of inflammatory mediators, such as IL-1β, IL-6, TNF-α, and COX-2, even in lipopolysaccharide-stimulated cells (LPS) [37–41]. The neuroprotective properties of

quercetin have also been reported in studies with animal models subjected to neuronal injury induced by trauma, hypoxia, or LPS. In animals with traumatic brain injury, quercetin administration reduced inflammatory response, oxidative stress, neuronal apoptosis, and brain edema [42,43], improving cognitive functions, biogenesis, and mitochondrial function [43–46]. Quercetin treatment also modulated the inflammatory response, minimized oxidative stress, and reduced neuronal apoptosis in animals with cerebral ischemia, suppressing the expression and synthesis of inflammatory cytokines (TNF-α, Il-1β, and Il-6), as well as inhibiting NF-kB activation [41,47]. In addition to modulating tissue responses induced by hypoxia, quercetin inhibited blood-brain barrier disruption and cerebral infarction, attenuating the neurological deficit [47].

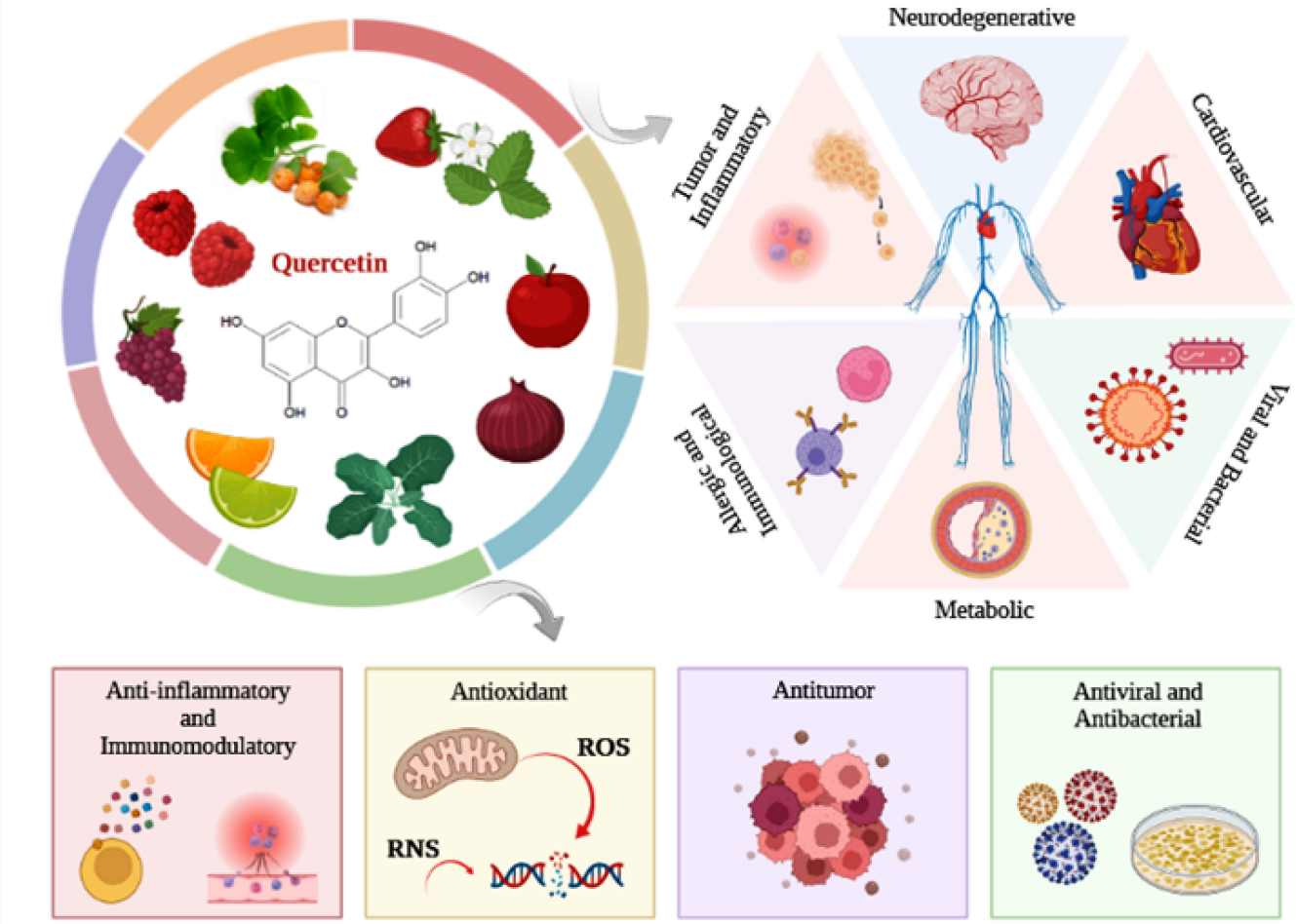

Figure 2. Quercetin is a dietary flavonoid widely distributed among a diversity of fruits, vegetables, and medicinal plants. Quercetin has anti-inflammatory, antioxidant, antitumor, antiviral, antibacterial, and neuroprotective properties. Due to its properties, quercetin can exert beneficial biological activity, acting in the prevention of various pathologies, such as cancer, bacterial and viral infections, cardiovascular, neurodegenerative, inflammatory, immunological, and metabolic diseases. Reactive Nitrogen Species (RNS).

In addition, under conditions of cerebral hypoxia, a synergistic pharmacological effect was obtained by the association of quercetin administration with the transplantation of human umbilical cord mesenchymal stromal cells (HUMSCs) [48]. In this study, treatment with quercetin and HUMSCs reduced cellular apoptosis and the synthesis of inflammatory mediators (IL-1β and IL-6), while favoring the synthesis of anti-inflammatory cytokines (IL-4, IL-10 and TGF-β1). Additionally, the combined treatment favored the survival of HUMSCs at the site of injury and promoted an improvement in the recovery

of neurological functions [48]. In LPS-induced animal models, quercetin administration reduced ROS production and the synthesis of inflammatory mediators (Il-1β, TNF-α and COX-2), minimizing neurotoxicity and neurodegeneration, in addition to improving memory function [38,49]. Similar results were obtained in studies that used quercetin to treat animals with neurodegenerative or metabolic diseases. In rotenone-induced parkinsonian rats, quercetin minimized neurological deficits and downregulated the expression of inflammatory mediators, such as Il-1β, TNF-α and NF-kB [50]. Similarly, an inhibition of inflammatory mediator synthesis (Il-1β and TNF-α) was obtained in diabetic peripheral neuropathy animal model treated with quercetin [51]. Other in vivo studies have also reported that the administration of quercetin promoted a beneficial effect by alleviating neuropathic pain [52–55].

In general, in several studies conducted with animal models, quercetin has shown beneficial effects on the microenvironment of nervous tissue, modulating the inflammatory response, and minimizing oxidative stress, cell apoptosis and neurodegenerative disorders, in addition to alleviating neuropathic pain.

3. Therapeutic Effect of Quercetin

3.1. Animal Models with Central and Peripheral Nervous System Injuries

The influence of the neuroprotective properties of quercetin on the regeneration and functional recovery of the nervous system after injuries or traumas has also been reported in several studies. This review selected studies that investigated the effect of quercetin administration in animal models of spinal cord injury (SCI) or peripheral nerve injury and, for the most part, investigated the effect of quercetin used alone, without association with other agents [56–61]. Two studies compared the effect of administration of quercetin alone or in combination with other agent or with stem cells [62,63]. Some studies also compared the effect of quercetin administration in relation to the effect of other agents with pharmacological action, such as methylprednisolone, SB203580 (p38 mitogen-activated protein kinases inhibitor), and nerve growth factor (NGF) [64,65].

In general, the effects of the treatment with quercetin were measured using different methods of analysis, such as behavioral and electrophysiological assessment, quantitative real-time reverse-transcriptase polymerase chain reaction (qRT-PCR), Western blot, immunohistochemistry, immunofluorescence, histological assays, and motor nerve conduction velocity analysis. The main outcomes of these studies showed that quercetin favored the regeneration and recovery of the functional capacity. Table 1 synthesizes the experimental design and summarizes the main outcomes of studies that evaluated the effect of quercetin administration in animal models with spinal cord injury (SCI) or peripheral nerve injury.

3.1.1. Spinal Cord Injury (SCI)

In the studies of this review that investigated the effect of quercetin administration in SCI animal models, the behavioral assessment was performed using the Basso, Beattie, Bresnahan Locomotor Rating Scale (BBB scores), which is a valid measure to detect alterations in locomotor performance after SCI [66]. In SCI animals, quercetin administration reduced histopathological damage, inflammatory cytokine synthesis, and cellular oxidative stress, promoting a significant recovery of neurophysiological functions and locomotor capacity.

Table 1. In vivo studies that evaluated the effect of quercetin administration in animal models with spinal cord injury (SCI) or peripheral nerve injury (sciatic nerve).

References	Animals Models	Treatment Groups	Intervention	Main Analysis	Main Outcomes
Wang et al., (2011) [60]	Sprague Dawley rats. Sciatic Nerve Injury	G1: Saline solution G2: Quercetin 0.1 µg/mL G3: Quercetin 1 µg/mL G4: Quercetin 10 µg/mL	Implantation of silicone rubber nerve chamber filled with the quercetin or saline solutions in the gaps (15 mm) (n = 10). Analyses were performed after 8 weeks of the procedures.	Electrophysiological and histological analysis.	Quercetin-treated groups showed a considerable increase in the number and density of myelinated axons in relation to the control, with satisfactory reinnervation of the gastrocnemius muscle. Quercetin (1 µg/mL) had a considerably larger area of evoked muscle action potential than the control group.
Song et al., (2013) [65]	Male Sprague Dawley rats. Spinal Cord Injury (SCI)	G1: Sham surgery G2: SCI G3: SCI + Quercetin 0.2 mg/kg/day G4: SCI + Methylprednisolone (MP) 30 mg/kg/day G5: SCI + specific p38MAPK inhibitor SB20358 (SB) 10 mg/kg/day	Intraperitoneal injections of quercetin, MP, or SB solutions (n = 8). Analyses were performed until the 14th day after the procedures.	Behavioral assessment (BBB: Basso, Beattie and Bresnahan scores), qRT-PCR, Western blot, and immunohistochemical analysis.	Quercetin significantly improved BBB scores, similarly to the positive control (MP). Quercetin suppressed the expression of inducible nitric oxide synthase (iNOS) similarly to SB, showing a neuroprotective effect by inhibiting cellular oxidative stress.
Jiang et al., (2016) [57]	Female Sprague Dawley rats. Spinal Cord Injury (SCI)	G1: Sham G2: SCI G3: SCI + Saline solution (vehicle) G4: SCI + Quercetin solution 100 mg/Kg	Intraperitoneal injections with quercetin or vehicle solutions at 12-h intervals for 3 days (n = 5). Analyses were performed until the 14th day after the procedures.	Behavioral assessment (BBB scores), Western blot, histological assays, and biochemical analysis.	Quercetin promoted a significant improvement in functional recovery, reducing histopathological damage, inflammatory cytokines synthesis, and reactive oxygen species production.

Table 1. *Cont.*

References	Animals Models	Treatment Groups	Intervention	Main Analysis	Main Outcomes
Chen et al., (2017) [64]	Male C57BL/6J mice. Sciatic Nerve Crush Injury	G1: Sham G2: Saline solution G3: Quercetin 0.2 mg/kg/day G4: Quercetin 2 mg/kg/day G5: Quercetin 20 mg/kg/day G6: mice-derived nerve growth factor (mNGF) 4.86 µg/kg/day	Injection of the solutions into the plantar muscle of the left hind limb once a day (n = 10). Analyses were performed at 7, 14 and 35 days after the procedures.	Behavioral test, qRT-PCR, Western blot, immunofluorescence, transmission electron microscopy, and motor nerve conduction velocity analysis.	Quercetin (mainly at 20 mg/kg/day) and mNGF favored the expression of genes related to intrinsic axon growth and promoted an increase in the number of myelinated fibers. At 20 mg/kg/day, quercetin significantly accelerated sensory and motor function recovery. In addition, quercetin (20 mg/kg/day) and mNGF significantly reduced muscle atrophy.
Turedi et al., (2018) [59]	Male Sprague Dawley rats. Sciatic Nerve Crush Injury (T)	G1: Sham (S-7) G2: Sham (S-28) G3: Quercetin (Q-7) 200 mg/kg/day G4: Quercetin (Q-28) 200 mg/kg/day G5: T (T-7) G6: T (T-28) G7: T + Quercetin (T + Q-7) 200 mg/kg/day G8: T + Quercetin (T + Q-28) 200 mg/kg/day	Intragastric administration of quercetin solutions for 7 days (n = 6). Analyses were performed at 7 and 28 days after the procedures.	TUNEL assay, histopathological assay, and biochemical analysis.	Quercetin significantly decreased the index of apoptosis. Nerve fiber regeneration was significantly more expressive in T + Q-28 than in T + Q-7. In addition, T + Q-28 showed significantly more myelinated nerve fibers with thicker myelin sheaths than T + Q-7.
Wang et al., (2018) [62]	Female Sprague Dawley rats. Spinal Cord Injury (SCI)	G1: Sham G2: Culture medium G3: Human umbilical cord mesenchymal stromal cells (HUSMCs) G4: Quercetin 50 µmol/kg G5: HUSMCs + Quercetin 50 µmol/kg	Administration of quercetin or saline solutions at 12-h intervals for 3 days. HUSMCs transplantation (2 dosages) into the injured spinal cord. (n = 28). Analyses were performed until the 4th week after the procedures.	Behavioral assessment (BBB scores) and immunohistochemical analysis.	HUMSCs + Quercetin promoted significant improvement in neurological function in relation to the other groups. Similarly, HUMSCs + Quercetin reduced cystic cavities formation, inflammatory cytokines synthesis, and iNOS production, while favoring pro-inflammatory cytokines synthesis.

Table 1. *Cont.*

References	Animals Models	Treatment Groups	Intervention	Main Analysis	Main Outcomes
Wang et al., (2018) [61]	Male Sprague Dawley rats. Spinal Cord Injury (SCI)	G1: Sham G2: SCI G3: SCI + Quercetin 20 mg/kg/day	Intraperitoneal injections of quercetin for 7 days (n = 10). Analyses were performed after 7 days of the procedures.	Behavioral assessment (BBB scores), qRT-PCR, Western blot, immunofluorescence, histological assays, and electrophysiological analysis.	Quercetin significantly improved functional capacity and electrophysiological recovery. Quercetin reduced cavity formation, favored axonal regeneration, and promoted astrocyte activation, upregulating the expression of glial fibrillary acidic protein (GFAP) and S100 calcium binding protein B (S100β).
Fan et al., (2019) [56]	Male Sprague Dawley rats. Spinal Cord Injury (SCI)	G1: Sham G2: SCI + saline solution (vehicle) G3: SCI + Quercetin 7,5 mg/kg	Intraperitoneal injections of quercetin or vehicle solutions twice daily for 10 days (n = 6). Analyses were performed until the 21st day after the procedures.	Behavioral assessment (BBB scores), qRT-PCR, Western blot, immunohistochemical assays, and electron microscopic analysis.	Quercetin significantly improved functional recovery. Quercetin considerably prevented oligodendrocyte necropsies, in addition to significantly reducing myelin loss and axonal loss after SCI.
Qiu et al., (2019) [58]	Male ICR mice. Sciatic Nerve Crush Injury	G1: Sham G2: Saline solution (vehicle) G3: Isoquercitrin (quercetin-3-glucoside) 20 mg/kg/day	Intraperitoneal injections of isoquercitrin or vehicle solutions. Analyses were performed until the 23rd day after the procedures.	Behavioral assessment (sciatic functional index), cell proliferation and migration assays qRT-PCR, Western blot, and electrophysiological analysis.	Isoquercitrin favored peripheral nerve remyelination, improved motor function recovery, reduced muscle atrophy, and inhibited autophagy. In addition, isoquercitrin suppressed cellular oxidative stress, favoring the proliferation and migration of Schwann cells.
Wang et al., (2021) [63]	Male Sprague Dawley rats. Spinal Cord Injury (SCI)	G1: Sham surgery + saline solution G2: SCI + saline solution G3: SCI + Quercetin 20 mg/kg/day G4: SCI + Quercetin + 3-methyladenine (3-MA; 400 nmol)	Intraperitoneal injections of solutions for 1, 3, or 7 days (n = 10). Analyses were performed until the 14th days after the procedures.	Behavioral assessment (BBB scores), Western blot and immunohistochemical analysis.	Quercetin favored axonal regeneration and promoted a significant recovery of locomotor capacity, minimizing histological alterations and cavity formation. 3-MA partially abrogated the neuroprotective effects of quercetin.

Several biological conditions resulting from spinal cord injuries can influence the recovery of neurophysiological functions, such as the inflammatory process and oxidative stress, which can cause secondary damage in the injury area. Considering these issues, studies have investigated whether the use of an agent with potential to modulate the inflammatory process and oxidative stress could constitute a strategy to favor the regeneration of nervous tissue. Song et al., (2013) evaluated the effect of quercetin on cellular oxidative stress resulting from acute spinal cord injury in rats, which were treated with quercetin (0.2 mg/kg/day), methylprednisolone (30 mg/kg/day), or SB203580 (10 mg/kg/day) [65]. Methylprednisolone has been used as a neuroprotective agent in the treatment of central nervous system injuries. SB203580 is a specific inhibitor of p38 mitogen-activated protein kinases (p38MAPK) signaling. The results showed that quercetin administration significantly downregulated the expression of phosphorylated p38MAPK and iNOS, similarly to SB203580, contributing to minimize cellular oxidative stress. In contrast, the expression of these factors was significantly increased in the SCI group.

These authors also evaluated malondialdehyde (MDA) content and superoxide dismutase (SOD) activity, which are biomarkers related to oxidative stress. MDA constitutes an end product of lipid peroxidation and acts in the activation of pro-inflammatory cytokines. SOD is an antioxidant enzyme responsible for scavenging free radicals [67,68]. Quercetin treatment significantly reduced MDA content and increased SOD activity compared to SB203580. In this study, BBB scores showed that quercetin significantly improved the functional capacity of SCI animals, similarly to the positive control methylprednisolone. These authors concluded that the inhibition of p38MAPK/iNOS signaling may constitute one of the mechanisms of neuroprotective action of quercetin [65]. Corroborating with these data, Jiang et al., (2016) reported that the administration of quercetin (100 mg/kg) promoted a significant improvement in the functional recovery of SCI rats from the 3rd postoperative day, according to BBB scores [57]. SCI caused an increase in the formation of reactive oxygen species, in the production of TNF-α, and in the synthesis of pro-inflammatory cytokines, such as IL-1β and interleukin-18 (IL-18), which were significantly reduced by quercetin. Additionally, quercetin minimized histopathological damage, providing a considerable reduction in congestion, edema, neutrophil infiltration, and structural disruption in the lesion area [57].

The functional recovery of nervous tissue can also be favored by treatment with quercetin and cells with regenerative potential. Wang et al., (2018) evaluated the effect of quercetin administration (50 μmol/kg) associated with transplantation of human umbilical cord mesenchymal stromal cells (HUMSCs) in SCI rats [62]. The behavioral assessment measured by BBB scores showed that the neurological functions of the animals were significantly improved by the treatment with quercetin and HUMSCs, differing significantly from the other groups. Furthermore, the treatment combining quercetin and HUMSCs reduced the formation of cystic cavities, exhibited greater axonal preservation, and showed a significant reduction in the levels of pro-inflammatory cytokines, such as IL-1β and IL-6, in addition to exhibiting an increase in the levels of anti-inflammatory cytokines, such as IL-10, interleukin-4 (IL-4), and transforming growth factor beta 1 (TGF-β1). These authors concluded that the administration of quercetin combined with the transplantation of HUMSCs had a synergistic effect, which may constitute a strategy to favor the recovery of neurological functions and to minimize the damage resulting from SCI [62].

Some studies with SCI animal models have investigated the effect of quercetin on nerve cells, such as astrocytes and oligodendrocytes. Wang et al., (2018) evaluated the effect of quercetin (20 mg/kg/day) on astrocyte activation and on the expression of factors, such as glial fibrillary acidic protein (Gfap) and S100 calcium binding protein B (S100b) [61]. Gfap and S100b are biomarkers related to neurological damage. S100b constitutes a neurotrophic protein present in astrocytes [69]. Gfap, in turn, is the main component of the cytoskeleton of astrocytes and constitutes a marker of differentiation and activation of these cells [70,71]. Analyses showed that the quercetin-treated group showed an overexpression of Gfap and S100b at 7 days post-SCI, evidencing a positive effect on astrocyte activation. Astrocytes

perform several functions in nervous tissue, being responsible for neuronal homeostasis [72]. In the early stages of the regenerative process, activation of astrocytes can be considered beneficial. However, prolonged activation of astrocytes can lead to tissue damage, making it difficult to regenerate the injured area [72]. Additionally, histological analyses also showed that quercetin considerably reduced the area of cavities at the site of injury and favored axonal regeneration, minimizing tissue damage, and promoting an increase in axon density. Thus, quercetin treatment promoted a significant improvement in functional recovery and electrophysiological capacity of SCI rats [61].

Fan et al., (2019) investigated the effect of the anti-inflammatory properties of quercetin (7.5 mg/kg) on oligodendrocyte necroptosis after SCI [56]. Oligodendrocytes are present in the central nervous system, and they act in the formation of the myelin sheath [73]. Necroptosis of oligodendrocytes is often involved with the inflammatory process, and it can be exacerbated after SCI, leading to more severe neurological damage. In this study, quercetin administration improved the functional recovery of the animals, significantly reducing myelin and axonal loss, which were markedly expressive in the SCI group. Immunofluorescence staining showed that quercetin minimized the reduction of myelin basic protein (Mbp) and neurofilament (NF200) in the white matter of SCI mice. Mbp constitutes the main component of the myelin sheath of oligodendrocytes. NF200 is a structural constituent of the cytoskeleton, and it is involved in axon development. Analysis by qRT-PCR also showed that the mRNA expression of factors involved in the inflammatory process, such as *TNF-α* and *iNOS*, were significantly downregulated by quercetin. Additionally, according to immunohistochemistry, quercetin favored the survival of oligodendrocytes by approximately 80%, significantly reducing the necroptosis of these cells after SCI [56].

The effect of quercetin administration (20 mg/kg/day), alone or associated with a specific autophagy inhibitor (3-methyladenine, 3-MA, 400 nmol) was investigated by Wang et al., (2021) [63]. BBB scores were employed over time to assess locomotor performance and recovery of functional capacity in SCI rats, with assessments performed at 1-, 3-, 7- and 14-days post-SCI. The results showed that there was no significant difference between the scores of the three groups (SCI, SCI + quercetin, SCI + quercetin + 3-MA) on day 1. However, quercetin administration promoted a significant recovery of locomotor capacity from the 3rd day, which increased over time, differing from the SCI group. In addition, the SCI + quercetin group showed better recovery of functional capacity than the SCI + quercetin + 3-MA group, but with no significant difference between them. Similarly, treatment with quercetin favored the electrophysiological recovery of the animals, while 3-MA partially reduced the beneficial effects of quercetin. In this study, histological analysis showed that SCI caused the disruption of nerve fibers, leading to cavity formation. However, quercetin administration reduced the deformity and the degree of histological alterations in the nervous tissue, so that the lesion area and the presence of cavities were reduced in the SCI + quercetin group.

However, 3-MA partially minimized the effects of quercetin. Additional analyses performed at 14 days post-SCI showed that SCI led to other significant changes in the nervous tissue. Immunofluorescence staining showed that the SCI group had a reduction of 5-hydroxytryptamine (5-HT) or serotonin positive nerve fibers and neurofilament (NF200) positive neurons, in addition to an increase in the detection of Gfap-positive astrocytes. Quercetin administration improved this condition, promoting an increase in 5-HT positive nerve fibers and NF200 positive neurons and a decrease in Gfap-positive astrocytes, which is favorable for tissue regeneration at this more advanced stage. Quercetin also downregulated *Gfap* expression and upregulated the expression of RNA binding fox-1 homolog 3 (*Neun*), confirmed in this study by Western blotting. Immunohistochemistry staining also showed a high number of Gfap-positive cells and a reduced number of NF200 and Neun-positive cells in the SCI group. Quercetin treatment reduced Gfap-positive cells and increased NF-200 and Neun-positive cells; however, these effects were also partially inhibited by 3-MA. Another important parameter investigated in this study was cellular autophagy, evaluated by the expression of the biomarkers Beclin 1 (Beclin 1) and

microtubule-associated protein 1 light chain 3 alpha (LC3-II). Autophagy is essential for neuronal homeostasis. The SCI group showed an overexpression of Beclin 1 and LC3-II in relation to Sham, on days 1 to 3 post-SCI. Quercetin upregulated the expression of these biomarkers and 3-MA partially minimized this effect. According to the data from this study, quercetin favored autophagy, which contributed to minimize neuronal damage and to improve recovery of functional capacity after SCI [63].

3.1.2. Peripheral Nerve Injury

The studies of this review that investigated the effect of quercetin on the regeneration and functional recovery of the peripheral nervous system were conducted with animal models with sciatic nerve injuries. In these animal models, quercetin administration also modulated the inflammatory response and significantly inhibited oxidative stress and cellular apoptosis, favoring nerve fiber remyelination and improving sensory and motor recovery. Wang et al., (2011) implanted a silicone rubber nerve chamber filled with quercetin or saline solutions into the sciatic nerve gaps (15 mm) of rats [60]. After 8 weeks, morphometric analysis showed that the groups treated with different dosages of quercetin (0.1, 1 and 10 μg/mL) showed an adequate reinnervation of the gastrocnemius muscle and a considerable increase in the number and density of myelinated axons compared to the control.

However, at this stage, the gastrocnemius muscle still showed significant atrophy, exhibiting relatively smaller muscle fibers at the injury site. Among the experimental groups, the group treated with quercetin, at a dosage of 1 μg/mL, presented an area of evoked muscle action potential significantly greater in relation to the control. These authors also found that quercetin, at all concentrations (0.1, 1 and 10 μg/mL), significantly favored the survival and growth of Schwann cells in vitro, not inducing cellular apoptosis [60]. Chen et al., (2017) also reported that quercetin administration promoted functional recovery after sciatic nerve crush injury in mice [64]. In this study, animals were treated with quercetin, at different dosages (0.2, 2, and 20 mg/kg/day), or with mice-derived nerve growth factor (m-NGF, 4.86 μg/kg/day). Sciatic nerve crush injury caused a significant deficit in the number of myelinated fibers.

Therefore, analyses showed that quercetin (mainly at 20 mg/kg/day) and mNGF favored the expression of genes related to intrinsic axon growth and promoted an increase in the number of myelinated fibers. Intrinsic neuronal growth was evaluated by the expression of cyclic adenosine monophosphate (cAMP) and growth associated protein 43 (Gap43). In all the evaluated periods (7, 14 and 35 days), quercetin at the highest dose tested (20 mg/kg/day) showed the best results, upregulating the expression of these two factors. At 20 mg/kg/day, quercetin also significantly accelerated sensory and motor function recovery, exhibiting sensory responses more rapid than the m-NGF group. In addition, quercetin (20 mg/kg/day) and mNGF significantly reduced muscle atrophy [64].

Corroborating with these studies, Turedi et al., (2018) investigated the effects of quercetin in a rat sciatic nerve crush injury model and obtained promising results [59]. In this study, untreated (T) or quercetin (Q) treated animals (200 mg/kg/day) were sacrificed at 7 or 28 days. Morphometric analyses were performed considering several parameters, such as the thickness of the myelin sheath, the diameter of the nerve fibers and the number of myelinated nerve fibers in the injured sciatic nerve. Analyses showed that the trauma caused axonal edema, in addition to degeneration in most of the myelinated axons and in the myelin sheath, signs indicative of Wallerian degeneration. The thickness of the myelin sheath and the number of myelinated nerve fibers were significantly compromised by the injury to the sciatic nerve, so that the T-7 and T-28 groups had a lower number of myelinated nerve fibers, with a thinner myelin sheath, compared to the Sham groups (S-7 and S-28).

Regarding the evaluated periods, analyses showed that the T-7 group presented a more expressive degree of nerve fiber degeneration; however, the T-28 group already exhibited the presence of nerve fibers indicating a process of initiated regeneration. Comparing the

treated and untreated groups, analyses showed that quercetin favored and accelerated the recovery of the injured nerve, since the T + Q-28 group showed a more advanced degree of regeneration compared to the T-28 group, exhibiting visible histopathological findings. Thus, T + Q-28 presented a greater number of myelinated nerve fibers, showing thicker myelin sheaths compared to T-28, with significant differences between these groups. Considering quercetin treatment and experimental periods, analyses showed that quercetin promoted an improvement in morphological parameters over time, since the T + Q-28 group had a significantly greater number of myelinated nerve fibers with thicker myelin sheaths in relation to the group treated for only 7 days (T + Q-7).

Therefore, the regeneration of the nervous fiber structure was significantly more expressive in the T + Q-28 group compared to the T + Q-7 group, which indicates that the regeneration process advanced over the days. These authors also performed biochemical analyses to evaluate the apoptosis index among the Schwann cells of the sciatic nerve. The data from these analyses showed that injury to the sciatic nerve increased the rate of cell apoptosis, as this rate was significantly higher for the T-7 and T-28 groups compared to the Sham groups (S-7 and S-28). In animals submitted to trauma, the administration of quercetin significantly reduced the apoptosis index, which was evident in the comparison of T + Q-7 in relation to T-7, as well as between T + Q-28 and T-28, with no increase in this index over time for all groups. Considering the results of the analyses, the authors concluded that quercetin had beneficial effects and potential to shorten the period of nerve regeneration [59].

Qiu et al., (2019) evaluated the effect of isoquercitrin (quercetin-3-glucoside), at 20 mg/kg/day, in mice sciatic nerve crush injury model [58]. Sciatic nerve injury resulted in a significant reduction in the thickness and number of layers of the myelin sheath, in addition to a reduction in the expression of proteins involved in the formation and conservation of the myelin sheath, such as myelin-associated glycoprotein (Mag) and peripheral myelin protein 22 (Pmp22). Mag is expressed by oligodendrocytes of the central nervous system and by Schwann cells present in the peripheral nervous system. Pmp22 is involved in several functions, including the formation and conservation of the myelin sheath of cells in the peripheral nervous system. Analyses performed at 15 days post-injury showed that the administration of isoquercitrin reversed part of these events, upregulating the expression of Mag and Pmp22, as well as the expression of factors involved with axonal growth, such as Gap43 and NF200. Isoquercitrin showed beneficial effects, favoring peripheral nerve remyelination, improving motor function recovery, and reducing muscle atrophy.

Additionally, isoquercitrin suppressed cellular oxidative stress resulting from sciatic nerve injury, downregulating the expression of proteins related to ROS production, such as NADPH oxidase 4 (Nox4) and dual oxidase 1 (Duox1), and upregulating the expression of proteins involved with the inhibition of free radical production, such as nuclear factor erythroid 2-related factor-2 (Nrf2) and superoxide dismutase 2 (Sod2). In this study, in vitro assays also showed that isoquercitrin promoted the proliferation and migration of Schwann cells in a dose-dependent manner. These authors concluded that isoquercitrin may have considerable therapeutic potential as a neuroprotective agent [58].

Figure 3 illustrates and summarizes the main outcomes of the in vivo studies that were included in this literature review, considering the effects of quercetin administration in animal models with SCI or sciatic nerve injury.

In addition to the content reported in this review, complementary therapies can also be considered, which can also be used in peripheral nerve regeneration, such as the use of Mesenchymal Stem Cells (MSCs) [74], fibrin sealants or fibrin "glues" [75], and photobiomodulation therapy (PBM), with the use of low-level laser (LLLT) [76] or light emitting diode (LED) [77], to improve the process of morphological and functional recomposition of injured nervous tissues, in which we envisage future studies to be carried out.

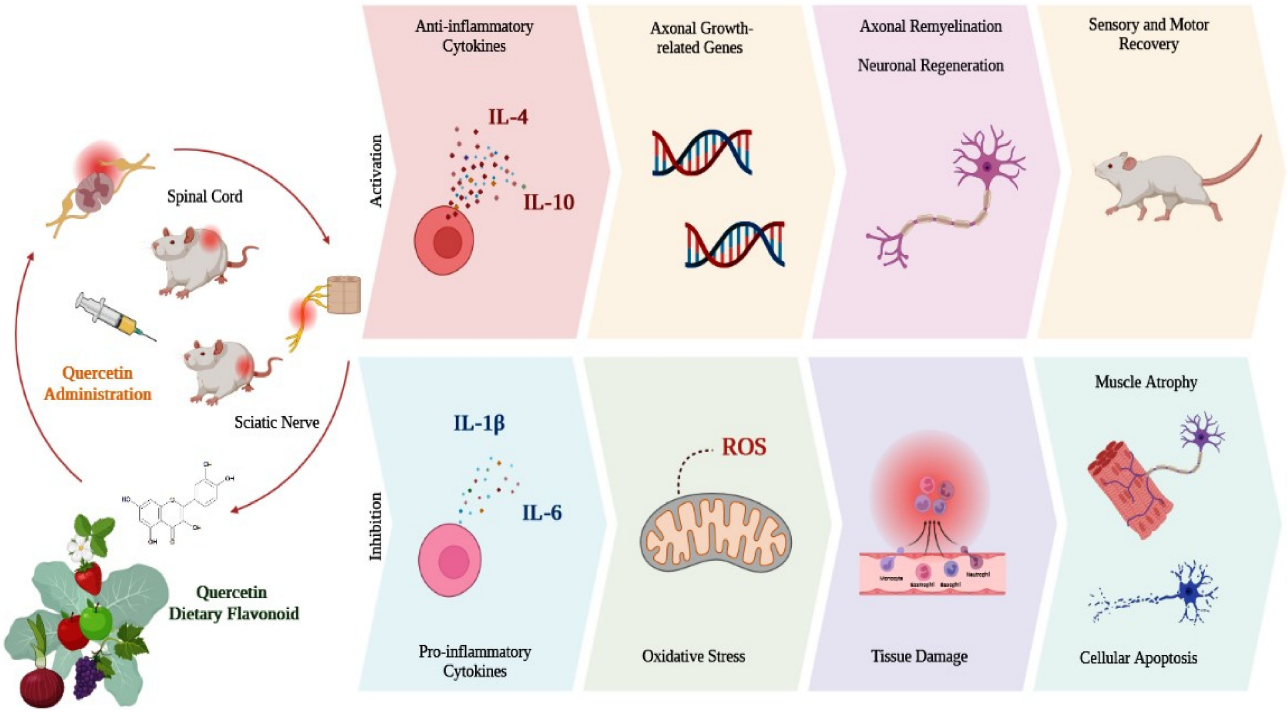

Figure 3. Schematic illustration of the main outcomes of the studies included in this literature review. In SCI and sciatic nerve injury models, quercetin administration inhibited the synthesis of pro-inflammatory cytokines, oxidative stress, and cell apoptosis, thus minimizing tissue damage and muscle atrophy. Similarly, quercetin favored the synthesis of anti-inflammatory cytokines and the expression of growth-related genes, promoting axonal remyelination and neuronal regeneration, accelerating sensory and motor recovery, and improving locomotor capacity. Interleukin-4 (IL-4); Interleukin-10 (IL-10); Interleukin-1 beta (IL-1β); Interleukin-6 (IL-6); Reactive Oxygen Species (ROS).

4. Conclusions

Injuries and traumas that affect the nervous system cause an imbalance in tissue homeostasis, leading to several physiopathological alterations, such as increased synthesis of inflammatory mediators, oxidative stress, and cellular apoptosis. These alterations may result in secondary damage in the injury site that can impair adequate nerve regeneration, compromising the recovery of functional capacity. The use of agents with antioxidant and anti-inflammatory properties, such as flavonoids, may constitute a strategy to favor the regeneration of nervous tissue. Quercetin is a dietary flavonoid, from the flavonols subgroup, which has neuroprotective properties and biological activity on nervous tissue. In animal models with SCI or sciatic nerve injuries, quercetin administration reduced histopathological damage, inflammatory cytokine synthesis, and cellular oxidative stress, promoting a significant recovery of neurophysiological functions and locomotor capacity. Although there is still a lack of clinical research, in vivo studies have shown that quercetin may have a beneficial effect on the nervous system, with the potential to minimize deleterious alterations, to favor regeneration and to improve the recovery of neurological functions.

Author Contributions: Conceptualization, S.O.M.F., A.d.C.O., R.L.B.; Methodology, S.O.M.F., A.d.C.O.; Formal Analysis, S.O.M.F., A.d.C.O.; Investigation, S.O.M.F., A.d.C.O.; Resources, M.R.d.C.; Data Curation, E.d.S.B.M.P., M.J.B.M.P. and J.d.O.R.; Writing—Original Draft Preparation, S.O.M.F. and A.d.C.O.; Writing—Review & Editing, S.O.M.F., A.d.C.O., D.V.B. and R.L.B.; Visualization, W.C.S. and A.T.d.S.; Supervision, R.L.B. All authors have read and agreed to the published version of the manuscript.

Funding: This research received no external funding.

Conflicts of Interest: The authors declare no conflict of interest.

References

1. Fan, B.; Wei, Z.; Yao, X.; Shi, G.; Cheng, X.; Zhou, X.; Zhou, H.; Ning, G.; Kong, X.; Feng, S. Microenvironment Imbalance of Spinal Cord Injury. *Cell Transplant.* **2018**, *27*, 853–866. [CrossRef] [PubMed]
2. Radi, E.; Formichi, P.; Battisti, C.; Federico, A. Apoptosis and oxidative stress in neurodegenerative diseases. *J. Alzheimers Dis.* **2014**, *42* (Suppl. S3), S125–S152. [CrossRef]
3. Modrak, M.; Talukder, M.A.H.; Gurgenashvili, K.; Noble, M.; Elfar, J.C. Peripheral nerve injury and myelination: Potential therapeutic strategies. *J. Neurosci. Res.* **2020**, *98*, 780–795. [CrossRef] [PubMed]
4. Guérout, N. Plasticity of the Injured Spinal Cord. *Cells* **2021**, *10*, 1886. [CrossRef] [PubMed]
5. Brett, B.L.; Gardner, R.C.; Godbout, J.; Dams-O'Connor, K.; Keene, C.D. Traumatic Brain Injury and Risk of Neurodegenerative Disorder. *Biol. Psychiatry* **2022**, *91*, 498–507. [CrossRef] [PubMed]
6. Vella, M.A.; Crandall, M.L.; Patel, M.B. Acute Management of Traumatic Brain Injury. *Surg. Clin. N. Am.* **2017**, *97*, 1015–1030. [CrossRef] [PubMed]
7. Houdek, M.T.; Shin, A.Y. Management and complications of traumatic peripheral nerve injuries. *Hand. Clin.* **2015**, *31*, 151–163. [CrossRef] [PubMed]
8. Wang, M.L.; Rivlin, M.; Graham, J.G.; Beredjiklian, P.K. Peripheral nerve injury, scarring, and recovery. *Connect. Tissue Res.* **2019**, *60*, 3–9. [CrossRef]
9. Grewal, A.K.; Singh, T.G.; Sharma, D.; Sharma, V.; Singh, M.; Rahman, M.H.; Najda, A.; Walasek-Janusz, M.; Kamel, M.; Albadrani, G.M.; et al. Mechanistic insights and perspectives involved in neuroprotective action of quercetin. *Biomed. Pharm.* **2021**, *140*, 111729. [CrossRef]
10. Barreca, D.; Bellocco, E.; D'Onofrio, G.; Nabavi, S.F.; Daglia, M.; Rastrelli, L.; Nabavi, S.M. Neuroprotective Effects of Quercetin: From Chemistry to Medicine. *CNS Neurol. Disord. Drug Targets* **2016**, *15*, 964–975. [CrossRef]
11. Islam, M.T. Oxidative stress and mitochondrial dysfunction-linked neurodegenerative disorders. *Neurol. Res.* **2017**, *39*, 73–82. [CrossRef] [PubMed]
12. Deepika; Maurya, P.K. Health Benefits of Quercetin in Age-Related Diseases. *Molecules* **2022**, *27*, 2498. [CrossRef] [PubMed]
13. Cassidy, A.; Minihane, A.M. The role of metabolism (and the microbiome) in defining the clinical efficacy of dietary flavonoids. *Am. J. Clin. Nutr.* **2017**, *105*, 10–22. [CrossRef] [PubMed]
14. Birt, D.F.; Jeffery, E. Flavonoids. *Adv. Nutr.* **2013**, *4*, 576–577. [CrossRef]
15. Crasci, L.; Basile, L.; Panico, A.; Puglia, C.; Bonina, F.P.; Basile, P.M.; Rizza, L.; Guccione, S. Correlating In Vitro Target-Oriented Screening and Docking: Inhibition of Matrix Metalloproteinases Activities by Flavonoids. *Planta Med.* **2017**, *83*, 901–911. [CrossRef]
16. Hwang, S.L.; Yen, G.C. Neuroprotective effects of the citrus flavanones against H_2O_2-induced cytotoxicity in PC12 cells. *J. Agric. Food Chem.* **2008**, *56*, 859–864. [CrossRef] [PubMed]
17. Li, X.; Chen, B.; Xie, H.; He, Y.; Zhong, D.; Chen, D. Antioxidant Structure(-)Activity Relationship Analysis of Five Dihydrochalcones. *Molecules* **2018**, *23*, 1162. [CrossRef]
18. Dias, M.C.; Pinto, D.; Silva, A.M.S. Plant Flavonoids: Chemical Characteristics and Biological Activity. *Molecules* **2021**, *26*, 5377. [CrossRef]
19. Shen, P.; Lin, W.; Deng, X.; Ba, X.; Han, L.; Chen, Z.; Qin, K.; Huang, Y.; Tu, S. Potential Implications of Quercetin in Autoimmune Diseases. *Front. Immunol.* **2021**, *12*, 689044. [CrossRef]
20. Chen, B.H.; Park, J.H.; Ahn, J.H.; Cho, J.H.; Kim, I.H.; Lee, J.C.; Won, M.H.; Lee, C.H.; Hwang, I.K.; Kim, J.D.; et al. Pretreated quercetin protects gerbil hippocampal CA1 pyramidal neurons from transient cerebral ischemic injury by increasing the expression of antioxidant enzymes. *Neural Regen. Res.* **2017**, *12*, 220–227. [CrossRef]
21. Li, Y.; Yao, J.; Han, C.; Yang, J.; Chaudhry, M.T.; Wang, S.; Liu, H.; Yin, Y. Quercetin, Inflammation and Immunity. *Nutrients* **2016**, *8*, 167. [CrossRef] [PubMed]
22. Andres, S.; Pevny, S.; Ziegenhagen, R.; Bakhiya, N.; Schäfer, B.; Hirsch-Ernst, K.I.; Lampen, A. Safety Aspects of the Use of Quercetin as a Dietary Supplement. *Mol. Nutr. Food Res.* **2018**, *62*, 1700447. [CrossRef]
23. Shabbir, U.; Rubab, M.; Daliri, E.B.; Chelliah, R.; Javed, A.; Oh, D.H. Curcumin, Quercetin, Catechins and Metabolic Diseases: The Role of Gut Microbiota. *Nutrients* **2021**, *13*, 206. [CrossRef] [PubMed]
24. Suganthy, N.; Devi, K.P.; Nabavi, S.F.; Braidy, N.; Nabavi, S.M. Bioactive effects of quercetin in the central nervous system: Focusing on the mechanisms of actions. *Biomed. Pharm.* **2016**, *84*, 892–908. [CrossRef] [PubMed]
25. Guo, Y.; Bruno, R.S. Endogenous and exogenous mediators of quercetin bioavailability. *J. Nutr. Biochem.* **2015**, *26*, 201–210. [CrossRef] [PubMed]
26. Kawabata, K.; Mukai, R.; Ishisaka, A. Quercetin and related polyphenols: New insights and implications for their bioactivity and bioavailability. *Food Funct.* **2015**, *6*, 1399–1417. [CrossRef]
27. Murota, K.; Nakamura, Y.; Uehara, M. Flavonoid metabolism: The interaction of metabolites and gut microbiota. *Biosci. Biotechnol. Biochem.* **2018**, *82*, 600–610. [CrossRef]
28. Ghosh, A.; Sarkar, S.; Mandal, A.K.; Das, N. Neuroprotective role of nanoencapsulated quercetin in combating ischemia-reperfusion induced neuronal damage in young and aged rats. *PLoS ONE* **2013**, *8*, e57735. [CrossRef]

29. Huang, C.; Fu, C.; Qi, Z.P.; Guo, W.L.; You, D.; Li, R.; Zhu, Z. Localised delivery of quercetin by thermo-sensitive PLGA-PEG-PLGA hydrogels for the treatment of brachial plexus avulsion. *Artif. Cells Nanomed. Biotechnol.* **2020**, *48*, 1010–1021. [CrossRef]
30. Sadalage, P.S.; Patil, R.V.; Havaldar, D.V.; Gavade, S.S.; Santos, A.C.; Pawar, K.D. Optimally biosynthesized, PEGylated gold nanoparticles functionalized with quercetin and camptothecin enhance potential anti-inflammatory, anti-cancer and anti-angiogenic activities. *J. Nanobiotechnol.* **2021**, *19*, 84. [CrossRef]
31. Testa, G.; Gamba, P.; Badilli, U.; Gargiulo, S.; Maina, M.; Guina, T.; Calfapietra, S.; Biasi, F.; Cavalli, R.; Poli, G.; et al. Loading into nanoparticles improves quercetin's efficacy in preventing neuroinflammation induced by oxysterols. *PLoS ONE* **2014**, *9*, e96795. [CrossRef] [PubMed]
32. Thipkaew, C.; Wattanathorn, J.; Muchimapura, S. Electrospun Nanofibers Loaded with Quercetin Promote the Recovery of Focal Entrapment Neuropathy in a Rat Model of Streptozotocin-Induced Diabetes. *BioMed Res. Int.* **2017**, *2017*, 2017493. [CrossRef] [PubMed]
33. Alizadeh, S.R.; Ebrahimzadeh, M.A. Quercetin derivatives: Drug design, development, and biological activities, a review. *Eur. J. Med. Chem.* **2022**, *229*, 114068. [CrossRef] [PubMed]
34. Mendoza, E.E.; Burd, R. Quercetin as a systemic chemopreventative agent: Structural and functional mechanisms. *Mini Rev. Med. Chem.* **2011**, *11*, 1216–1221. [CrossRef] [PubMed]
35. Wang, Y.; Tao, B.; Wan, Y.; Sun, Y.; Wang, L.; Sun, J.; Li, C. Drug delivery based pharmacological enhancement and current insights of quercetin with therapeutic potential against oral diseases. *Biomed. Pharm.* **2020**, *128*, 110372. [CrossRef]
36. Yi, H.; Peng, H.; Wu, X.; Xu, X.; Kuang, T.; Zhang, J.; Du, L.; Fan, G. The Therapeutic Effects and Mechanisms of Quercetin on Metabolic Diseases: Pharmacological Data and Clinical Evidence. *Oxi. Med. Cell Longev.* **2021**, *2021*, 6678662. [CrossRef]
37. Güran, M.; Şanlıtürk, G.; Kerküklü, N.R.; Altundağ, E.M.; Süha Yalçın, A. Combined effects of quercetin and curcumin on anti-inflammatory and antimicrobial parameters in vitro. *Eur. J. Pharm.* **2019**, *859*, 172486. [CrossRef]
38. Han, X.; Xu, T.; Fang, Q.; Zhang, H.; Yue, L.; Hu, G.; Sun, L. Quercetin hinders microglial activation to alleviate neurotoxicity via the interplay between NLRP3 inflammasome and mitophagy. *Redox. Biol.* **2021**, *44*, 102010. [CrossRef]
39. Luo, X.; Bao, X.; Weng, X.; Bai, X.; Feng, Y.; Huang, J.; Liu, S.; Jia, H.; Yu, B. The protective effect of quercetin on macrophage pyroptosis via TLR2/Myd88/NF-κB and ROS/AMPK pathway. *Life Sci.* **2022**, *291*, 120064. [CrossRef]
40. Tang, J.; Diao, P.; Shu, X.; Li, L.; Xiong, L. Quercetin and Quercitrin Attenuates the Inflammatory Response and Oxidative Stress in LPS-Induced RAW264.7 Cells: In Vitro Assessment and a Theoretical Model. *BioMed Res. Int.* **2019**, *2019*, 7039802. [CrossRef]
41. Wang, C.P.; Shi, Y.W.; Tang, M.; Zhang, X.C.; Gu, Y.; Liang, X.M.; Wang, Z.W.; Ding, F. Isoquercetin Ameliorates Cerebral Impairment in Focal Ischemia Through Anti-Oxidative, Anti-Inflammatory, and Anti-Apoptotic Effects in Primary Culture of Rat Hippocampal Neurons and Hippocampal CA1 Region of Rats. *Mol. Neurobiol.* **2017**, *54*, 2126–2142. [CrossRef] [PubMed]
42. Song, J.; Du, G.; Wu, H.; Gao, X.; Yang, Z.; Liu, B.; Cui, S. Protective effects of quercetin on traumatic brain injury induced inflammation and oxidative stress in cortex through activating Nrf2/HO-1 pathway. *Restor. Neurol. Neurosci.* **2021**, *39*, 73–84. [CrossRef] [PubMed]
43. Yang, T.; Kong, B.; Gu, J.W.; Kuang, Y.Q.; Cheng, L.; Yang, W.T.; Xia, X.; Shu, H.F. Anti-apoptotic and anti-oxidative roles of quercetin after traumatic brain injury. *Cell Mol. Neurobiol.* **2014**, *34*, 797–804. [CrossRef]
44. Li, X.; Wang, H.; Gao, Y.; Li, L.; Tang, C.; Wen, G.; Yang, Y.; Zhuang, Z.; Zhou, M.; Mao, L.; et al. Quercetin induces mitochondrial biogenesis in experimental traumatic brain injury via the PGC-1α signaling pathway. *Am. J. Transl. Res.* **2016**, *8*, 3558–3566. [PubMed]
45. Li, X.; Wang, H.; Gao, Y.; Li, L.; Tang, C.; Wen, G.; Zhou, Y.; Zhou, M.; Mao, L.; Fan, Y. Protective Effects of Quercetin on Mitochondrial Biogenesis in Experimental Traumatic Brain Injury via the Nrf2 Signaling Pathway. *PLoS ONE* **2016**, *11*, e0164237. [CrossRef] [PubMed]
46. Qu, X.; Qi, D.; Dong, F.; Wang, B.; Guo, R.; Luo, M.; Yao, R. Quercetin improves hypoxia-ischemia induced cognitive deficits via promoting remyelination in neonatal rat. *Brain Res.* **2014**, *1553*, 31–40. [CrossRef]
47. Wang, Y.Y.; Chang, C.Y.; Lin, S.Y.; Wang, J.D.; Wu, C.C.; Chen, W.Y.; Kuan, Y.H.; Liao, S.L.; Wang, W.Y.; Chen, C.J. Quercetin protects against cerebral ischemia/reperfusion and oxygen glucose deprivation/reoxygenation neurotoxicity. *J. Nutr. Biochem.* **2020**, *83*, 108436. [CrossRef]
48. Zhang, L.L.; Zhang, H.T.; Cai, Y.Q.; Han, Y.J.; Yao, F.; Yuan, Z.H.; Wu, B.Y. Anti-inflammatory Effect of Mesenchymal Stromal Cell Transplantation and Quercetin Treatment in a Rat Model of Experimental Cerebral Ischemia. *Cell Mol. Neurobiol.* **2016**, *36*, 1023–1034. [CrossRef]
49. Khan, A.; Ali, T.; Rehman, S.U.; Khan, M.S.; Alam, S.I.; Ikram, M.; Muhammad, T.; Saeed, K.; Badshah, H.; Kim, M.O. Neuroprotective Effect of Quercetin Against the Detrimental Effects of LPS in the Adult Mouse Brain. *Front. Pharm.* **2018**, *9*, 1383. [CrossRef]
50. Josiah, S.S.; Famusiwa, C.D.; Crown, O.O.; Lawal, A.O.; Olaleye, M.T.; Akindahunsi, A.A.; Akinmoladun, A.C. Neuroprotective effects of catechin and quercetin in experimental Parkinsonism through modulation of dopamine metabolism and expression of IL-1β, TNF-α, NF-κB, IκKB, and p53 genes in male Wistar rats. *Neurotoxicology* **2022**, *90*, 158–171. [CrossRef]

51. Zhang, Q.; Song, W.; Zhao, B.; Xie, J.; Sun, Q.; Shi, X.; Yan, B.; Tian, G.; Liang, X. Quercetin Attenuates Diabetic Peripheral Neuropathy by Correcting Mitochondrial Abnormality via Activation of AMPK/PGC-1α Pathway in vivo and in vitro. *Front. Neurosci.* **2021**, *15*, 636172. [CrossRef] [PubMed]
52. Espinosa-Juárez, J.V.; Jaramillo-Morales, O.A.; Déciga-Campos, M.; Moreno-Rocha, L.A.; López-Muñoz, F.J. Sigma-1 receptor antagonist (BD-1063) potentiates the antinociceptive effect of quercetin in neuropathic pain induced by chronic constriction injury. *Drug. Dev. Res.* **2021**, *82*, 267–277. [CrossRef] [PubMed]
53. Komirishetty, P.; Areti, A.; Gogoi, R.; Sistla, R.; Kumar, A. Combination strategy of PARP inhibitor with antioxidant prevent bioenergetic deficits and inflammatory changes in CCI-induced neuropathy. *Neuropharmacology* **2017**, *113*, 137–147. [CrossRef]
54. Muto, N.; Matsuoka, Y.; Arakawa, K.; Kurita, M.; Omiya, H.; Taniguchi, A.; Kaku, R.; Morimatsu, H. Quercetin Attenuates Neuropathic Pain in Rats with Spared Nerve Injury. *Acta Med. Okayama* **2018**, *72*, 457–465. [CrossRef] [PubMed]
55. Ye, G.; Lin, C.; Zhang, Y.; Ma, Z.; Chen, Y.; Kong, L.; Yuan, L.; Ma, T. Quercetin Alleviates Neuropathic Pain in the Rat CCI Model by Mediating AMPK/MAPK Pathway. *J. Pain Res.* **2021**, *14*, 1289–1301. [CrossRef] [PubMed]
56. Fan, H.; Tang, H.B.; Shan, L.Q.; Liu, S.C.; Huang, D.G.; Chen, X.; Chen, Z.; Yang, M.; Yin, X.H.; Yang, H.; et al. Quercetin prevents necroptosis of oligodendrocytes by inhibiting macrophages/microglia polarization to M1 phenotype after spinal cord injury in rats. *J. Neuroinflam.* **2019**, *16*, 206. [CrossRef] [PubMed]
57. Jiang, W.; Huang, Y.; Han, N.; He, F.; Li, M.; Bian, Z.; Liu, J.; Sun, T.; Zhu, L. Quercetin suppresses NLRP3 inflammasome activation and attenuates histopathology in a rat model of spinal cord injury. *Spinal Cord.* **2016**, *54*, 592–596. [CrossRef]
58. Qiu, J.; Yang, X.; Wang, L.; Zhang, Q.; Ma, W.; Huang, Z.; Bao, Y.; Zhong, L.; Sun, H.; Ding, F. Isoquercitrin promotes peripheral nerve regeneration through inhibiting oxidative stress following sciatic crush injury in mice. *Ann. Transl. Med.* **2019**, *7*, 680. [CrossRef]
59. Türedi, S.; Yuluğ, E.; Alver, A.; Bodur, A.; İnce, İ. A morphological and biochemical evaluation of the effects of quercetin on experimental sciatic nerve damage in rats. *Exp. Med.* **2018**, *15*, 3215–3224. [CrossRef]
60. Wang, W.; Huang, C.Y.; Tsai, F.J.; Tsai, C.C.; Yao, C.H.; Chen, Y.S. Growth-promoting effects of quercetin on peripheral nerves in rats. *Int. J. Artif. Organs* **2011**, *34*, 1095–1105. [CrossRef]
61. Wang, Y.; Li, W.; Wang, M.; Lin, C.; Li, G.; Zhou, X.; Luo, J.; Jin, D. Quercetin reduces neural tissue damage and promotes astrocyte activation after spinal cord injury in rats. *J. Cell Biochem.* **2018**, *119*, 2298–2306. [CrossRef] [PubMed]
62. Wang, X.; Wang, Y.Y.; Zhang, L.L.; Li, G.T.; Zhang, H.T. Combinatory effect of mesenchymal stromal cells transplantation and quercetin after spinal cord injury in rat. *Eur. Rev. Med. Pharm. Sci.* **2018**, *22*, 2876–2887. [CrossRef]
63. Wang, Y.; Xiong, M.; Wang, M.; Chen, H.; Li, W.; Zhou, X. Quercetin promotes locomotor function recovery and axonal regeneration through induction of autophagy after spinal cord injury. *Clin. Exp. Pharm. Physiol.* **2021**, *48*, 1642–1652. [CrossRef] [PubMed]
64. Chen, M.M.; Qin, J.; Chen, S.J.; Yao, L.M.; Zhang, L.Y.; Yin, Z.Q.; Liao, H. Quercetin promotes motor and sensory function recovery following sciatic nerve-crush injury in C57BL/6J mice. *J. Nutr. Biochem.* **2017**, *46*, 57–67. [CrossRef] [PubMed]
65. Song, Y.; Liu, J.; Zhang, F.; Zhang, J.; Shi, T.; Zeng, Z. Antioxidant effect of quercetin against acute spinal cord injury in rats and its correlation with the p38MAPK/iNOS signaling pathway. *Life Sci.* **2013**, *92*, 1215–1221. [CrossRef]
66. Basso, D.M.; Beattie, M.S.; Bresnahan, J.C. A sensitive and reliable locomotor rating scale for open field testing in rats. *J. Neurotrauma* **1995**, *12*, 1–21. [CrossRef]
67. Huang, T.T.; Zou, Y.; Corniola, R. Oxidative stress and adult neurogenesis–effects of radiation and superoxide dismutase deficiency. *Semin. Cell Dev. Biol.* **2012**, *23*, 738–744. [CrossRef]
68. Pong, K. Oxidative stress in neurodegenerative diseases: Therapeutic implications for superoxide dismutase mimetics. *Expert Opin. Biol* **2003**, *3*, 127–139. [CrossRef]
69. Kleindienst, A.; Hesse, F.; Bullock, M.R.; Buchfelder, M. The neurotrophic protein S100B: Value as a marker of brain damage and possible therapeutic implications. *Prog. Brain Res.* **2007**, *161*, 317–325. [CrossRef]
70. Li, D.; Liu, X.; Liu, T.; Liu, H.; Tong, L.; Jia, S.; Wang, Y.F. Neurochemical regulation of the expression and function of glial fibrillary acidic protein in astrocytes. *Glia* **2020**, *68*, 878–897. [CrossRef]
71. Yang, Z.; Wang, K.K. Glial fibrillary acidic protein: From intermediate filament assembly and gliosis to neurobiomarker. *Trends Neurosci.* **2015**, *38*, 364–374. [CrossRef]
72. Kovacs, G.G. Cellular reactions of the central nervous system. *Handb. Clin. Neurol.* **2017**, *145*, 13–23. [CrossRef] [PubMed]
73. Kuhn, S.; Gritti, L.; Crooks, D.; Dombrowski, Y. Oligodendrocytes in Development, Myelin Generation and Beyond. *Cells* **2019**, *8*, 1424. [CrossRef] [PubMed]
74. Ortiz, A.d.C.; Fideles, S.O.M.; Pomini, K.T.; Bellini, M.Z.; Pereira, E.d.S.B.M.; Reis, C.H.B.; Pilon, J.P.G.; de Marchi, M.Â.; Trazzi, B.F.d.M.; da Silva, W.S.; et al. Potential of Fibrin Glue and Mesenchymal Stem Cells (MSCs) to Regenerate Nerve Injuries: A Systematic Review. *Cells* **2022**, *11*, 221. [CrossRef] [PubMed]
75. Buchaim, R.L.; Andreo, J.C.; Barraviera, B.; Ferreira Junior, R.S.; Buchaim, D.V.; Rosa Junior, G.M.; de Oliveira, A.L.; de Castro Rodrigues, A. Effect of low-level laser therapy (LLLT) on peripheral nerve regeneration using fibrin glue derived from snake venom. *Injury* **2015**, *46*, 655–660. [CrossRef] [PubMed]

76. Rosso, M.P.d.O.; Buchaim, D.V.; Kawano, N.; Furlanette, G.; Pomini, K.T.; Buchaim, R.L. Photobiomodulation Therapy (PBMT) in Peripheral Nerve Regeneration: A Systematic Review. *Bioengineering* **2018**, *5*, 44. [CrossRef] [PubMed]
77. Araujo, T.; Andreo, L.; Tobelem, D.D.C.; Silva, T.; Malavazzi, T.C.D.S.; Martinelli, A.; Lemes, B.; Fernandes, K.P.S.; Bussadori, S.K.; Mesquita-Ferrari, R.A. Effects of systemic vascular photobiomodulation using LED or laser on sensory-motor recovery following a peripheral nerve injury in Wistar rats. *Photochem. Photobiol. Sci.* **2022**, *in press*. [CrossRef] [PubMed]

antioxidants

MDPI

Review

Bioactive Compounds of Citrus Fruits: A Review of Composition and Health Benefits of Carotenoids, Flavonoids, Limonoids, and Terpenes

Ramesh Kumar Saini [1], Arina Ranjit [2], Kavita Sharma [2], Parchuri Prasad [3], Xiaomin Shang [4], Karekal Girinur Mallikarjuna Gowda [5] and Young-Soo Keum [1,*]

[1] Department of Crop Science, Konkuk University, Seoul 143-701, Korea; saini1997@konkuk.ac.kr
[2] Biomedical and Pharmaceutical Sciences, Kasiska Division of Health Sciences, College of Pharmacy, Pocatello, ID 83209, USA; arinaranjit@isu.edu (A.R.); sharkum2@isu.edu (K.S.)
[3] Institute of Biological Chemistry, Washington State University, Pullman, WA 99164, USA; prasad.parchuri@wsu.edu
[4] Jilin Provincial Key Laboratory of Nutrition and Functional Food, Jilin University, Changchun 130062, China; xmshang@jlu.edu.cn
[5] Department of Biochemistry, Padmashree Institute of Management and Sciences, Bengaluru 560060, India; mallikarjunagowda367@gmail.com
* Correspondence: rational@konkuk.ac.kr

Abstract: The increased consumption of fruits, vegetables, and whole grains contributes to the reduced risk of many diseases related to metabolic syndrome, including neurodegenerative diseases, cardiovascular disease (CVD), diabetes, and cancer. Citrus, the genus *Citrus* L., is one of the most important fruit crops, rich in carotenoids, flavonoids, terpenes, limonoids, and many other bioactive compounds of nutritional and nutraceutical value. Moreover, polymethoxylated flavones (PMFs), a unique class of bioactive flavonoids, abundantly occur in citrus fruits. In addition, citrus essential oil, rich in limonoids and terpenes, is an economically important product due to its potent antioxidant, antimicrobial, and flavoring properties. Mechanistic, observational, and intervention studies have demonstrated the health benefits of citrus bioactives in minimizing the risk of metabolic syndrome. This review provides a comprehensive view of the composition of carotenoids, flavonoids, terpenes, and limonoids of citrus fruits and their associated health benefits.

Keywords: orange; mandarin; polymethoxylated flavones (PMFs); nobiletin; essential oil; β-citraurin; limonene; metabolic syndrome; neurodegenerative diseases; cardiovascular disease (CVD)

1. Introduction

Mechanistic, observational, and intervention studies have shown that increased consumption of fruits, vegetables, and whole grains contributes to the reduced risk of many diseases related to metabolic syndrome, including neurodegenerative diseases, cardiovascular disease (CVD), type 2 diabetes, and cancer [1,2]. These diseases are primarily associated with systemic and low-grade chronic inflammation prompted by oxidative stress. The bioactive compounds present in fruits, vegetables, and whole grains prevent the oxidative damage of cells by detoxifying the free radicals, thus minimizing the incidence of such diseases [3].

Citrus, the genus *Citrus* L. of the family Rutaceae, subfamily Aurantioideae [4], is one of the most important fruit crops, including pomelo, sweet orange, sour, lemon, lime, citron, grapefruit, kumquat, and hybrids [5,6]. The citrus fruit species widely investigated for their bioactive composition and their health benefits are listed in Table 1.

Table 1. The list of citrus fruit species widely investigated for their composition of bioactive compounds and their health benefits.

Botanical Name	Common Name
C. aurantifolia (Christm.) Swingle or *C.* × *lumia* Risso. & Poit.	Lime, key lime, lumy, ancient Mediterranean citrus
C. × *aurantium* L.	Bitter/sour orange
C. × *clementina*	Clementine
C. × *deliciosa* Tanore	Montenegrin mandarin
C. japonica Thunb.	Kumquat
C. junos Siebold ex Tanaka	Junos, yuzu
C. × *latifolia* (Yu.Tanaka) Tanaka	Persian lime
C. limon (L.) Osbeck)	Lemon
C. × *limonia* Osbeck	Rangpur lime
C. maxima (J. Burman) Merr. or *C. grandis* (L.) Osbeck	Pomelo, pummelo
C. medica L.	Citron, finger citron
C. poonensis Hort. ex Tanaka	Ponkan
C. × *paradisi* Macfad. or *C.* × *paradise* Macfad	Grapefruit, pink/white grapefruit
C. reticulata × *C. paradisi*	Tangelo
C. reticulata Blanco	Mandarin, tangerine, Phlegraean mandarin, ougan
C. reticulata × *C. sinensis*	Tangor
C. × *sinensis* (L.) Osbeck	Orange, Valencia orange, blood orange, sweet orange
C. unshiu Marc.	Satsuma mandarin, Mandarin orange

Southeast Asia, especially the Yunnan province of Southwest China, Myanmar, and Northeastern India in the Himalayan foothills, is generally considered the origin of *Citrus* [4]. Citrus plants are now widely cultivated in the tropical and subtropical areas of the world, especially China, followed by Brazil and the European Union, with annual production of approximately 102 million tons [7]. Oranges account for half of the production/exports, followed by tangerines/mandarins (one third of total citrus production), lemons/limes (≈8%), and grapefruit (≈7%) [7].

The *Citrus* genus is popular worldwide because of its pleasant flavor and richness of bioactive and nutrients. Citrus fruits are an excellent source of bioactive compounds [3], mainly phenolic compounds (flavonoids, phenolic acids, and coumarins), terpenoids (limonoids and carotenoids), and pectin [5,8,9]. In addition, citrus fruits are rich in nutrients, such as ascorbic acid (vitamin C), tocopherols and tocotrienols (vitamin E), and minerals (selenium, zinc, copper, iron, and manganese) [3,5,8].

Several outstanding reviews have recently been published on citrus' bioactive composition and health benefits (Table 2), centering primarily on flavonoids and essential oil (terpenes and limonoids). However, a comprehensive review of all major bioactive components of citrus fruits is lacking. Thus, this review provides a comprehensive view of the composition of flavonoids, carotenoids, terpenes, and limonoids of citrus fruits and their associated health benefits. Most importantly, this review highlights the significant recent advancement in this area.

Table 2. List of recently published outstanding reviews on composition and health benefits of citrus bioactive compounds.

Compounds	Review Highlights	Reference
Essential oil	Extraction, purification, detection methods, composition, and applications of citrus essential oil	[10]
	Composition of volatile compounds from peel, leaves, and flowers of different citrus species	[11]
Flavanones (hesperidin and naringin)	The intestinal fate, bioavailability, intestinal metabolism, and interaction with the gut microbiota	[12]
Flavones	Sources, antioxidant, anti-inflammatory, antimicrobial, anticancer properties	[13]
Flavonoids	Chemistry, biosynthesis, composition, extraction techniques, health benefits, and industrial applications	[14]
	Composition, antioxidant evaluation, and regulation of Nrf2-Keap1 pathway by citrus flavonoids	[15]
	Role of citrus flavonoids in brain health: evidence from preclinical and human studies	[16]
	Biosynthesis, location, and distribution of flavonoids in citrus plants, factors affecting biosynthesis, and health-promoting properties	[17]
	In vitro, in vivo, and human studies of citrus flavonoids in minimizing the incidence of inflammatory bowel disease	[18]
	Antidiabetic potential of 19 citrus flavonoids, including diosmin, hesperidin, hesperetin, naringin, naringenin, nobiletin, neohesperidin, quercetin, rutin, and tangeretin	[19]
	Therapeutic potential in diabetes and diabetic cardiomyopathy, endothelial dysfunction, atherosclerosis, and platelet function	[20]
	Chemistry, metabolism, bioavailability, biotransformation and delivery systems, and health benefits	[6]
Hesperidin and vitamin C	Antiviral properties against acute respiratory syndrome coronavirus 2 (SARS-CoV-2)	[21]
Naringenin	Antidiabetic properties; in vitro, in vivo, and human studies	[22]
	Combating oxidative stress disorders: cardiovascular disease, diabetes mellitus, neurodegenerative disease, pulmonary disease, cancer, and nephropathy	[23]
Nobiletin	Beneficial effects against Alzheimer's disease (AD) and Parkinson's disease (PD)	[24]
Nobiletin, 5-demethylnobiletin, and derivatives	Beneficial effects against colon cancer, pharmacokinetics, and bioavailability	[25]
Nutrients and bioactive	Description of the genus *Citrus*, the composition of nutrients and bioactive components, and biological activities of lemon extract and essential oil	[26]
	Nutrients (proteins, lipids, vitamins, minerals, fiber) and bioactive (flavonoids, essential oil, limonoids, carotenoids, synephrine) content, their structural characteristics, and health benefits	[5]
Polymethoxyflavones (PMF)	Biological properties against metabolic disorder, atherosclerosis, inflammation, neuroinflammation, cancer, and oxidation	[27]

2. Literature Search Methodology

Available electronic databases, especially Web of Science, PubMed, and Google Scholar, were searched for studies (review or experimental) that analyzed the composition of bioactive compounds in citrus fruits and their health benefits (in vitro, in vivo, and epidemiological). The primary search keywords were: (1) **Citrus** (title) and **antioxidants** (topic) or **health** (topic) and (2) **Citrus** (title) and **bioactive** (topic) or **health** (topic). The other keywords were: (1) **Citrus** (title) and **flavonoid** (title) or **health** (topic); (2) **Citrus** (title) and **carotenoids** (title) or **health** (topic); (3) **Citrus** (title) and **essential oil** (title) or **health** (topic); (4) **Citrus** (title) and **essential oil** (title) or **health** (topic); (5) **Fruits** (title) and **health** (topic); and (6) **Diet** (title) and **health** (topic). The relevant 320 articles were downloaded; they had been published mostly between 2018 and 2022. A total of 135 articles, including 128 published in the years 2022 (02), 2021 (37), 2020 (35), and 2019 (30), are discussed in this review.

3. Bioactive Compounds of Citrus Fruits

3.1. Flavonoids

Flavonoids, a significant contributor of antioxidant components within the human diet, are a class of polyphenolic secondary metabolites widely found in plants. Chemically, flavonoids are composed of a 15-carbon skeleton (C6-C3-C6) with two six-carbon phenyl rings joined by a heterocyclic ring containing the embedded oxygen. According to the substitution patterns of a heterocyclic ring, flavonoids can be divided into subgroups, such as flavones, flavonols, flavanones, flavanonols, flavanols (flavan-3-ols), isoflavones, and anthocyanins. Citrus fruits contain a substantial amount of flavanone-7-O-glycosides (e.g., naringin, eriocitrin, hesperidin, and narirutin), flavones (e.g., rhoifolin, vitexin, diosmin), polymethoxylated flavones (PMFs, e.g., nobiletin, tangeritin, and 5-demethyl nobiletin), flavonols (quercetin, rutin, and kaempferol), and anthocyanin (cyanidin and peonidin glucosides) [28–31] (Figure 1).

PMFs are a unique class of bioactive flavonoids with more than two methoxyl (–OCH_3) groups on their chemical skeletons, and they abundantly occur in citrus fruits [29]. PMFs have attracted growing interest in recent years due to their anti-inflammatory [32], anti-atherosclerosis [33], anti-obesity [34,35], and anti-cancer properties [36]. Moreover, de-methylated PMFs, a product of fruit metabolism, chemical reactions during the drying process, and human metabolism, possess greater anticancer and anti-inflammatory activities than their corresponding methylated counterparts [37].

Deng et al. [38] isolated 11 flavonoids from (*cv.* Shatianyu) pulp; among them, naringin and rhoifolin showed the highest oxygen radical absorbance capacity (ORAC) activity. However, melitidin, bergamjuicin, and naringin were the major contributors to the ORAC activity in flavonoid extracts. In the albedo (inner layer) of ancient Mediterranean citrus fruit, flavonoids occupied 89.34% of polyphenolic fractions, dominated by flavanones eriocitrin and hesperidin as significant components, which accounted for 52.81% and 31.31% of the total flavonoids, respectively [30].

Citrus fruits contain the highest amount of flavonoids during the middle stages (60–80 days after pollination (DAP)) of development, and a decrease during complete maturation, probably due to the high expression of *Chalcone synthase-1* (*CHS-1*) and *chalcone isomerase*, the rate-limiting enzymes in flavonoid biosynthesis [28,39,40]. In contrast, hesperidin peaked at the last developmental stage in the juice sacs of lemon (*cv.* Akragas) [41]. Moreover, the citrus fruit peel flavedo (outer layer) and the albedo contain more flavonoids than the juice sacs [41]. Among the 116 citrus accessions screened by Peng et al. [28], the highest amounts of PMFs, especially OCH_3-PMFs (nobiletin and tangeritin), were recorded in loose-skin mandarins (including mandarins and tangerines) and their hybrids, followed by tangelo (*C. reticulata* × *C. paradisi*), sweet orange, junos, Rangpur lime, sour orange, and grapefruit [28]. Interestingly, the content of nobiletin, 5-demethylnobiletin, and tangeritin increased during the maturation and reached the highest at 60 DAP and decreased again (60–210 DAP). In the Persian lime, the highest amounts of flavanones (hes-

peridin, 2005 μg/g; eriocitrin, 1171 μg/g; and narirutin, 1207 μg/g) and flavones (disomin, 366 μg/g; rhoifolin, 285 μg/g; and vitexin, 237 μg/g) were recorded at 12 weeks of growth and found to reduce at complete maturity (16 weeks). In contrast, in this study, the contents of flavanols (rutin and quercetin) were found to be highest at five weeks of maturation.

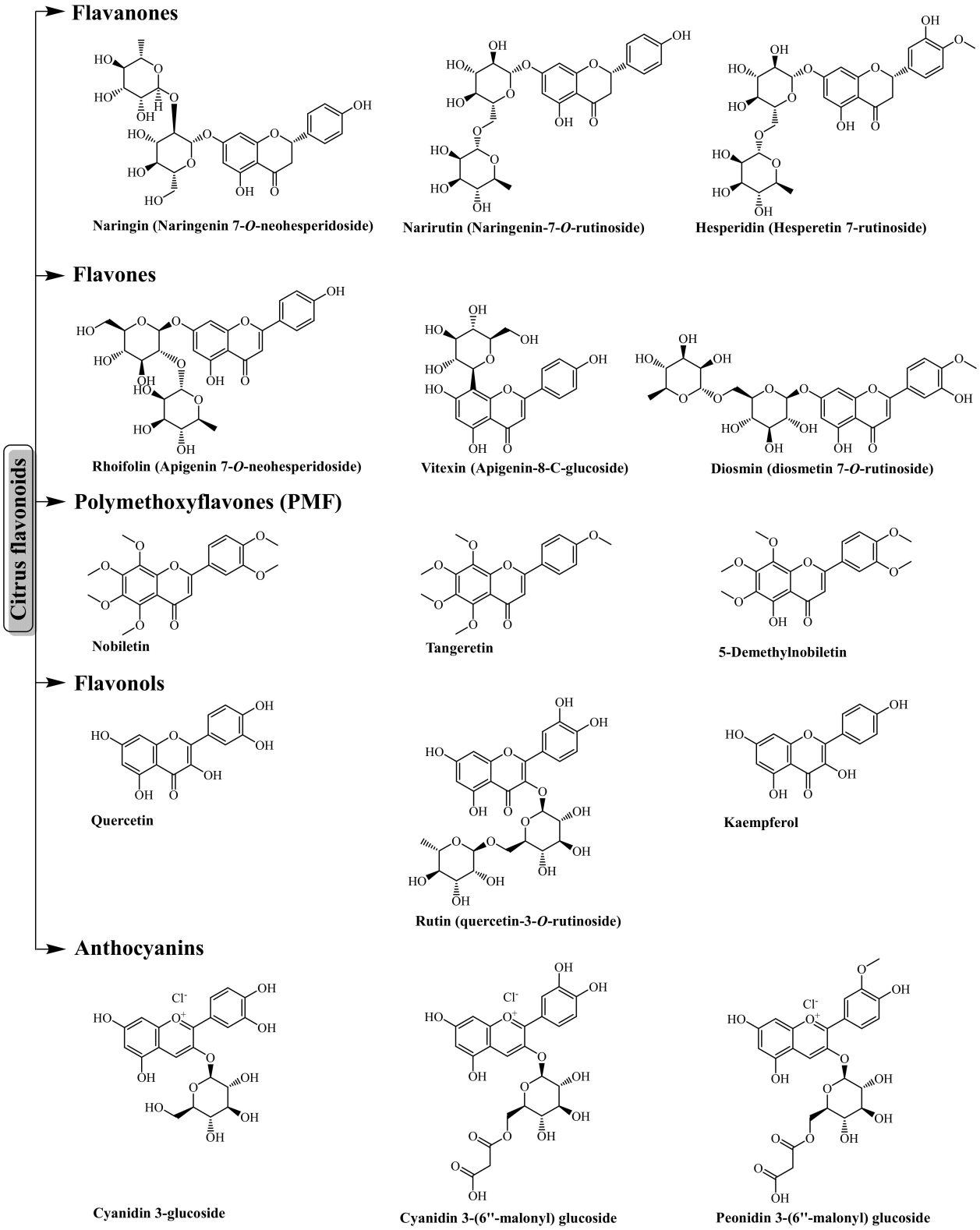

Figure 1. The major flavonoids of citrus fruits.

In a comparative study, the highest amounts of total phenolic compounds were recorded in the albedo of unripe sweet orange (*cv*. Washington navel, 10910 mg kg^{-1} DW) and accounted for 50% of the cumulative content (flavedo + albedo + juice sacs), followed by orange (*cv*. Tarocco) flavedo, lemon (*cv*. Akragas) flavedo, and pummelo (*cv*. Chandler) albedo of unripe stages [41]. In this study, in the juice sacs of ripened fruits, flavanone hesperidin was the dominating phenolic compound in lemon (2213 mg/kg DW) and oranges (1957 and 1975 mg/kg DW in Washington novel and Tarocco, respectively), whereas flavanone narirutin was the most prevalent in pummelo (292 mg/kg DW). A significant amount of flavanone eriocitrin was recorded from lemon (913 mg/kg DW).

In the fruit pulp of Sanguinello and Tarocco blood oranges, hesperidin (78–143 mg/100 g) dominated, followed by narirutine (37.0–93.0 mg/100 g) and quercetin (28.1–42 mg/100 g) [8]. In addition, in this study, cyanidin 3-(6″-malonylglucoside) and cyanidin 3-glucoside were detected in the fruit pulp.

3.2. Carotenoids and Apocarotenoids

Carotenoids are a ubiquitous class of isoprenoid pigments involved in photosynthesis and signaling [42,43]. Based on their chemical structure, the carotenoids are divided into two major groups: (a) carotenes—the hydrocarbon carotenoids, such as α- and β-carotene, and lycopene; (b) xanthophylls—oxygenated derivatives of hydrocarbon carotenoids, such as neoxanthin, violaxanthin, lutein, and β-cryptoxanthin [42,43]. The oxygenated functional groups of xanthophylls can be esterified with fatty acids, and thus found in free or fatty acid esterified forms, while, due to the simple hydrocarbon structure, carotenes are found only in free form (no esterification possible due to the absence of oxygenated functions groups). In citrus fruits, xanthophylls are commonly acylated with saturated and unsaturated fatty acids, including caprate (C10:0), laurate (C12:0), myristate (C14:0), palmitate (C16:0), stearate (C18:0), palmitoleate (C16:1), and oleate (C18:1) acyl moieties (Figure 2) [44,45].

Apart from the carotenes and xanthophylls, apocarotenoids are another category of carotenoids. The carotenoid cleavage dioxygenases, i.e., the (CCDs)/9-cis-epoxycarotenoid dioxygenase (NCED)-mediated cleavage of carotenoids, gives rise to ecologically and nutritionally important apocarotenoids [46]. In citrus, β-citraurin is generated from the CCD4b1/CitCCD4-catalyzed asymmetric cleavage (at either position 7, 8 or 7′, 8′) of β-cryptoxanthin or zeaxanthin [47].

The presence of carotenoids and apocarotenoids confers the orange-red color to the peel and pulp of citrus fruits [47]. The carotenoid composition of citrus fruits is dominated by carotenoid fatty acid esters (xanthophyll esters) [44,45]. The occurrence of specific xanthophyll esters and total carotenoids largely depends on the species, maturity stage, and fruit parts [44,45]. For instance, at the fully mature stage, the total carotenoid contents of the flavedo of sweet orange were nine-fold higher (12.6 mg/100 g FW) than those in the pulp (1.4 mg/100 g FW) [45]. In this study, the most abundant carotenoids in the endocarp and flavedo of fully mature oranges were (all-*E*)- and (9*Z*)-violaxanthin, monoesters, and diesters esters carrying caprate, laurate, myristate, palmitate, stearate, palmitoleate, and oleate acyl moieties. The other major carotenoids were (all-*E*)-antheraxanthin, (all-*E*)-lutein, and (all-*E*)-β-carotene. In contrast, in this study, (all-*E*)-violaxanthin, (all-*E*)-lutein, (all-*E*)-α-carotene, and (all-*E*)-β-carotene were also found to be prevalent in the flavedo of fully mature green fruits. Moreover, the esters of β-citraurin were also detected in the flavedo of fully mature oranges.

In the Valencia orange fruit pulp, esters of violaxanthin, antheraxanthin, β-cryptoxanthin, and mutatoxanthin esterified mainly with laurate, myristate, and palmitate as monoesters or diesters are the most dominant carotenoids. Meanwhile, free xanthophylls and carotenes, such as α-, β-, and ζ-carotene, are found in a small amount [44]. In the extracted juice, the natural acidity of the juice catalyzes the isomerization and rearrangement of 5,6-epoxy-carotenoids (e.g., violaxanthin and antheraxanthin) to their respective 5,8-epoxy-carotenoids (e.g., luteoxanthin, mutatoxanthin, auroxanthin) [44]. Although xanthophylls

dominate in the citrus fruits, a substantial amount of lycopene is also found in the red-fleshed pomelo and grapefruit [48,49].

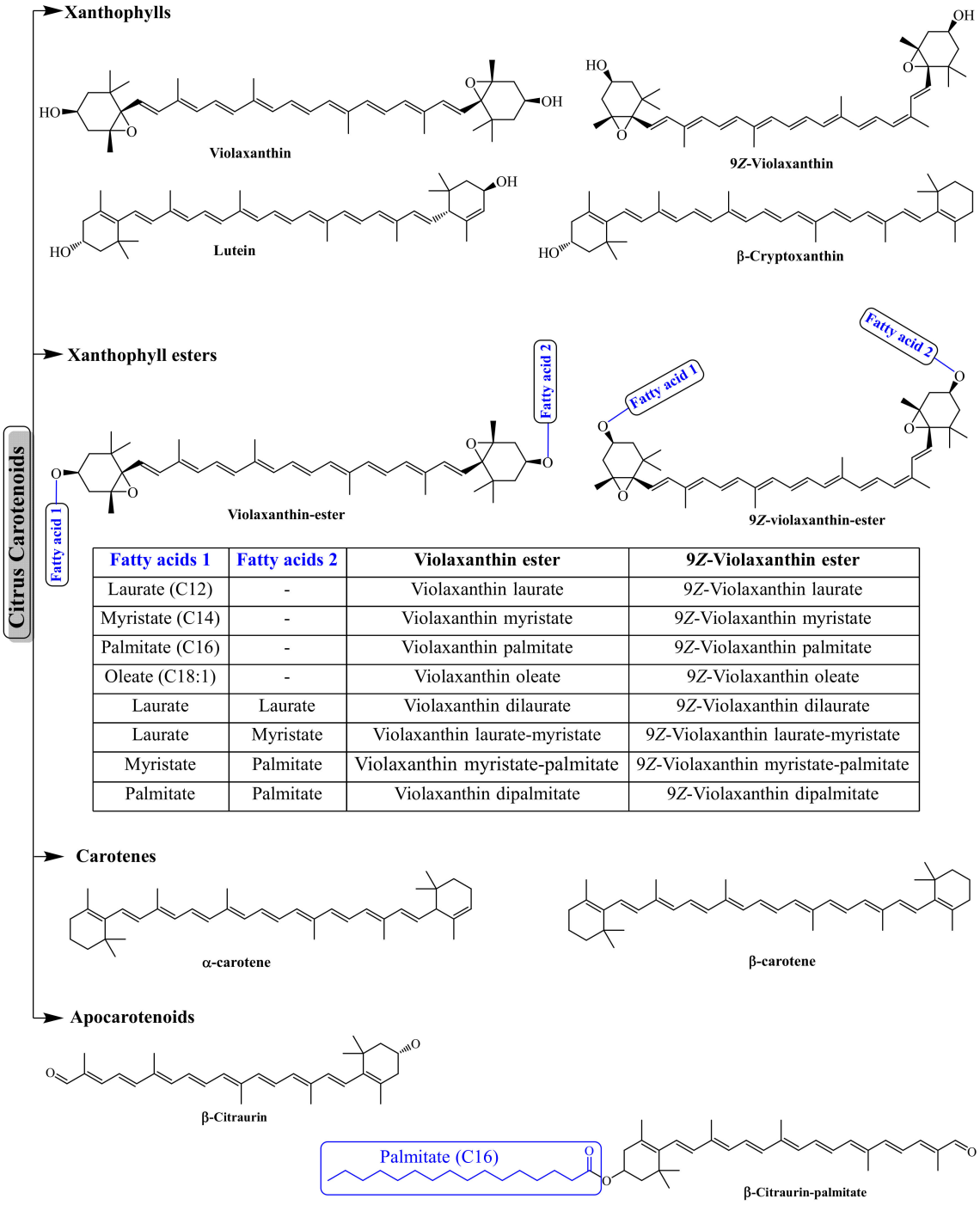

Fatty acids 1	Fatty acids 2	Violaxanthin ester	9Z-Violaxanthin ester
Laurate (C12)	-	Violaxanthin laurate	9Z-Violaxanthin laurate
Myristate (C14)	-	Violaxanthin myristate	9Z-Violaxanthin myristate
Palmitate (C16)	-	Violaxanthin palmitate	9Z-Violaxanthin palmitate
Oleate (C18:1)	-	Violaxanthin oleate	9Z-Violaxanthin oleate
Laurate	Laurate	Violaxanthin dilaurate	9Z-Violaxanthin dilaurate
Laurate	Myristate	Violaxanthin laurate-myristate	9Z-Violaxanthin laurate-myristate
Myristate	Palmitate	Violaxanthin myristate-palmitate	9Z-Violaxanthin myristate-palmitate
Palmitate	Palmitate	Violaxanthin dipalmitate	9Z-Violaxanthin dipalmitate

Figure 2. The major carotenoids and apocarotenoids of citrus fruits.

The β-cryptoxanthin content is commonly used to distinguish mandarins from sweet oranges [50]. In sweet orange (*cv.* 'Pêra'), (9Z)-violaxanthin, and (9′Z)- or (9Z)-antheraxanthin dominate, while it is low in (all-*E*)-β-cryptoxanthin [50]. In contrast, (all-*E*)-β-cryptoxanthin dominates in tangor (*C. reticulata* × *C. sinensis cv.* Murcott), followed by (9Z)-violaxanthin. Interestingly, in this study, the hybrids between *cv.* 'Pêra' (female genitor) and *cv.* 'Murcott' (female genitor) produced several orange-like groups with low β-cryptoxanthin content, and the mandarin-like group contained the highest level of β-cryptoxanthin xanthophyll

(80.6–124.8 μg/g, 25-fold higher than sweet orange and twice that of tangor), suggesting the transgressive segregation of carotenoid biosynthesis.

Similar to the phenolic compounds, the citrus fruit peel flavedo contains a higher amount of carotenoids than the juice sacs [41]. However, unlike phenolic compounds, carotenoid contents increase during maturation [41,50]. In addition, in contrast to phenolic compounds, the albedo contains only a trace amount of carotenoids [41]. In a comparative study among oranges (*cv*. Washington navel and *cv*. Tarocco), lemon (*cv*. Akragas), and pummelo (*cv*. Chandler), the highest amount of total carotenoids was recorded in the flavedo of ripened Washington navel orange (159 mg/kg DW), while, among the juice sacs of ripened fruits, the highest content of total carotenoids was recorded from Tarocco orange (63.7 mg/kg DW). In this study, lutein was the most dominating carotenoid in the juice sacs of the studied fruits, accounting for 83% of the total carotenoids in the juice sacs of Tarocco orange, whereas violaxanthin, antheraxanthin, β-cryptoxanthin, and β-carotene were minor carotenoids.

3.3. Essential Oil (Terpenes and Limonoids)

The essential oil obtained mainly from the flavedo of citrus fruits is an economically important product with beneficial health activities due to the presence of terpenes and limonoids with other bioactive components, including flavonoids, carotenoids, and coumarins [51,52]. The citrus essential oils are widely used in the pharmaceutical, cosmetics, perfumery, and food industries due to their natural fruity perfumes [11,53]. Moreover, citrus essential oils possess potent antioxidant, analgesic, anxiolytic, neuroprotective, and antimicrobial activities [11,54,55]. In particular, bioactive compounds from citrus essential oil are well known for their potential antimicrobial properties, as they cause significant lysis of the bacterial cell wall, intracellular ingredient leakage, and, subsequently, cell death [54]. Due to its potent antimicrobial activities, in recent years, the citrus essential oil has received significant attention as a preservation agent of fruits, vegetables, meat, and processed food products [53].

The monoterpene hydrocarbons (e.g., D-limonene, γ-terpinene, p-cymene, β-phellandrene, β-pinene, δ-3-carene, myrcene), oxygenated monoterpenes (e.g., geranial, nonanal, and (*Z*)-neral), terpene alcohol (e.g., linalool, (*E*)-carveol, (*E*)-verbenol, geraniol, and α-terpineol), sesquiterpenes (e.g., (*Z*)-α-bergamotene), aldehyde (e.g., decanal), and esters (e.g., ethyl cinnamate and ethyl p-methoxycinnamate) are the major chemical constituents of the volatile fractions of citrus essential oil (Figure 3) [5,54]. Moreover, the non-volatile fraction (1 to 15% of cold-pressed citrus essential oil) is mainly composed of fatty acids, long-chain hydrocarbons, sterols, wax, and limonoids (e.g., limonin) [51]. In mandarin/tangerine, grapefruit, orange, citron, and lemon essential oil, D-limonene accounts for nearly 45–90% of the total terpenoids [51,54,56,57]. In lemon and mandarin essential oil, γ-terpinene and β-pinene account for 8–20% and 0.3–11% of the total compounds, respectively [51]. Among the cold-pressed citrus essential oil from lemon, bergamot, sweet orange, clementine, bitter orange, blood orange, mandarin (green, yellow, red), and pink grapefruit, the highest amount of limonin (21.2 mg/L) was recorded from bergamot essential oil, while essential oils from clementine and blood orange presented the lowest (0.5–0.9 mg/L) limonin content [58]. In this study, among the green, yellow, and red mandarin, green mandarin showed four-times higher limonin (4.5 mg/L) than yellow and red mandarin (1.1 mg/L).

In the essential oil obtained from the fruit peel of Montenegrin mandarin, D-limonene and γ-terpinene were the major fractions, with the minor presence of citronellol and β-linalool [59]. Surprisingly, in this study, the presence of these minor components favored the antioxidant activity, while colorectal cancer HT-29 cells' cytotoxicity was significantly decreased. In a comparative study among essential oils obtained from grapefruit, lemon, mandarin, and orange, the highest 2,2′-Azino-bis(3-ethylbenzothiazoline-6-sulfonic acid (ABTS) radical cation reducing activities and ferric reducing antioxidant power (FRAP) was obtained from mandarin essential oil, while lemon essential oil showed the highest

2,2-diphenyl-1-picrylhydrazyl (DPPH) free radical scavenging and cupric ion reducing antioxidant capacity (CUPRAC) [51].

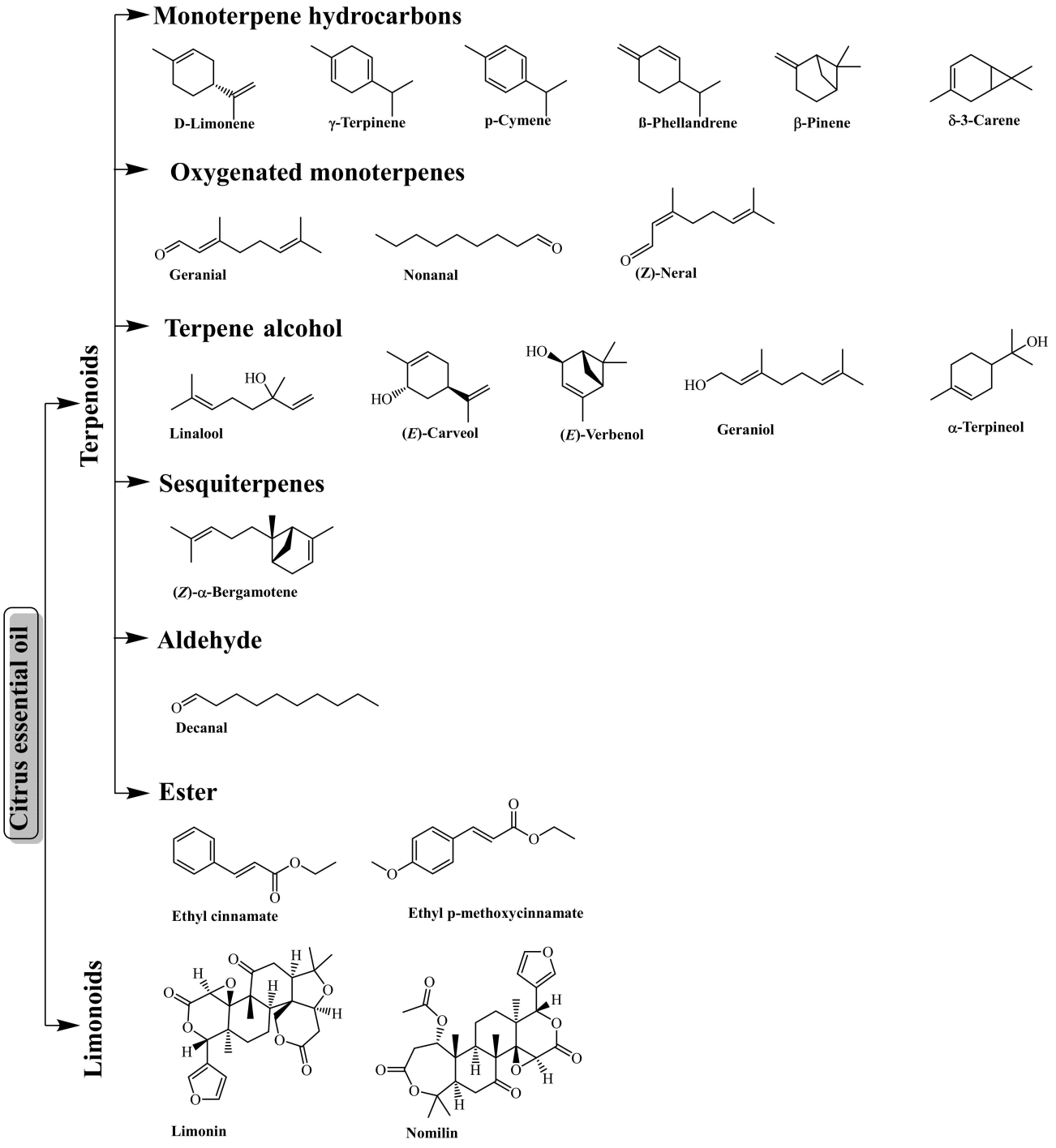

Figure 3. The major bioactive compounds (terpenes and limonoids) of citrus essential oil.

4. Bioactive Compounds of Citrus Fruit Byproducts

The domestic and industrial processing of citrus fruit generates a considerable amount of peel, pulp, and seeds as byproducts, called pomace. A significant amount of research has been conducted to recover the commercially vital compounds from citrus fruit pomace [60–62]. Citrus peel is a rich source of essential oils [63], carotenoids [64–66], pectin [67,68], flavonoids [69–71], and several other bioactive components with excellent

antioxidant [69] and health-promoting potential [62,72–74]. Among the flavonoids, hesperidin, naringin, rutin, and neohesperidin are the major flavonoids found in the peel of citrus fruits [71,74], with especially high amounts in mandarins, which exhibit high antioxidant potency [71]. Surprisingly, the peel of most citrus fruits contains more polyphenols and other antioxidant compounds than edible pulp [65,75]. Therefore, peels from citrus fruits can potentially be used to recover these health-beneficial compounds. Moreover, given the low lignin content, the citrus peel can serve as a promising alternative to lignocellulosic biomass to produce biofuels [76].

Similar to citrus peel, the seeds are rich in nutritionally vital proteins [73], ascorbic acid [65], fatty acids, phytosterols and tocopherols, limonoids, dietary fibers, and flavonoids [65,77]. A comparative study among the seeds, peel, and pulp of fruits of three cultivars of mandarins, including Phlegraean mandarin (*C. reticulata*), kumquat (*C. japonica*), and clementine (*C clementina*), revealed that Phlegraean mandarin is richer in bioactive compounds, including total polyphenols (seeds > peel > pulp), antioxidant activity (seeds > peel > pulp), and ascorbic acid (seeds > peel > pulp) [65].

Hesperidin and narirutin are the major flavonoids of *C. unshiu* peel [78,79]. Using the response surface model (RSM), the optimal extraction temperatures for the semi-continuous subcritical water extraction (SWE) of hesperidin and narirutin from *C. unshiu* peel were predicted as 164.4 °C and 154.6 °C, respectively, with an optimal flow rate of 2.25 mL/min. With these extraction conditions, the predicted yields of hesperidin and narirutin were 45.2 and 8.76 mg/g DW, respectively, corresponding to a recovery rate of 90.4% and 94.4%, respectively. In another study, Hwang et al. [78] optimized the extraction of hesperidin and narirutin from *C. unshiu* peel using SWE aided by pulsed electric field (PEF) treatments. In this study, PEF treatment for 2 min, combined with SWE at 150 °C for 15 min, provided the highest (46.96 mg/g DW) yield of hesperidin, while the narirutin yield was highest (8.76 mg/g DW) after PEF treatment for 2 min, combined with SWE at 190 °C for 5 min.

In view of the above, citrus pomace presents enormous opportunities to recover bioactive compounds and has a wide range of commercial applications in the food, feed, and pharmaceuticals industries. Moreover, the utilization of citrus pomace can create a surplus revenue that can substantially improve the economics of citrus fruit processing.

5. Health Benefits of Citrus Fruit Bioactive Compounds

5.1. In Vitro Studies

5.1.1. Flavonoids

The antioxidant activity of citrus bioactive compounds, especially flavonoids, carotenoids, terpenes, and limonoids, can attenuate oxidative stress-related disorders [80,81]; they thus have potential applications against obesity [82], inflammatory diseases [32,83,84], atherosclerosis [85], neurodegenerative diseases [86–88], and cancer [89,90] (Table 3).

The pancreatic lipase (PL) is a crucial enzyme involved in triglycerides' hydrolysis in the gastrointestinal tract, and its inhibition can ameliorate obesity by minimizing lipid absorption [82]. Hesperidin, neohesperidin, naringin, narirutin, and eriocitrin were found to be the major components in the citrus peel extracts of grapefruit, pomelo, kumquat, mandarin, and ponkan [82]. Interestingly, in this study, among these flavonoids, hesperidin, the most dominant flavonoid in ponkan peel extract, showed the highest pancreatic lipase inhibition activities, suggesting its promising application in managing obesity.

Citrus peel flavonoid nobiletin suppresses the inflammatory response in lipopolysaccharide (LPS)-stimulated RAW264.7 cells by enhancing autophagy through decreasing the levels of inflammatory cytokines (inducible nitric oxide synthase (iNOS) and cyclooxygenase-2 (COX-2)) and activating the Interleukin-6 (IL-6)/signal transducer and activator of transcription 3 (STAT3)/forkhead box O3a (FOXO3a) signal pathway responsible for the induction of macrophage autophagy [32].

Dysregulation of IL-5 secretion by antigen-specific T helper 2 (Th2) cells has been linked to eosinophilic inflammation in asthma [84]. The Th2 cytokine expression is regulated by transcription factors, including the nuclear factor of activated T cells (NFAT) [84].

Moreover, Heme oxygenase-1 (HO-1) expression is known to suppress the asthmatic immune response modulation of phosphoinositide 3-kinase (PI3K)/protein kinase B (AKT), extracellular signal-regulated kinases (ERK)/c-Jun N-terminal kinases (JNK), nuclear factor erythroid 2 related factor 2 (Nrf2), and peroxisome proliferator-activated receptor γ (PPARγ) signaling [84]. Citrus flavonoid gardenin A and hesperidin exhibited a robust suppressive effect on IL-5 secretion by PMA/ionomycin-treated EL-4 murine T-lymphoma cells by downregulating NFAT protein expression [84]. In this study, hesperidin and gardenin A induced HO-1 protein expression and repressed IL-5 production through distinct pathways; hesperidin upregulated HO-1 production via Nrf2 protein expression combined with the activation of the ERK/JNK and PI3K/Akt signaling pathways, whereas gardenin A induced HO-1 expression through the transcription factor PPARγ.

Beyond the health-beneficial effects described above, bioactives present in citrus fruit juices were shown to have direct antiviral activity. Dong et al. [91] mentioned that hesperidin restricted the replication and progression of the Influenza virus in human lung carcinoma A549 cells by upregulating the p38 signaling pathway. Hesperidin, hesperetin, and naringenin were shown to inhibit key proteases involved in coronavirus replication and prevent virus entry into host cells [92–94].

The flavonoids (hesperidin, naringin, tangeritin, and rutin) rich in the hydro-ethanolic extract of *C. reticulata* Blanco peels have shown antiproliferative effects against BT-474 human breast carcinoma [95]. In this study, 500 μg/mL of extract treatment reduced the viability of BT-474 cells by 47% and 60% after 24 or 48 h of treatment, respectively.

5.1.2. Carotenoids

Carotenoids are widely investigated for their anticancer activities [96,97]. Carotenoids are well known for their antioxidant function in the normal cellular environment [42]. However, in cancer cells with an innately high intracellular ROS level, carotenoids may act as potent pro-oxidant molecules and promote ROS-mediated apoptosis [98]. In our study, we have demonstrated that the anticancer activities of β-cryptoxanthin derived from mandarin oranges on human cervical carcinoma (HeLa) cells are mediated through pro-oxidant action, which enhances the ROS generation, followed by the enhanced expression of caspase-3, -7, and -9, Bax, and p-53 at the mRNA, with the concordant suppression of antiapoptotic Bcl-2. These events trigger the nuclear condensation, loss of mitochondrial membrane potential, activation of caspase-3 proteins, and, finally, cleavage of nuclei DNA. In this study, β-cryptoxanthin substantially inhibited the proliferation of HeLa cells, with an IC50 value of 4.5 μM after 24 h of treatment.

5.1.3. Essential Oil (Terpenes and Limonoids)

The lumy essential oil rich in limonene (48.9%) and linalool (18.2%) has been shown to exhibit potent antioxidant and free radical scavenging properties with anti-acetylcholinesterase activities [86]. Moreover, in this study, lumy essential oil showed neuroactive effects by significantly reducing the burst frequency (MBR), assessed by the spontaneous electrical activity of rat cortical neuronal networks.

In the neuronal cells, K^+ imbalance, activation (phosphorylation) of extracellular signal-regulated protein kinase (ERK1), and reactive oxygen species (ROS) production are associated with the progression of Alzheimer's disease (AD) [87]. In addition, the acetylcholinesterase (AChE) enzyme involved in the hydrolysis of acetylcholine plays a vital role in triggering neuropsychiatric symptoms in AD [87]. Limonene has shown protective effects in $A\beta_{1–42}$ oligomer-triggered toxicity in primary cortical neurons (in vitro model of AD) by suppressing the AChE, ROS production, and voltage-gated K^+ channel KV3.4 hyperfunction, and downregulating phosphorylated (p)-ERK [87].

Citrus limonoids (limonexic acid, limonin, and nomilin) have been shown to induce apoptosis and inhibit the proliferation (IC50 values < 50 μM after 72 h) of pancreatic cancer cells Panc-28, by the enhanced cleavage of caspase-3, decreased mitochondrial membrane potential, and upregulation of the expression of B-cell lymphoma 2 (Bcl-2)-associated X

protein (Bax)/Bcl-2 proteins [90]. Moreover, in this study, limonoids upregulated the expression of cyclin-dependent kinase inhibitor (p21) and exhibited anti-inflammatory activity through downregulating the expression of proinflammatory proteins Cox-2, nuclear factor-kappa β (NF-κB), and IL-6.

5.1.4. Other Bioactives

Apart from the flavonoids, carotenoids, terpenes, and limonoids, citrus pectin and coumarin have beneficial health properties [85,99]. For instance, citrus pectin oligosaccharides and their microbial metabolites exhibited anti-atherosclerosis effects on LPS-treated human macrophages by regulating the expression of proinflammatory mediators (TNF-α, IL-6, IL-10, and NF-κB mRNA) [85]. Moreover, in this study, cholesterol efflux was also accelerated by the upregulation of the liver X receptor-α (LXRα) and adenosine triphosphate-binding cassette transporter (ABC) A1 and G1 (ABCG1) mRNA. Furthermore, pectin oligosaccharides repressed cholesterol synthesis by the downregulation of 3-hydroxy-3-methylglutaryl-coenzyme A reductase (HMGCR) mRNA.

The coumarins isolated from pomelo have shown hepatoprotective activities in D-galactosamine-treated normal human hepatic LO2 cells by suppressing the levels of alanine transaminase (ALT) and aspartate transaminase (AST), increasing the activities of antioxidant enzymes, including glutathione peroxidase (GSH-Px) and superoxide dismutase (SOD), and decreasing the level of malondialdehyde (MDA) [99].

Table 3. Health benefits of citrus fruit bioactive compounds demonstrated using in vitro experimental models.

Compounds	Experimental System	Disease Target	Mechanism of Action	Reference
Flavanone-rich mandarin juice extract (0.001–1 mg/mL)	6-hydroxydopamine (6-OHDA)-stimulated SH-SY5Y human neuroblastoma cells	Parkinson's disease (PD)	↓ROS and NO, restored SOD and CAT activity, ↓caspase 3 activity, ↑Bcl-2 mRNA, ↓p53 and Bax mRNA, restored mitochondrial membrane potential, ↓oxidative DNA damage, balanced α-synuclein, LRRK2, parkin, PINK1, and DJ-1 mRNA levels	[88]
Flavanones (10 μM)	Caco-2 cells stimulated with IL-1	Bowel diseases	↓IL-6, IL-8, and NO release	[83]
Hesperetin and gardenin A (5–10 μM)	PMA/ ionomycin-induced EL-4 murine T-lymphoma cell cells	Asthma	↓ROS and IL-5 production, ↓NFAT activity and IL-5 secretion, ↑HO-1 through ↑Nrf2, PPARγ, PI3K/AKT, or ERK/JNK signaling	[84]
Limonene (1–100 mg/mL)	$A\beta_{1-42}$ triggered toxicity in primary cortical neurons	Alzheimer's disease (AD)	↓AchE, ROS production, voltage-gated K+ channel KV3.4 hyperfunction, and phosphorylated ERK	[87]
Limonin, nomilin, and limonexic acid (20–60 μM)	Human pancreatic Panc-28 cells	Cancer (pancreatic)	↓Cell proliferation (IC_{50} values < 50 μm after 72 h), ↑cleavage of caspase-3, mitochondrial membrane potential, ↑Bax/Bcl2 expression, and p21, ↓COX-2, NF-κβ, and IL-6	[90]
Limonoids (Fortunellon and nomilin; 30 μM)	HeLa cells	Cancer (Cervical)	↑Adriamycin-dependent cell death	[89]

Table 3. *Cont.*

Compounds	Experimental System	Disease Target	Mechanism of Action	Reference
Naringenin (62.5–2000 μM)	Human A549 lung epithelial cells and primary human monocyte-derived dendritic cells	Zika virus infection	↓Replication or assembly of viral particles	[100]
Naringin- and hesperidin-rich junos peel extract (0.5 mg/mL)	Human lung basal epithelial NCI-H460 cells exposed to H_2O_2	Oxidative stress-induced diseases	↓p53, cytochrome c, and Bax proteins	[80]
Pectin oligosaccharides (5 mg/mL)	LPS-stimulated human macrophages	Atherosclerosis	↑Immune responses, ↓TNF-α, IL-6, IL-10, and NF-κβ mRNA, ↑cholesterol efflux via LXRα and ABCA1, and ABCG1 pathway, ↓cholesterol synthesis via ↓HMGCR	[85]
Phase-II flavanone metabolites (2–100 μM)	Pancreatic β-cell MIN6 cells exposed to cholesterol	Oxidative stress-induced diseases	↓Oxidative biomarkers (superoxide anion, H_2O_2, and MDA), ↓SOD and GPx, ↑insulin secretion, ↓apoptosis	[81]
PMF nobiletin (10–50 μM)	LPS-stimulated RAW264.7 cells	Inflammatory diseases	↓Release of NO, ↓expression of iNOS and COX-2, ↑autophagy, activation of the IL-6/STAT3/FOXO3a signal pathway	[32]
β-cryptoxanthin from mandarin oranges; IC_{50}—4.5μM (24 h treatment)	HeLa cells	Cancer (cervical)	↓Bcl-2 mRNA, ↑Bax, caspase-3, -7, and -9 mRNA, nuclear condensation and disruption of the integrity of the mitochondrial membrane, activation of caspase-3 proteins, nuclei DNA damage, and apoptosis	[101]

The upregulation and downregulation are denoted by upward (↑) and downward (↓) arrows, respectively. Abbreviations are as follows: ABCA1: adenosine triphosphate-binding cassette transporter subfamily A member 1; ABCG1: adenosine triphosphate-binding cassette transporter subfamily G member 1; AChE: acetylcholinesterase; AKT: protein kinase B; $A\beta_{1–42}$: amyloid β-protein; Bax: B-cell lymphoma 2 (Bcl-2)-associated X protein; Bcl2: B-cell lymphoma 2; CAT: catalase; COX-2: cyclooxygenase-2; DJ: Parkinson disease protein 1; EPO: eosinophil peroxidase; ERK: extracellular signal-regulated kinases; FOXO3a: Forkhead box O3a; GPx: glutathione peroxidase; H_2O_2: hydrogen peroxide; HeLa: human cervical cancer cells; HMGCR: 3-hydroxy-3-methylglutaryl-coenzyme A reductase; HO-1: Heme oxygenase-1; IL: Interleukin; iNOS: inducible nitric oxide synthase; JNK: c-Jun N-terminal kinases; LPS: lipopolysaccharide; LRRK2: leucine-rich repeat kinase 2; LXRα: liver X receptor-α; MDA: malondialdehyde; MPO: myeloperoxidase; NFAT: nuclear factor of activated T cells; NF-κβ: nuclear factor-kappa β; NO: nitric oxide; Nrf2: nuclear factor-erythroid 2 related factor 2; PI3K: phosphoinositide 3-kinase; PINK1: phosphatase and tensin homolog (PTEN)-induced putative kinase 1; PMA: phorbol 12-myristate 13-acetate; PMF: polymethoxylated flavone; PPARγ: peroxisome proliferator-activated receptor γ; ROS: reactive oxygen species; SOD: superoxide dismutase; STAT3: signal transducer and activator of transcription 3; TNF-α: tumor necrosis factor α.

5.2. In Vivo Studies

Excess caloric supply causes chronic hyperlipidemia and hyperglycemia, triggering atherosclerosis, hepatic steatosis, obesity, diabetes, and cardiovascular complications [102–104]. These metabolic diseases are linked to a wide array of metabolic complications [102]. Hyperlipidemia is the condition of disorder of lipid metabolism, resulting in abnormally elevated levels of low-density lipoprotein cholesterol (LDL-c) and very-low-density lipoprotein cholesterol (VLDL-c), triglyceride (TG), and total cholesterol (TC) in the blood, as well as reduced levels of high-density lipoprotein cholesterol (HDL-c) [102]. Similarly, chronic

hyperglycemia is the condition of persistent and unusually high postprandial (after a meal) blood glucose levels, primarily due to the flawed insulin production [104]. Several recent animal studies have demonstrated the beneficial effects of citrus flavonoids, carotenoids, terpenes, limonoids, and other bioactives (e.g., pectin and coumarins) against metabolic syndrome (Table 4). Moreover, the potent antioxidant activities of citrus bioactives have shown protection against primary dysmenorrhea (PD) [105], pulmonary edema [80], cancer [36], and neuropsychiatric [106] and neurodegenerative diseases [107,108].

5.2.1. Flavonoids

The citrus flavonoids are most widely investigated for their antihyperglycemic and antihyperlipidemic effects in animal models [104,108]. Citrus flavonoids, such as hesperetin, have shown potential in attenuating hyperglycemia in streptozotocin (STZ)-induced diabetes in rats by releasing insulin from β cells of islets [104]. In this study, hesperetin supplementation of 40 mg/kg for 45 days showed a significant decrease in plasma glucose levels and a significant increase in the level of plasma insulin. It restored the compromised antioxidant status by increasing the activity of SOD, catalase (CAT), and glutathione peroxidase (GPx). Moreover, in this study, hesperetin alleviated hyperlipidemia by lowering the cholesterol, free fatty acid (FFA), TG, and phospholipid (PL) levels in diabetic rats, probably via the insulin-mediated reduction in the synthesis of fatty acids and cholesterol. Moreover, the authors suggested that the cholesterol-lowering effect of hesperetin is possibly due to the capability of hesperetin and other flavonoids to bind to bile acids, resulting in enhanced bile acid secretion and a reduction in cholesterol absorption [104].

The flavanone aglycones present in fermented/non-fermented ougan (*cv*. Suavissima) juice exhibited anti-obesity properties in high-fat-diet (HFD)-fed C57BL/6J mice by reduced weight gain, decreased fat accumulation, enhanced glucose homeostasis and insulin sensitivity, lowered liver steatosis, enhanced white adipose tissue (WAT) browning, augmented brown adipose tissue (BAT) activity, and increased diversity of gut microbiota [109].

The gastrointestinal microbiota composition plays a vital role in host physiology, nutrition, and metabolism [110]. Changes in the gastrointestinal microbiota composition, the community of pathogenic symbiotic and microorganisms, are probably responsible for the anti-obesity effects of citrus bioactives, especially flavonoids [35,111]. The abundance of gut microbiota, *Firmicutes* over *Bacteroidetes*, is linked to obesity-related metabolic syndrome [35]. Moreover, the gut microbiome's branched-chain amino acid (BCAA) metabolism is considered responsible for metabolic syndrome [35]. It is likely that microbially produced BCAAs, such as imidazole propionate, impair insulin signaling through the activation of mammalian target of rapamycin (mTOR) complex 1 (mTORC1) and P70S6K [35]. Sterol regulatory element-binding proteins (SREBPs) play essential roles in regulating lipid homeostasis via mTOR. An extract rich in PMFs and hydroxy polymethoxyflavones (HOPMFs) (0.5% of HFD for 16 weeks) from citrus peel attenuated the obesity and modulated gut microbiota in male C57BL/6 mice fed a HFD by altering the gut microbiota, by increasing *Prevotella* and decreasing rc4–4 bacteria [111]. In this study, PMFs and HOPMFs alleviated the total body weight, decreased the lipids in 3T3-L1 preadipocytes, and reduced the adipocyte size and adipose tissue weight in the HFD mice. Moreover, in this study, PMFs and HOPMFs decreased the levels of lipid droplets (LD) and perilipin 1 protein and sterol regulatory element-binding protein 1 (SREBP-1) expression. Similarly, in another study, a citrus PMF (nobiletin and tangeretin)-rich extract was shown to ameliorate HFD-induced metabolic syndrome via gut dysbiosis (decreased *Firmicutes*-to-*Bacteroidetes* ratio), and regulated branched-chain amino acid (BCAA) metabolism [35]. In this study, the PMF-rich extract inhibited the phosphorylation of mTOR and P70S6K and decreased the expression of SREBPs in human liver HL-7702 cells and HFD-fed mice. Therefore, the authors hypothesized that the decreased BCAAs by the PMF-rich extract contribute to improving metabolic syndrome by inhibiting the mTOR/P70S6K/SREBP pathway.

Among the four flavanones tested for their anti-atherosclerosis potential in apolipoprotein E-deficient (ApoE$^{-/-}$) mice, naringin showed the most potent anti-atherogenic effect,

followed by hesperidin, naringenin, and hesperetin [33]. In this study, oral naringin admiration alleviated atherosclerosis by enhancing bile acid synthesis. Hesperidin upregulated ABCA1 to enhance cholesterol reverse transport, while the aglycones naringenin and hesperetin inhibited cholesterol synthesis significantly by downregulating 3-hydroxy-3-methyl-glutaryl-coenzyme A reductase (HMGCR).

Dietary administration of 0.05% PMF 5-demethylnobiletin has shown chemopreventive effects against azoxymethane/dextran sulfate sodium (DSS)-driven colorectal carcinogenesis in male CD-1 mice by reduced cell proliferation, increased apoptosis, and decreased mRNA and protein levels of proinflammatory cytokines IL-1β, IL-6, and TNF-α in the colon [36]. In this study, a significant amount of 5-Demethylnobiletin metabolites, namely 5,3′-didemethylnobiletin, 5,4′-didemethylnobiletin, and 5,3′,4′-tridemethylnobiletin, was documented in the colonic mucosa of the treated mice. Surprisingly, these metabolites showed more potent effects than 5-demethylnobiletin on inhibiting the proliferation, inducing cell cycle arrest, and the apoptosis of HCT116 human colorectal cancer cells.

Higher levels of circulating thyroid-stimulating hormone (TSH) are vital for greater longevity [112]. The upregulation of sirtuin 1, which deacetylates transcription factors that contribute to cellular regulation, may positively upregulate the exocytosis of TSH-containing granules [112]. Due to the antioxidant and anti-inflammatory properties, 15 mg/kg body mass (BM) of citrus naringenin has shown increased TSH secretion in 24-month-old male Wistar rats by upregulating the Sirt1 protein expression [112].

Neuroinflammation is also crucial in several neurodegenerative disorders, including Alzheimer's disease (AD) and Parkinson's disease (PD). Due to its antioxidant and anti-inflammatory properties, hesperetin has shown protective effects against LPS-induced neuroinflammation, neuronal apoptosis, oxidative stress, and memory impairments in C57BL/6 N mice via regulating the toll-like receptor 4 (TLR4)/NF-κB signaling pathways [107]. In this study, hesperetin repressed the inflammatory mediators (p-NF-κβ, TNF-α, and IL-1) and ROS/lipid peroxidation, and improved the antioxidant protein levels (Nrf2 and HO-1). Moreover, hesperetin reduced neuronal apoptosis by reducing the expression of Bax, phosphorylated-c-Jun *N*-terminal kinases (p-JNK), and caspase-3 protein and upregulating the Bcl-2 protein level. Moreover, hesperetin prompted the cognition, synaptic integrity, and memory processes by augmenting the postsynaptic density protein-95 (PSD-95), phosphorylated-cAMP response element-binding protein (p-CREB), and Syntaxin.

Hyperglycemia is considered a vital risk factor in developing neurodegenerative disorders, as it is known to promote brain astroglial activation, oxidative stress, inflammation, amyloid-β-accumulation, tau hyperphosphorylation, and memory impairment [108]. Tau hyperphosphorylation induces microtubule dysfunction, leading to the formation of neurofibrillary tangles (NFTs), which are often observed in AD [108]. The citrus auraptene and naringin have shown inhibitory effects against tau hyperphosphorylation, astroglial activation, and recovered the suppression of neurogenesis in the hippocampus of STZ-induced hyperglycemic mice [108].

Chronic inflammation is involved in the etiology of several intestinal disorders, including inflammatory bowel diseases (IBDs), which mainly comprise ulcerative colitis and Crohn's disease [113]. The *C. kawachiensis* peel powder rich in flavonoids (naringin, narirutin, and auraptene) and dietary fiber protected from the DSS-induced intestinal inflammation in a murine model of colitis [113]. In this study, supplementation of peel powder (5% of diet, *w*/*w*) ameliorated the DSS-induced body weight loss, colon shortening, increased expression of pro-inflammatory cytokines (e.g., TNF-α), and decreased expression of colonic tight junctions (TJs) (e.g., occluding).

5.2.2. Carotenoids

The provitamin A carotenoids (e.g., β-cryptoxanthin) from citrus fruits have also shown effectiveness against metabolic syndromes, such as type 2 diabetes [103]. In the body (intestine and liver), provitamin A carotenoids are bio-converted to retinol by the

activities of β-carotene 15,15′-oxygenase (BCO1). In a high-fructose-diet-induced type 2 diabetes model of Wistar male rats, feeding of citrus concentrate containing 0.086 mg β-cryptoxanthin, 5.69 mg hesperidin, and 7.5 mg pectin for eight weeks decreased insulinemia, glycemia, and dyslipidemia by restoring the LDL-c and TG levels to be similar to the healthy group [103]. Moreover, in this study, feeding purified β-cryptoxanthin alone or with a matrix containing hesperidin and pectin showed the synergy between these constituents. Furthermore, in this study, β-cryptoxanthin from citrus fruits was shown to restore the vitamin A status in both control and prediabetic (high-fructose fed) rats; however, prediabetic rats showed lower absorption bioconversion of β-cryptoxanthin into retinoids.

The synergy between carotenoids and flavonoids is probably due to the enhanced uptake of carotenoids in the presence of flavonoid glycosides [114]. In Caco-2 cells, it has been shown that flavanone O-glycosylation (at C_7 of the A ring) led to the highest promoting effect on β-carotene absorption via enhanced paracellular permeability by transient drop-in tight junction (TJ) protein expression, and the upregulation of peroxisome proliferator-activated receptor-gamma (PPARγ) and scavenger receptor class B type I (SR-BI; proteins involved in carotenoid absorption and transport) expression [114].

5.2.3. Essential Oil (Terpenes and Limonoids)

The overproduction of endometrial prostaglandins (PGs), especially prostaglandin F2α (PGF2α) and prostaglandin E2 (PGE2), is considered to be one of the critical factors for the progression of primary dysmenorrhea (PD) [105]. A higher ratio of PGF2α/PGE2 is considered to be a principal indicator of PD [105]. The citrus essential oil, particularly sweet orange essential oil rich in limonene, exhibited relief from estradiol benzoate- and oxytocin-induced PD in female Sprague Dawley rats via decreasing the level of PGF2α and increasing PGE2, resulting in a decrease in the ratio of PGF2α/PGE2. Moreover, in this study, citrus essential oil prevented a decrease in antioxidant status markers, including total antioxidant capacity (T-AOC), SOD, and CAT, and an increase in MDA levels.

Anxiety and depression are the most common forms of neuropsychiatric disorders [106]. The essential oil from oranges and its main component limonene have shown an antidepressant-like effect in a chronic unpredictable mild stress (CUMS) male Kunming mice mouse model by restoring the decreased curiosity and mobility, reduced body weight gain, reduced sucrose preference, decreased levels of monoamine neurotransmitter 5-hydroxytryptamine (5-HT), dopamine (DA), norepinephrine (NE), and brain-derived neurotrophic factor (BNDF) and its receptor tropomyosin receptor kinase B (TrkB) expression in the hippocampus, and increased levels of corticotropin-releasing factor (CRF) and corticosterone (CORT) [106].

The peel oil of mandarin, rich in limonene, myrcene, and carotenoids, has led to the dose-dependent growth inhibition of A549 non-small-cell lung cancer (NSCLC) cells and tumor growth in nude mice implemented with A479 cells [115]. In this study, supplementation of 5.25 mg/d of peel oil per mouse for seven days significantly decreased tumor growth by reducing the expression of membrane-bound Ras protein, increasing apoptosis, and inducing cell cycle arrest at the G0/G1 phase.

Table 4. Health benefits of citrus fruit bioactive compounds demonstrated using the animal models.

Bioactive and Doses	Experimental System	Disease Target	Mechanism of Action	Reference
Auraptene (50 mg/kg), naringin (50 mg/kg) for 14 days	STZ-induced hyperglycemia in C57BL/6 mice	Alzheimer's disease (AD)	↓Tau hyperphosphorylation, astroglial activation, and ↑neurogenesis in the hippocampus	[108]
Citrus concentrate containing 0.086 mg β-cryptoxanthin, 5.69 mg hesperidin, and 7.5 mg pectin for 8 weeks	Wistar male rats fed with high-fructose diet	Metabolic syndrome (type 2 diabetes)	↓Plasma glucose, glycemia, insulinemia, and LDL-C, VLDL-C, and TG levels, ↑liver retinyl palmitate, and plasma β-cryptoxanthin	[103]

Table 4. *Cont.*

Bioactive and Doses	Experimental System	Disease Target	Mechanism of Action	Reference
Coumarin (auraptene, 7.5–30 mg/kg for three days a week for total of 8 weeks)	TAA-induced hepatic fibrosis in male C57BL/6 mice	Hepatic fibrosis (cirrhosis and liver cancer)	↓Bile acids in liver by increasing their efflux, ↓activation of HSCs by suppressing the expression of TGF-β1 and -SMAα and ↓expression of NF-κB, TNF-α, and IL-1β	[116]
Coumarin auraptene (5–20 mg/kg)	17α-Ethinylestradiol (synthetic estrogen) induced cholestasis in male C57BL/6 mice	Estrogen-induced cholestasis	↑Bile acid transporters (Bsep and Mrp2) mRNA and proteins, ↑Shp and Fgf15, FXR, ↑bile acid metabolism, ↑SULT2A1, ↓Cyp7a1 and Cyp8b1 mRNA, ↓hepatic inflammation (↓TNF-α, IL-1β, and IL-6)	[117]
Essential oil (0.75% of the diet for 42 weeks)	Male SD rats fed with HFD	Metabolic syndrome (hyperlipidemia)	↓TC, LDL-C, hepatic TC, TG, and hepatic lipid droplet accumulation, ↓liver FFAs, TG, and CE	[102]
Essential oil (limonene; daily inhalation for 1.5 and 24 h, for five days)	CUMS male Kunming mice mouse model	Depression	↑Curiosity, body weight, sucrose preference, 5-HT, DA, NE, BNDF, TrkB, GR, ↓CRF, CORT	[106]
Flavanone aglycones rich ougan (*cv.* Suavissima) juice (20 mL/kg for 10 weeks)	HFD-fed C57BL/6J mice	Metabolic syndrome (obesity)	↓Weight gain, ↓fat accumulation, ↓liver steatosis, ↑glucose homeostasis and insulin sensitivity, ↑BAT activity, and ↑WAT browning, ↑diversity of gut microbiota	[109]
Flavanones (eriocitrin and eriodictyol), 25 and 50 mg/kg	BALB/c mice with LPS-induced periodontal disease	Periodontitis	↓Gingival IL-1β and TNF-α, ↑IL-10, ↓MPO and EPO activity, SOD, ↑CAT and GPx activities, ↓MDA	[118]
Flavanones (naringin, naringenin, hesperidin, and hesperetin; 100 mg/kg/day for 16 weeks)	ApoE$^{-/-}$ mice	Atherosclerosis	↑Bile acid synthesis (naringin), ↑cholesterol reverse transport (hesperidin), ↓cholesterol synthesis (naringenin and hesperetin)	[33]
Flavonoid-rich bitter/sour orange fruit peel extract (125–500 mg/kg for 3 days)	TNBS-induced IBD in male Sprague/Dawley (SD) rats	IBD	↓Weight loss and diarrhea, colitis inflammatory cell infiltration, and proinflammatory cytokines (TNF-α, iNOS, COX-2), ↓serum and colon NO and MPO activity	[119]
Hesperetin (40 mg/kg for 45 days)	STZ-induced diabetes in male albino Wistar strain rats	Diabetes	↓Plasma glucose, ↑plasma insulin and glycogen, ↑antioxidant system (↑SOD, CAT, GPx), ↑insulin secretion by renovating pancreatic β-cells, ↓dyslipidemia (hepatic cholesterol, FFAs, TG, and PLs), ↓serum levels of ALT, AST, and ALP, ↓renal damage (serum urea, creatinine, and uric acid)	[104]

Table 4. *Cont.*

Bioactive and Doses	Experimental System	Disease Target	Mechanism of Action	Reference
Hesperetin (50 mg/kg daily for five weeks)	LPS-induced neuroinflammation C57BL/6 N mice	Alzheimer's disease (AD) and Parkinson's disease (PD)	↓Inflammatory mediators (phosphorylated-NF-κβ, TNF-α, and IL-1), ROS/lipid peroxidation, ↑antioxidant protein (Nrf2 and HO-1), ↓phosphorylated-JNK, Bax, and caspase-3 protein, ↑Bcl-2, ↑synaptic integrity, cognition, and memory processes, ↑ phosphorylated-CREB, PSD-95, and Syntaxin	[107]
Hesperetin (50 mg/kg/day for 46 days)	STZ-induced diabetes in male Wistar rats	Diabetes-associated testicular injury	↓Body weight loss, ↓ serum glucose, ↓MDA, ROS, protein carbonyl, DNA fragmentation, and caspase 3 activity, ↑testicular antioxidant system (↑GSH, MMP, FRAP, SOD, CAT, GPx)	[120]
Hesperidin (100 mg/kg for eight weeks)	Male SD rats fed an obesogenic cafeteria diet	Metabolic syndrome (obesity)	↓TC, LDL-C, FFAs, MCP-1	[121]
Limonene-rich essential oil (0.0765 mL/kg for 7 days)	SD rats with estradiol benzoate and oxytocin-induced uterine contraction	Primary dysmenorrhea (PD)	↑Antioxidant status markers (SOD,T-AOC, CAT, and GSH), ↓MDA and iNOS, and PGF2α/PGE2	[105]
Naringin- and hesperidin-rich *C. junos* peel extract (200 mg/kg/day, 10 days	Acrolein-induced pulmonary apoptosis in male C57BL/6J mice	Pulmonary edema and COPD	↓Cleaved caspase 3, cleaved PARP, Bax and PUMA, p53, Prx-SO3	[80]
Pectin oligosaccharides (0.15–0.9 g/kg for 30 days)	Male C57BL/6 mice fed with HFD	Metabolic syndrome	↓Serum TC, LDL-C, ↓*Firmicutes* ↑*Bacteroidetes* ↑SCFAs (acetate, propionate, and butyrate)	[122]
PMF (nobilitin, tangeritin)-rich extract (30–120 mg/kg)	C57BL/6J male mice fed with HFD	Metabolic syndrome	↓*Firmicutes*-to-*Bacteroidetes* ratio, ↓serum BCAA, ↓mTORC1 and P70S6K activation, ↓SREBPs	[35]
PMF (nobilitin, tangeritin, and 5-OH nobiletin)-rich aged chenpi peel extract (0.25 and 0.5% of diet weight for 11 weeks)	Male C57BL/6J mice fed with HFD	Metabolic syndrome (obesity)	↑Fecal SCFAs (acetic acid and propionic acid), ↑healthy gut microbiota	[34]
PMF 5-Demethylnobiletin (12 mg per kg)	Azoxymethane/DSS-driven colorectal carcinogenesis in male CD-1 mice	Cancer (colorectal)	↓Cell proliferation, ↑apoptosis, and ↓mRNA and protein levels of IL-1β, IL-6, and TNF-α in the colon	[36]

Table 4. *Cont.*

Bioactive and Doses	Experimental System	Disease Target	Mechanism of Action	Reference
PMF- and HOPMF-rich extract (0.5% of HFD for 16 weeks)	Male C57BL/6 mice fed with HFD	Metabolic syndrome (obesity)	↓Adipocyte size, adipose tissue weight, and alleviated the total body weight, levels of lipid droplets, and perilipin 1 protein and SREBP-1 expression, ↑gut microbiota *Prevotella*, ↓rc4–4 bacteria	[111]

The upregulation and downregulation are denoted by upward (↑) and downward (↓) arrows, respectively. Abbreviations are as follows: 5-HT: 5-hydroxytryptamine; ALP: alkaline phosphatase; ApoE: apolipoprotein E; AST: aspartate aminotransferase; BAT: brown adipose tissue; Bax: B-cell lymphoma 2 (Bcl-2)-associated X protein; BCAA: branched-chain amino acid; Bcl-2: B-cell lymphoma 2; BNDF: brain-derived neurotrophic factor; Bsep: bile salt export pump; CAT: catalase; CE: cholesterol esters; COPD: obstructive pulmonary disease; CORT: corticosterone; COX-2: cyclooxygenase-2; CREB: cAMP response element-binding protein; CRF: corticotropin-releasing factor (CRF); CUMS: chronic unpredictable mild stress; Cyp7a1: cholesterol 7α-hydroxylase; Cyp8b1: sterol-12α-hydroxylase; DA: dopamine; DSS: dextran sulfate sodium; FFA: free fatty acids; FFAs: free fatty acids; Fgf15: fibroblast growth factor 15; FRAP: ferric reducing antioxidant; FXR: farnesoid X receptor; GPx: glutathione peroxidase; GR: glucocorticoid receptor; GSH: glutathione; HFD: high-fat diet;.HO-1: Heme oxygenase; HOPMFs: hydroxy polymethoxyflavones; HSCs hepatic stellate cells; HSCs: hepatic stellate cells; IBD: inflammatory bowel disease; IL: Interleukin; iNOS: inducible nitric oxide synthase; JNK: c-Jun N-terminal kinases; LDL-C: low-density lipoprotein cholesterol (LDL-c); LPS: lipopolysaccharide; MCP-1: monocyte chemoattractant protein 1; MDA: malondialdehyde; MMP: mitochondrial membrane potential; MPO: myeloperoxidase; Mrp2: multidrug-resistance-related protein 2; mTOR: mammalian target of rapamycin; mTORC1: mammalian target of rapamycin (mTOR) complex1; NE: norepinephrine; NF-κβ: nuclear factor-kappa β; NO: nitric oxide; Nrf2: nuclear factor-erythroid 2 related factor 2; P70S6K: phospho-p70 S6 kinase; PARP: poly (ADP-ribose) polymerase; PGE2: prostaglandin E2; PGF2α: prostaglandin F2α;.PLs: phospholipids; PMF: polymethoxyflavones; Prx-SO3: oxidized peroxiredoxin; PSD-95: postsynaptic density protein-95; PUMA: p53 upregulated modulator of apoptosis; ROS: reactive oxygen species; SCFAs: short-chain fatty acids; SD: Sprague Dawley; Shp: small heterodimer partner; SMAα: α-smooth muscle actin; SOD: superoxide dismutase; SREBP-1Sterol regulatory element-binding protein 1; STZ: streptozotocin;SULT2A1: sulfotransferase family 2a member 1; TAA: thioacetamide; T-AOC: total antioxidant capacity; TC: total cholesterol; TG: triglyceride and hepatic lipid droplet accumulation; TGF-β1: transforming growth factor-β1; TNBS: trinitrobenzene sulfonic acid; TNF-α: tumor necrosis factor α; TrkB: tropomyosin receptor kinase B; VLDL-C: very-low-density lipoprotein-cholesterol; WAT: white adipose tissue.

5.3. Human Studies

Similar to the in vitro and animal studies, case–control, cohort, and interventional studies have also demonstrated the health benefits of bioactive compounds derived from citrus fruits. A pooled meta-analysis of 14 case–control (13 hospital-based and two population-based) and two cohort studies showed that people with the highest citrus fruit intake had a 50% reduction in risk of oral cavity and pharyngeal cancer compared to the lowest intake [123]. In this meta-analysis, the protective effect of citrus fruit was substantially higher in case–control studies (OR 0.47; 95% CI 0.40–0.55) compared to cohort studies (OR 0.73; 95% CI 0.55–0.96).

The oxidized (ox)-low-density lipoprotein (LDL) plays a vital role in converting macrophages to foam cells and the formation and progression of atherosclerotic lesions [124]. In a 3-month randomized, double-blind, controlled study, 23 untreated human subjects (16 males and seven females, mean age of 41.9 years) with cardiovascular risk (total cholesterol level >200 mg/dL and LDL-c > 130 mg/dl) consumed a commercially available flavonoid-rich hydroethanolic extract (Citrolive™; 1000 mg/day for 90 d) from bitter orange and olive leaf (*Olea europaea* L.), and they showed a significant reduction in ox-LDL-c and LDL-oxidase/LDL-c ratio and increased serum paraoxonase activity (PON1; athero-protective by preventing LDL oxidation) as compared to controls [124]. In another eight-week study of 96 healthy human subjects (51 intervention and 45 placeboes), supplementation of Citrolive™ (1000 mg/day for 8 weeks) improved endothelial function, as measured by flow-mediated vasodilation (FMD), reduced blood pressure and lipid metabolism-related parameters (TC, LDL-c, LDL-oxidase, oxidized/reduced glutathione (GSSH/GHS) ratio, protein carbonyl, and IL-6), and improved antioxidant and inflammatory status [125].

In a randomized, parallel, double-blind, placebo-controlled trial of 153 participants (53 women and 106 men; age 18 to 65) with pre- or stage-1 hypertensive conditions, supplementation of 500 mL/day of orange juice (containing 345 mg hesperidin) or hesperidin-enriched orange juice (containing 600 mg of hesperidin) for 12 weeks reduced systolic BP (SBP; −6.35 and −7.36 mmHg) and pulse (PP) pressure. Interestingly, the SBP and PP decreased dose-dependently relative to the hesperidin intake.

Visvanathan and Williamson [126] reviewed acute (13 studies) as well as chromic (22 studies) human intervention studies of the effect of citrus fruits and juice intake on the risk of developing type 2 diabetes and concluded that the direct acute effect of citrus polyphenols on the postprandial glycemic response (a risk factor for type 2 diabetes) is subtle. However, citrus juice intake for longer periods (e.g., 500 mL/day for 12 weeks) showed improved fasting glucose, fasting insulin (9–32%), and insulin resistance.

The lower solubility hampers the bioavailability and microbial metabolism of flavonoids, thus probably yielding high inter-individual variability, resulting in inconsistent health benefits [127]. In a randomized crossover human pharmacokinetic study, 16 healthy subjects (eight men and eight women) were administered a single dose of 3.1 g lemon extract containing 260 mg eriocitrin (main flavanone of lemon) or 1.95 g orange extract containing 260 mg hesperidin (main flavanone of orange) and showed higher bioavailability of eriocitrin, compared to hesperidin, probably due to the higher solubility of eriocitrin [127]. Thus, the authors suggested that consumption of eriocitrin-rich lemon extract could provide better health benefits.

The emerging evidence has suggested that the bioactive compounds present in orange fruits are associated with the metabolism of the gut microbiota [128]. Brasili et al. [128] revealed that daily consumption of juice of *cv*. Cara Cara and *cv*. Bahia oranges, differing in vitamin C, flavanone, and carbohydrate content, affects the fecal microbiota and metabolome differently. Intake of Cara Cara orange juice increased the Mogibacteriaceae and Tissierellaceae families (Firmicutes), while the Odoribacteraceae family and the Odoribacter genus (Bacteroidetes) decreased. In contrast, in the Bahia group, the Enterococcaceae and Veillonellaceae families increased while the Mogibacteriaceae and Ruminococcaceae families and the *Faecalibacterium prausnitzii* decreased. The abundance of Mogibacteriaceae was found in healthy subjects.

The PGs, thromboxanes (TXs), leukotrienes (LT), and isoprostane (IsoPs) metabolites derived from arachidonic acid are generally considered proinflammatory mediators, and the hallmark of increased secretion of these metabolites in the urine indicates enhanced inflammation in the body [129]. In a randomized, double-blind, placebo-controlled, and crossover study on 16 elite triathletes (6 women and 10 men), consumption of 200 mL of polyphenol-rich *Aronia-citrus* juice (95% citrus juice + 5% *Aronia melanocarpa* juice) for 45 d led to reduced excretion of 2,3-dinor-11β-$PGF_{2\alpha}$ and 11-dehydro-thromboxin B2 (11-dh-TXB2), although the levels of other metabolites related to vascular homeostasis and smooth muscle function, such as PGE2, 15-keto-15-F2t-IsoP, 20-OH-PGE2, leukotrienes E4 (LTE4), and 15-epi-15-E2t-IsoP, were increased after juice supplementation compared to the placebo, suggesting a positive effect on the cardiovascular system [129].

6. Toxicity and Safety Profile of Citrus Fruit Bioactive Compounds

Bioactive compounds derived from citrus fruits have shown a good safety profile in animal toxicological evaluation. In a 90 d sub-chronic and acute oral toxicity study on Sprague Dawley rats, hesperidin isolated from the dehydrated peel of *C. sinensis* showed a low observed adverse effect level (LOAEL) at 1 g/kg, and a median lethal dose (LD_{50}) of 4.83 g/kg [130]. These observations suggest a good safety profile in the animals, as this concentration is much lower than the flavonoids administered in animal models (10–200 mg/kg) to obtain the health benefits (Table 4). Moreover, other citrus flavonoids, including nobiletin, tangeretin, and naringin, have shown a good safety profile [131,132].

The limonene, and other terpene-rich citrus flavor ingredients, such as oil, essential oil, whole fruit extract, and peel extract, are generally recognized as safe (GRAS) [133].

R-(+)-limonene has shown no observed adverse effect level (NOAEL) in rodents ranging from <75 to 500 mg/kg, and LD_{50} values range from 4.40 to 6.60 g/kg [134].

7. Conclusions

Citrus fruits are a rich and exceptional source of bioactive flavonoids, especially polymethoxylated flavones (PMFs), including nobiletin, tangeritin, and 5-demethyl nobiletin. Moreover, citrus fruits are a dense source of bioactive xanthophylls (e.g., violaxanthin esters), provitamin A carotenoids (e.g., β-cryptoxanthin), and apocarotenoids (e.g., β-citraurin). These bioactive compounds reduce the inflammatory mediators and reactive oxygen species (ROS) in the body, thus minimizing the risk of metabolic syndrome, including neurodegenerative diseases, cardiovascular disease (CVD), diabetes, and cancer. In addition, citrus essential oil, rich in terpenes (e.g., D-limonene) and limonoids (limonin), is an economically important product due to its flavoring, antimicrobial, antioxidant, and other health-beneficial properties.

Significant advancements have been made to study the composition, content, and health-promoting activities of citrus fruit bioactives. However, in future investigations, the following fields should be addressed to overcome the bottlenecks: (1) screening of traditional and new cultivars with modern analytical techniques to identify the genetic variation in content and composition; these data can help to select bioactive-rich cultivars for food formulations; moreover, precise identification of the bioactive-rich growth stage of citrus fruits suitable for consumption is necessary; (2) the elucidation of cellular and molecular mechanisms of functioning of citrus bioactives in the body; (3) more human interventional studies are required to demonstrate the health benefits of citrus bioactives; (4) the synergetic effects in the bioavailability and bioactivity among different citrus bioactive need more exploration; in addition, synergetic effects between citrus bioactives and clinically used drugs should be explored; (5) citrus fruit wastes can potentially serve as a low-cost and eco-friendly source of bioactives; however, further research is needed in the context of the efficient extraction and utilization of bioactives from citrus fruit waste.

Funding: This work and article processing charges (APC) were supported by the Konkuk University research fund (2021A0190061).

Institutional Review Board Statement: Not applicable.

Informed Consent Statement: Not applicable.

Data Availability Statement: Data are contained within the article.

Acknowledgments: This paper was supported by the KU research professor program of Konkuk University, Seoul, Korea.

Conflicts of Interest: The authors declare no conflict of interest.

References

1. Lapuente, M.; Estruch, R.; Shahbaz, M.; Casas, R. Relation of Fruits and Vegetables with Major Cardiometabolic Risk Factors, Markers of Oxidation, and Inflammation. *Nutrients* **2019**, *11*, 2381. [CrossRef]
2. Medina-Remón, A.; Kirwan, R.; Lamuela-Raventós, R.M.; Estruch, R. Dietary patterns and the risk of obesity, type 2 diabetes mellitus, cardiovascular diseases, asthma, and neurodegenerative diseases. *Crit. Rev. Food Sci. Nutr.* **2018**, *58*, 262–296. [CrossRef]
3. Zou, Z.; Xi, W.; Hu, Y.; Nie, C.; Zhou, Z. Antioxidant activity of Citrus fruits. *Food Chem.* **2016**, *196*, 885–896. [CrossRef]
4. Wu, G.A.; Terol, J.; Ibanez, V.; Lopez-Garcia, A.; Perez-Roman, E.; Borreda, C.; Domingo, C.; Tadeo, F.R.; Carbonell-Caballero, J.; Alonso, R.; et al. Genomics of the origin and evolution of Citrus. *Nature* **2018**, *554*, 311–316. [CrossRef]
5. Lu, X.; Zhao, C.; Shi, H.; Liao, Y.; Xu, F.; Du, H.; Xiao, H.; Zheng, J. Nutrients and bioactives in citrus fruits: Different citrus varieties, fruit parts, and growth stages. *Crit. Rev. Food Sci. Nutr.* **2021**, 1–24. [CrossRef] [PubMed]
6. Zhang, M.; Zhu, S.Y.; Yang, W.J.; Huang, Q.R.; Ho, C.T. The biological fate and bioefficacy of citrus flavonoids: Bioavailability, biotransformation, and delivery systems. *Food Funct.* **2021**, *12*, 3307–3323. [CrossRef]
7. United States Department of Agriculture Foreign Agricultural Service. Citrus: World Markets and Trade. 2021. Available online: https://www.fas.usda.gov/data/citrus-world-markets-and-trade (accessed on 23 December 2021).

8. Cebadera-Miranda, L.; Dominguez, L.; Dias, M.I.; Barros, L.; Ferreira, I.; Igual, M.; Martinez-Navarrete, N.; Fernandez-Ruiz, V.; Morales, P.; Camara, M. Sanguinello and Tarocco (*Citrus sinensis* L. Osbeck): Bioactive compounds and colour appearance of blood oranges. *Food Chem.* **2019**, *270*, 395–402. [CrossRef]
9. Lado, J.; Gambetta, G.; Zacarias, L. Key determinants of citrus fruit quality: Metabolites and main changes during maturation. *Sci. Hortic.* **2018**, *233*, 238–248. [CrossRef]
10. Bora, H.; Kamle, M.; Mahato, D.K.; Tiwari, P.; Kumar, P. Citrus Essential Oils (CEOs) and Their Applications in Food: An Overview. *Plants* **2020**, *9*, 357. [CrossRef] [PubMed]
11. Gonzalez-Mas, M.C.; Rambla, J.L.; Lopez-Gresa, M.P.; Blazquez, M.A.; Granell, A. Volatile Compounds in Citrus Essential Oils: A Comprehensive Review. *Front. Plant Sci.* **2019**, *10*, 12. [CrossRef]
12. Stevens, Y.; Van Rymenant, E.; Grootaert, C.; Van Camp, J.; Possemiers, S.; Masclee, A.; Jonkers, D. The Intestinal Fate of Citrus Flavanones and Their Effects on Gastrointestinal Health. *Nutrients* **2019**, *11*, 1464. [CrossRef] [PubMed]
13. Barreca, D.; Mandalari, G.; Calderaro, A.; Smeriglio, A.; Trombetta, D.; Felice, M.R.; Gattuso, G. Citrus Flavones: An Update on Sources, Biological Functions, and Health Promoting Properties. *Plants* **2020**, *9*, 288. [CrossRef] [PubMed]
14. Addi, M.; Elbouzidi, A.; Abid, M.; Tungmunnithum, D.; Elamrani, A.; Hano, C. An Overview of Bioactive Flavonoids from Citrus Fruits. *Appl. Sci.* **2022**, *12*, 29. [CrossRef]
15. Wang, Y.; Liu, X.J.; Chen, J.B.; Cao, J.P.; Li, X.; Sun, C.D. Citrus flavonoids and their antioxidant evaluation. *Crit. Rev. Food Sci. Nutr.* **2021**, 1–22. [CrossRef]
16. Pontifex, M.G.; Malik, M.; Connell, E.; Muller, M.; Vauzour, D. Citrus Polyphenols in Brain Health and Disease: Current Perspectives. *Front. Neurosci.* **2021**, *15*, 640648. [CrossRef] [PubMed]
17. Zhao, C.Y.; Wang, F.; Lian, Y.H.; Xiao, H.; Zheng, J.K. Biosynthesis of citrus flavonoids and their health effects. *Crit. Rev. Food Sci. Nutr.* **2020**, *60*, 566–583. [CrossRef]
18. Musumeci, L.; Maugeri, A.; Cirmi, S.; Lombardo, G.E.; Russo, C.; Gangemi, S.; Calapai, G.; Navarra, M. Citrus fruits and their flavonoids in inflammatory bowel disease: An overview. *Nat. Prod. Res.* **2020**, *34*, 122–136. [CrossRef]
19. Gandhi, G.R.; Vasconcelos, A.B.S.; Wu, D.T.; Li, H.B.; Antony, P.J.; Li, H.; Geng, F.; Gurgel, R.Q.; Narain, N.; Gan, R.Y. Citrus Flavonoids as Promising Phytochemicals Targeting Diabetes and Related Complications: A Systematic Review of In Vitro and In Vivo Studies. *Nutrients* **2020**, *12*, 2907. [CrossRef] [PubMed]
20. Mahmoud, A.M.; Bautista, R.J.H.; Sandhu, M.A.; Hussein, O.E. Beneficial Effects of Citrus Flavonoids on Cardiovascular and Metabolic Health. *Oxid. Med. Cell. Longev.* **2019**, *2019*, 5484138. [CrossRef]
21. Bellavite, P.; Donzelli, A. Hesperidin and SARS-CoV-2: New Light on the Healthy Function of Citrus Fruits. *Antioxidants* **2020**, *9*, 742. [CrossRef]
22. Den Hartogh, D.J.; Tsiani, E. Antidiabetic Properties of Naringenin: A Citrus Fruit Polyphenol. *Biomolecules* **2019**, *9*, 99. [CrossRef] [PubMed]
23. Zaidun, N.H.; Thent, Z.C.; Abd Latiff, A. Combating oxidative stress disorders with citrus flavonoid: Naringenin. *Life Sci.* **2018**, *208*, 111–122. [CrossRef]
24. Nakajima, A.; Ohizumi, Y. Potential Benefits of Nobiletin, A Citrus Flavonoid, against Alzheimer's Disease and Parkinson's Disease. *Int. J. Mol. Sci.* **2019**, *20*, 3380. [CrossRef] [PubMed]
25. Goh, J.X.H.; Tan, L.T.H.; Goh, J.K.; Chan, K.G.; Pusparajah, P.; Lee, L.H.; Goh, B.H. Nobiletin and Derivatives: Functional Compounds from Citrus Fruit Peel for Colon Cancer Chemoprevention. *Cancers* **2019**, *11*, 867. [CrossRef] [PubMed]
26. Klimek-Szczykutowicz, M.; Szopa, A.; Ekiert, H. *Citrus limon* (Lemon) Phenomenon—A Review of the Chemistry, Pharmacological Properties, Applications in the Modern Pharmaceutical, Food, and Cosmetics Industries, and Biotechnological Studies. *Plants* **2020**, *9*, 119. [CrossRef]
27. Gao, Z.; Gao, W.; Zeng, S.L.; Li, P.; Liu, E.H. Chemical structures, bioactivities and molecular mechanisms of citrus polymethoxyflavones. *J. Funct. Foods* **2018**, *40*, 498–509. [CrossRef]
28. Peng, Z.X.; Zhang, H.P.; Li, W.Y.; Yuan, Z.Y.; Xie, Z.Z.; Zhang, H.Y.; Cheng, Y.J.; Chen, J.J.; Xu, J. Comparative profiling and natural variation of polymethoxylated flavones in various citrus germplasms. *Food Chem.* **2021**, *354*, 129499. [CrossRef]
29. Zhang, H.J.; Tian, G.F.; Zhao, C.Y.; Han, Y.H.; DiMarco-Crook, C.; Lu, C.; Bao, Y.M.; Li, C.X.; Xiao, H.; Zheng, J.K. Characterization of polymethoxyflavone demethylation during drying processes of citrus peels. *Food Funct.* **2019**, *10*, 5707–5717. [CrossRef]
30. Smeriglio, A.; Cornara, L.; Denaro, M.; Barreca, D.; Burlando, B.; Xiao, J.B.; Trombetta, D. Antioxidant and cytoprotective activities of an ancient Mediterranean citrus (*Citrus lumia* Risso) albedo extract: Microscopic observations and polyphenol characterization. *Food Chem.* **2019**, *279*, 347–355. [CrossRef]
31. Mazzotti, F.; Bartella, L.; Talarico, I.R.; Napoli, A.; Di Donna, L. High-throughput determination of flavanone-O-glycosides in citrus beverages by paper spray tandem mass spectrometry. *Food Chem.* **2021**, *360*, 130060. [CrossRef]
32. Rong, X.; Xu, J.; Jiang, Y.; Li, F.; Chen, Y.L.; Dou, Q.P.; Li, D.P. Citrus peel flavonoid nobiletin alleviates lipopolysaccharide-induced inflammation by activating IL-6/STAT3/FOXO3a-mediated autophagy. *Food Funct.* **2021**, *12*, 1305–1317. [CrossRef] [PubMed]
33. Wang, F.; Zhao, C.Y.; Yang, M.K.; Zhang, L.; Wei, R.J.; Meng, K.; Bao, Y.M.; Zhang, L.N.; Zheng, J.K. Four Citrus Flavanones Exert Atherosclerosis Alleviation Effects in ApoE(−/−) Mice via Different Metabolic and Signaling Pathways. *J. Agric. Food Chem.* **2021**, *69*, 5226–5237. [CrossRef]

34. Zhang, M.; Zhu, J.Y.; Zhang, X.; Zhao, D.G.; Ma, Y.Y.; Li, D.L.; Ho, C.T.; Huang, Q.R. Aged citrus peel (chenpi) extract causes dynamic alteration of colonic microbiota in high-fat diet induced obese mice. *Food Funct.* **2020**, *11*, 2667–2678. [CrossRef] [PubMed]
35. Zeng, S.L.; Li, S.Z.; Xiao, P.T.; Cai, Y.Y.; Chu, C.; Chen, B.Z.; Li, P.; Li, J.; Liu, E.H. Citrus polymethoxyflavones attenuate metabolic syndrome by regulating gut microbiome and amino acid metabolism. *Sci. Adv.* **2020**, *6*, eaax6208. [CrossRef]
36. Song, M.Y.; Lan, Y.Q.; Wu, X.; Han, Y.H.; Wang, M.Q.; Zheng, J.K.; Li, Z.Z.; Li, F.; Zhou, J.Z.; Xiao, J.; et al. The chemopreventive effect of 5-demethylnobiletin, a unique citrus flavonoid, on colitis-driven colorectal carcinogenesis in mice is associated with its colonic metabolites. *Food Funct.* **2020**, *11*, 4940–4952. [CrossRef] [PubMed]
37. Li, S.; Pan, M.-H.; Lo, C.-Y.; Tan, D.; Wang, Y.; Shahidi, F.; Ho, C.-T. Chemistry and health effects of polymethoxyflavones and hydroxylated polymethoxyflavones. *J. Funct. Foods* **2009**, *1*, 2–12. [CrossRef]
38. Deng, M.; Jia, X.C.; Dong, L.H.; Liu, L.; Huang, F.; Chi, J.W.; Ma, Q.; Zhao, D.; Zhang, M.W.; Zhang, R.F. Structural elucidation of flavonoids from Shatianyu (*Citrus grandis* L. Osbeck) pulp and screening of key antioxidant components. *Food Chem.* **2022**, *366*, 130605. [CrossRef]
39. Chen, J.; Yuan, Z.; Zhang, H.; Li, W.; Shi, M.; Peng, Z.; Li, M.; Tian, J.; Deng, X.; Cheng, Y.; et al. Cit1,2RhaT and two novel CitdGlcTs participate in flavor-related flavonoid metabolism during citrus fruit development. *J. Exp. Bot.* **2019**, *70*, 2759–2771. [CrossRef]
40. Ledesma-Escobar, C.A.; Priego-Capote, F.; Olvera, V.J.R.; de Castro, M.D.L. Targeted Analysis of the Concentration Changes of Phenolic Compounds in Persian Lime (*Citrus latifolia*) during Fruit Growth. *J. Agric. Food Chem.* **2018**, *66*, 1813–1820. [CrossRef]
41. Multari, S.; Licciardello, C.; Caruso, M.; Martens, S. Monitoring the changes in phenolic compounds and carotenoids occurring during fruit development in the tissues of four citrus fruits. *Food Res. Int.* **2020**, *134*, 109228. [CrossRef]
42. Saini, R.K.; Nile, S.H.; Park, S.W. Carotenoids from fruits and vegetables: Chemistry, analysis, occurrence, bioavailability and biological activities. *Food Res. Int.* **2015**, *76*, 735–750. [CrossRef]
43. Saini, R.K.; Keum, Y.S. Carotenoid extraction methods: A review of recent developments. *Food Chem.* **2018**, *240*, 90–103. [CrossRef] [PubMed]
44. Etzbach, L.; Stolle, R.; Anheuser, K.; Herdegen, V.; Schieber, A.; Weber, F. Impact of Different Pasteurization Techniques and Subsequent Ultrasonication on the In Vitro Bioaccessibility of Carotenoids in Valencia Orange (*Citrus sinensis* (L.) Osbeck) Juice. *Antioxidants* **2020**, *9*, 534. [CrossRef]
45. Lux, P.E.; Carle, R.; Zacarias, L.; Rodrigo, M.J.; Schweiggert, R.M.; Steingass, C.B. Genuine Carotenoid Profiles in Sweet Orange *Citrus sinensis* (L.) Osbeck cv. Navel Peel and Pulp at Different Maturity Stages. *J. Agric. Food Chem.* **2019**, *67*, 13164–13175. [CrossRef] [PubMed]
46. Zheng, X.J.; Mi, J.N.; Deng, X.X.; Al-Babili, S. LC-MS-Based Profiling Provides New Insights into Apocarotenoid Biosynthesis and Modifications in Citrus Fruits. *J. Agric. Food Chem.* **2021**, *69*, 1842–1851. [CrossRef] [PubMed]
47. Luan, Y.T.; Wang, S.S.; Wang, R.Q.; Xu, C.J. Accumulation of red apocarotenoid beta-citraurin in peel of a spontaneous mutant of huyou (*Citrus changshanensis*) and the effects of storage temperature and ethylene application. *Food Chem.* **2020**, *309*, 125705. [CrossRef]
48. Dhakane-Lad, J.; Kar, A. Supercritical CO2 extraction of lycopene from pink grapefruit (*Citrus paradise* Macfad) and its degradation studies during storage. *Food Chem.* **2021**, *361*, 130113. [CrossRef] [PubMed]
49. Wang, F.; Lin, J.R.; Xu, L.L.; Peng, Q.Q.; Huang, H.Y.; Tong, L.J.; Lu, Q.; Wang, C.C.; Yang, L. On higher nutritional and medical properties of a carotenoid-rich mutant pomelo (*Citrus maxima* (L.) Osbeck). *Ind. Crop. Prod.* **2019**, *127*, 142–147. [CrossRef]
50. Petry, F.C.; de Nadai, F.B.; Cristofani-Yaly, M.; Latado, R.R.; Mercadante, A.Z. Carotenoid biosynthesis and quality characteristics of new hybrids between tangor (*Citrus reticulata* × *C. sinensis*) cv. 'Murcott' and sweet orange (*C. sinensis*) cv. 'Pera'. *Food Res. Int.* **2019**, *122*, 461–470. [CrossRef]
51. Raspo, M.A.; Vignola, M.B.; Andreatta, A.E.; Juliani, H.R. Antioxidant and antimicrobial activities of citrus essential oils from Argentina and the United States. *Food Biosci.* **2020**, *36*, 100651. [CrossRef]
52. Gao, Z.P.; Zhong, W.M.; Chen, K.Y.; Tang, P.Y.; Guo, J.J. Chemical composition and anti-biofilm activity of essential oil from *Citrus medica* L. var. sarcodactylis Swingle against Listeria monocytogenes. *Ind Crop. Prod.* **2020**, *144*, 112036. [CrossRef]
53. Mahato, N.; Sharma, K.; Koteswararao, R.; Sinha, M.; Baral, E.; Cho, M.H. Citrus essential oils: Extraction, authentication and application in food preservation. *Crit. Rev. Food Sci. Nutr.* **2019**, *59*, 611–625. [CrossRef]
54. Li, Z.H.; Cai, M.; Liu, Y.S.; Sun, P.L.; Luo, S.L. Antibacterial Activity and Mechanisms of Essential Oil from *Citrus medica* L. var. sarcodactylis. *Molecules* **2019**, *24*, 1577. [CrossRef]
55. Ambrosio, C.M.S.; Ikeda, N.Y.; Miano, A.C.; Saldana, E.; Moreno, A.M.; Stashenko, E.; Contreras-Castillo, C.J.; Da Gloria, E.M. Unraveling the selective antibacterial activity and chemical composition of citrus essential oils. *Sci. Rep.* **2019**, *9*, 17719. [CrossRef]
56. Denkova-Kostova, R.; Teneva, D.; Tomova, T.; Goranov, B.; Denkova, Z.; Shopska, V.; Slavchev, A.; Hristova-Ivanova, Y. Chemical composition, antioxidant and antimicrobial activity of essential oils from tangerine (*Citrus reticulata* L.), grapefruit (*Citrus paradisi* L.), lemon (*Citrus lemon* L.) and cinnamon (*Cinnamomum zeylanicum* Blume). *Z. Nat. Sect. C J. Biosci.* **2021**, *76*, 175–185. [CrossRef]
57. Paw, M.; Begum, T.; Gogoi, R.; Pandey, S.K.; Lal, M. Chemical Composition of *Citrus limon* L. Burmf Peel Essential Oil from North East India. *J. Essent. Oil Bear. Plants* **2020**, *23*, 337–344. [CrossRef]
58. Zoccali, M.; Arigo, A.; Russo, M.; Salafia, F.; Dugo, P.; Mondello, L. Characterization of Limonoids in Citrus Essential Oils by Means of Supercritical Fluid Chromatography Tandem Mass Spectrometry. *Food Anal. Methods* **2018**, *11*, 3257–3266. [CrossRef]

59. Rossi, R.C.; da Rosa, S.R.; Weimer, P.; Moura, J.G.L.; de Oliveira, V.R.; de Castilhos, J. Assessment of compounds and cytotoxicity of *Citrus deliciosa* Tenore essential oils: From an underexploited by-product to a rich source of high-value bioactive compounds. *Food Biosci.* **2020**, *38*, 100779. [CrossRef]
60. Yu, M.; Xia, Y.; Xie, W.; Li, Y.; Yu, X.; Zheng, J.; Zhang, Y. Enzymatic extraction of pectic oligosaccharides from finger citron (*Citrus medica* L. var. *sarcodactylis* Swingle) pomace with antioxidant potential. *Food Funct.* **2021**, *12*, 9855–9865. [CrossRef] [PubMed]
61. Zema, D.A.; Calabro, P.S.; Folino, A.; Tamburino, V.; Zappia, G.; Zimbone, S.M. Valorisation of citrus processing waste: A review. *Waste Manag.* **2018**, *80*, 252–273. [CrossRef] [PubMed]
62. Mahato, N.; Sharma, K.; Sinha, M.; Cho, M.H. Citrus waste derived nutra-/pharmaceuticals for health benefits: Current trends and future perspectives. *J. Funct. Foods* **2018**, *40*, 307–316. [CrossRef]
63. Singh, B.; Singh, J.P.; Kaur, A.; Yadav, M.P. Insights into the chemical composition and bioactivities of citrus peel essential oils. *Food Res. Int.* **2021**, *143*, 110231. [CrossRef] [PubMed]
64. Saini, A.; Panesar, P.S.; Bera, M.B. Valuation of *Citrus reticulata* (kinnow) peel for the extraction of lutein using ultrasonication technique. *Biomass Convers. Biorefinery* **2021**, *11*, 2157–2165. [CrossRef]
65. Costanzo, G.; Iesce, M.R.; Naviglio, D.; Ciaravolo, M.; Vitale, E.; Arena, C. Comparative Studies on Different Citrus Cultivars: A Revaluation of Waste Mandarin Components. *Antioxidants* **2020**, *9*, 517. [CrossRef] [PubMed]
66. Murador, D.C.; Salafia, F.; Zoccali, M.; Martins, P.L.G.; Ferreira, A.G.; Dugo, P.; Mondello, L.; De Rosso, V.V.; Giuffrida, D. Green Extraction Approaches for Carotenoids and Esters: Characterization of Native Composition from Orange Peel. *Antioxidants* **2019**, *8*, 613. [CrossRef]
67. Nuzzo, D.; Picone, P.; Giardina, C.; Scordino, M.; Mudò, G.; Pagliaro, M.; Scurria, A.; Meneguzzo, F.; Ilharco, L.M.; Fidalgo, A.; et al. New Neuroprotective Effect of Lemon IntegroPectin on Neuronal Cellular Model. *Antioxidants* **2021**, *10*, 669. [CrossRef] [PubMed]
68. Colodel, C.; Vriesmann, L.C.; Teofilo, R.F.; Petkowicz, C.L.D. Extraction of pectin from ponkan (*Citrus reticulata* Blanco cv. Ponkan) peel: Optimization and structural characterization. *Int. J. Biol. Macromol.* **2018**, *117*, 385–391. [CrossRef] [PubMed]
69. Long, X.Y.; Zeng, X.G.; Yan, H.T.; Xu, M.J.; Zeng, Q.T.; Xu, C.; Xu, Q.M.; Liang, Y.; Zhang, J. Flavonoids composition and antioxidant potential assessment of extracts from Gannanzao Navel Orange (*Citrus sinensis* Osbeck Cv. Gannanzao) peel. *Nat. Prod. Res.* **2021**, *35*, 702–706. [CrossRef]
70. El-Kersh, D.M.; Ezzat, S.M.; Salama, M.M.; Mahrous, E.A.; Attia, Y.M.; Ahmed, M.S.; Elmazar, M.M. Anti-estrogenic and anti-aromatase activities of citrus peels major compounds in breast cancer. *Sci. Rep.* **2021**, *11*, 7121. [CrossRef] [PubMed]
71. Chen, Y.; Pan, H.L.; Hao, S.X.; Pan, D.M.; Wang, G.J.; Yu, W.Q. Evaluation of phenolic composition and antioxidant properties of different varieties of Chinese citrus. *Food Chem.* **2021**, *364*, 130413. [CrossRef] [PubMed]
72. Liu, N.; Li, X.; Zhao, P.; Zhang, X.Q.; Qiao, O.; Huang, L.Q.; Guo, L.P.; Gao, W.Y. A review of chemical constituents and health-promoting effects of citrus peels. *Food Chem.* **2021**, *365*, 130585. [CrossRef]
73. Gogoi, M.; Boruah, J.L.H.; Bora, P.K.; Das, D.J.; Famhawite, V.; Biswas, A.; Puro, N.; Kalita, J.; Haldar, S.; Baishya, R. Citrus macroptera induces apoptosis via death receptor and mitochondrial mediated pathway as prooxidant in human non-small cell lung cancer cells. *Food Biosci.* **2021**, *43*, 101293. [CrossRef]
74. Abdelghffar, E.A.; El-Nashar, H.A.S.; Al-Mohammadi, A.G.A.; Eldahshan, O.A. Orange fruit (*Citrus sinensis*) peel extract attenuates chemotherapy-induced toxicity in male rats. *Food Funct.* **2021**, *12*, 9443–9455. [CrossRef] [PubMed]
75. Singh, B.; Singh, J.P.; Kaur, A.; Singh, N. Phenolic composition, antioxidant potential and health benefits of citrus peel. *Food Res. Int.* **2020**, *132*, 109114. [CrossRef] [PubMed]
76. Jeong, D.; Park, H.; Jang, B.K.; Ju, Y.B.; Shin, M.H.; Oh, E.J.; Lee, E.J.; Kim, S.R. Recent advances in the biological valorization of citrus peel waste into fuels and chemicals. *Bioresour. Technol.* **2021**, *323*, 124603. [CrossRef]
77. Zayed, A.; Badawy, M.T.; Farag, M.A. Valorization and extraction optimization of Citrus seeds for food and functional food applications. *Food Chem.* **2021**, *355*, 129609. [CrossRef] [PubMed]
78. Hwang, H.J.; Kim, H.J.; Ko, M.J.; Chung, M.S. Recovery of hesperidin and narirutin from waste *Citrus unshiu* peel using subcritical water extraction aided by pulsed electric field treatment. *Food Sci. Biotechnol.* **2021**, *30*, 217–226. [CrossRef]
79. Kim, D.-S.; Lim, S.-B. Semi-Continuous Subcritical Water Extraction of Flavonoids from *Citrus unshiu* Peel: Their Antioxidant and Enzyme Inhibitory Activities. *Antioxidants* **2020**, *9*, 360. [CrossRef] [PubMed]
80. Kim, J.W.; Jo, E.H.; Moon, J.E.; Cha, H.; Chang, M.H.; Cho, H.T.; Lee, M.K.; Jung, W.S.; Lee, J.H.; Heo, W.; et al. In Vitro and In Vivo Inhibitory Effect of Citrus Junos Tanaka Peel Extract against Oxidative Stress-Induced Apoptotic Death of Lung Cells. *Antioxidants* **2020**, *9*, 1231. [CrossRef]
81. Anacleto, S.L.; Milenkovic, D.; Kroon, P.A.; Needs, P.W.; Lajolo, F.M.; Hassimotto, N.M.A. Citrus flavanone metabolites protect pancreatic-beta cells under oxidative stress induced by cholesterol. *Food Funct.* **2020**, *11*, 8612–8624. [CrossRef]
82. Huang, R.; Zhang, Y.; Shen, S.Y.; Zhi, Z.J.; Cheng, H.; Chen, S.G.; Ye, X.Q. Antioxidant and pancreatic lipase inhibitory effects of flavonoids from different citrus peel extracts: An in vitro study. *Food Chem.* **2020**, *326*, 126785. [CrossRef]
83. Denaro, M.; Smeriglio, A.; Trombetta, D. Antioxidant and Anti-Inflammatory Activity of Citrus Flavanones Mix and Its Stability after In Vitro Simulated Digestion. *Antioxidants* **2021**, *10*, 140. [CrossRef] [PubMed]
84. Yang, W.L.; Chen, S.Y.; Ho, C.Y.; Yen, G.C. Citrus flavonoids suppress IL-5 and ROS through distinct pathways in PMA/ionomycin-induced EL-4 cells. *Food Funct.* **2020**, *11*, 824–833. [CrossRef]

85. Hu, H.J.; Zhang, S.S.; Pan, S.Y. Characterization of Citrus Pectin Oligosaccharides and Their Microbial Metabolites as Modulators of Immunometabolism on Macrophages. *J. Agric. Food Chem.* **2021**, *69*, 8403–8414. [CrossRef] [PubMed]
86. Smeriglio, A.; Alloisio, S.; Raimondo, F.M.; Denaro, M.; Xiao, J.B.; Cornara, L.; Trombetta, D. Essential oil of *Citrus lumia* Risso: Phytochemical profile, antioxidant properties and activity on the central nervous system. *Food Chem. Toxicol.* **2018**, *119*, 407–416. [CrossRef]
87. Piccialli, I.; Tedeschi, V.; Caputo, L.; Amato, G.; De Martino, L.; De Feo, V.; Secondo, A.; Pannaccione, A. The Antioxidant Activity of Limonene Counteracts Neurotoxicity Triggered byAβ1-42 Oligomers in Primary Cortical Neurons. *Antioxidants* **2021**, *10*, 937. [CrossRef]
88. Cirmi, S.; Maugeri, A.; Lombardo, G.E.; Russo, C.; Musumeci, L.; Gangemi, S.; Calapai, G.; Barreca, D.; Navarra, M. A Flavonoid-Rich Extract of Mandarin Juice Counteracts 6-OHDA-Induced Oxidative Stress in SH-SY5Y Cells and Modulates Parkinson-Related Genes. *Antioxidants* **2021**, *10*, 539. [CrossRef]
89. Kitagawa, T.; Matsumoto, T.; Imahori, D.; Kobayashi, M.; Okayama, M.; Ohta, T.; Yoshida, T.; Watanabe, T. Limonoids isolated from the Fortunella crassifolia and the *Citrus junos* with their cell death-inducing activity on Adriamycin-treated cancer cell. *J. Nat. Med.* **2021**, *75*, 998–1004. [CrossRef]
90. Murthy, K.N.C.; Jayaprakasha, G.K.; Safe, S.; Patil, B.S. Citrus limonoids induce apoptosis and inhibit the proliferation of pancreatic cancer cells. *Food Funct.* **2021**, *12*, 1111–1120. [CrossRef] [PubMed]
91. Dong, W.; Wei, X.; Zhang, F.; Hao, J.; Huang, F.; Zhang, C.; Liang, W. A dual character of flavonoids in influenza A virus replication and spread through modulating cell-autonomous immunity by MAPK signaling pathways. *Sci. Rep.* **2014**, *4*, 7237. [CrossRef]
92. Lin, C.W.; Tsai, F.J.; Tsai, C.H.; Lai, C.C.; Wan, L.; Ho, T.Y.; Hsieh, C.C.; Chao, P.D. Anti-SARS coronavirus 3C-like protease effects of Isatis indigotica root and plant-derived phenolic compounds. *Antivir. Res.* **2005**, *68*, 36–42. [CrossRef]
93. De Clercq, E. Potential antivirals and antiviral strategies against SARS coronavirus infections. *Expert Rev. Anti-Infect. Ther.* **2006**, *4*, 291–302. [CrossRef]
94. Tutunchi, H.; Naeini, F.; Ostadrahimi, A.; Hosseinzadeh-Attar, M.J. Naringenin, a flavanone with antiviral and anti-inflammatory effects: A promising treatment strategy against COVID-19. *Phytother. Res.* **2020**, *34*, 3137–3147. [CrossRef] [PubMed]
95. Ferreira, S.S.; Silva, A.M.; Nunes, F.M. *Citrus reticulata* Blanco peels as a source of antioxidant and anti-proliferative phenolic compounds. *Ind. Crop. Prod.* **2018**, *111*, 141–148. [CrossRef]
96. Saini, R.K.; Rengasamy, K.R.R.; Mahomoodally, F.M.; Keum, Y.S. Protective effects of lycopene in cancer, cardiovascular, and neurodegenerative diseases: An update on epidemiological and mechanistic perspectives. *Pharm. Res.* **2020**, *155*, 104730. [CrossRef] [PubMed]
97. Saini, R.K.; Keum, Y.S.; Daglia, M.; Rengasamy, K.R. Dietary carotenoids in cancer chemoprevention and chemotherapy: A review of emerging evidence. *Pharm. Res.* **2020**, *157*, 104830. [CrossRef]
98. Shin, J.; Song, M.H.; Oh, J.W.; Keum, Y.S.; Saini, R.K. Pro-Oxidant Actions of Carotenoids in Triggering Apoptosis of Cancer Cells: A Review of Emerging Evidence. *Antioxidants* **2020**, *9*, 532. [CrossRef]
99. Tian, D.M.; Wang, F.F.; Duan, M.L.; Cao, L.Y.; Zhang, Y.W.; Yao, X.S.; Tang, J.S. Coumarin Analogues from the *Citrus grandis* (L.) Osbeck and Their Hepatoprotective Activity. *J. Agric. Food Chem.* **2019**, *67*, 1937–1947. [CrossRef]
100. Cataneo, A.H.D.; Kuczera, D.; Koishi, A.C.; Zanluca, C.; Silveira, G.F.; de Arruda, T.B.; Suzukawa, A.A.; Bortot, L.O.; Dias-Baruffi, M.; Verri, W.A.; et al. The citrus flavonoid naringenin impairs the in vitro infection of human cells by Zika virus. *Sci. Rep.* **2019**, *9*, 16348. [CrossRef]
101. Gansukh, E.; Nile, A.; Sivanesan, I.; Rengasamy, K.R.R.; Kim, D.H.; Keum, Y.S.; Saini, R.K. Chemopreventive Effect of beta-Cryptoxanthin on Human Cervical Carcinoma (HeLa) Cells Is Modulated through Oxidative Stress-Induced Apoptosis. *Antioxidants* **2019**, *9*, 28. [CrossRef]
102. Feng, K.L.; Zhu, X.A.; Liu, G.; Kan, Q.X.; Chen, T.; Chen, Y.J.; Cao, Y. Dietary citrus peel essential oil ameliorates hypercholesterolemia and hepatic steatosis by modulating lipid and cholesterol homeostasis. *Food Funct.* **2020**, *11*, 7217–7230. [CrossRef] [PubMed]
103. Dhuique-Mayer, C.; Gence, L.; Portet, K.; Tousch, D.; Poucheret, P. Preventive action of retinoids in metabolic syndrome/type 2 diabetic rats fed with citrus functional food enriched in beta-cryptoxanthin. *Food Funct.* **2020**, *11*, 9263–9271. [CrossRef]
104. Revathy, J.; Srinivasan, S.; Abdullah, S.H.S.; Muruganathan, U. Antihyperglycemic effect of hesperetin, a citrus flavonoid, extenuates hyperglycemia and exploring the potential role in antioxidant and antihyperlipidemic in streptozotocin-induced diabetic rats. *Biomed. Pharmacother.* **2018**, *97*, 98–106. [CrossRef]
105. Bi, W.Y.; Zhou, J.X.; Zhao, L.; Wang, C.T.; Wu, W.; Zhang, L.B.; Ji, B.P.; Zhang, N.H.; Zhou, F. Preventive effect of different citrus essential oils on primary dysmenorrhea: In vivo and in vitro study. *Food Biosci.* **2021**, *42*, 101135. [CrossRef]
106. Zhang, L.L.; Yang, Z.Y.; Fan, G.; Ren, J.N.; Yin, K.J.; Pan, S.Y. Antidepressant-like Effect of *Citrus sinensis* (L.) Osbeck Essential Oil and Its Main Component Limonene on Mice. *J. Agric. Food Chem.* **2019**, *67*, 13817–13828. [CrossRef] [PubMed]
107. Muhammad, T.; Ikram, M.; Ullah, R.; Rehman, S.U.; Kim, M.O. Hesperetin, a Citrus Flavonoid, Attenuates LPS-Induced Neuroinflammation, Apoptosis and Memory Impairments by Modulating TLR4/NF-kappa B Signaling. *Nutrients* **2019**, *11*, 648. [CrossRef] [PubMed]

108. Okuyama, S.; Nakashima, T.; Nakamura, K.; Shinoka, W.; Kotani, M.; Sawamoto, A.; Nakajima, M.; Furukawa, Y. Inhibitory Effects of Auraptene and Naringin on Astroglial Activation, Tau Hyperphosphorylation, and Suppression of Neurogenesis in the Hippocampus of Streptozotocin-Induced Hyperglycemic Mice. *Antioxidants* **2018**, *7*, 109. [CrossRef] [PubMed]
109. Guo, X.; Cao, X.D.; Fang, X.G.; Guo, A.L.; Li, E.H. Inhibitory effects of fermented Ougan (*Citrus reticulata* cv. *Suavissima*) juice on high-fat diet-induced obesity associated with white adipose tissue browning and gut microbiota modulation in mice. *Food Funct.* **2021**, *12*, 9300–9314. [CrossRef]
110. Lazar, V.; Ditu, L.-M.; Pircalabioru, G.G.; Picu, A.; Petcu, L.; Cucu, N.; Chifiriuc, M.C. Gut Microbiota, Host Organism, and Diet Trialogue in Diabetes and Obesity. *Front. Nutr.* **2019**, *6*, 21. [CrossRef]
111. Tung, Y.C.; Chang, W.T.; Li, S.M.; Wu, J.C.; Badmeav, V.; Ho, C.T.; Pan, M.H. Citrus peel extracts attenuated obesity and modulated gut microbiota in mice with high-fat diet-induced obesity. *Food Funct.* **2018**, *9*, 3363–3373. [CrossRef]
112. Miler, M.; Zivanovic, J.; Ajdzanovic, V.; Milenkovic, D.; Jaric, I.; Sosic-Jurjevic, B.; Milosevic, V. Citrus Flavanones Upregulate Thyrotroph Sirt1 and Differently Affect Thyroid Nrf2 Expressions in Old-Aged Wistar Rats. *J. Agric. Food Chem.* **2020**, *68*, 8242–8254. [CrossRef]
113. Kawabata, A.; Hung, T.V.; Nagata, Y.; Fukuda, N.; Suzuki, T. Citrus kawachiensis Peel Powder Reduces Intestinal Barrier Defects and Inflammation in Colitic Mice. *J. Agric. Food Chem.* **2018**, *66*, 10991–10999. [CrossRef] [PubMed]
114. Zhang, Z.Y.; Nie, M.M.; Liu, C.Q.; Jiang, N.; Liu, C.J.; Li, D.J. Citrus Flavanones Enhance beta-Carotene Uptake in Vitro Experiment Using Caco-2 Cell: Structure-Activity Relationship and Molecular Mechanisms. *J. Agric. Food Chem.* **2019**, *67*, 4280–4288. [CrossRef]
115. Castro, M.A.; Rodenak-Kladniew, B.; Massone, A.; Polo, M.; de Bravo, M.G.; Crespo, R. Citrus reticulata peel oil inhibits non-small cell lung cancer cell proliferation in culture and implanted in nude mice. *Food Funct.* **2018**, *9*, 2290–2299. [CrossRef] [PubMed]
116. Gao, X.G.; Wang, C.Y.; Ning, C.Q.; Liu, K.X.; Wang, X.Y.; Liu, Z.H.; Sun, H.J.; Ma, X.D.; Sun, P.Y.; Meng, Q. Hepatoprotection of auraptene from peels of citrus fruits against thioacetamide-induced hepatic fibrosis in mice by activating farnesoid X receptor. *Food Funct.* **2018**, *9*, 2684–2694. [CrossRef]
117. Wang, J.Q.; Fu, T.; Dong, R.C.; Wang, C.Y.; Liu, K.X.; Sun, H.J.; Huo, X.K.; Ma, X.D.; Yang, X.B.; Meng, Q. Hepatoprotection of auraptene from the peels of citrus fruits against 17 alpha-ethinylestradiol-induced cholestasis in mice by activating farnesoid X receptor. *Food Funct.* **2019**, *10*, 3839–3850. [CrossRef] [PubMed]
118. Carvalho, J.D.; Ramadan, D.; Goncalves, V.D.; Maquera-Huacho, P.M.; Assis, R.P.; Lima, T.F.O.; Brunetti, I.L.; Spolidorio, D.M.P.; Cesar, T.; Manthey, J.A.; et al. Impact of citrus flavonoid supplementation on inflammation in lipopolysaccharide-induced periodontal disease in mice. *Food Funct.* **2021**, *12*, 5007–5017. [CrossRef]
119. He, W.; Li, Y.M.; Liu, M.Y.; Yu, H.Y.; Chen, Q.; Chen, Y.; Ruan, J.Y.; Ding, Z.J.; Zhang, Y.; Wang, T. Citrus aurantium L. and Its Flavonoids Regulate TNBS-Induced Inflammatory Bowel Disease through Anti-Inflammation and Suppressing Isolated Jejunum Contraction. *Int. J. Mol. Sci.* **2018**, *19*, 3057. [CrossRef]
120. Samie, A.; Sedaghat, R.; Baluchnejadmojarad, T.; Roghani, M. Hesperetin, a citrus flavonoid, attenuates testicular damage in diabetic rats via inhibition of oxidative stress, inflammation, and apoptosis. *Life Sci.* **2018**, *210*, 132–139. [CrossRef]
121. Guirro, M.; Gual-Grau, A.; Gibert-Ramos, A.; Alcaide-Hidalgo, J.M.; Canela, N.; Arola, L.; Mayneris-Perxachs, J. Metabolomics Elucidates Dose-Dependent Molecular Beneficial Effects of Hesperidin Supplementation in Rats Fed an Obesogenic Diet. *Antioxidants* **2020**, *9*, 79. [CrossRef]
122. Hu, H.J.; Zhang, S.S.; Liu, F.X.; Zhang, P.P.; Muhammad, Z.; Pan, S.Y. Role of the Gut Microbiota and Their Metabolites in Modulating the Cholesterol-Lowering Effects of Citrus Pectin Oligosaccharides in C57BL/6 Mice. *J. Agric. Food Chem.* **2019**, *67*, 11922–11930. [CrossRef] [PubMed]
123. Cirmi, S.; Navarra, M.; Woodside, J.V.; Cantwell, M.M. Citrus fruits intake and oral cancer risk: A systematic review and meta-analysis. *Pharmacol. Res.* **2018**, *133*, 187–194. [CrossRef] [PubMed]
124. Victoria-Montesinos, D.; Abellán Ruiz, M.S.; Luque Rubia, A.J.; Guillén Martínez, D.; Pérez-Piñero, S.; Sánchez Macarro, M.; García-Muñoz, A.M.; Cánovas García, F.; Castillo Sánchez, J.; López-Román, F.J. Effectiveness of Consumption of a Combination of Citrus Fruit Flavonoids and Olive Leaf Polyphenols to Reduce Oxidation of Low-Density Lipoprotein in Treatment-Naïve Cardiovascular Risk Subjects: A Randomized Double-Blind Controlled Study. *Antioxidants* **2021**, *10*, 589. [CrossRef]
125. Sánchez Macarro, M.; Martínez Rodríguez, J.P.; Bernal Morell, E.; Pérez-Piñero, S.; Victoria-Montesinos, D.; García-Muñoz, A.M.; Cánovas García, F.; Castillo Sánchez, J.; López-Román, F.J. Effect of a Combination of Citrus Flavones and Flavanones and Olive Polyphenols for the Reduction of Cardiovascular Disease Risk: An Exploratory Randomized, Double-Blind, Placebo-Controlled Study in Healthy Subjects. *Nutrients* **2020**, *12*, 1475. [CrossRef] [PubMed]
126. Visvanathan, R.; Williamson, G. Effect of citrus fruit and juice consumption on risk of developing type 2 diabetes: Evidence on polyphenols from epidemiological and intervention studies. *Trends Food Sci. Technol.* **2021**, *115*, 133–146. [CrossRef]
127. Ávila-Gálvez, M.Á.; Giménez-Bastida, J.A.; González-Sarrías, A.; Espín, J.C. New Insights into the Metabolism of the Flavanones Eriocitrin and Hesperidin: A Comparative Human Pharmacokinetic Study. *Antioxidants* **2021**, *10*, 435. [CrossRef]
128. Brasili, E.; Hassimotto, N.M.A.; Del Chierico, F.; Marini, F.; Quagliariello, A.; Sciubba, F.; Miccheli, A.; Putignani, L.; Lajolo, F. Daily Consumption of Orange Juice from *Citrus sinensis* L. Osbeck cv. Cara Cara and cv. Bahia Differently Affects Gut Microbiota Profiling as Unveiled by an Integrated Meta-Omits Approach. *J. Agric. Food Chem.* **2019**, *67*, 1381–1391. [CrossRef]

129. Garcia-Flores, L.A.; Medina, S.; Gomez, C.; Wheelock, C.E.; Cejuela, R.; Martinez-Sanz, J.M.; Oger, C.; Galano, J.M.; Durand, T.; Hernandez-Saez, A.; et al. Aronia-citrus juice (polyphenol-rich juice) intake and elite triathlon training: A lipidomic approach using representative oxylipins in urine. *Food Funct.* **2018**, *9*, 463–475. [CrossRef]
130. Li, Y.; Kandhare, A.D.; Mukherjee, A.A.; Bodhankar, S.L. Acute and sub-chronic oral toxicity studies of hesperidin isolated from orange peel extract in Sprague Dawley rats. *Regul. Toxicol. Pharmacol.* **2019**, *105*, 77–85. [CrossRef]
131. Nakajima, A.; Nemoto, K.; Ohizumi, Y. An evaluation of the genotoxicity and subchronic toxicity of the peel extract of Ponkan cultivar 'Ohta ponkan' (*Citrus reticulata* Blanco) that is rich in nobiletin and tangeretin with anti-dementia activity. *Regul. Toxicol. Pharmacol.* **2020**, *114*, 104670. [CrossRef]
132. Li, P.; Wu, H.; Wang, Y.; Peng, W.; Su, W. Toxicological evaluation of naringin: Acute, subchronic, and chronic toxicity in Beagle dogs. *Regul. Toxicol. Pharmacol.* **2020**, *111*, 104580. [CrossRef] [PubMed]
133. Cohen, S.M.; Eisenbrand, G.; Fukushima, S.; Gooderham, N.J.; Guengerich, F.P.; Hecht, S.S.; Rietjens, I.M.C.M.; Bastaki, M.; Davidsen, J.M.; Harman, C.L.; et al. FEMA GRAS assessment of natural flavor complexes: Citrus-derived flavoring ingredients. *Food Chem. Toxicol.* **2019**, *124*, 192–218. [CrossRef] [PubMed]
134. Ravichandran, C.; Badgujar, P.C.; Gundev, P.; Upadhyay, A. Review of toxicological assessment of d-limonene, a food and cosmetics additive. *Food Chem. Toxicol.* **2018**, *120*, 668–680. [CrossRef] [PubMed]

MDPI AG
Grosspeteranlage 5
4052 Basel
Switzerland
Tel.: +41 61 683 77 34

Antioxidants Editorial Office
E-mail: antioxidants@mdpi.com
www.mdpi.com/journal/antioxidants

Academic Open
Access Publishing

mdpi.com

ISBN 978-3-7258-4400-5